ISSN 1018-5593

itu

Institute for Transuranium Elements

Annual Report 96

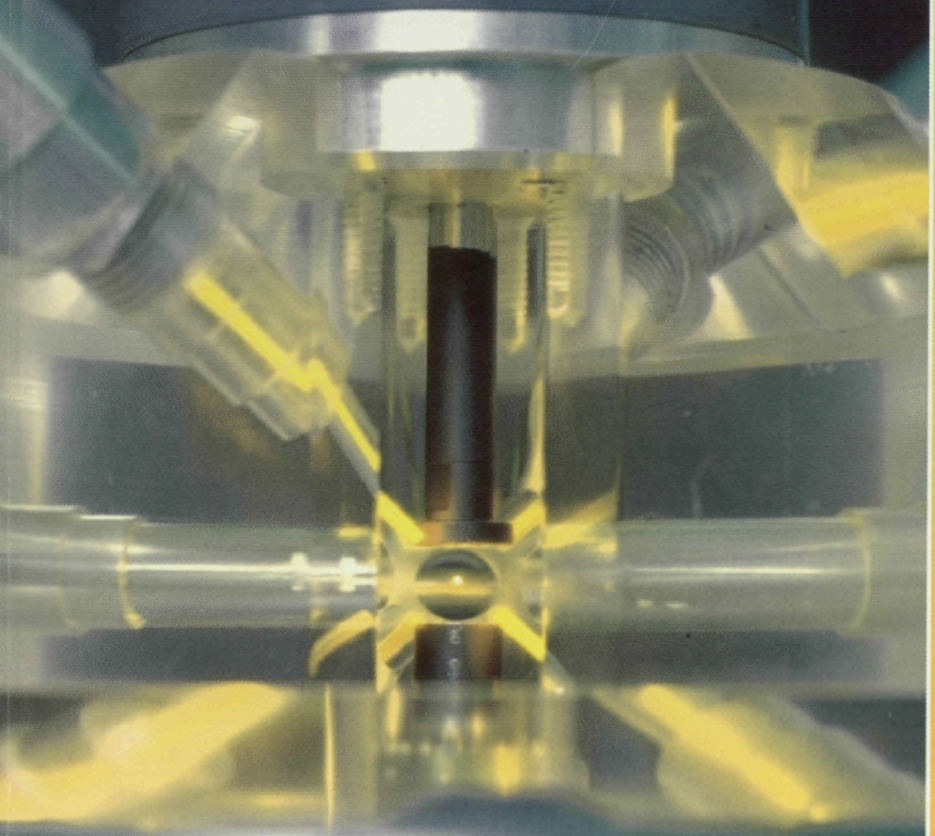

JOINT RESEARCH CENTRE
EUROPEAN COMMISSION

Report EUR 17296 EN

EUROPEAN COMMISSION

Directorate-General JRC
Joint Research Centre

Institute for Transuranium Elements Karlsruhe

Annual Report 1996

TUAR-96

1997

EUR 17296 EN

Published by the
EUROPEAN COMMISSION
Directorate-General JRC

INSTITUTE FOR TRANSURANIUM ELEMENTS
D-76125 Karlsruhe

LEGAL NOTICE

Cataloguing data can be found at the end of this publication

This report was compiled and edited by R. Schenkel, J. Richter, J. Magill, D. Pel

Inquiries for more details should be addressed to the Programme Office,
Institute for Transuranium Elements, P.O. Box 2340, D-76125 Karlsruhe,
Phone ++49-7247-951386, FAX ++49-7247-951591

This publication and more information on the Institute may be found on the Web page:
http://www.jrc.org/

Luxembourg: Office for Official Publications of the European Communities, 1997
ISBN 92-828-0049-0

Printed in Germany

Table of Contents

Foreword

by J. van Geel, Director

This report provides a description of the work performed and the progress achieved in 1996. It covers the various scientific and technical activities of the Institute, placing emphasis on the institutional activities, but summarizing in a succinct manner also the various competitive activities.

Some of the major scientific/technical achievements are outlined in the section "Highlights 1996". I am grateful to the staff of the Institute for this broad range of high quality and dedicated work carried out. It covers applied research such as the application of the alpha emitting nuclides to treat certain types of leukemia, the development of unique equipment for the micro-characterization of spent fuel, or new fabrication techniques for targets for transmutation or incineration. The highlights include subjects with a high potential for future application, like nuclear forensic analysis and related data bases.
There are excellent examples of new preparation techniques and instrument developments for basic thermophysical and material science research of actinides. The highlight reporting on the the first detection of surface magnetism of UO_2 by synchrotron X-rays is an example of the relevance of basic actinide research for the scientific community and the close collaboration of the Institute with major research institutions in this area.

As a new feature of the Annual Report, a review article on "Limits and Prospects for High Burn-up LWR fuel" provides a survey of the state of the art of high burn-up fuel based on experience available in the Institute.

In November 1996 a visiting group evaluated the Institute on behalf of the JRC's Board of Governors. This evaluation was a follow up of a previous assessment in February 1994. We are encouraged by the result of this evaluation and consider the recommendations made as very helpful.

In the year ahead we are faced with the retirement of several leading scientists and technicians. Their replacement with equally qualified personnel will be given highest priority in order to guarantee a smooth transition.

Some outstanding issues, such as the extension of our Minor Actinide Laboratory, the renovation and upgrading of the Institute's infrastructure, and the further discharge of radioactive wastes will be tackled during 1997 and 1998. I look forward again to the support of the Institute's staff to the solution of these challenges.

J. van Geel

Executive Summary

Introduction

The safety of actinides in the nuclear fuel cycle continued to be the major institutional contribution of the Institute to the Programme 'Nuclear Fission Safety'. Major research areas were basic actinide research, safety of nuclear fuels, mitigation of long-lived actinides and spent fuel characterisation.

ITU also provided scientific and technical support for Community policies in the area of nuclear safety and safeguards, predominantly related to the implementation of on-site laboratories at Sellafield and Cap la Hague, but also related to nuclear safety in Eastern countries and the Russian Federation. In addition, ITU continued to carry out contractual work in request of various customers.

Fuel Cycle Safety

Basic Actinide Research

The central objective of actinide research is the elucidation of the electronic structure of actinide metals and compounds, in particular, the behaviour of the 5f electrons. The dualism between localized and itinerant characteristics, as it is particularly clearly demonstrated in the actinide series, is a key problem in these studies.

The preparation of new compounds, study of phase diagrams, and synthesis of single crystals play a key role in this endeavour. Important results have been obtained in the understanding of uranium-based heavy fermion superconductors doped with neptunium and plutonium. Other themes include the use of pressure to study trends in structural transitions and changes in resistance at low temperature, the theory of light-solid interactions, and the use of neutron and synchrotron experiments to complement the bulk property measurements obtained in Karlsruhe.

The X-ray magnetic scattering experiments on surface magnetism in UO_2 performed in collaboration with the National Synchrotron Light Source at Brookhaven are featured as a ITU highlight at the front of this report.

The work on alpha-immunotherapy entered into a decisive phase: First clinical tests and evaluations were performed in December 1996 in the Memorial Sloan Kettering Cancer Center in New York.

Safety of Nuclear Fuels

In the area of safety of nuclear fuel, microstructure and fuel cladding interaction of fuel at very high burn-up (up to 60 GWd/t) was measured and evaluated. Structural properties of fuel with simulated burn-ups of up to 200 GWd/t were examined and compared with real high burn-up fuel to understand the rim effect formation processes. Fission gas release of high burn-up fuel was analysed and source term measurements with the Knudsen cell continued including specimens from the Phebus FP experiment. Oxidation and creep measurements on SIMFUEL were carried out and radiation damage studies on UO_2 continued.

The fuel performance code TRANSURANUS was further amended with data from high burn-up fuel.

Four highlights at the front of the report feature work in this area: new micro X-ray diffraction equipment for the characterisation of irradiated fuel, new preparation for the characterisation of irradiated fuel, new preparation technique to study radiation damage in UO_2 and a novel approach for the fabrication of transmutation/incineration targets.

Mitigation of long-lived actinides and fission products

In the area of mitigation of long-lived actinides and fission products, ITU continued its collaborative work with leading national laboratories, in order to study the further reduction of radiotoxicity of highly active wastes.

The major task of ITU is the fabrication and characterisation of fuel targets for irradiation experiments and the post-irradiation examination to compare the results with theoretical predictions. Also new extraction processes for the effective separation of long-lived actinides are tested under realistic conditions.

The initial layout of the minor actinide laboratory was modified and the purchase of major components has been initiated. Actinides were separated from irradiated fuel (Superfact 1) on a 100 g scale, including a final separation step for lanthanides. Radiation damage and basic physical property studies were performed on different inert matrices.

Spent fuel characterization in view of long term storage

In the area of spent fuel characterisation, major emphasis of the work performed was the investigation of the oxidation kinetics and corrosion effects of irradiated UO_2 and MOX fuel, leaching tests of UO_2 and on fuel rod segments with pre-set defects have been caried out.

The chemical interaction of fuel and cladding has been further investigated. Initial electrochemical measurements show lower corrosion rates for MOX fuel than for uranium fuel. Extensive work to study the leaching of simulated high burn-up fuel was carried out leading to an explanation for the buffering behaviour of molybdenum on the oxidation potential of spent fuel. Non destructive measurements based on CdTe detectors were performed on spent fuel under hot cell conditions.

Safeguards and fissile material management

Nuclear safeguards on fissile material is performed in the European Union within the framework of the Euratom and the Non-Proliferation Treaty. The Institute contributes to the objectives of these treaties by performing research and development of methods, techniques and instruments, by provision of analytical services and expertise and by direct in-field measurement support.

In support for DG XVII, major progress was achieved towards the implementation of the on-site laboratory at Sellafield. Analytical procedures and working procedures in accordance with ISO 9001 and preparation for the shipment of glove boxes and equipment to Sellafield were completed. Verification measurements on samples taken at Cap la Hague and Sellafield continued.

The technical specifications for the on-site laboratory at Cap la Hague were discussed with the architect and engineering company in charge of the pre-project. Routine analytical measurements on samples sent to the Institute continued in the framework of ECSAM (European Commission's Safeguards Analytical Measurements). ITU also continued to receive and analyse seized nuclear materials. A nuclear material data bank was set up in close collaboration with the Bochvar Institute in Moscow. (This achievement is featured as a highlight at the front of the report).

Test samples with extremely low concentrations of radionuclides and samples from in-field experiments from environmental monitoring were measured on request from the IAEA and DG XVII.

Competitive activities

During 1996 work was started in collaboration with our European partners in shared cost action activities under the framework programme *Nuclear Fission Safety*. One new contract was obtained on the investigation of corium interactions and thermochemistry.

As far as technology transfer projects are concerned, three new projects submitted by the Institute were accepted, all in the area of alpha-immunotherapy and related to new actinium production techniques, conjugation work and new application of radioimmunotherapy to multiple myelonic cancer cells present in the human bone marrow.

As in previous years, the Institute has carried out work for third parties, with major contracts in the area of post-irradiation examination of irradiated fuel, fabrication and characterization of fuels for transmutation and examination of high burn-up oxide and mixed oxide fuels for different customers.

Several new proposals were submitted for the TACIS/PHARE programme, covering assistance in combatting illicit trafficking of nuclear materials, the setting up of analytical, metrological and forensic capabilities in the Russian Federation for nuclear material accountancy and control and a cooperation in the area of fuel modelling to improve the safety of reactor operation.

Taking all competitive activities together, new contracts with a volume of 3.7 MECU were signed. The payments received from work carried out during 1996 totalled 3.6 MECU.

Highlights 1996

Pioneering Work on Alpha-Radioimmunotherapy

Alpha-emitting radioisotopes are amongst the most promising nuclides for the treatment of blood borne and micro-metastatic cancer cells. Because of their short range (60 to 100 micrometer) and high linear energy transfer values, alpha emitters can deliver a very large radiation dose over the distance of a few cell diameters. When alpha emitters are conjugated to tumour seeking monoclonal antibodies, the resulting product is expected to be an efficient cancer drug. (A schematic description of the coupling of antibody, chelator and the α-emitter is shown in the attached figure).

Following several years of joint development, implementation of phase I clinical trials using ^{213}Bi-immunotherapy on patients with acute myelogeneous leukaemia started in the Memorial Sloan Kettering Cancer Center in New York. ^{213}Bi generators are sent regularly from ITU to the US on request of the hospital, depending upon the availability of a patient in a more or less stable situation. The special requirements related to the stability under transport and the safe processing of such generator at the hospital were solved by ITU researchers. They developed both the transport arrangement (a quartz ampoule in which the ^{225}Ac is fixed as a chloride in colloid free form) and a dissolution, elution and purification procedure, allowing the ^{213}Bi to be extracted in the hospital, directly before the coupling to the antibody HuM^{195} and before the injection of the radioimmunoconjugate into the patient. In the pre-clinical study it was found that the radio-labelled HuM195 is rapidly internalized into the HL60 leukaemia cells. The in vitro stability and non-specific toxicity in mice were acceptable. The results of the first clinical trials on several patients provide the confirmation that the drug in the human body is behaving as predicted from the pre-clinical data. No acute side effects were observed and a significant anti-leukaemia effect was shown.

The production of ^{225}Ac through irradiation of ^{226}Ra in a cyclotron with protons (a process patented by ITU) is a new project which is expected to allow a flexible and clean production of the mother isotope for the ^{213}Bi-generator. Experiments to prove the feasability of this approach were started in collaboration with the Forschungszentrum Karlsruhe.

In collaboration with the Institut National de la Santé et de la Recherche Médicale (INSERM) and the Laboratoire de Physique Subatomique et de Technologies Associées (SUBATECH) in Nantes, the use of both ^{213}Bi and ^{225}Ac for killing multiple myelomic cancer cells in human bone marrow will be studied. These cancer cells are very well suited to be treated with short range alpha particles because the onset of the myelomic cancer is restricted to the bone marrow (and therefore easy to locate and target) and the modular type of tumours consists of a few hundreds of cells (corresponding to the distance traveled by the α-particles).

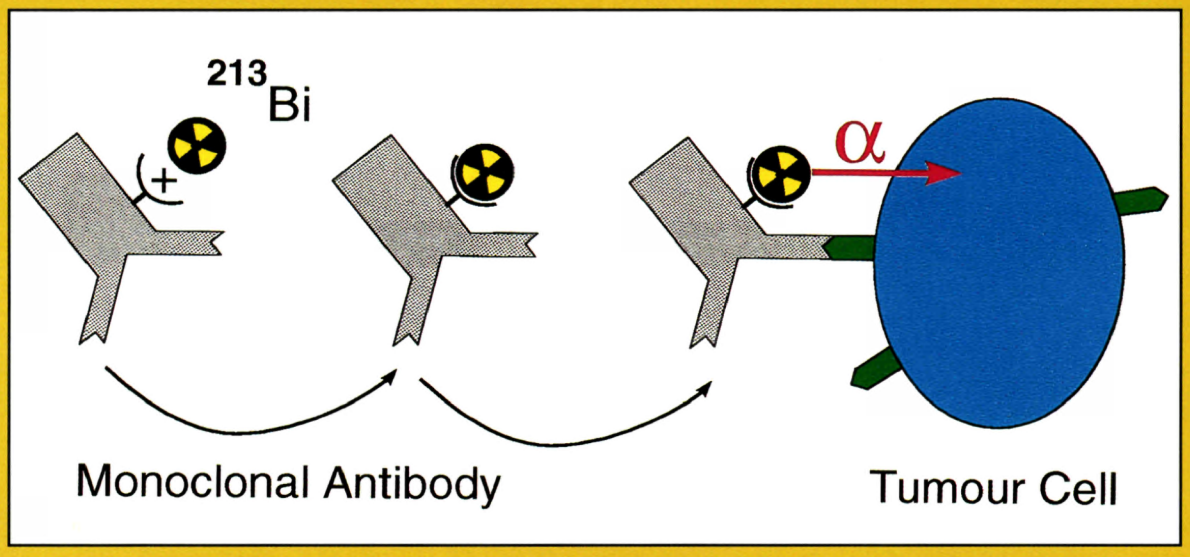

Conjugation and coupling of an alpha-emitting radio-immunoconjugate.

Surface Magnetism as observed by Synchrotron X-rays

The design of high-density storage media, magneto-optical recording devices, corrosion, the leaching of nuclear fuels, and fundamental questions concerning so-called "dimensionality" all agree on one thing – the *surface* is where the action is. Many techniques have been invented to look at surfaces, including new ones such as the scanning-tunneling microscope, but few have the capability of giving information on the spatial configuration of the surface layer. In general obtaining the latter requires the use of scattering techniques, using electrons, X-rays, or neutrons, although getting information on just the surface presents a considerable challenge.

With the advent of the high X-ray intensities from synchrotrons, many structural surface studies have been performed that give a good idea of surface morphology, and have led to the concept of surface roughness as a quantifiable parameter. Structural correlations, both perpendicular and parallel to the surface, may be studied as a function of temperature and these studies have shown how the surface melts before the bulk. However, studies of *magnetic* surfaces are at a more primitive stage – the technique of neutron scattering, which couples strongly to the magnetism, being unfavourable because of the low intensities and high penetration of neutron beams.

Scientists working at the National Synchrotron Light Source at Brookhaven National Laboratory, New York, USA, including an important collaboration with the JRC-Karlsruhe, have now reported the first use of synchrotron X-rays to study *magnetic* surfaces. At first sight X-rays would seem unsuitable for this job, as their interaction with magnetic moments is very weak, but this is enormously enhanced if the photon energy is tuned close to an absorption edge of a magnetic element in the solid. One of the largest enhancements is found at the M-edges of the actinides (energy around 4 keV) and this is what motivated the team to select a highly polished single crystal of UO_2 and attempt to see what happens to the magnetism near the temperature T_o at which the magnetic moments disorder in the bulk – in this case 30 K. Surprisingly, the ordering arrangement and T_o of the surface layers are the same as found in the bulk. However, the exact mechanism for the disordering when heating the sample from low temperature is quite different.

The figure shows what happens on heating towards T_o and the dramatic increase in magnetic "roughness" as the surface is approached. These data are of interest to theorists, who have laboured without much experimental information, but there are important differences between what is found in UO_2 and predicted from theories of so-called surface melting.

Although basic in nature, these experiments, together with the increased X-ray intensities from the new third generation synchrotrons, such as the European Synchrotron Radiation Facility in Grenoble, France, open the way for more studies on both structural and magnetic effects at surfaces. No doubt the knowledge gained will be of importance in future high-density storage media and the associated read/write process. For more information reference is made to an article in Phys. Rev. Lett. *77* (1996) 751.

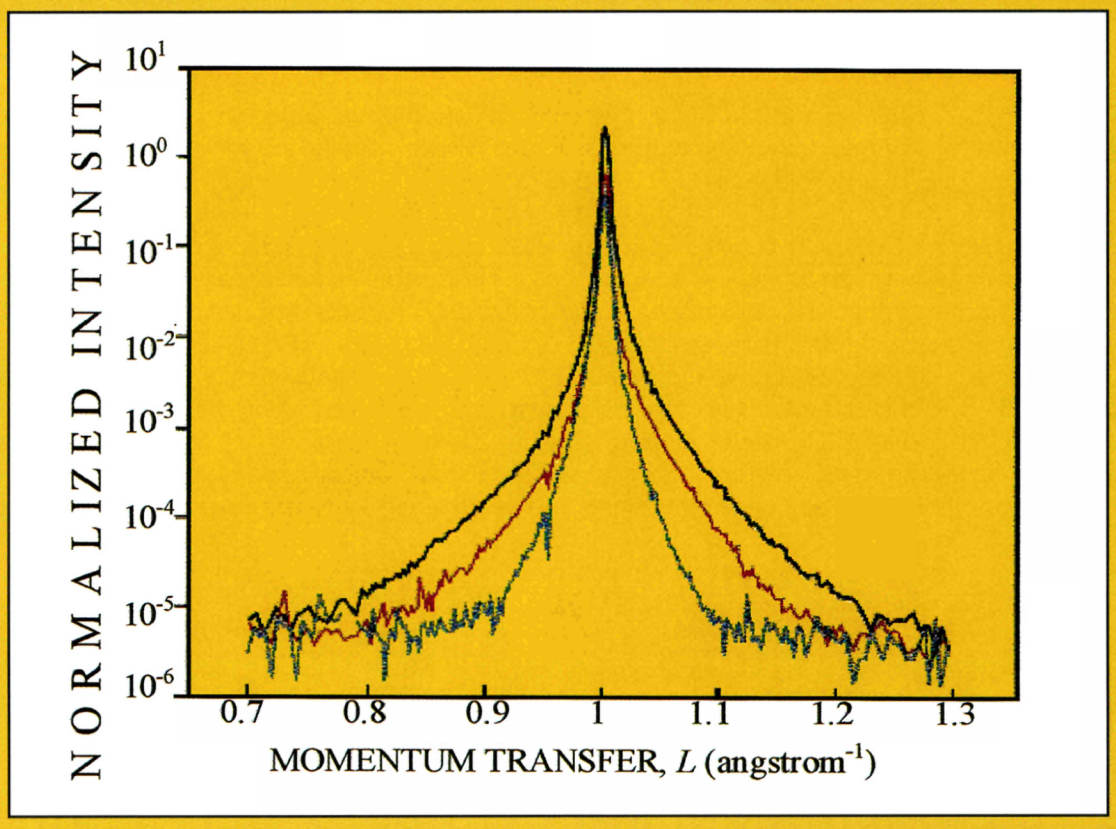

Approaching magnetic disorder. The magnetic reflectivity as a function of momentum transfer for 3 different temperatures [black – 10 K, red – 26.9 K, blue 29.6 K]. The width of the scattering in momentum space (x-axis) gives a measure of the width of the interface between the disordered region at the surface and the ordered bulk. In momentum space a wide distribution indicates a narrow distribution in real space. Thus as the material is heated from 10 to 29.6 K (the magnetism disappears at To = 30 K) the interfacial width increases, as shown by the decrease in the width in momentum space. (figure with courtesy of Physics Today, November 1996)

Development and Application of a new Micro X-ray Diffraction Technique for the Characterization of Irradiated Fuels

The increase of burn-up and thus the residence time of fuel in light water reactors is one of the major objectives of plant operators. The achievement of this goal will lead not only to economic advantages but also to a decrease of transports and radioactive waste arising.

It has been observed in recent years that microstructure changes occur in the fuel at very high burn-up. The investigation of these effects requires new methods in the material characterization of irradiated fuels. These requirements concern the determination of the structural, chemical and mechanical properties of the heavily irradiated fuel, often restricting the area of analysis to sample dimensions as small as 10-20 micrometers. Such a strong demand in the materials sampling stems from the fact that the main property changes of the high burn-up fuels occur at the pellet periphery, in a region which at most extends to some hundreds microns in depth. Despite its reduced size, this peripheral region (rim) would determine to a large extent the thermal behaviour of the fuel, as well as its mechanical response under reactor operation conditions and its corrosion resistance during intermediate and long term storage.

Concerning the mechanical properties of the high burn-up fuel, a microindentation study was started in 1995 in collaboration with nuclear industry. The study demonstrated that the fracture toughness of the rim material increases considerably with the accumulated burn-up, mainly as a consequence of the grain size reduction taking place in this region. As a complement of this study, a new programme for the characterization of the lattice structure variations of the high burn-up fuel has been initiated, with the aim to widen the understanding of the physical processes affecting the fuel properties at high burn-ups. For this purpose, a micro X-ray diffraction system for powder diffractometry was developed with a collimation of the incident beam to a dimension of 3x0.01 mm, allowing the aquisition of diffraction spectra of irradiated fuel samples at intervals as small as 20-30 micrometers in the radial direction. With this system, also the structural characterization of different nuclear and non-nuclear thin interface materials will be possible, as for instance those appearing in light water reactor fuel under severe accident conditions.

MICRO XRD-ANALYSIS OF INTERFACE MATERIALS

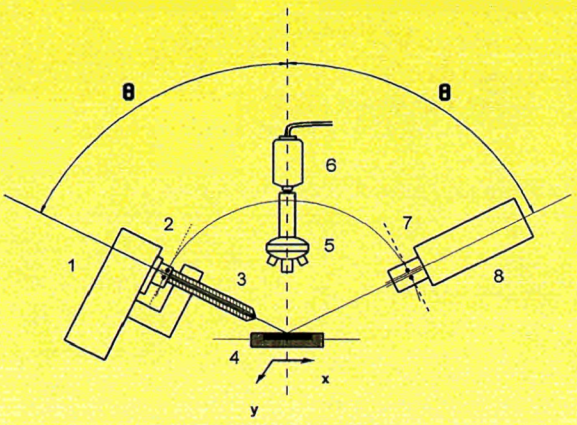

MICRO XRD APPARATUS

1 X-Ray tube
2 Soller slit
3 Collimator (10 µm width)
4 Sample (x-y table)
5 Microscope
6 Video Camera
7 Receiving slit
8 Scintillation counter

θ = diffraction angle

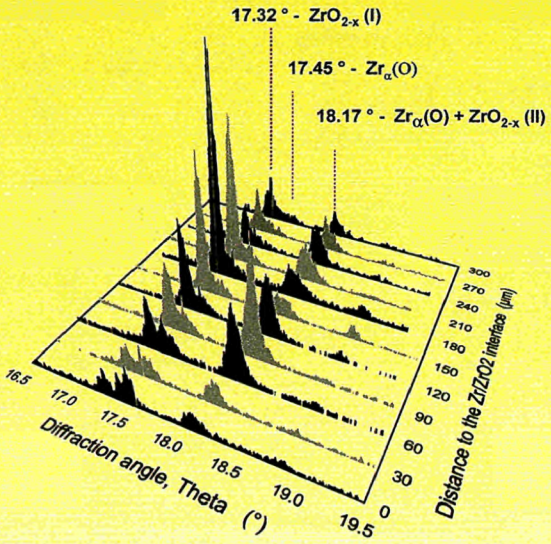

XRD peak intensity vs. diffraction angle (θ) at various distances from the Zr/ZrO_2 interface

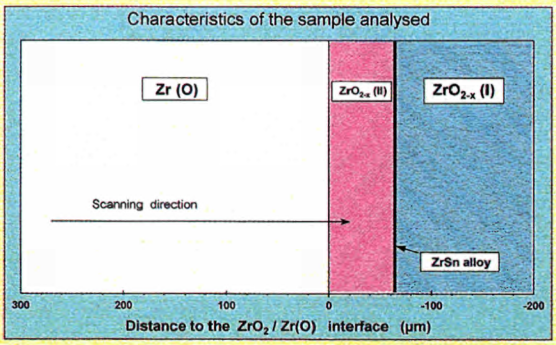

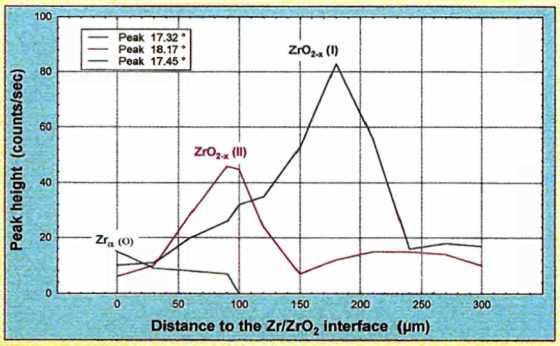

Infiltration of Highly Radioactive Materials: A Novel Approach to the Fabrication of Transmutation and Incineration Targets

Mitigation of long lived actinides and fission products by transmutation and incineration requires the development of advanced fuel and target fabrication procedures suitable for safe handling of radioactive materials with high dose rates (e.g. Am).

A method based on the infiltration of aqueous solutions of the required radioactive material into porous pellets with subsequent sintering has been developed and successfully tested at the Institute.

Tailored distributions of the infiltrant can be achieved by changing fabrication parameters, e.g. infiltration time.

A complete infiltration results in a relatively homogeneous distribution of the infiltrant within the pellet (Fig. 1), while a partial infiltration leeds to a deposition of the infiltrant only in the outer shell of a pellet as shown in Fig. 2.

The new process offers several advantages:

- minimal number of fabrication steps involving handling of highly radioactive materials
- suitable for remote handling and extensive automation
- minimization of wastes
- low dust generation, i.e. reduced contamination of exposed surfaces
- reduction of radiation exposure

So far the process has been used to produce spinel targets containing 11 w/o Am for the heterogeneous transmutation and incineration of americium. These targets are now under irradiation at HFR Petten (EFTTRA-T4 experiment).

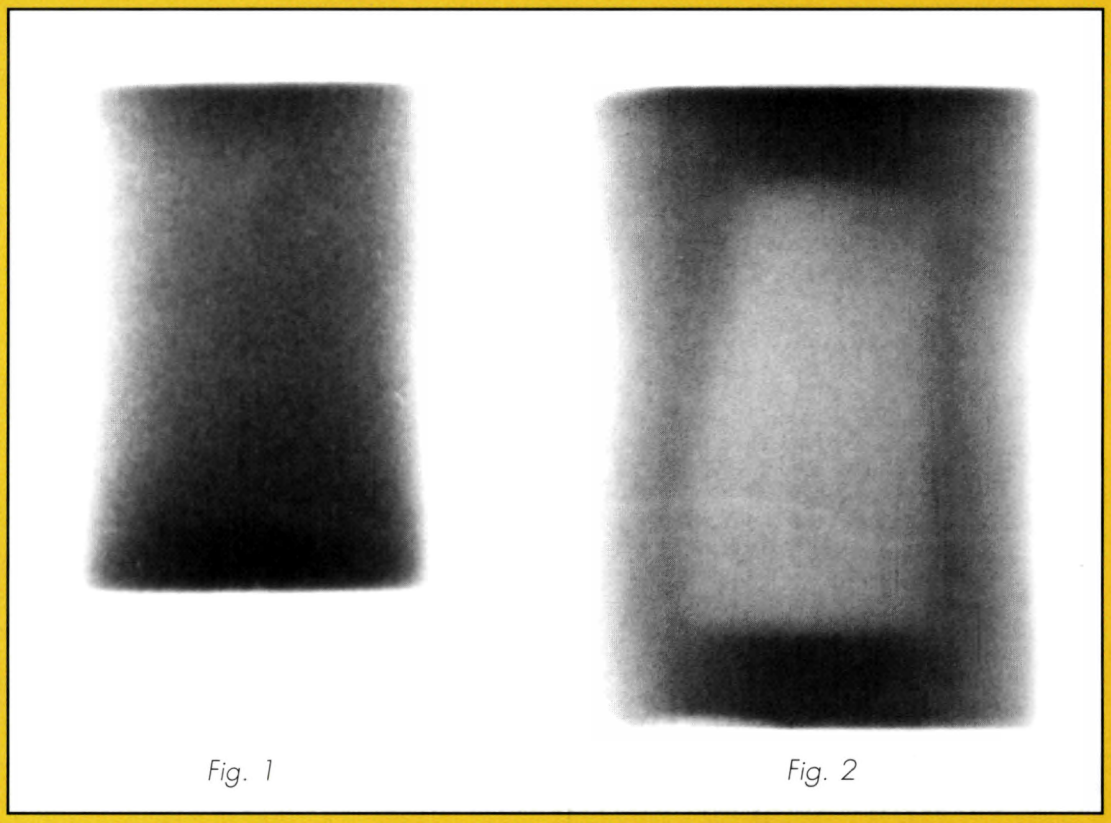

Fig. 1 Fig. 2

Fig. 1 X-ray radiography determination of the americium distribution in a spinel pellet prepared by complete infiltration of an americium nitrate solution.

Fig. 2 X-ray radiography determination of the plutonium distribution in a spinel pellet prepared by partial infiltration of a plutonium nitrate solution. The light region in the centre of the photograph corresponds to a Pu-free region of the pellet.

Development of a Nuclear Material Database for Support of Nuclear Forensic Analyses

A significant number of cases of illicit trafficking of nuclear material were detected in recent years. Law-enforcement authorities require to know not only the basic characteristics of such materials, but also their origin and intended use. From cases which occurred in the European Union more than 20 seized materials were analysed and assessed at ITU Karlsruhe.

The analysis scheme is highly case-specific and is guided by the pattern of interim results which builds up in the course of the investigation. The figure shows a photograph of seized nuclear material. To provide necessary background information and support for a subsequent evaluation, ITU experts are establishing a comprehensive database which will eventually give a complete coverage of fuel cycle and reactor facilities in the EU countries, Russia, as well as Eastern Europe. The database will be interfaced with a retrieval system.

The main objectives of the database system are:

- to guide the analyst by selection of appropriate techniques for more detailed measurements,
- to reveal the origin and intended use of seized material.

Two separate ORACLE databases were installed: one for covering source-characteristic, but non-sensitive information, the second for sample-specific data. Their internal structures differ significantly. Parameters of the source-characteristics database can be divided into three groups:

- Characteristic parameters: e.g. fuel material, fuel form, pellet dimensions, initial enrichment, impurities.
- Query results concerning origin and intended use: fuel supplier, reactor type, reactor unit.
- Auxiliary parameters for relating tables to each other: e.g. fuel type, assembly model.

Conversely, the sample-specific database covers information about actual materials analysed at ITU, including

- their morphological description,
- types of samples taken,
- analytical technique used, as well as element and isotope composition of the sample.

It is designed for materials of unknown origin as well as for samples of already known or partially identified origin.

A large fraction of development activities focused on defining which parameters are indeed characteristic for individual fuel production processes and facilities. In May 1996 a project on international co-operation between the ITU and the All-Russia Research Institute of Inorganic Materials (VNIINM), Moscow was launched, in the framework of which two VNIINM specialists made essential contributions to both contents and structure of the database. To obtain more comprehensive characteristics for irradiated fuel, ITU specialists also perform ORIGEN burn-up calculations. A number of new cross sections libraries covering the reactor types, for which fresh fuel data are available, was already established.

As main result of this years' activities, a first operational version of the database system has been set up. The corresponding data include a comprehensive list of power and prototype reactors working with U or MOX fuel as well as fuel cycle facilities situated either in Russia or in the EU. In this context, studies for identification of simple cases were carried out successfully.

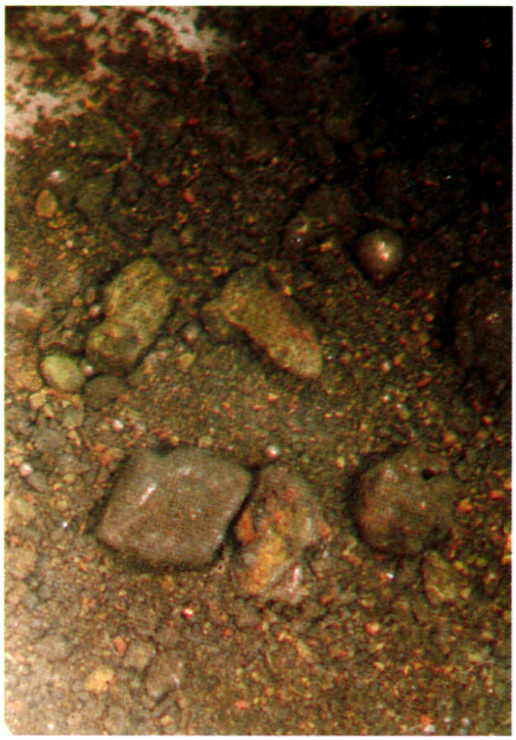

Nuclear material find analysed at ITU.

Multi- Property Thermophysical Apparatus

Combined thermophysical property measurements up to very high temperatures

When, at the beginning of the 60's, flash lamps were first introduced to measure heat propagation in solids, old techniques for thermal diffusivity measurements soon became obsolete in view of the new more elegant and flexible methods. Furthermore, experimenters soon realised that the analysis of the flash perturbations, produced in the form of temperature spikes, could be extended to calorimetric measurements. Yet, for a number of reasons, all attempts in this sense were doomed to fail, and flash calorimetry remained for a long time considered as a merely virtual method.

Now, after five years' research and development in this domain, we succeeded in constructing an apparatus which is indeed capable to produce flash pulses suitable for calorimetric analysis, and, moreover, with high-temperature steady-state heating produced by continuous-wave lasers.

The apparatus consist of a very simple cell provided with two windows and a three-pin sample mounting. The two surfaces of the sample are heated to the conditioning temperature, and, when this is achieved, a laser pulse is applied: the evolution of the thermal perturbation is recorded on the two surfaces of the sample by two special, very sensitive pyrometers. The excellent homogeneity of the laser beams used, as well as the high quality of the instrumentation for control and measurement of temperature and power input, make it possible to obtain from a single shot analysis:

- the thermal diffusivity
- the heat capacity and
- the thermal conductivity of the sample.

The uncertainty achieved is smaller than for most other methods (< 3-5%).

In addition,

- the radiative heat loss properties can be measured.

Furthermore,

- samples can be heated up to very high temperatures in the presence of a suitable gas pressure, to reduce vaporisation.

Successful measurements have been carried out on graphite up to 3500 K, but higher temperatures can be achieved.

At present, measurements on molten refractory materials are also being attempted. Finally, the accurate record of the transient temperature (< 0,1 K) provides

- a very accurate "thermal-arrest" analysis, revealing possible solid-solid or solid-liquid phase transitions under controlled environmental conditions.

The prototype, shown in the figure at the right hand side, is provided with two cells for medium (1 MPa) and high (700 MPa) buffer gas pressure.

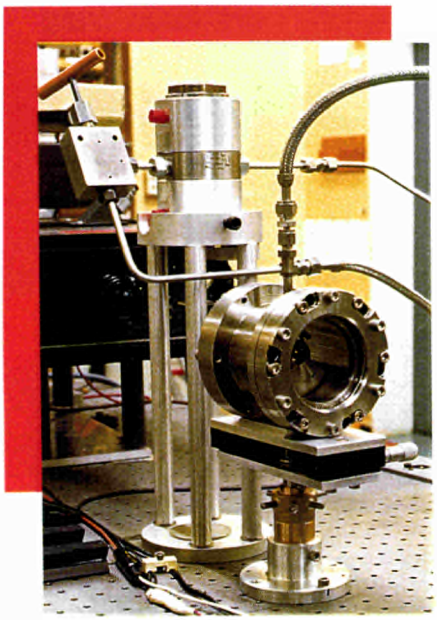

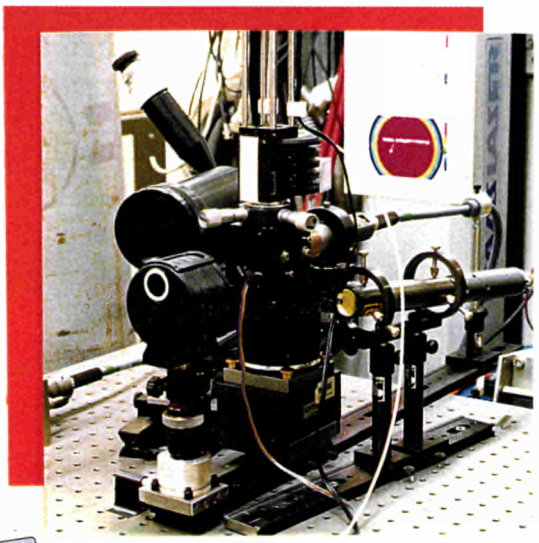

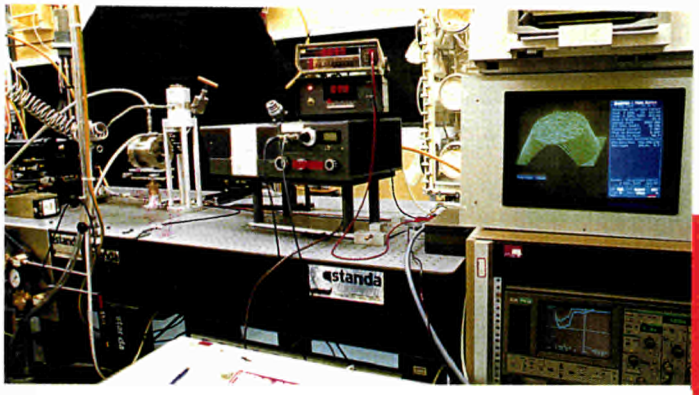

-THERMAL CAPACITY
-DIFFUSIVITY
-CONDUCTIVITY
-MELTING POINT

Schematic Diagram of The Laser Flash Thermal Diffusivity and Capacity Apparatus for Very High Temperature Applications Based on CW Power Laser Heating

On the front page the scheme of MPA.1 is shown; top left: the two vessels respectively used for measurements in vacuo or under low pressures, and for pressures uo to 2500 bar; top right: the laser focusing and beam diagnostic system; bottom: a partial view of the set-up.

New Preparation Technique to Study Radiation Damage in UO_2 by Electron Microscopy

The main source of heat production in UO_2 nuclear fuel is the slowing down of energetic heavy ions (fission products). A thorough knowledge of this process helps to understand fuel performance and behaviour at extended burnup.

In order to use well defined experimental conditions, beams of energetic ions from different large accelerators were used to study the physics of energy deposition in UO_2. The upper part of the figure shows the calculated energy deposition of different ions in UO_2 as a function of energy. The red area shows the conditions for fission products. The reported work aims to investigate in detail the consequences of this energy deposition and to approach this area from both higher and lower energies. The technique to observe the damage was high resolution transmission electron microscopy (HRTEM). Conventional specimen preparation yields thin discs (~100 nm) transparent to the electron beam. With such specimens, only a very small fraction of the tracks of the ions can be seen. To solve this problem, cross-sectional HRTEM specimens of UO_2 were successfully prepared for the first time, i.e. a special technique was developed to produce thin specimens perpendicular to the original sample surface rather than parallel as in conventional specimen preparation. Some typical results are shown in figures a and b. Fig. a shows a conventionally prepared specimen. The energetic ions produce a track, visible as 10 nm dots, showing only a fraction of a percent of the total track. With cross-sectional specimens, the tracks can, for the first time, be seen for significant parts of their length, and thus for different energy loss values or velocities of the ions.
Fig. c shows another progress in HRTEM, i.e. an edge dislocation in UO_2, using Fourier transform techniques to make it clearly visible.[1]

This new preparation/examination technique can be useful in other material science areas, where radiation damage effects need to be investigated (i.e. semiconductors, advanced materials).

[1] Hj. Matzke and L. M. Wang, J. Nucl. Mater. 231 (1996) 155

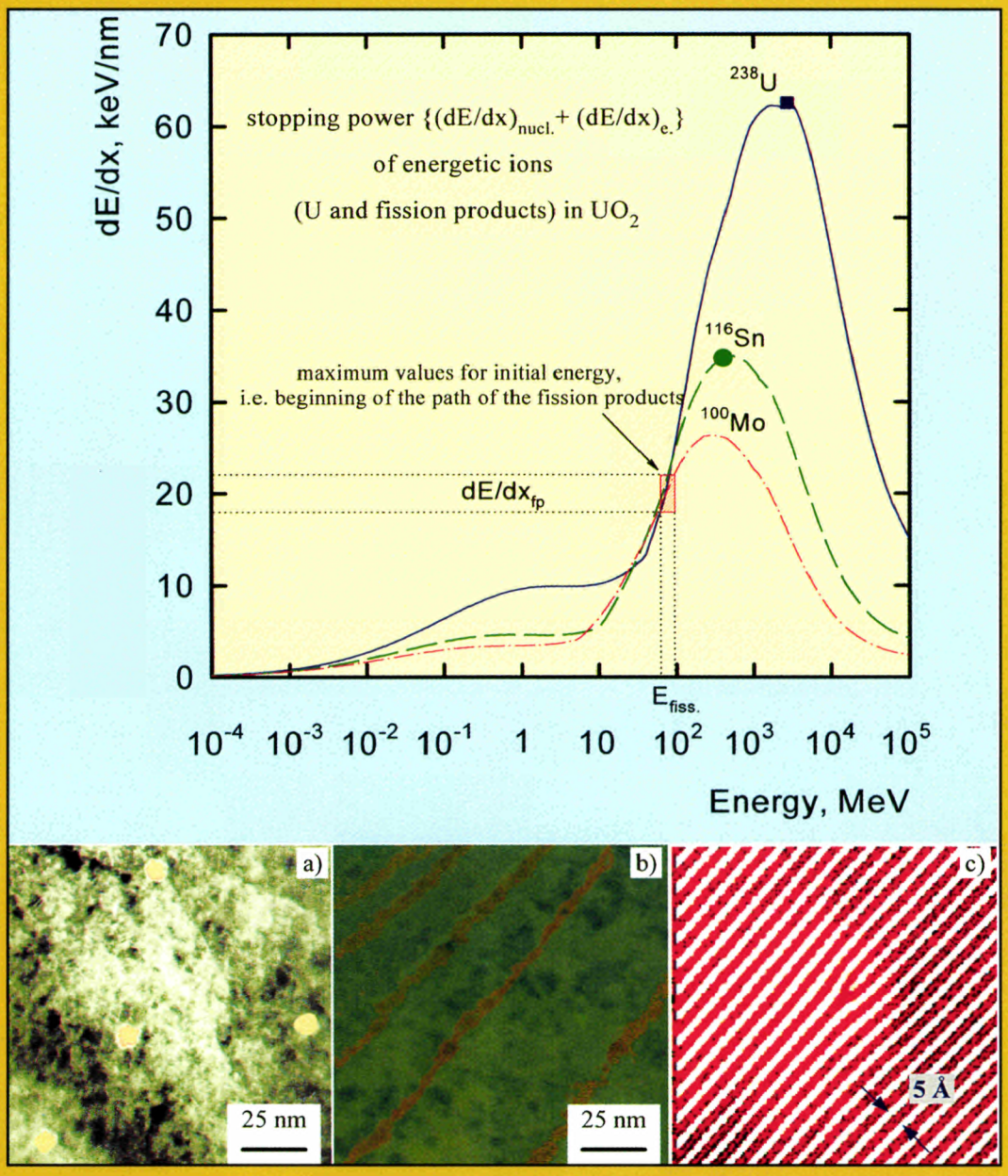

High resolution transmission electron microscopy showing a) tracks of 2.6 GeV U-ions near the surface (conventional TEM) b) tracks of 400 MeV Sn-ions in bulk UO_2 (new cross sectional technique) c) a dislocation line in UO_2 made clearly visible by a Fourier transformation. The three pictures are in false colours.

Review article

Limits and Prospects for High Burn-up LWR fuels

M. Coquerelle, J. Spino

1. Introduction

A first generation of power reactors has come of age during the last 30 years during which pioneers have explored many possible combinations of fuel, moderator and coolant. Today, apart from a few fast reactors and the gas-cooled reactors in U.K., all power reactors are (light or heavy) water-cooled and basically fuelled with UO_2. In addition, most of these reactors are water moderated, the only exception being the graphite moderated Russian RBMK's.

Some European power reactors will reach their 30 years operation limit in 5 to 10 years. Licensing extensions for a further 10 years operation are being considered to bridge the gap until a second generation of reactors is introduced. The new reactor types will only be fully developed if there is a further need for nuclear energy, if they are competitive and if they are accepted as safe enough.

At present, there is constant pressure to reduce fuel cycle costs. This can be achieved primarily by increasing the burn-up. In this way the fuel inventory, reprocessing, transport and storage costs are reduced. Furthermore, longer use of the fuel assemblies allow fewer refuellings and, consequently, less reactor operation costs. But such a strategy has its limits. From the analysis carried out at the Institute for Transuranium Elements (ITU) on fuel rods belonging to KWU-Siemens and from the results of a co-operation programme with Électricité de France (EDF) on fuel-clad chemical interaction (FCCI) and fuel-clad mechanical interaction (FCMI), limiting factors in the burn-up extension are the increase of the fission gas pressure inside the fuel rod, the marked outer corrosion of the zircaloy (Zry) cladding and the resulting hydrogen pick-up after prolonged irradiation time.

This report is focused on the thermal and mechanical behaviour of fuel irradiated up to burn-ups of 80 GWd/tM, with emphasis in those aspects which may limit the fuel rod life-time. The main topics to be treated will be fission gas release, its correlation to the fuel restructuring, the mechanical properties of the fuel and some aspects related to the FCMI and FCCI problems. Limiting factors concerned with the outer corrosion of the Zry cladding materials are not envisaged here. We start with a concise state of the art review of the power reactor fuel rod behaviour.

2. Current status of the fuel rod behaviour in power reactors.

Reliable, failure-free fuel rod operation continues to be the priority of all fuel vendors and users. According to the last ANS International Topical Meeting on LWR Fuel Performance held at Palm Beach in April 1994 [1], potential areas of optimisation can be foreseen in the fields of fuel design, extended burn-up operation, MOX fuel technology and cladding corrosion. The current state of development can be summarised as follows:

Fuel design improvements

The need to meet challenging performance goals, combined with competitive pressures among the fuel vendors, has brought about extensive fuel design modifications to improve the global core behaviour.

Nearly all fuel vendors designed new PWR and BWR debris filters to reduce the fraction of debris that can be transported to the active fuel region, thereby reducing the probability of fuel failures by fretting damage of the cladding.

New spacer grids represent the most significant design changes, and have been developed by Framatome, Siemens, ASEA Brown Boveri – Combustion Engineering, and Mitsubishi Atomic Power Industries. The major objective is to improve the thermal hydraulic performance of the spacers by changes in their mechanical configuration to provide a more efficient cooling of the fuel rods. Advanced zirconium alloys with improved cladding corrosion resistance [2], as discussed later, are also being used for other structural components.

Extended burn-up

There is a strong trend to extend the fuel burn-up targets in order to reduce the waste volume at the back-end of the fuel cycle. Minimising the number of fuel assemblies per unit energy generated is desirable whether the fuel is reprocessed or stored. Currently, batch average burn-up targets of about 45 GWd/tM are normal for PWRs, with maximum assembly average exposures of about 50 GWd/tM.

For PWRs, successful irradiation results of whole fuel assemblies were already reported up to average burn-ups of 45 GWd/tM (Russian VVER's) [3], 55 GWd/tM (Siemens, Westinghouse and Mitsubishi) [4,5], 57 GWd/tM (Babcock and Wilcox) [6] and 48 GWd/tM (Fragema) [7]. Also, successful pilot fuel rod exposures above 60 GWd/tM were reported independently by ABB Atom, Framatome and Siemens [8,7,4]. For BWRs, usual fuel assemblies exposures range between 35 and 40 GWd/tM batch average, with peak assembly expo-

sures slightly over 40 GWd/tM. Successful load irradiations of modern fuel assemblies were reported up to 49 GWd/tM (ABB) [8] and up to 53 GWd/tM (Kernkraftwerk Gundremmingen Betreibergesellschaft (KGB) and Siemens) [9,4].

Ramp testing of PWR fuels pre-irradiated to high burn-ups continues to confirm that the margin to the pellet cladding interaction (PCI) failure threshold is large. In this respect, ramp tests of fuel rods exposed to 42 GWd/tM (Japan Atomic Energy Research Institute) [10] and 62 GWd/tM (B&W Fuel Co.) [6] showed successful failure-free behaviour.

Concerning the effects of the burn-up dependent fuel thermal properties on fuel performance [11], measurements carried out on simulated fuels at Battelle and ITU [16,13] and on irradiated UO_2 in the High Burn up Chemistry Programme [14] showed that the largest impact is due to the degradation of the thermal conductivity with increasing burn-up, in particular, in the temperature range between 400 and 1000 °C.

At an average burn-up in the vicinity of about 50 GWd/tM [16] accelerated fission gas release occurs for BWR and PWR fuel. A narrow plutonium-rich zone appears at the pellet periphery (outer rim), developing a highly porous and fine grain size fuel structure. Fission gas is retained within this structure, probably as bubbles and pores, and it is not released unless the fuel is ramped. In addition, other microstructural changes occur in the central part of the fuel characterized by the formation of intergranular porosity. Between the periphery and the central zone a transition zone is formed with incipient outer rim microstructure whose extent increases with burn-up. These zones produce by thermally activated diffusion mechanisms a gradually increasing fission gas release rate as burn-up is accumulated (see point 6).

According to microstructural studies, at EDF and the Commissariat à l'Energie Atomique (CEA) [15], and at Siemens and ITU [16], carried out on commercial PWR fuels exposed to burn-ups greater than 60 GWd/tM, the inner region of the fuel constitutes the main source of gas release. The threshold amount is mainly determined by the local fuel temperature [15]. The 'outer rim' contributes less to the fission gas release. More important is its effect on the thermal gap conductance and by power 'edge-peaking' due to the plutonium fissioning near the pellet surface.

MOX fuel performance

New data continue to support the extensive "good performance" record of MOX fuel in PWRs and BWRs. No failures or degraded performance have been observed due to MOX. Preussen Elektra reported the irradiation of over 500 MOX assemblies in its PWRs with an assembly average burn-up of up to 40 GWd/tM [17]. EDF has irradiated a smaller number of assemblies in commercial PWRs and reported the examination of fuel rods with up to 43 GWd/tM [18]. In both cases, the irradiations occurred failure-free.

Successful ramp tests to a linear power as high as 480 W/cm were reported by Siemens with PWR rods pre-exposed to 48 GWd/tM [19]. Also, ramp tests by Japanese investigators were successful to 600 W/cm with BWR rods pre-irradiated in Dodewaard to 50 GWd/tM. The irradiation behaviour was found to be better than UO_2 [20].

Cladding corrosion and hydrogen pick-up

An increasing rate of the oxidation (and consequently of the hydrogen pick-up) observed in standard and modified Zircaloy-4 PWR cladding initiates between 30 and 40 GWd/tM and increases with burn-up. This sets a limit to the upper exposure of the material.This quantitative limit depends largely on the coolant temperature, heat flux and water chemistry. Aiming at extending this limit, alloy development programmes have been started and shown positive initial results.

The materials with the most extensive commercial application to date, combined with the best water corrosion resistance, are the Duplex clad of Siemens [2] and the ZIRLO alloy of Westinghouse. The Duplex, or Extra Low Sn (ELS), is a Zry-4 clad with a 100 µm outer layer of more corrosion resistant, low Sn-Fe-Cr alloy. The ZIRLO is a 1% Sn-1% Nb zirconium alloy. Duplex clad irradiation experience has exceeded 60 GWd/tM and ZIRLO has reached 46 GWd/tM in commercial plants and 60 GWd/tM in a test reactor, with oxidation rates significantly lower than standard or even modified Zry-4 alloys. Further oxidation data on zirconium alloys are expected in the next ANS meeting to be held in Portland, USA, in March 1997.

From the above, it can be concluded that UO_2 target burn-ups of 50 to 60 GWd/tM for PWRs can be considered as realistic and are already authorised in Germany and USA. Improvements, of course, will be necessary in order to guarantee a safe behaviour of these fuels, especially in the case of burnable poison (Gd, Er) utilisation, if long cycles (18-24 months) are requested. Further aspects to be considered are:

- The pellet-cladding interaction, when reactors are operated under load-following conditions.
- The behaviour under fast reactivity induced accidents (RIA): analysis of UO_2 fuel rods, ramped under these conditions in the CABRI reactor, using pins pre-irradiated in BR3 to 25 GWd/tM, is still under analysis in France.
- High burn-up MOX fuels may show higher fission gas release than UO_2 fuels due to their comparatively higher linear ratings [18].

3. Safety relevant factors for high burn-up fuel

The safe use or the life limitation of a fuel rod for a definite type of power reactor depends on the factors which can lead to rod failure. These factors are of different nature and can be summarised as follows:

3.1 In-reactor modifications of the Zry-cladding

Water-side corrosion inducing an outer ZrO_2 layer and an increase of the hydrogen content of the cladding are the main factors limiting the insertion time of the fuel rod. This leads to the build-up of a supplementary thermal barrier and a worsening of the mechanical properties of the cladding. A review of data up to 1994 has been described in the preceding chapter.

3.2 Consequences of the fuel behaviour with increasing burn-up

The following aspects have to be considered when fuel is irradiated under steady state conditions:

Fission gas release

This is an important feature for the thermal and mechanical design analysis of LWR fuel rods, especially at higher burn-ups. A high release leads to internal rod pressure built-up which could exceed the coolant pressure. Furthermore, increase of internal pressure can cause stresses on the cladding during storage of the spent fuels. To mitigate this pressure increase, it is important to understand the correlation between the fission gas release and the burn-up induced fuel restructuring.

Fuel-cladding mechanical interaction (FCMI)

Two contrary mechanisms lead to mechanical fuel cladding interaction, namely the cladding creepdown and the fuel swelling. The latter, in turn, leads to a stress reversal situation (cladding tensile stresses) at around 45 GWd/tM burn-up. From this point, the fuel swelling is the main factor contributing to radial and axial constraints on the cladding. At 70 GWd/tM obvious plastic deformations of the cladding can be measured at the pellet interface and the disappearance of the Cs-137 activity drop (γ-scanning) at this position indicates a complete dishing filling as a result of the axial fuel swelling. To compute this mechanical interaction (FCMI) in a realistic form, a reliable estimation of the fuel mechanical properties, in particular at the pellet periphery, is needed. A relatively plastic behaviour of the fuel and a good resistance to crack propagation, such as developed at high burnups (see point 8), can be considered as positive factors.

Fuel-cladding chemical interaction (FCCI)

Above a certain burn-up the formation of a fuel-cladding interaction compound, as an intermediate layer between the internally oxidised cladding and the fuel, has been reported. If the phases resulting from this process have good plastic properties and do not display worse thermal properties than the irradiated fuel, FCCI effects at high burn-ups are not detrimental to safe operation conditions.

From the above points, it is clear that the mechanical resistance of the cladding is the main factor determining the safe use of LWR fuel rods at burn-ups higher than those currently specified.

4. Characteristics and irradiation history of LWR fuel rods analysed at ITU

The operating fuel temperatures have to be considered also as an important parameter determining the fuel behaviour at high burn-ups. In order to reach higher burn-ups with complete reloads, higher fuel enrichments than those previously used are necessary. As a consequence, the fuel rods are operated at higher average power over a longer period of time and hence at higher fuel temperatures. As a result, higher fractional fission gas release than previously observed appear with increasing burn-ups. In this section, fission gas release measurements and their correlation with the fuel microstructural changes will be presented. In addition some aspects concerning the outer rim structure and its mechanical properties will be mentioned.

The fuel rods analysed under contract for KWU-Siemens were irradiated in a commercial PWR plant with a 15 x 15 fuel rod array. All fuel rods examined were pre-characterized before irradiation. Zirconium-base alloys were used as cladding material and the UO_2-fuel was produced by the AUC-process. Characteristic fuel rod data were:

Fuel rod length	= 3842 mm
Fuel rod diameter	= 10.75 mm
Fuel/clad diametrical gap	= 180 to 195 μm
He fill gas pressure	= 22.5 bar
Fuel density	= 10.40 g/cm^3
Fuel grain size (linear intercept)	= 7–10 μm
Initial enrichment (^{235}U)	= 3.8 / 4.2 w/o (and few rods with 3.5 w/o)

The fuel rods were operated for up to six consecutive cycles to maximum rod average burn-ups of 72 GWd/tM. In order to achieve such high burn-ups, a number of fuel rods were withdrawn from the fuel assemblies after reaching their target burn-ups, and reinserted into fresh assemblies for further irradiation. Such procedures achieve relatively high power levels at high burn-ups. Typical cycle average linear heat generation rates (LHGR) for the examined rods are given in Tab. 1.

Tab. 1 Typical irradiation data of the examined fuels.

Cycle	Cycle Average LHGR W/cm	Cumulative Average Burn-up GWd/tM
1	270-310	15.0-20.0
2	230-270	29.5-30.0
3	210-230	41.5-44.0
4	180-200	51.5-54.0
5	170-180	60.0-64.0
6	160-170	71.0-72.0

5. Experimental techniques

Standard fuel rod puncturing technique and mass spectrometric analysis were applied to determine the integral amount and composition of the fission gases released into the rod free volume.

Detailed analysis of the fission gas release behaviour centred on the fuel restructuring by optical and scanning electron microscopy on polished and fractured cross sections respectively. In order to quantify the radial distribution of fission gases, as well as to perform local burn-up determinations, radial profiles of Xe, Cs, Pu and Nd concentrations in the fuel pellet were obtained with a shielded electron microprobe analyzer (EMPA). The radial distributions of retained Xe in the UO_2 grains were determined by point analysis at intervals of 50 μm and 150 μm along the fuel radius. The point analyses were made away from the grain boundaries to avoid the interference produced by the gas contained in intergranular bubbles.

Scanning electron microscopy (SEM) was used to correlate the radial distribution of xenon to the fuel restructuring. In addition, porosity and pore density profiles, as well as grain size of the fuel at the pellet (outer rim), were determined by quantitative ceramography.

To assess the modifications of fuel mechanical properties as a function of burn-up at the fuel pellet periphery, the fuel-cladding interaction layer, the local Vickers hardness (H_V), and the fracture toughness parameter (K_{IC}) were determined. For this purpose, the microhardness device of a remote-controlled optical microscope was used. In addition, the chemical composition and the fracture appearance of the fuel-cladding interaction layer was characterized by EMPA and SEM respectively.

6. Fission gas release results

The results of the standard puncturing and mass spectrometric analysis are plotted in Fig. 1 in the form of fractional fission gas release as function of the rod average burn-up.

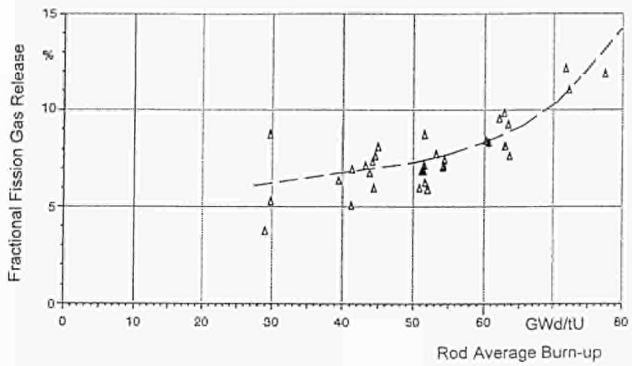

Fig.1 Fractional fission gas release of PWR fuel rods with enrichments of 3.5 w/o as a function of burn-up.

As can be seen, the fractional fission gas release values are around 5% at burn-ups of about 30 GWd/tM and increase linearly to about 7% at 50 GWd/tM. Above that burn-up, the fractional release increases more steeply to about 12 a/o burn-ups of 72 to 75 GWd/tM, in spite of the decreased rod power. Although the decreasing thermal conductivity of the fuel tends to keep the fuel temperatures up, there is a general tendency of decreasing fuel temperatures with increasing burn-up. Therefore, the increasing fractional fission gas release with burn-up might be attributed also to other effects than those of strictly thermal nature.

An electron probe microanalysis has been performed to determine the radial concentrations of retained xenon within the individual UO_2 grains on fuel cross sections. Three different burn-up levels of about 50 GWd/tM, 70 GWd/tM and 83 GWd/tM have been examined. The radial concentration profiles measured are compared to the theoretically-calculated concentrations of xenon generated (Fig. 2).

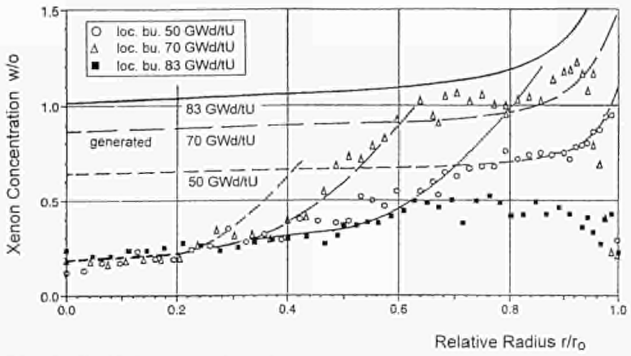

Fig. 2 Radial xenon distribution in PWR fuel pellets as a function of relative radius from EMPA measurements.

At all three burn-up levels, an equally low xenon concentration of about 0. 2 w/o exists in the centre region of the pellets. With increasing relative radius (r/r_0) the amount of xenon retained within the grains increases. This increase occurs not as a continuous function of r/r_0, but in several steps with different slopes. These steps are associated with consecutive steps in the power history, for instance due to reshuffling. They mark regions of the fuel with different levels of fission gas release at certain time intervals of operation.

The results of the EMPA are supplemented by optical ceramography. Etching across a section revealed various dark rings in the optical microscopy. Detailed examinations have shown that these rings contain a large number of fission gas bubbles precipitated within the grains.

At a relative radius r/r_0 of about 0.8 and up to a burn-up of 70 GWd/tM xenon concentrations within the grains are measured by electron probe microanalysis (EMPA) that correspond to the theoretical values. At the burn-up of 83 GWd/tM the xenon concentration deviates everywhere from the amount of xenon theoretically calculated.

At the pellet periphery (pellet rim), moving towards the fuel cladding the xenon concentration decreases continuously at all three burn-up levels analysed. The decrease in xenon concentration was first observed at a pellet burn-up of about 45 GWd/tM. This threshold value is a function of the initial U-235 enrichment and

corresponds to a local burn-up at the pellet rim of about 60 GWd/tM.

At pellet burn-ups exceeding 45 GWd/tM basically three different restructured fuel regions have been observed :

- A central zone being characterized by grain growth, and the formation of intergranular porosity with a high degree of coalescence (formation of channels)
- A transition zone exhibiting a heterogeneous structure. The smaller grains show grain subdivision and a structure of the same type as found at the outer rim ("cauliflower structure"). Subdivision is not noticed in the larger grains. These show the usual transgranular fracture mode. Grain boundaries appear partially to be decorated with the „cauliflower structure". The heterogeneity in the fuel structure is also reflected in the results of the SEM analysis shown in Fig. 3 on page 134.

  At a pellet burn-up of 70 GWd/tM, a coexistence of original grains, containing the theoretical concentration of xenon and subdivided grains, whose xenon content is only about half the theoretical value, has been found. The restructuring of this transition zone progresses with increasing burn-up at the expense of the original microstructure.
- The outer rim zone characterized by the "cauliflower structure" – subdivided equiaxed grains of $0.1 < \varnothing < 1\mu m$ with intergranular fracture mode and faceted bubbles of micron to submicron size (0.5 to 2 μm) precipitated most likely on the new grain boundaries. Porosity measurements in this zone yield values of 15 to 17%.

  The correlation between fission gas retained in the fuel and the corresponding fuel restructuring leads to the conclusion that the thermally activated release mechanisms give the essential contribution to the overall fission gas release. This has been proven by fission gas release calculations based on the EMPA results. In general, EMPA over-predicts fission gas release because the analysis does not take into account fission gases accumulated on grain boundaries and in bubbles. However, based on fuel microstructural observations it is possible to at least qualitatively take that into account.

  The equilibrium xenon concentration in the centre region of the pellets up to a relative radius r/r_0 of ~ 0.4 is an indication of an open channel system and ceramography shows very few separate fission gas bubbles on grain boundaries. Hence, most of the fission gases released from the grains must have also been released into the rod free volume. At a burn-up of 50 GWd/tM the release from that region accounts for about 90% of the total release. At higher burn-ups the fraction of gas release from the centre region (r/r_0 up to 0.4) to the total release decreases progressively to about 70% at a burn-up of 83 GWd/tM and the fraction from the intermediate pellet zones of the total release increases. Since these intermediate pellet zones are operated at lower fuel temperature most of the fission gases released from the grains accumulate on grain boundaries or in bubbles in case of restructuring. Without such retention on grain boundaries and in bubbles, EMPA results would yield overall fission gas releases up to twice as high as measured by puncturing.

  The xenon depletion of the UO_2-matrix at the pellet periphery operated at temperatures below 500 °C is a result of restructuring in this zone. The restructuring is an athermal process directly related to the accumulation of radiation damage. The released xenon is most probably contained in the large number of bubbles there.

  Fuel micro-coring had already indicated that the xenon released from the UO_2-matrix is still confined to the porous rim structure. EMPA has confirmed a high xenon concentration in micro-bubbles just below the specimen surface. Also from X-ray fluorescence measurements it has been concluded that a significant fraction of the xenon produced was retained in that zone.

  At a pellet average burn-up of 83 GWd/tM the outer rim structure and the transition zones extend from the pellet rim to a relative radius of about 0.65 (transition zone), and hence into a region, where thermally activated processes begin to operate. Release may start from that area ($1 > r/r_0 > 0.65$) of high bubble concentration by a re-solution and bubble fragmentation mechanism. It can be anticipated that such a mechanism may finally lead to a fission gas release from that region into the free volume of the rod, although, this may be insignificant at the burn-ups reached so far.

Further results, obtained from filling gas analysis, display a Kr enrichment and a Xe depletion [21]. This result which implies a larger mobility of Kr than Xe, or otherwise a larger effective diffusion coefficient for Kr (including atomic diffusion, defect trapping, bubble precipitation and resolution effects [22,23]), contrasts with the traditional results of low burn-up fuels where no differentiation in the release of both species was noticed [23,24].

Concerning the integral gas release, the acceleration of this process as the burn-up increases and the fuel temperature decreases bring into question the validity of the applicable diffusion coefficients at higher fission product concentrations. It is interesting to remark that, contrary to the observations, the single atom diffusion coefficients in a matrix with increasing damage concentration (burn-up) should decrease, due to the increased trapping probability in lattice defects [23,25].

7. Microstructural characterisation of the 'outer rim' zone

In a previous paper [26], the porosity and other relevant microstructure features of the rim and adjacent zones of commercial PWR-UO_2 fuels with average burn-ups between 40 and 67 GWd/tM have been determined as function of the radial position and the average burn-up.

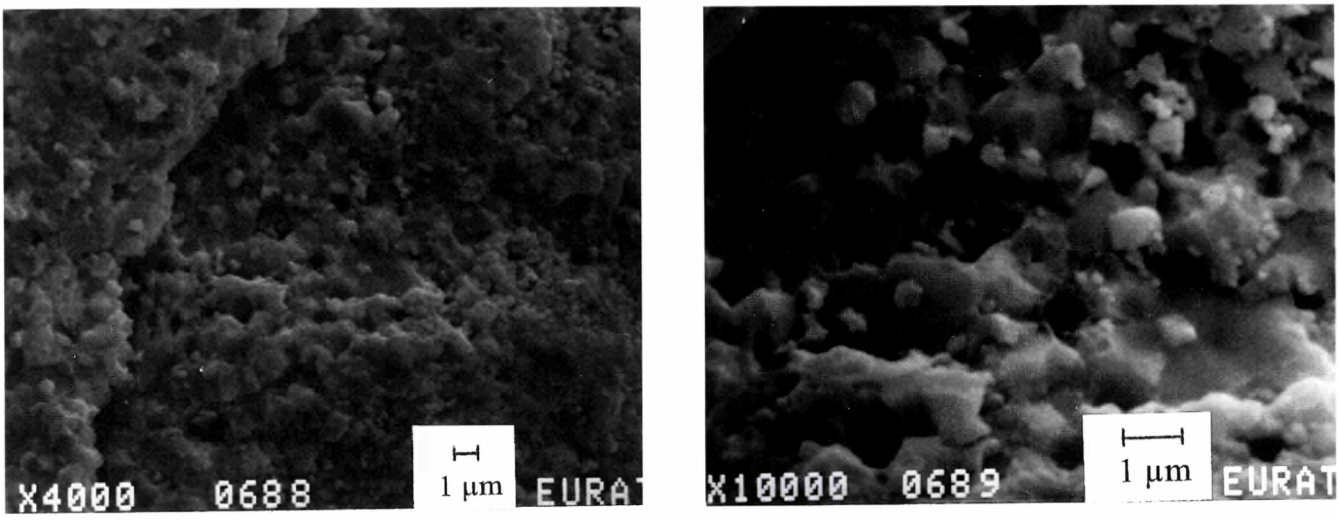

pellet rim $r/r_o = 0.97$

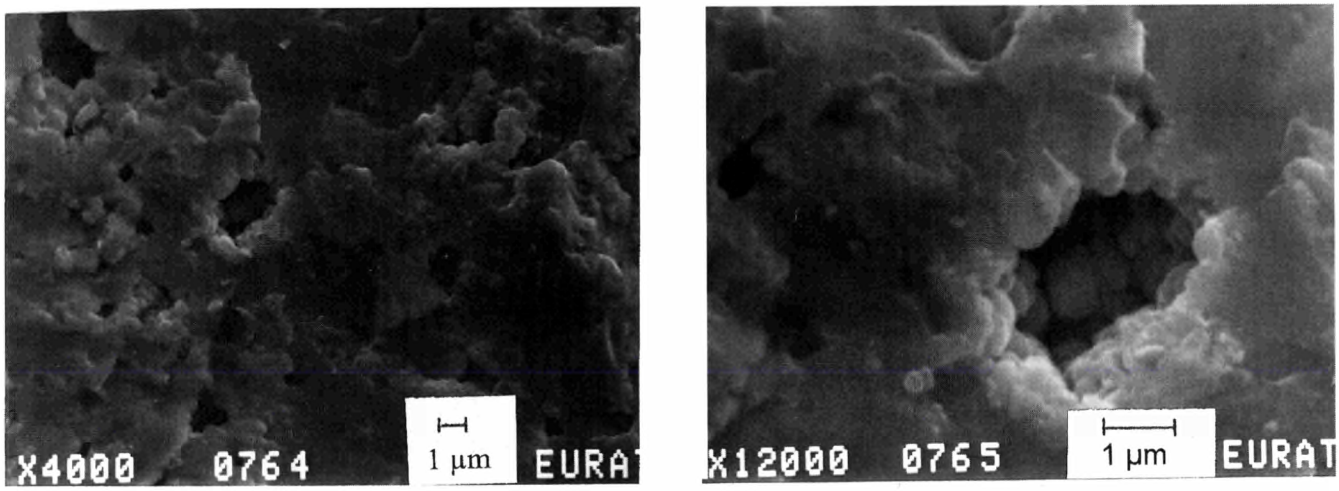

transition zone $r/r_o = 0.63$

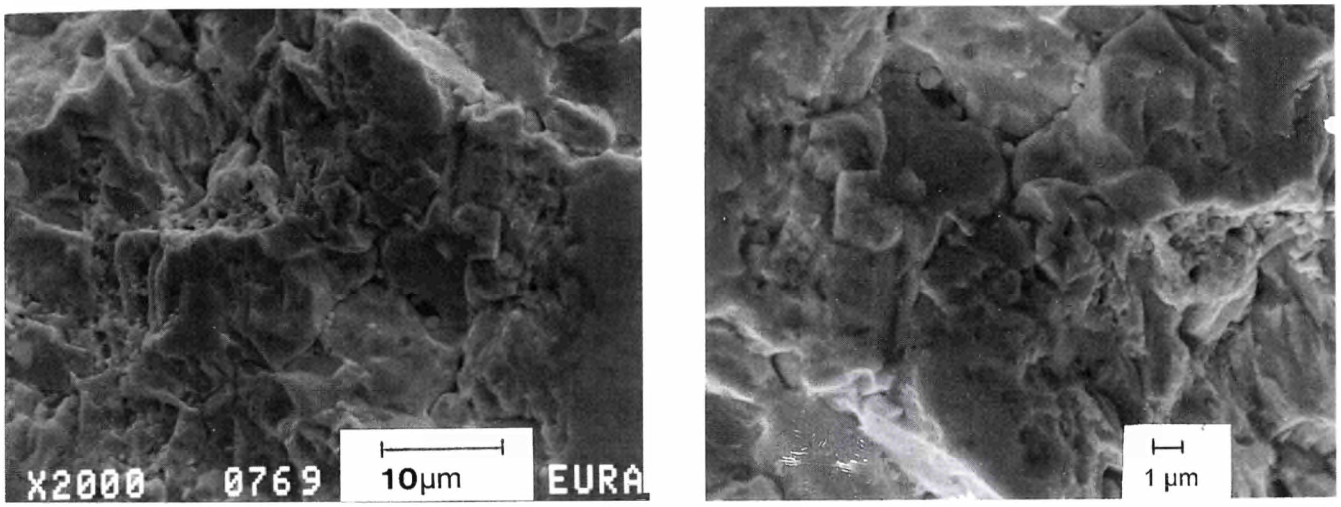

central zone $r/r_o = 0.04$

Fig. 3 Characteristic SEM fuel microstructure of a PWR fuel pellet with an average burn up of 83 GWd/tM

This work showed that at the pellet periphery, within a region of a few tens to several hundreds of microns (increasing with burn-up), an exponential growth of the fuel porosity and the pore density takes place. This results in 3 to 4 times larger porosities at the pellet edge, and typically one order of magnitude larger pore densities, compared to the values observed at the onset of the rim zone (Fig. 4 on page 135).

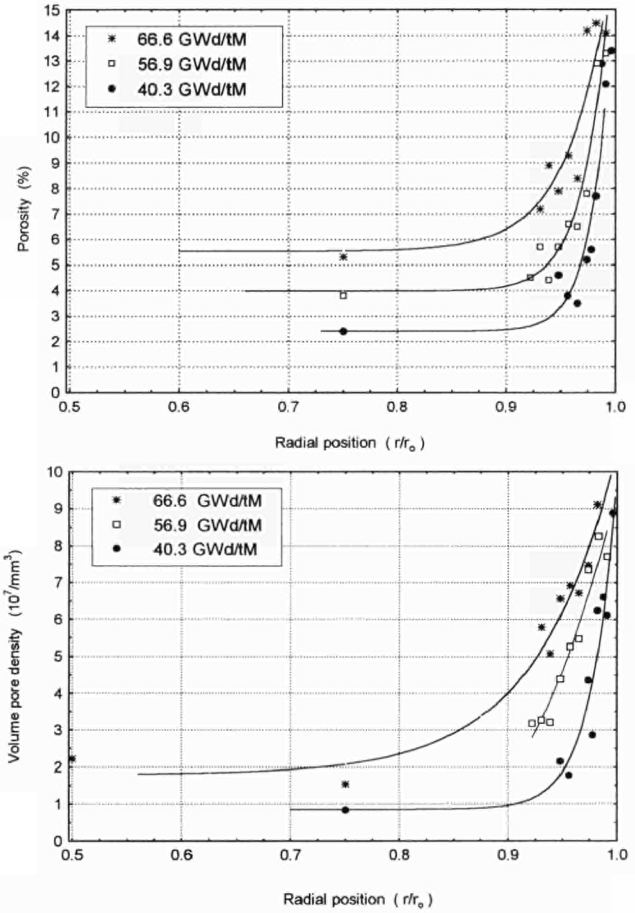

Fig. 4 Variation of the fuel porosity and pore density with the radial position and burn-up.

Accompanying this porosity and pore density increase, a grain subdivision process is also verified in the rim zone, and leads to a typical 'submicron' grain structure after irradiation, in contrast to the relatively large grain size of the as-fabricated material (7-10 μm) (Fig. 5).

A characteristic of this 'in-reactor' grain subdivision is that it appears as a homogeneous structure only in a narrow band of material near the pellet edge. Moving to the centre of the fuel a transition zone is formed, with a mixture of unrestructured and restructured matrix areas, the concentration of these decreasing gradually towards the pellet centre. In the same direction, the location of the restructured areas is observed first indistinctly at intragranular and intergranular positions, and then unambiguously at the grain boundaries of the original fuel matrix [26] (Fig. 5). Inside the restructured areas, a clear localisation of the grain subdivision around pores is observed [26] (Fig. 6 on page 136).

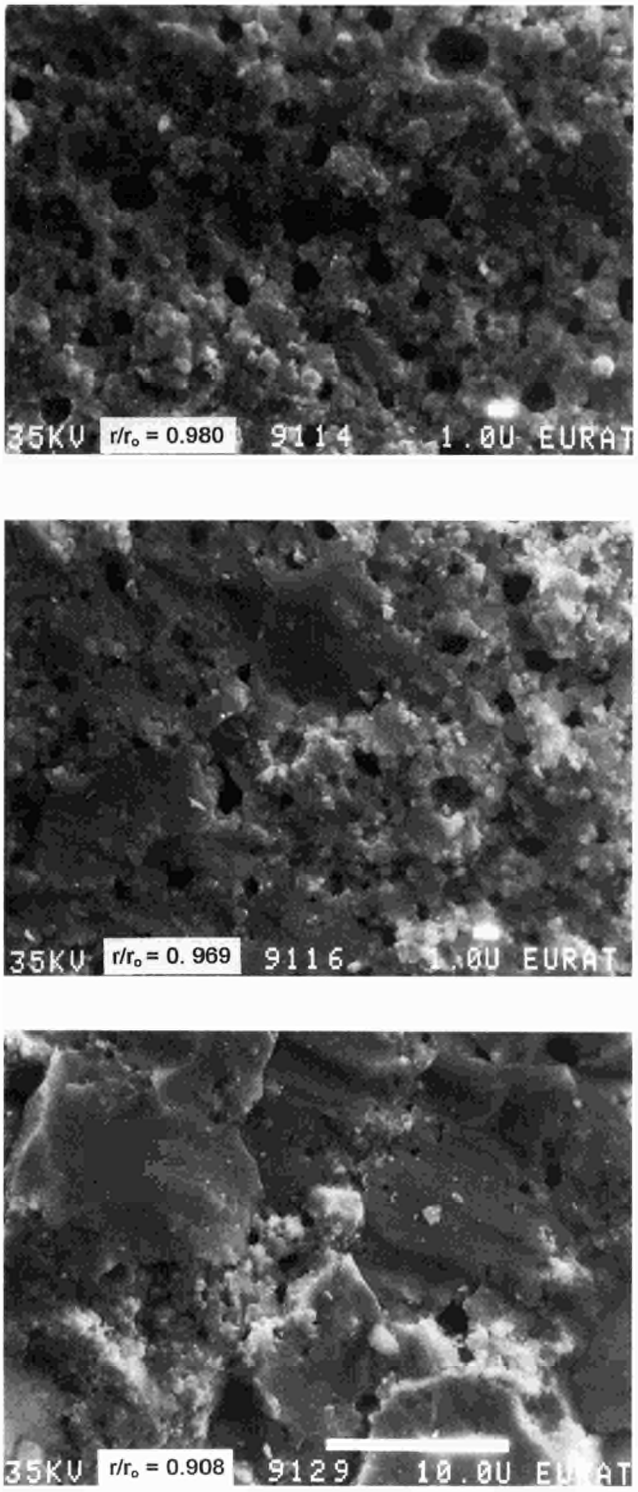

Fig. 5 Microstructural changes along the pellet radius of a PWR fuel with an average burn-up of 67 GWd/tM

8. Fuel mechanical properties as determined by microindentation

Tests and parameters description

Using a remotly-controlled microscope, room temperature determinations of the microhardness (H_V) and the fracture toughness (K_{IC}) variations with the radial position and burn-up were performed via Vickers microindentations at small loads (20-100 g). Details of the technique are described elsewhere [27]. For all samples studied, measurements were done on four orthogonal radii at intervals of 50 μm, with a minimum distance between imprints of at least 3 diagonal lengths. The results described below correspond thus to the statistical average of four independent measurements, the error bands being placed with a confidence level of 95%.

The hardness values given were calculated with the expression

$H_V = 1854.4\ P/d\ (kg/mm^2)$

and the fracture toughness via the relationship

$K_{IC} = 0.057 \cdot H_V \cdot a^{1/2} \cdot (E/H_V)^{0.4} \cdot (c/a)^{-3/2}\ (MPa.m^{1/2})$,

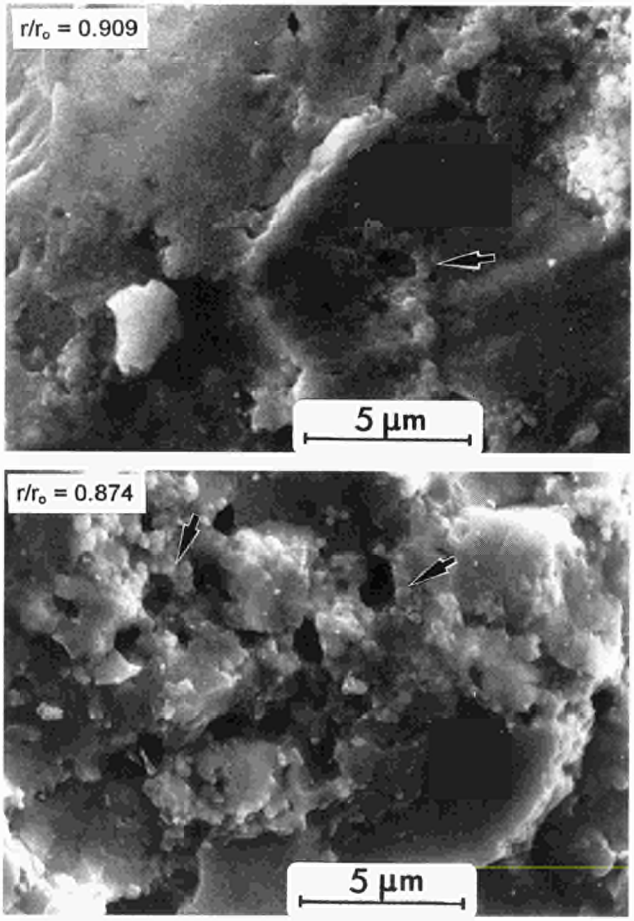

Fig. 6 Grain subdivision around pores at different radial positions. Top: Intragranular pore. Bottom: Intergranular pores (average pellet burn-up: 67 GWd/tM)

where

P(g) is the indentation load, d (µm) the print diagonal length, E (MPa) the Young modulus, a (m) the half-print diagonal length, and c (m) the crack length measured from the imprint centre [7]. For the values of the Young modulus a correction due to the local porosity p (%) variation was used.
E (MPa) = $2.2 \cdot 10^5 - (5.1 \cdot 10^3) \cdot p$ (%) [27].

Microindentation results

Microhardness

A characteristic observation for all fuels studied is that the hardness remains relatively constant along most of the pellet radius, except at the periphery region showing the rim structure, where a reduction of up to 30% towards the pellet edge is usually measured, independent of the indentation load applied and the average burn-up examined (Fig. 7).

It can be seen that, for any sample, the hardness and the local porosity profiles coincide spatially rather well (Fig. 4 vs. Fig. 7). With respect to the constant part of the curves at the fuel centre and intermediate regions ('plateaus' in Fig. 7), a monotonic increase of the hardness level is observed as the burn-up increases, provided that the indentation load is maintained the same.

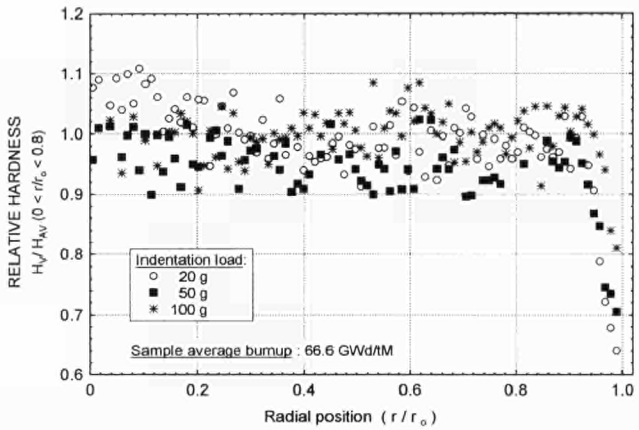

Fig. 7 Variation of the fuel hardness with the radial position at different loads. (H_V-data normalised with respect to the average values in the range $0<r/r_o<0.8$)

Crack length and fracture toughness

Similarly to the previously shown hardness profiles (Fig. 7), the average length of the cracks produced by the indentation remain relatively constant along most of the pellet radius ($r/r_o \pm 0.8$), and then starts to decrease on approaching the outer parts of the fuel (Fig. 8).

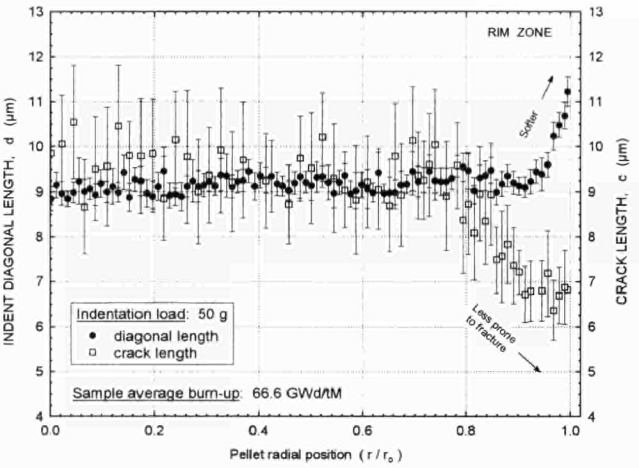

Fig. 8 Variation of the Vickers diagonal lengths and crack lengths along the pellet radius at constant indentation load (average pellet burn-up : 67 GWd/tM)

This indicates obviously a smaller propensity to crack propagation of the outer fuel regions, which in combination with the diagonal length increase (hardness decrease), results in a clear improvement of the fracture toughness of the rim zone (Fig. 8).

In contrast to the hardness values, the derived K_{IC} values were rather independent of the indentation load used, allowing direct comparison of the results without any normalisation. Fig. 9 shows the derived fracture toughness (K_{IC}) profiles for three of the fuels tested, at the indentation load of 50 g.

As is evident from the plots, a toughening effect can be associated with the rim zone, whose width of influence clearly increases with the average burn-up (Fig. 9).

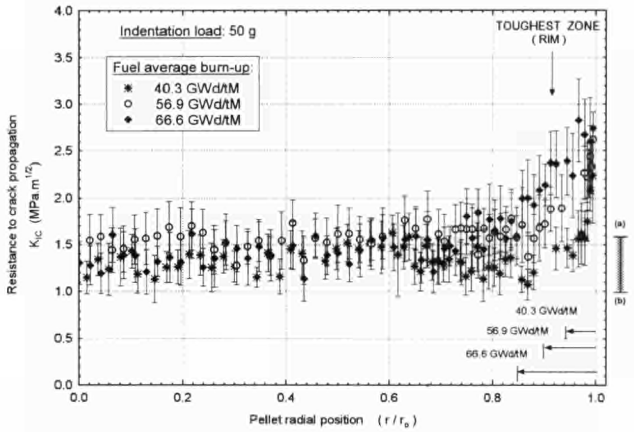

Fig. 9 Radial variation of the fuel fracture toughness (K_{IC}) at different average burn-ups. The bar on the right side indicates the differences in the K_{IC} values for unirradiated UO_2 as determined in this work (a) (low loads) and as given in the literature (b) (high loads).

Also in Fig. 9 the range of K_{IC} values for unirradiated UO_2 is given, according to measurements by other authors at higher loads [8] and the control measurements performed in our case under the same conditions as for the irradiated fuels.

The higher K_{IC} value derived in our case is due to the abundant lateral crack formation. Within the scatter of both measured and reference results, the plots of Fig. 9 show primarily that the fracture toughness of the central parts of the irradiated fuels roughly is comparable to the range of values for unirradiated UO_2, while the fracture toughness of the rim zone can be twice as large.

9. Characteristics of the fuel-cladding interaction phase

As mentioned already in section 3, when solid pellet-cladding contact is established in PWR fuels after a certain (high) burn-up, the formation of a fuel-cladding interaction layer is usually found in the post-irradiation examinations, as an intermediate phase between the internally oxidised cladding and the fuel (rim). The formation of this layer is not always uniform; it presents often an irregular thickness (of maximum 10-15 μm), being sometimes discontinuous, and sporadically shows the presence of large voids (several μm in diameter) (Fig. 10). The composition, can be basically described as a mixed Zr-U (Pu)-oxide, containing up to 3-4 w/o Cs according to EMPA results [29].

Despite this low dopant content (evaporation of Cs during EMPA measurements not excluded), the mechanical response of this phase seems to depart largely from that of the usually hard and brittle Zr-U-oxides. This is due to the filling of thin cracks and fuel interstices (for instance pellet-pellet interfaces) (Fig. 11). In addition the microindentation test at room temperature reveals that this phase is significantly softer than its neighbour (ZrO_2 and outer rim) phases (Tab. 2).

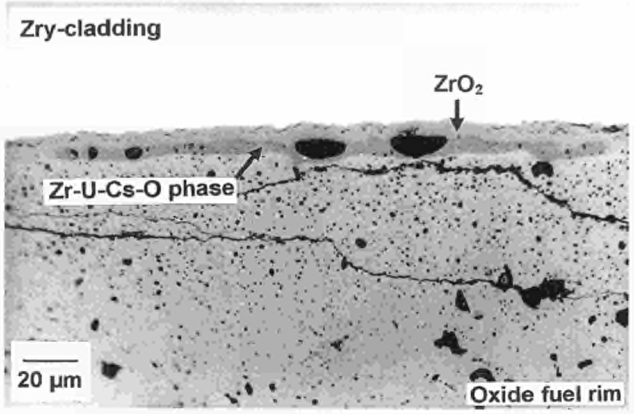

Fig. 10 Fuel-cladding interaction layer in high burn-up PWR fuel (pellet middle position), (average pellet burn-up : 45.7 GWd/tM)

Fig. 11 Fuel-cladding interaction layer in high burn up PWR fuel at the pellet-pellet interface (average pellet burn up: 51.2 GWd/tM)

Tab. 2 Typical microhardness values of fuel-cladding gap phases in high burn up LWR fuels.

ZrO_2 at the inner clad face	Fuel-clad interaction layer	Oxide fuel (rim) ($0<r/r_0<0.8$)
H_v = 1200-1300 Kg/mm^2	H_v = 450-500 Kg/mm^2	H_v = 800-1000 Kg/mm^2

In agreement with the above description for PWR fuels, a similar type of 'bonding' layer has been reported for high burn-up BWR fuels, described as a mixture of cubic (stabilised) U-Zr-O and a second 'amorphous' phase not yet completely identified [30]. It is therefore highly probable that the formation of this *a priori* softer phase at high burn-ups will be responsible for the better PCI behaviour of the LWR fuels after several irradiation cycles. The determination of the high temperature mechanical properties of this interaction phase remains therefore an important open question, especially with regard to the verification of its hypothetical 'softening' point.

10. Assessment and prospects concerning the behaviour of UO_2 irradiated at high burn-up

The analysis of the properties, described above, that may influence the mechanical integrity of the cladding, leads to the following conclusions concerning the fuel behaviour at extended burn-ups:

- The fuel at the periphery (outer rim) presents higher crack resistance and plasticity in the zone directly in contact with the cladding than in other parts of the fuel. From this point of view the 'outer rim' cannot be considered as detrimental at least when irradiated under steady state conditions.

  In-pile transient irradiations generally resulted in a better behaviour than that found with low burn-up fuels. This can be explained by considering two reasons, namely the elimination of heterogeneous local stresses on the cladding due to the uniform closure of the fuel-cladding gap, and the improvement of the fuel plasticity at the periphery as burn-up increases.

  Furthermore, under transient conditions simulated in hot cells by annealing tests, burst release was found to occur during the temperature rise, ceasing thereafter when the annealing temperature is stable and does not exceed 1500 °C. The situation is here more worrying if the temperature rise reaches the level of 1700 °C. In this case, not only the burst is quantitatively more important, but the release goes on when holding the fuel at this temperature.

- The analysis of the filling gas of fuel rods irradiated under realistic conditions indicate an acceleration of the fission gas release as burn-up increases, under conditions where the fuel temperature decreases continuously. The acceleration of the fission gas release as burn-up increases can constitute a possible limitation factor should UO_2 be irradiated for longer periods of time.

- The fact that the internal rod pressure in PWRs cannot exceed the external coolant pressure and the need for a safer utilization of the fuel requires a reduction of the gas release rate. This could be achieved by operating fuels at lower temperature or by a design modification to increase the free volume (e.g. by increasing the plenum volume).

  Possible solutions in this direction, most of them assuming the 'thermally activated' diffusion as the predominant release mechanism, could be the use of:

  - Large grains to increase the diffusion path. This solution is currently under study, the burn-up limit at which this positive effect is annulled is not known. It has the drawback that by enlarging the grain size the plasticity of the fuel worsens. This requires more detailed investigation.
  - Dispersed fuels in a matrix to impede the gas diffusion.
  - Annular pellets to decrease the operation temperature.
  - Fuel as 'coated' particles within which the fission gases are retained.
  - Fuel or matrix with a higher thermal conductivity.

A prerequisite for these studies is of course a justification for the burn-up extension, under the basic assumption that an adequate cladding material is available. Recent studies [31] based on the cycle economics seem to anticipate no further advantage beyond burn-ups of 80 GWd/tM. Such studies, of course, cannot quantify gains in safety aspects.

For the fission gas release, assuming the thermally activated diffusion as the determining release mechanism, possible mitigating solutions can be considered. Decreasing the impact of diffusion can be achieved by decreasing the fuel temperature, or the use of fuels with lower diffusion coefficient. Of course, a further possible solution is a design modification of the fuel rod by increasing the plenum volume, but this possibility is strongly limited.

We suggest that all the following proposals should lead to a lower impact of the diffusion mechanism:

1. Decrease of the fuel temperature by using highly enriched UO_2 particles diluted in a matrix with a

better thermal conductivity (e.g. Zr or Zry). The drawback is of course the fabrication and the absence of Pu build-up. Irradiations are necessary to demonstrate the efficiency of the gas retention. This solution can also be applied to MOX fuel. Tentative irrradiations made by the CEA showed a strong increase of fission gas retention by using a cermet of the type UO_2-Mo due to the low irradiation temperature (2% release). [32]. Russian scientists have investigated systems such as Al-U_3Si_2, UO_2-Zr, UO_2-Al, U_3(Si-Zr) and U_3(Si-Al), UO_2-silumin [33,34,35] and UO_2-Mg. A more sophisticated design is the use of coated UO_2 particles offering an additional barrier and dispersed in a Zr or Zry matrix.

2. Another approach is to use fuels either as alloys or ceramics with a better thermal conductivity than UO_2. In this category, one can mention the silicides (U_3Si_2) and the nitrides (UN) which can be irradiated as ceramics or alloys (UN-ZrN, U_3Si-Al, U_3Si-Zr). The problems associated with these solutions are the fabrication, the compatibility with the matrix and coolant and the behaviour under transient condition (off-normal, accident conditions). In the particular case of nitrides some attention has to be paid to the neutronic properties of nitrogen.

3. The diffusion can progress slowly under similar fuel temperatures when the diffusion path increases by using sintered UO_2 with large grain size ($\varnothing \geq 40$ μm). Various types of large grain undoped UO_2 [7], UO_2 doped with metal oxides ((Nb_2O_5, TiO_2, Cr_2O_3, La_2O_3 [36,37,38]) or with Al and Ti-silicates [36] have been tested in-pile.

   The results are inconclusive because high burn-up levels have not been reached and it is necessary to check the burn-up at which the cancellation of the positive effects due to large grains occurs. Another aspect to be considered is the need to counteract the poor creep and PCI behaviour due to large grain size. Current results suggest the use of silicates doping for improving grain boundary sliding. In this field more information have to be gained by further irradiations.

4. A further possibility to mitigate the impact of the fission gas release is to envisage a design based on the use of annular pellets. Such a design results in a reduction of the fuel centre temperature and an increase of the fuel rod free volume. These aspects contribute to a safer performance of the fuel rod. Nevertheless, the possible loss of fuel pellet segments is generally considered as detrimental.

References

[1] Proceedings of the ANS Topical Meeting on Light Water Reactor Fuel Performance,West Palm Beach, Florida, April 17-21, (1994)
[2] L.F. van Swam, F. Garzarelli, E. Steinberg; id. [1], 303
[3] Y.K. Bibilasvily, K. P. Dubrovin, A. A. Enin, V.G. Hadeev, P.I. Lavrenryuk, V.A. Tsibulya, J.N. Vasilschenko; id. [1], 360
[4] J.N. Morgan, R. Holzer, W.D. Krebs; id. [1], 55
[5] S. Suzuki, K. Murakami, T. Takahashi; id. [1], 352
[6] D.A. Wesley, K. Mori, S. Inoue; id. [1], 343
[7] M. Morel, P. Melin, A. Dumont; id. [1], 15
[8] G. Vesterlund, L.V. Corsetti; id. [1], 62
[9] R.W. Seepolt; id. [1], 96
[10] K. Yanagisawa, S. Katanishi, T. Fujishiro; id. [1], 248
[11] D.D. Lanning, C.E. Beyer, M.E. Cunningham; id. [1], 229
[12] Hj. Matzke, P.G. Lucuta, R.A. Verral, J.P. Hiernaut; 22nd Int. Conf. on Thermal Conductivity, 7-10 Nov. 1993, Tempe. AZ. Proc. Thermal Conductivity 22, ed. T. Toup (1994) 904
[13] P.G. Lucuta, Hj. Matzke, H.A. Tasman; J. Nucl. Mater. **188** (1992) 198
[14] S. Shibab; Belgonucléaire High Burnup Chemistry, Topical Report HBC 91/34 (1991) and private communication
[15] J.P. Piron, B. Bordin, G. Geoffroy, C. Maunier, D. Baron; id. [1], 321
[16] R. Manzel, M. Coquerelle, M.R. Billaux; id. [1], 335
[17] K. Baur, R. Lisdat, H. Puschel; id. [1], 22
[18] P. Blanpain, X. Thibault, M. Trotabas; id. [1], 718
[19] J.N. Morgan, W.-D. Krebs; id. [1], 712
[20] K. Ashai (NNFD), T. Matsumoto (Toshiba), M. Oguma (Hitachi), T. Toyaba; id. [1], 726
[21] M. Coquerelle; to be published (1997)
[22] D.R. Olander; Fundamental aspects on nuclear reactor fuel elements, TID-26711-P1, 1976
[23] Hj. Matzke; Rad. Effects **53** (1980) 219-242
[24] C.A. Friskney; J.A. Turnbull; J. Nucl. Mater. **79** (1979) 184-198
[25] J.R. MacEwan, W.H. Stevens; J. Nucl. Mater. **11** (1969) 77
[26] J. Spino, K. Vennix, M. Coquerelle; J. Nucl. Mater., **231** (1996) 179-190
[27] J. Spino, M. Coquerelle, D. Baron; IAEA Tech. Committee Meeting on Advances in Pellet Technology for Improved Performance at High Burn ups, Tokyo, Japan, 28 Oct.-1 Nov. 1996
[28] T.R.G. Kutty, A.K. Sengupta, C. Ganguly; European Appl. Res. Rept.-Nucl. Sci. Technol., (Hj. Matzke, E. Toscano, Eds), Hardwood Academic Publishers, 1990, p. 1473
[29] EUR 16152 EN, (TUAR-1994), p. 112
[30] K. Nogita, K. Une; IAEA Tech. Committee Meeting on Advances in Pellet Technology for Improved Performance at High Burn ups, Tokyo, Japan, 28.Oct.-1.Nov. 1996
[31] Rycroft; Proceedings of an ENS Topical Meeting, Brussels, 4-6 June 1996, 134
[32] Ph. Dehaudt, s. Mocellin, G. Eminet, L. Caillot, G. Delette, M. Bauer, I. Viallard; IAEA. Technical Committee meeting on Research of Fuel aimed at Low Fission Gas Release, Moscow, Russia, 1-4 Oct. 1996.
[33] A.V. Vatulin, Yu.A. Stetsky, V.B. Suprun, G.I. Khotyaskov; id. [32]
[34] V.V. Popov, A.D. Karpin, I.A. Isupov, V.N. Rumyantrev, V.M. Troyanov, V.N. Sugonyaev, N.A. Melnichenko, I. Scheinker; id. [32]
[36] T. Kuba; id. [1], [32]
[35] L.I. Moseev, A.N. Ryzkkov, B.S. Kirionov, S.I. Porollo; id. [1], 650
[37] J.C. Killeen; J. Nucl. Mater. **58** (1975) 39
[38] J.C. Killeen; J. Nucl. Mater. **88** (1980) 177

A. Institutional Research in Fuel Cycle Safety

1. Basic Actinide Research

Introduction

The central objective of actinide research in ITU and in its numerous collaborations is the elucidation of the electronic structure of actinide metals and actinide compounds, in particular of the behaviour of the 5f electrons. The dualism between localized and itinerant characteristics as it is particularly clearly demonstrated in the actinide series, is a key problem in these studies.

These goals are approached by experiment and theory. Experimental studies are either selective investigations on the basis of theoretical or other experimental information which indicates that a particular material and method are promising, or they can involve a systematic approach to a whole class of compounds. Theoretical calculations can indicate to the experimentalist where he can expect to find important results, and theory can on the other hand try to combine experimental evidence from different sources into a general picture. An important basis for the experimental study is the preparation of polycrystalline and single crystal samples of actinides of high specific activity, and their careful characterization by X-ray diffraction, chemical, and electron microprobe analysis. As far as possible, study of physical properties concentrates on the most interesting of the available actinide compounds, and an attempt is made to study them by several different methods to obtain a maximum of information on their physical behaviour. Many of the experimental investigations take place at the special facilities in the Institute, but we also make use of unique large facilities, such as neutron, X-ray synchrotron, and muon sources, in other locations.

As a side line to the above research area, the work related to radioimmunotherapy entered into a decisive phase: pre-clinical and first clinical evaluations took place in the Memorial Sloan-Kettering Cancer Center in New York.

1.1 Samples Preparation and Characterization

During 1996, few really new families of compounds were investigated. Instead, efforts were concentrated on the growth of single crystals of previously reported systems, the understanding of the appearance and stability of given phases, the study of $Pu_{1-x}Am_x$ solid solutions, and the encapsulation for physical studies in house or for external organizations.

1.1.1 Preparation and single crystal growth

In 1994 and 1995, many requests for single crystals of the U_2T_2X family of compounds (where T is a transition metal and X a metalloid, e.g. Sn, In) were expressed by our collaborators. We continued our efforts to provide suitable size crystals by the mineralization growth technique and particularly on U_2T_2In compounds. Success was obtained for U_2Pd_2In, U_2Pt_2In and U_2Ni_2In. Crystals obtained were characterized by Laue and single crystal X-ray diffraction and sent to other groups. Determination of optimal single crystal growth conditions on these systems are now established, and further attempts on transuranium systems may be envisaged.

On the other hand, single crystals of NaCl type are still requested by the international community. In recent years the interest has shifted to solid solutions type ($An^1_{1-x}An^2_xSb$) compounds. Single crystal growths of $Pu_{1-x}U_xSb$ with x= 0.5 and 0.25 were successfully performed and large crystals obtained.

Finally, synthesis of $UNiSb_2$, $URuSb_2$ and $UPdSb_2$ polycrystalline samples were performed for neutron diffraction experiments to allow the determination of their magnetic structure.

1.1.2 Crystallochemistry of $An_4T_7Ge_6$ systems

Among the family of intermetallic compounds, the ternary cubic compounds $An_4T_7(Si \text{ or } Ge)_6$ where An is an actinide and T a 4d or 5d transition metal are an example of a family with the potential to possess interesting physical properties [1,2]. Previous investigations of the 4:7:6 phases showed that very few systems are forming in this phase [3,4] (namely with T= Ru and Os see TUAR-95, p. 36 Tab. 1.1) as the more stable $AnT_2(Si \text{ or } Ge)_2$ phases are often preferentially formed. To understand the parameters allowing the formation of the 4:7:6, we started to investigate, from a crystallochemistry point of view, various solid solutions of $An_4Ru_7(Si_xGe_{1-x})_6$, $An_4Os_7(Si_xGe_{1-x})_6$, $An_4(Ru_{1-x}Rh_x)_7Ge_6$, $An_4(Os_{1-x}Rh_x)_7Ge_6$ and $An_4(Ru_{1-x}Co_x)_7Ge_6$. Single-phase samples were obtained for different percentages x of the doping elements (see Fig. 1.1) in each system. For higher concentration the second phase observed was mainly the alternative 1:2:2. In Fig. 1.1 we present the variation of the lattice parameters observed over the range of stability found.

These results show that the 4:7:6 phase exists only in a small range of the lattice parameter a (8.25 to 8.33 Å) and explains why other expected phases, such as $Pu_4Os_7Ge_6$ or $Np_4Rh_7Ge_6$ could not be obtained. It is also interesting that substitution on the transition-metal site does not noticeably affect the lattice parameters. This is a demonstration that the hypothesis made by some authors [5,6] that the stability of the phase is determined by the relative size of An and T atoms, is not correct.

1.1.3 Synthesis of $Pu_{1-x}Am_x$ solid solutions

The localization-delocalization of the 5f/4f/3d electrons, in the actinides/lanthanides/d transition metals based materials is one of the most important problems in solid state physics. It is important to understand the competition between these two aspects as they are

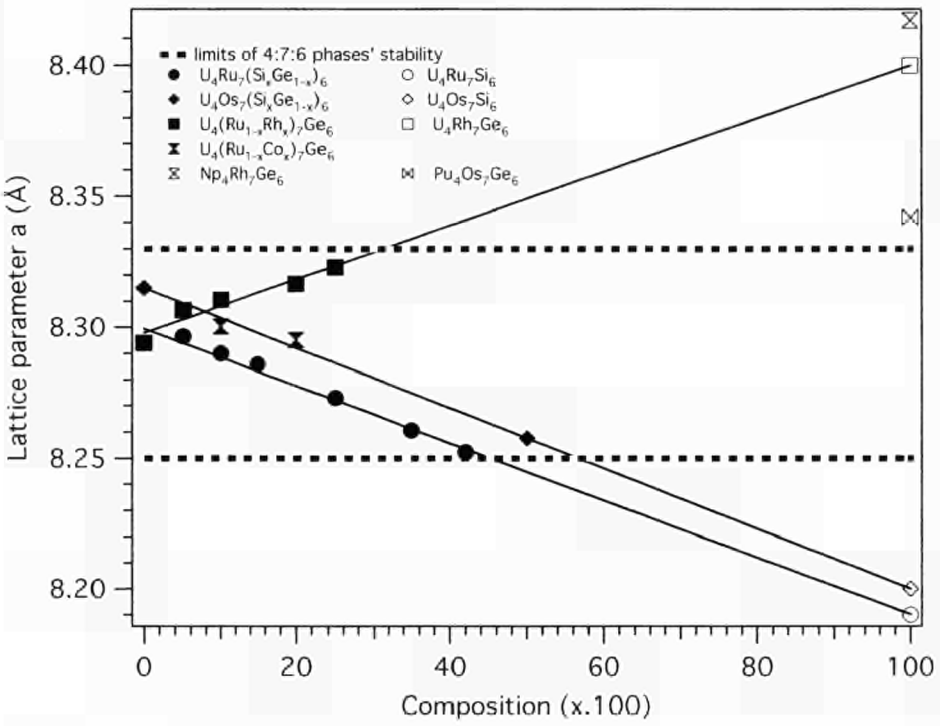

Fig. 1.1 Variation of the 4:7:6 phase's lattice parameters as function of the concentration of the doping element (open symbols are for extrapolated parameters).

claimed to be the driving force in phenomena such as heavy fermion or high T_c superconductors. Actinides are of particular interest due to their dual character. In this series, the transition between localization and delocalization occurs between plutonium and americium. Therefore the solid solutions $Pu_{1-x}Am_x$ may be seen as good materials to study the 5f electron localization. Samples with a nominal americium concentration x of 0.1, 0.25, 0.37 and 0.5 were synthesized by arc melting stoichiometric amount of materials. The samples were then obtained as a thin foil (of about 400 microns thickness) by splat-cooling technique. They were characterized by X-ray diffraction and their composition checked by chemical analysis. All samples were found to crystallize in the fcc structure and their lattice parameters are shown in Fig. 1.2. They are in relatively good agreement with previous results reported in the literature [7]. A slight discrepancy was observed between the nominal composition and the results of the analysis, probably due to the vapourization of the americium during the synthesis process.

At low concentrations of Am (x<0.6) a Vegard type law of the cell parameters is observed. Characterized samples were then encapsulated for resistivity measurements at low and high temperatures; the results are discussed in section 1.2.4.

1.1.4 Encapsulation of samples for collaborative studies

We developed, in collaboration with ETH-Zürich, a new type of encapsulation for magnetic studies at high temperature. The encapsulation of the sample is done by sealing it in a fine quartz tube introduced in a pure gold sample holder. The gold sample holder is then sealed by mechanical strangling of its lower part and melting a gold foil. Illustration of this new encapsulation type is given in Fig. 1.3a. Fig. 1.3b shows NpTe single crystals encapsulated for optical reflectivity measurements.

A complete list of the different samples encapsulated in the reporting period for collaborative studies is given in Tab. 1.1.

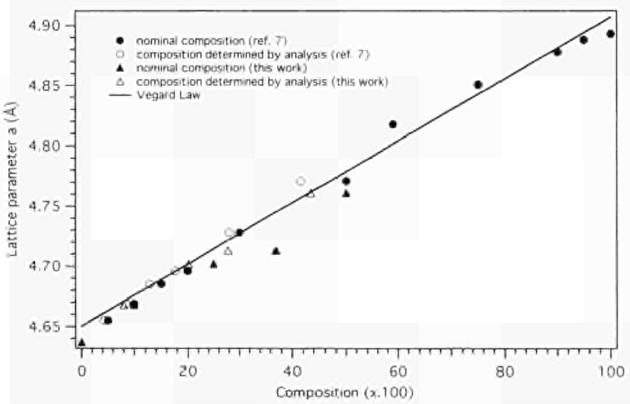

Fig. 1.2 Variation of the lattice constant in $Pu_{1-x}Am_x$ solid solutions.

References

[1] C. Jeandey, J.P. Sanchez, J.L. Oddou, J. Rebizant, J.C. Spirlet, F. Wastin; J. Phys. Condens. Matter. **8** (1996) 4259

[2] F. Wastin, E. Bednarczyk, J. Rebizant, J.P. Sanchez; 26ièmes Journées des Actinides, April 11-14, 1996, Zsklarka Poreba (Poland)

[3] F. Wastin, J. Rebizant, J.P. Sanchez, A. Blaise, J. Goffart, J.C. Spirlet, C.T. Walker, J. Fuger; J. Alloys and Comp. **210** (1994) 83

[4] E.J. Higgins, J. Rebizant, A.D. Stalios, C.T. Walker, F. Wastin, M.J. Hynes; 26ièmes Journées des Actinides, April 11-14, 1996, Zsklarka Poreba (Poland)

[5] N. Engel, B. Chabot, E. Parthé; J. Less-Common Met. **96** (1984) 291

[6] M.. François, G. Venturini, J.F. Marêché, B. Malaman, B. Roques; J. Less-Common Met. **113** (1985) 231

[7] F.H. Ellinger, K.A. Johnson, V.O. Struebing; J. Nucl. Mater. **20** (1966) 83

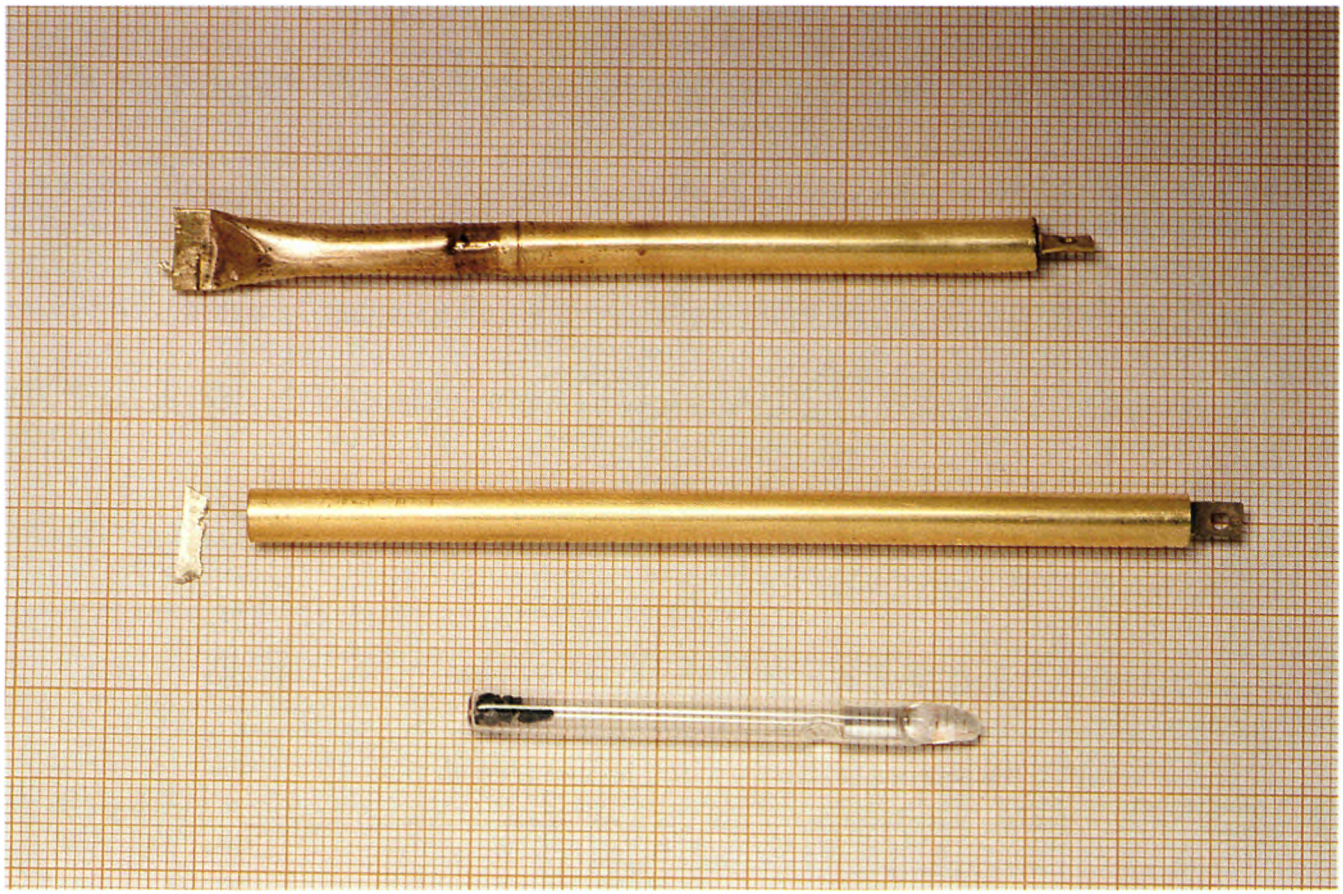

Fig. 1.3a Encapsulation of samples for high-temperature magnetic susceptibility measurements.

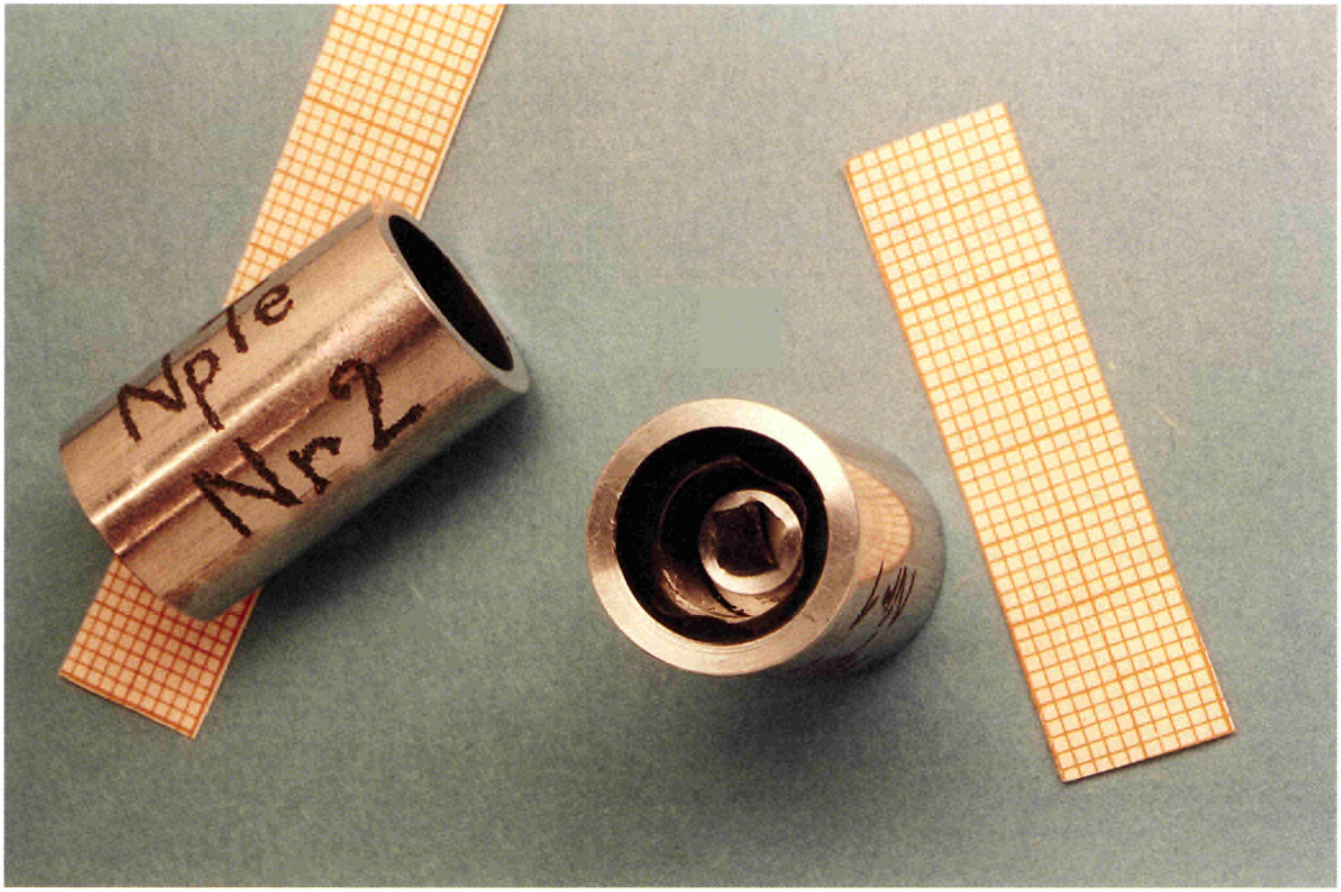

Fig. 1.3b Encapsulated NpTe single crystals for optical reflectivity measurements.

Tab. 1.1 Samples prepared, characterized and encapsulated in 1996 for the indicated measurements.

Measurements	Laboratories	Compounds	Form
Resistivity	ITU-Karlsruhe	Pu_2T_2Sn (T = Ni, Pd, Pt) Pu_2T_2In (T = Ni, Pd, Pt) $U_{1-x}Np_xPd_2Al_3$ (x = 0.005) $U_{1-x}Pu_xPd_2Al_3$ (x = 0.8) $U_{1-x}Np_xRu_2Si_2$ (x = 0.01, 0.1, 0.3, 0.5, 0.7, 0.9) $U_{1-x}Pu_xSb$ (x=0.5, 0.75) $Y_{1-x}Pu_xSb$ (x=0.4, 0.6) $Pu_{1-x}Am_x$ (x=0.1, 0.25, 0.37, 0.5, 1) $NpBe_{13}$	AcM AcM AcM AcM AcM SC SC AcM P
Mössbauer Spectroscopy	TU-München	$NpNi_2Al_3$ NpIrSn, NpNiSn NpSb Np_2Ir_2In	AcM AcM G-SC AcM
Neutron Scattering	CEN Grenoble	$UNiSb_2$, $URuSb_2$, $UPdSb_2$	AcM
Magnetism	ITN Sacavem	U_2T_2In (T = Ni, Pd, Pt)	SC
	ETH-Zürich	$U_{1-x}Pu_xSb$ (x= 0.75) $Y_{1-x}Pu_xSb$ (x=0.3, 0.4, 0.6)	SC SC
Optical Properties	ETH-Zürich	NpTe, AmTe	SC
Photoemission	Los Alamos	PuX (X= Sb, Te, S) NpX (X=Sb, Bi, S, Se, Te, As)	SC SC
Magnetization High-Temperature	ETH-Zürich	PuX (X= Sb, Te, S, Se, Bi, As, P) NpX (X=Sb, Bi, S, Se, Te, As, P) AmX (X=Bi,Te)	SC SC SC
Resistivity High-Temperature	ITU-Karlsruhe	$Pu_{1-x}Am_x$ (x=0, 0.1, 0.25, 0.37, 0.5, 1)	AcM

AcM = arc melting SC = single crystal P = powders, polycrystalline sample G-SC= grinding single crystals

1.2 Measurements of Bulk Physical Properties

1.2.1 Electrical resistivity of $U_{1-x}Np_xPd_2Al_3$

Continuing our study of the $U_{1-x}Np_xPd_2Al_3$ with very low concentration of Np, we measured the electrical resistivity of a sample doped with 0.5% of Np. At very low concentration (x<0.01), no strong influence was seen on the magnetic properties (T_N does not change significantly). On the other hand, a significant shift of the superconducting transition temperature is observed (see Fig. 1.4).

The superconducting transition observed in our pure UPd_2Al_3 sample was around 1.9 K, it was not observed down to 1.4 K in the 1% Np-doped sample, and is clearly seen at 1.5 K by doping with 0.5% Np. These results suggest that for low concentration of the doping element the superconductivity is not removed but shifted to lower temperatures.

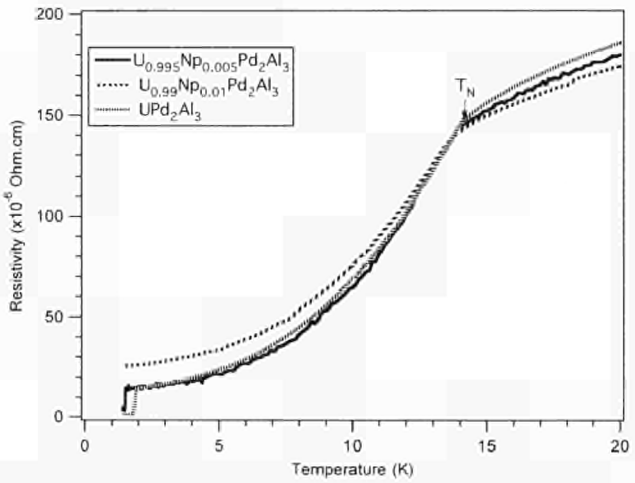

Fig. 1.4 Resistivity of $U_{1-x}Np_xPd_2Al_3$ at low temperature for x= 0, 0.005 and 0.01.

1.2.2 Electrical resistivity of $U_{1-x}Np_xRu_2Si_2$

Mössbauer results in $U_{1-x}Np_xRu_2Si_2$ systems, with x= 0.1, 0.3, 0.5, 0.7 and 0.9 were already presented and discussed in TUAR-95, p. 42. We extended our study to the resistivity measurements of these systems with x= 0.01, 0.1, 0.3, 0.5, 0.7 and 0.9. Curves obtained are displayed in Fig. 1.5.

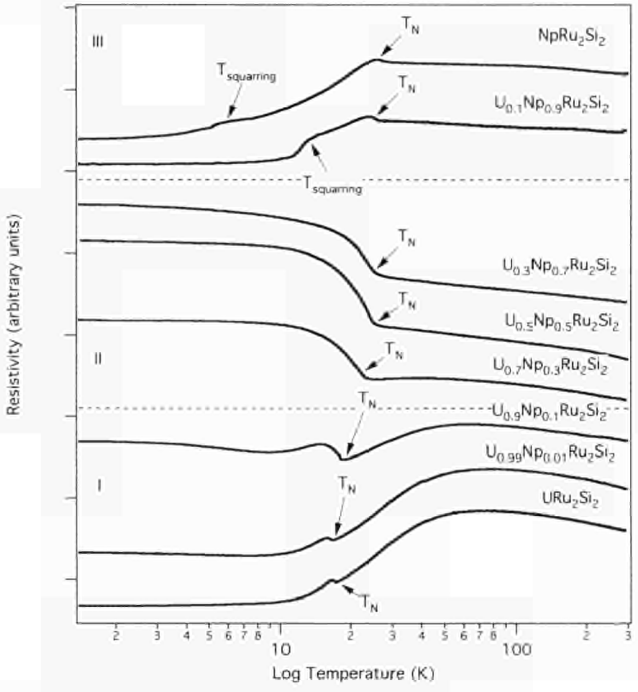

Fig. 1.5 Electrical resistivity of $U_{1-x}Np_xRu_2Si_2$.

Anomalies clearly indicate a magnetic ordering at temperatures in good agreement with those determined by Mössbauer spectroscopy [1]. We may distinguish three types of behaviour (I, II and III) depending on the Np-concentration. For x= 0.01 and 0.1 (region I), the variation of the resistivity with the temperature is similar to that observed in the case of pure URu_2Si_2. However, the maximum observed around the magnetic ordering temperature is more marked and broader for the diluted samples. Also, at low temperature, an increase of the resistivity is observed contrary to what happens for the pure U compound. These differences herald the strong increase of the resistivity observed in region II after the magnetic transition for x= 0.3, 0.5 and 0.7. Resistivities of these systems display similar comportment, the strongest effect being observed for the 50% dilution. This may suggest that in these systems the magnetic transition induces a gap in part of the conduction electron excitation spectrum, leading to a distinct increase of $\rho(T)$ just below T_N. For the last system (in region III), x=0.9, the variation of $\rho(T)$ at high temperature remains similar to that observed in the pure $NpRu_2Si_2$ compound. Below T_N (slightly reduced in comparison to the pure Np compound) another anomaly is observed around 15 K. A similar one was also observed in x= 1.0 at 6 K and correlated with the squarring of the modulation of the magnetic structure [2]. More studies and diffraction studies are necessary for a full understanding of these systems.

1.2.3 Susceptibility and electrical resistivity of Pu_2T_2X

During the last few years, intensive investigations have been devoted to the An_2T_2X isostructural family of ternary intermetallics (with An = U, Np , T= transition element and X= a p-element) [3-5]. To complete this study, we have investigated their Pu isostructural compounds. Magnetic susceptibility and resistivity measurements on Pu_2Ni_2Sn, Pu_2Ni_2In, Pu_2Pd_2Sn, Pu_2Pd_2In, Pu_2Pt_2Sn and Pu_2Pt_2In samples were performed. The temperature dependence of the magnetic susceptibility is shown in Fig. 1.6. The high temperature data for all compounds can be fit rather well to a modified Curie-Weiss law.

The calculated effective moments obtained are lower than the values expected for an isolated ion Pu $5f^5$ configuration, suggesting a strong hybridization of the f-electrons with the conduction band. With the exception of Pu_2Ni_2In and Pu_2Pt_2Sn, no clear indication of a magnetic transition is found.

The temperature dependence of the electrical resistivity is shown in Figs. 1.7 and 1.8. Some of these curves show similarities with the corresponding curves of some Pu intermetallics that proved to be spin fluctuation systems. This is the case for Pu_2Pt_2In. One can also find different but typical spin fluctuation characteristics for Pu_2Pt_2In which shows a T-square dependence confirming a spin behaviour in narrow bands.

In Pu_2Ni_2In and Pu_2Pt_2Sn the electrical resistivity results reinforce the idea of an antiferromagnetic behaviour predicted from the susceptibility results. The sudden increase of the electrical resistivity below the temperature anomaly, around 60 K for Pu_2Ni_2In and 80 K for Pu_2Pt_2Sn, typical for an antiferromagnetic behaviour, is probably due to the anisotropic gapping of the Fermi surface due to an increase of the magnetic unit cell compared to the crystallographic one. Comparing both, magnetic and resistivity results for each compound, it can be seen that the temperatures for which anomalies occur are not coincident, and are almost an order of magnitude higher in the resistivity curves. This suggests the existence of large pre-transitional fluctuations.

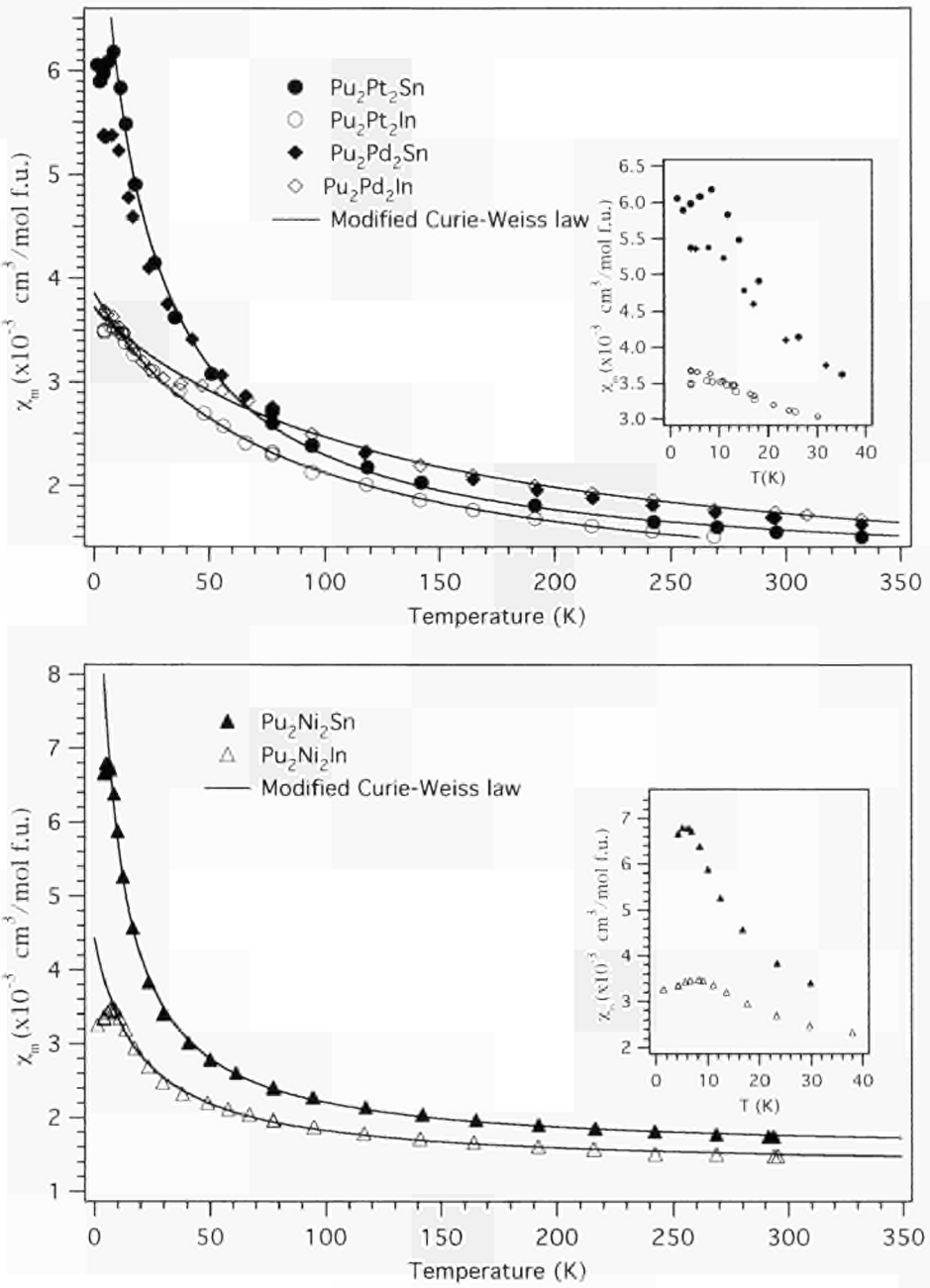

Fig. 1.6 Temperature dependence of the magnetic susceptibility of Pu_2T_2X compounds.

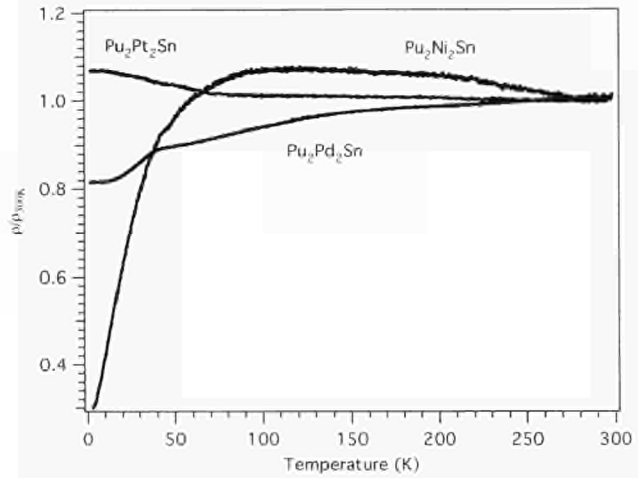

Fig. 1.7 Temperature dependence of the resistivity ratio of ρ/ρ_{300} of Pu_2T_2Sn compounds.

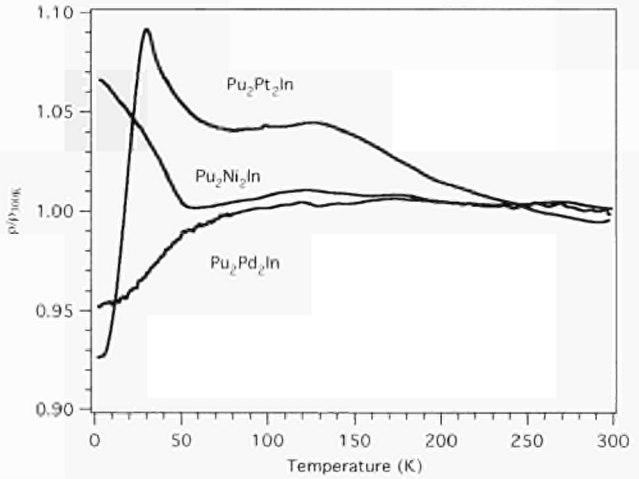

Fig. 1.8 Temperature dependence of the resistivity ratio of ρ/ρ_{300} of Pu_2T_2In compounds.

1.2.4 Electrical resistivity of $Pu_{1-x}Am_x$ solid solutions

Electrical resistivity measurements at low and high temperatures of $Pu_{1-x}Am_x$ solid solutions (see also 1.1.3), were performed. Pure Pu and Am metals were also measured in order to characterize our starting materials. Curves obtained for all systems investigated from 1.4 K to 800 K are displayed in Fig. 1.9.

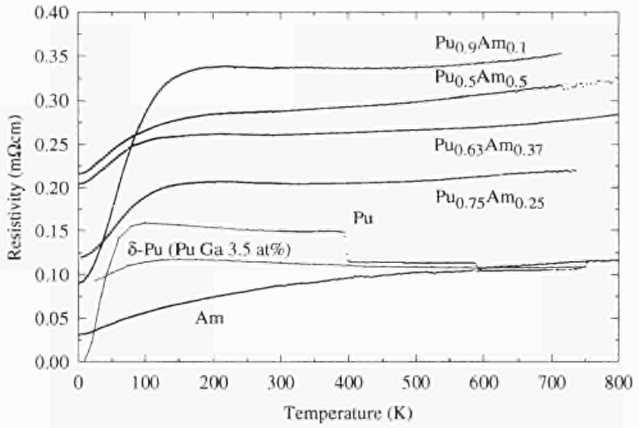

Fig. 1.9 Temperature dependence of the resistivity of $Pu_{1-x}Am_x$ solid solutions.

The resistivity curves of the pure Pu and Am metal obtained are in very good agreement with previously reported data [6,7]. In the case of the $Pu_{1-x}Am_x$ solid solutions, a T^2 type law is observed at low temperature. This can be explained by two phenomena: first, by an interband diffusion common for all ranges of concentrations and second, for low Am concentration, by an enhancement, in comparison to the pure Pu, of the spin fluctuation phenomena. At high temperatures, a Kondo type behaviour according to a law: $\rho = a\text{-}b.\ln T$ fits well the experimental data. In such a comportment b/a is a characteristic parameter which is proportional to the exchange integral J of the conduction electrons with the atomic moments. Values obtained are summarized in Tab. 1.2.

Tab. 1.2 Parameters obtained in the fits by a Kondo type law, $\rho = a\text{-}b.\ln T$, for the $Pu_{1-x}Am_x$ samples measured.

Sample	a ($\mu\Omega$.cm)	b ($\mu\Omega$.cm)	b/a	Temperature range
δ-Pu [8]	225.5	33.70	0.149	> 300 K
$Pu_{0.90}Am_{0.10}$	370.3	24.88	0.067	230-500 K
$Pu_{0.75}Am_{0.25}$	178.2	18.72	0.105	250-480 K
$Pu_{0.63}Am_{0.37}$	112.0	12.00	0.107	270-600 K
$Pu_{0.50}Am_{0.50}$	84.9	4.34	0.051	270-470 K

For low concentration in americium, b/a is dominated by correlations between the 5f electrons. By increasing the Am content, the Pu interdistance has the tendency to increase and these correlations are reduced as the moment on Am is zero. The b/a ratio initially decreases by increasing the Am content. For higher concentration (between $0.1<x<0.25$) the Pu 5f electrons have the tendency to localize, and the solid solutions may be considered as "isolated impurities Kondo" systems. These results strongly enhance the interest in this study for low Am concentration systems (below 30%) to determine where the transition to localized behaviour of the Pu-f electrons occurs.

1.2.5 Physical properties of $Np_4Ru_7Ge_6$

In the course of the study of the formation of ternary neptunium transition germanides, we reported the existence of $Np_4Ru_7Ge_6$ compound [9]. The physical properties of isostructural $U_4Ru_7Ge_6$ mentioned by the Bordeaux group [10] and investigated thoroughly by the Leiden group [11] indicated that this compound exhibits interesting characteristics. Indeed $U_4Ru_7Ge_6$ can be classified as a dense Kondo lattice which orders ferromagnetically (T_C=6.8 K) with strongly reduced U moments (0.2 μ_B).

Surprisingly, since normally Np compounds are more magnetic than their U analogs, a Mössbauer study of $Np_4Ru_7Ge_6$ at low temperature revealed a well resolved axially symmetric quadrupole interaction, and no onset of magnetic order could be detected down to 4.2 K [12]. A further Mössbauer study with a field applied showed that $Np_4Ru_7Ge_6$ is a non-magnetic compound with an enhanced susceptibility ($\chi_0 \approx 2.4\text{x}10^{-3}$ emu/mol. Np).The non-magnetic ground state of $Np_4Ru_7Ge_6$, as well as the behaviour of $U_4Ru_7Ge_6$, can be understood in terms of the competition between the Kondo effect and the RKKY exchange interaction, $Np_4Ru_7Ge_6$ being close to a magnetic instability[12]. We concentrate here on the resistivity and susceptibility measurements performed on $Np_4Ru_7Ge_6$.

Fig. 1.10 shows the temperature dependence of the resistivity down to 1.5 K. Some features are interesting to point out. The smooth linear decrease of the resistivity observed from 300 K to 50 K is followed by a steep drop. Below 25 K, the resistivity is well represented by a quadratic temperature dependence. This behaviour is very similar to the one observed in spin fluctuators or non-magnetic heavy fermion compounds [13]. Moreover, below 1.7 K, a second anomaly seems to

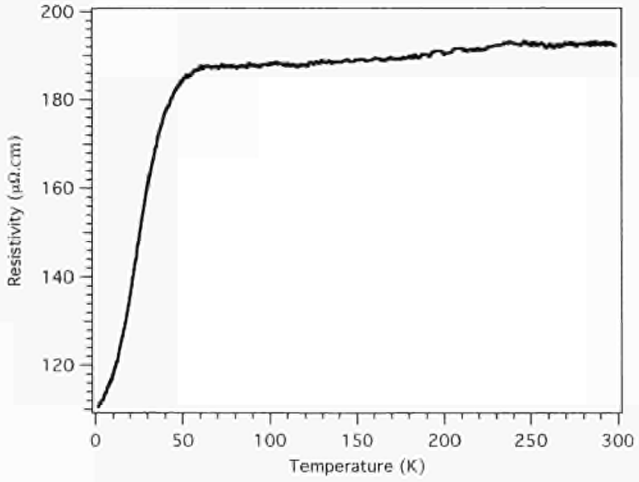

Fig. 1.10 Temperature dependence of the resistivity of $Np_4Ru_7Ge_6$.

occur, but the restricted range of experimental points (lowest temperature reachable with our equipment is 1.4 K) limits the reliability of this observation.

The AT^2 law observed at low temperature gives $A \approx 0.06$ $\mu\Omega$.cm/K^2. This relatively high A value substantiates that $Np_4Ru_7Ge_6$ is near a magnetic instability.

The magnetic susceptibility measurements performed at the FZK-ITC, down to 4.2 K are displayed in Fig.1.11.

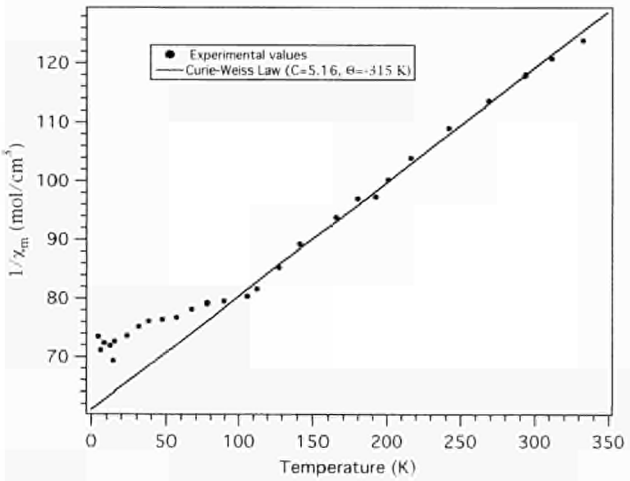

Fig. 1.11 Inverse of the magnetic susceptibility of $Np_4Ru_7Ge_6$.

No indication for magnetic order was observed in the whole temperature range, as expected from Mössbauer experiments. Down to 90 K a Curie-Weiss law is deduced from the experimental data with an effective moment on the Np of 1.6 μ_B. Around 10 K, an almost temperature-independant susceptibility is observed. The value of this temperature-independent magnetic susceptibility of about $3.4.10^{-3}$ emu/mol Np, is an enormous value for a Pauli-type susceptibility of an intermetallic compound and is consistant with Mössbauer-effect measurements in a magnetic field [12].

These results highlight the interest of the 4.7.6 compounds and give $Np_4Ru_7Ge_6$ as the best new candidate for a new heavy fermion Np compound.

References

[1] S. Zwirner, J.C. Waerenborgh, F. Wastin, A. Seret, J. Rebizant, J.C. Spirlet , W. Potzel, G.M. Kalvius; to be published in Physica B (1997)

[2] M. Bogé, D. Bonnisseau, P. Burlet, J.M. Fournier, E. Pleska, S. Quezel, J. Rebizant, J. Rossat-Mignod, J.C. Spirlet, M. Wulff; J. Nucl. Mater. **166** (1989) 77

[3] N. Péron, Y. Kergadallan, J. Rebizant, D. Meyer, J.M. Winand, S. Zwirner, L. Havela, H. Nakotte, J.C. Spirlet , G.M. Kalvius, E. Colineau, J.L. Oddou, C. Jeandey, J.P. Sanchez; J. Alloys Comp. **201** (1993) 203

[4] F. Mirambet, P. Gravereau, B. Chevalier, L. Trut, J. Etourneau; J. Alloys Comp. **203** (1993) 29

[5] L.C.J. Pereira, J.M. Winand, F. Wastin, J. Rebizant, J.C. Spirlet; 24ièmes Journées des Actinides, April 15-19, 1994, Obergurgl (Austria)

[6] T.A. Sandenaw, R.B. Gibney; J. Phys. Chem. Solids **6** (1958) 81

[7] R. Schenkel, W. Müller; J. Phys. Chem. Solids **38** (1977) 1301

[8] R.B. Gibney, T.A. Sandenaw; Report LA-1883 (1954) 26p.

[9] F. Wastin, J. Rebizant, J.P. Sanchez, A. Blaise, J. Goffart, J.C. Spirlet, C. Sari, C.T. Walker, J. Fuger; J. Alloys Comp. **210** (1994) 83

[10] B. Lloret, B. Buffat, B. Chevalier, J. Etourneau; J. Magn. Magn. Mater. **67** (1987) 232

[11] S.M.A. Mentink, G.J. Nieuwenhuys, A.A. Menovsky, J.A. Mydosch; J. Appl. Phys. **69** (1991) 5484

[12] C. Jeandey, J.P. Sanchez, J.L. Oddou, J. Rebizant, J.C. Spirlet, F. Wastin; J. Phys. Condens. Matter. **8** (1996) 4259

[13] A.R. Ott, Z. Fisk; in Handbook on the Physics and Chemistry of the Actinides, eds. A.J. Freeman and G.H. Lander, Vol. 5 (1987) 85

1.3 Spectroscopic Studies of Solid Surfaces

We continued synthesis and study of thin films of actinide materials using the sputter source we developed over the last years. Emphasis was put on the preparation of more complex films by using multicomponent targets (alloys) and by adding reactive gases to the plasma (reactive sputtering). We investigated the electronic structure of thin films and studied overlayer-substrate reactions such as interdiffusion. As part of collaboration with other groups we did surface analysis and thin layer preparation work.

1.3.1 Study of thin U layers on Mg-Al-Be

We concluded the study of thin layers of U on Mg and Al substrates, and did some complementary work on the U layers on Be. Because the surface electronic structure in these systems is strongly dependent on the mode of growth, and in particular on possible interdiffusion of overlayer and substrate [1,2], we studied the depth distribution of U on Mg and Al by analyzing the U4f background at high binding energy (BE), which is produced by inelastic scattering of photoelectrons originating from buried U atoms (Fig. 1.12).

Modelling this background by a depth distribution function [3] gives the thickness of the U containing

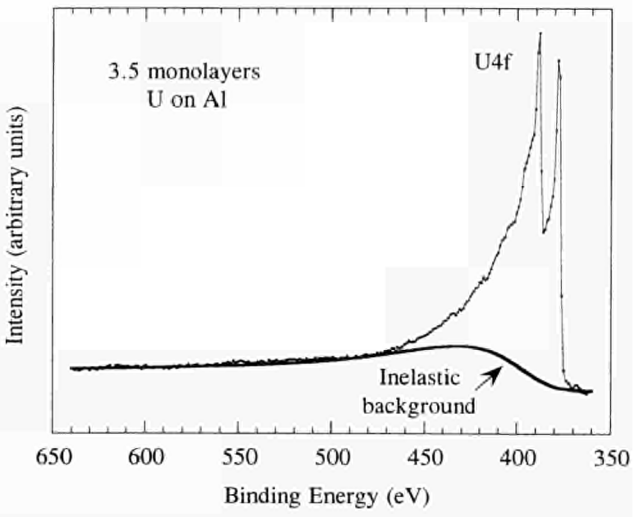

Fig. 1.12 U4f photoemission line with its inelastic background, calculated following Tougaard's model [3].

layer, independent of the film composition. If U diffuses deeper into the bulk forming a more dilute interdiffusion layer, than the depth distribution function will indicate a higher thickness. This thickness is compared to the total amount of U present at the surface, which has been measured by intensity comparisons, and which gives the thickness of a pure U overlayer without any interdiffusion ("Reference Overlayer Thickness") . The ratio of the two thickness values gives an estimate for U-substrate interdiffusion. Fig. 1.13 confirms that for U/Mg a pure overlayer is formed at all coverages while on U/Al interdiffusion takes place in the low coverage range.

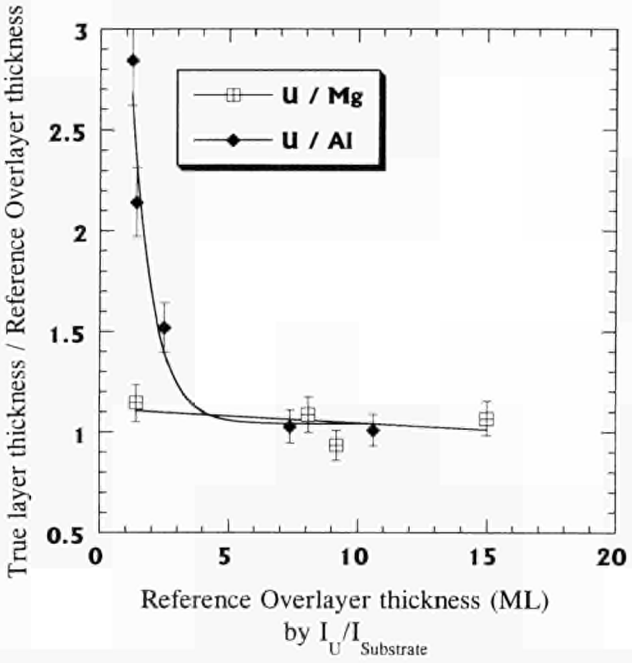

Fig. 1.13 Ratio of the actual layer thickness and the thickness of the layer assuming no interdiffusion. A higher ratio indicates more pronounced interdiffusion.

As we reported last year, U4f correlation satellites are observed at 6 eV from the main lines for U/Al while on U/Mg they are missing. Exact analysis of the U4f spectra revealed, however, that these satellites are superimposed onto plasmon loss peaks and the exact analysis of the correlation effects requires removal of the plasmon contributions. This was done by comparing the photoemission spectra to Reflection Electron Energy Loss Spectra (REELS) taken under the same experimental conditions (Fig. 1.14). It is seen that the intensity of the plasmon at 395 eV BE is too weak to account for all or even for a major part of the 395 eV peak, which thus is attributed partially to a 6 eV correlation satellite of the $U4f_{7/2}$ peak.

The plasmon losses are characteristic for pure Al - they where not observed in UAl_2 [4]. This shows that U4f photoelectrons pass through pure Al regions, i.e. U has to be buried below Al regions. Again this points to U-Al interdiffusion which probably takes place along the grain boundaries of the polycrystalline substrate thus leaving the inner grain regions unchanged. Similar plasmons where observed in the U/Be system.

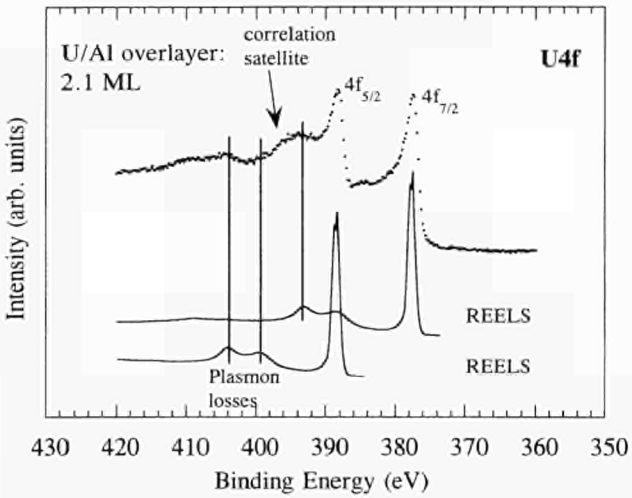

Fig. 1.14 Comparison of plasmon peaks in U4f and Electron Energy Loss (ELS) spectra of U overlayers on Al. The ELS spectra, taken at primary energies identical to the $U4f_{5/2}$ and $U4f_{7/2}$ emissions, show plasmon loss features which appear also in the U4f spectra.

1.3.2 Study of $(U_{0.7}Th_{0.3})Ni_5$

We studied the pseudoternary $(U_{0.7}Th_{0.3})Ni_5$. The goal of this work was to investigate the electronic structure and chemical reactivity of this complex actinide compound, and determine the suitability of our sputter source to make correct thin film replicates of complex or highly active actinide systems. We first investigated the composition of in situ deposited films as a function of various deposition conditions: substrate temperature (80 K to 1000 K), target voltage (200 to 800 V) and current (1 to 10 mA), and argon pressure (5.10^{-3} to 1.10^{-1} Torr). The thin films were compared to sputter cleaned and scraped bulk samples. Most remarkably the U/Th did not correspond to the composition of the target. There was a general tendency for Th enrichment at the surface ($U_{0.59}Th_{0.41}$) (Fig. 1.15a) when compared to a scraped surface, which has a nominal bulk composition. A depth profiling study showed that this enrichment takes place only at the top surface, independent of film thickness: sputter removal of the top surface layers (Fig. 1.15b) shows a similar subsurface composition both for film and bulk materials. Thus the average film composition appears to be correct. U surface enrichment after film deposition could be due to a reorganization within the top surface layer at the end of the deposition process, rather than a wrong intrinsic film composition, which could have been produced by different sticking probabilities, thermal diffusion inside the target, etc. Reorganization of the surface could be explained by a lower surface energy of Th when compared to U. It could also be due to a higher affinity of U for Ni, driving Th out of the Th-Ni bonding and resulting in an accumulation of Th in the low co-ordination environment at the surface. Th surface enrichment could be avoided by making the films in presence of oxygen, i.e. under reactive sputtering conditions, resulting in an actinide oxide composition of $U_{0.70}Th_{0.30}$ (Fig. 1.15c). Our work suggests surface reorganization characteristic of the metal phase is important.

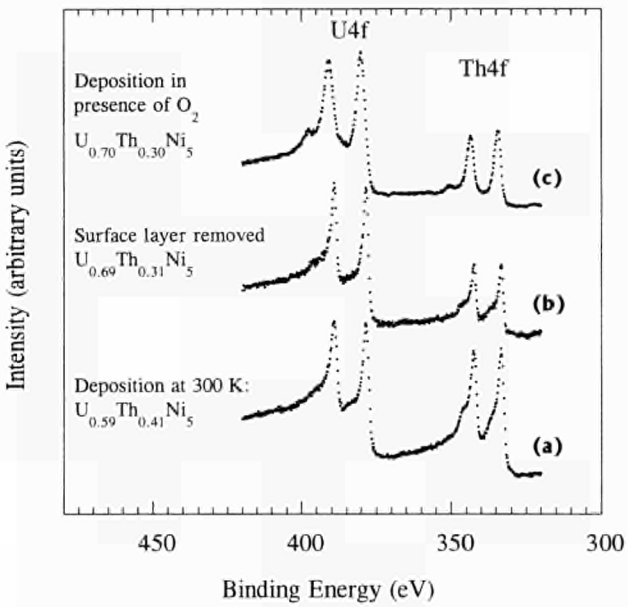

Fig. 1.15 U4f spectra of thin films deposited from a $U_{0.70}Th_{0.30}Ni_5$ target under various conditions. Metallic films exhibit surface segregation of Th while oxidized surfaces appear to have the right composition.

This work will be continued during the next year. In particular we will study the reaction of these films with corrosive gases (O_2, CO_2, ...) to obtain information on chemical and thermal stability of complex actinide systems. UThNi is a prototype study and will be followed by other ternary compounds of interest for the actinide research and more applied technological research.

1.3.3 Supplementary co-operative work

We did surface analysis work for other groups in the Institute. In particular we studied the surface composition of a UO_2-SiC pellet, started depth profiling experiments of CsOH/stainless steel and studied the initial surface composition of UO_2 single crystals after various annealing treatments and storage under air (C. Muggelberg, Univ. Oxford). We prepared thin films of UN and UNO on Al by reactive sputter deposition. We concluded the characterisation of the sputter source by monitoring deposition rates under controlled deposition conditions.

References

[1] T. Gouder; (TUAR-95, p. 44)
[2] T. Gouder; submitted for publication in Surf. Sci.
[3] S. Tougaard; Surf. Sci. **216** (1989) 343
[4] J.R. Naegele, L. Manes, J.C. Spirlet, J.M. Fournier; Appl. Surf. Sci. **4** (1980) 510

1.4 High Pressure Studies

1.4.1 Mössbauer study of NpSb under high pressure

We have studied NpSb by Mössbauer spectroscopy under high pressures up to 9 GPa. This extends the previous pressure studies on the pnictides NpX (X=As, Sb, Bi, crystallizing in the cubic NaCl structure) via electrical resistance [1] and X-rays [2] performed in ITU, and Mössbauer spectroscopy on NpAs [3]. Fig. 1.16 shows that the Néel temperature of the three systems decreases with increasing pressure. This is surprising, since in compounds where a more pronounced 5f-delocalization is expected T_N is almost pressure independent, e.g. as in UP, or even rises, as in UAs [4]. Furthermore, the slope of the T_N versus volume dependence is steeper in NpSb than in NpAs although the 5f states of the latter are expected to be more delocalized. Our present study allows one to examine whether the strong decrease of T_N in NpSb is connected with an enhanced suppression of the ordered moment, i.e. strong 5f delocalization. Furthermore, NpSb undergoes a structural transition from the NaCl to a tetragonal structure which is accompanied by a volume collapse of ~10%. Until these experiments the influence of this transition on the electronic state was unknown.

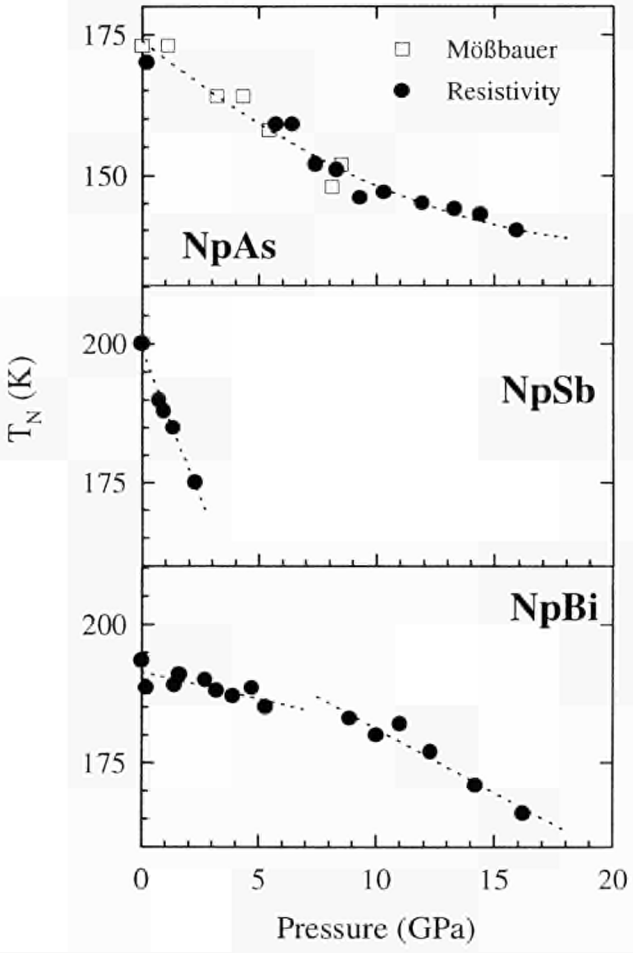

Fig. 1.16 Pressure dependencies of T_N in NpAs [1,3], NpSb [1], and NpBi [1]. Note that the two different slopes in NpBi are due to a similar structural transition as found for NpSb (see text).

In Fig. 1.17 the hyperfine parameters obtained for NpSb are plotted versus volume change. Their relatively weak volume dependencies in the B1 phase (o) indicate a rather weak 5f delocalization, which cannot explain the comparably strong decrease of T_N. For example in NpSb the slopes of the B_{hf} and S versus volume curves are smaller by a factor of ~2 as compared to NpAs. In contrast to the situation in NpAs, e^2qQ of NpSb is almost pressure independent. A careful analysis suggests that T_N is reduced rather by a decrease of the susceptibility of the conduction band than by 5f delocalization.

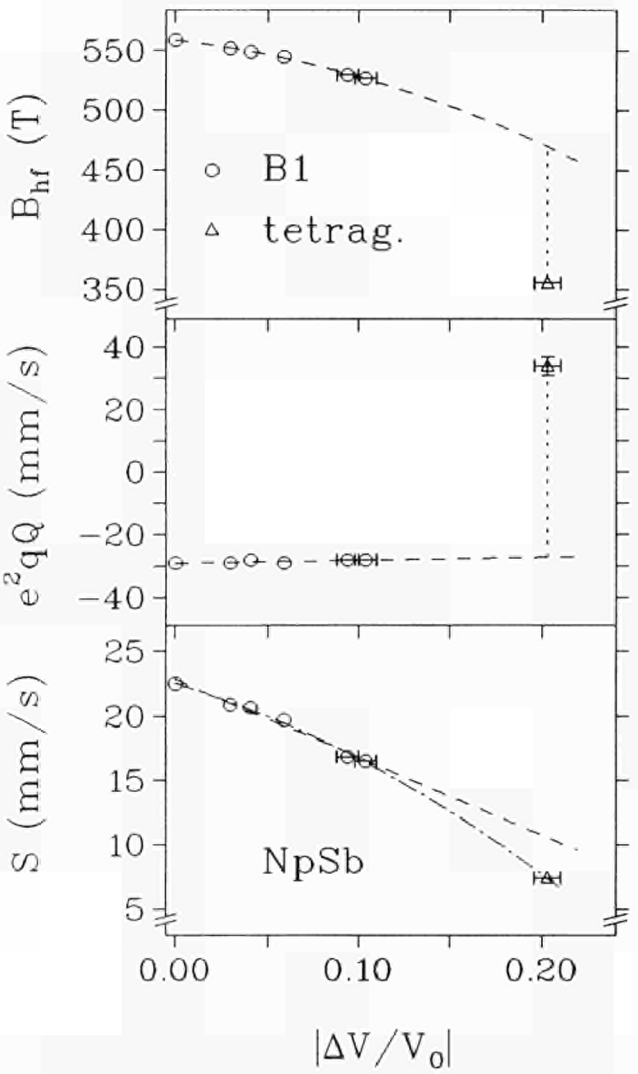

Fig. 1.17 NpSb: The magnetic hyperfine field B_{hf}, the coupling constant of the electric quadrupole interaction e^2qQ, and the isomer shift S relative to $NpAl_2$ plotted versus volume change.

In the high pressure tetragonal phase (Δ) the strong reduction of B_{hf} by ~170 T gives evidence for an enhanced 5f delocalization. The strong increase of e^2qQ is very likely due to a considerable distortion of the 6d and 5f orbitals which may be caused by a strong anisotropic hybridization. The isomer shift displays a weakly nonlinear volume dependence which is also expected in localized f systems [5]. Due to the *structural* change, however, several effects can partly compensate. This makes an interpretation of *S* in terms of 5f delocalization difficult.

References

[1] M. Amanowicz, D. Braithwaite, V. Ichas, U. Benedict, J. Rebizant, J.C. Spirlet; Phys. Rev. B **50** (1994) 6577
[2] S. Dabos-Seignon, U. Benedict, S. Heathman, J.C. Spirlet, M. Pages; J. Less-Common Met. **160** (1990) 35
[3] U. Potzel; Ph.D. thesis, Technische Universität München (1987)
[4] I.N. Goncharenko, J.M. Mignot, V.A. Somenkov, J. Rossat-Mignod, O. Vogt; Physica B **199&200** (1994) 625
[5] A. Gleissner, W. Potzel, J. Moser, G.M. Kalvius; Phys. Rev. Lett. **70** (1993) 2032

1.4.2 High pressure X-ray diffraction studies of AnX_3 compounds

Further high pressure X-ray diffraction studies of AnX_3 compounds were performed on UAl_3 using the synchrotron radiation source at Hasylab DESY Hamburg and $NpSn_3$, which was studied in Karlsruhe. The anomalous compression curve for UAl_3 previously reported in (TUAR-95, p. 46-47) was studied using an ethanol methanol water mixture in the ratio 16:3:1 to confirm that the solidification of the pressure transmitting medium is the source of the anomaly. As can be seen in Fig. 1.18 the anomaly shifted to higher pressure using the ethanol mixture, which was to be expected as this medium solidifies in the pressure cell at around 15 GPa as compared to silicone oil used in the previous experiments which solidifies at around 9 GPa.

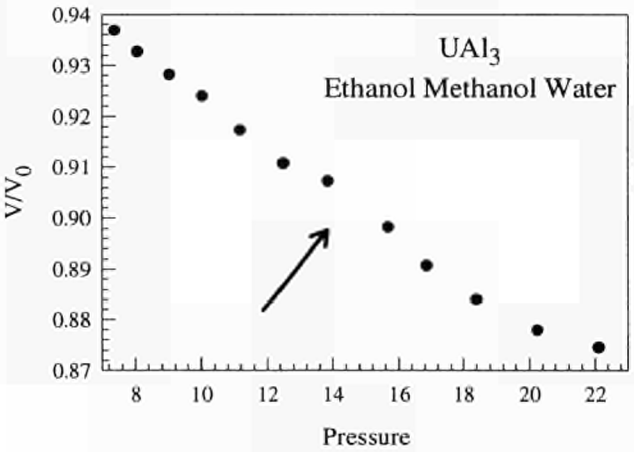

Fig. 1.18 Relative volume as a function of pressure for UAl_3 (pressure transmitting fluid : ethanol-methanol-water). The anomaly is marked with an arrow.

$NpSn_3$ was studied under pressure up to 45 GPa using the energy dispersive equipment in Karlsruhe. The sample showed no anomalous behaviour in its compression curve and also no phase change was observed up to the highest pressure attained. The compressibility was calculated using the Birch and Murnaghan equations of state and gave results of B_0 = 84.8 GPa, B'_0 = 4.9 for the Birch equation and B_0 = 86.8 GPa, B'_0 = 4.3 for the Murnaghan equation.

1.4.3 High pressure X-ray diffraction experiments on NpS and PuS up to 60 GPa

Neptunium and plutonium monosulfides were studied under high pressure up to ~60 GPa using a diamond anvil cell in an energy dispersive X-ray diffraction facility in the Institute. Samples of NpS and PuS were synthesized at our Institute by chemical vapour reaction. Pure elements in stoichiometric amounts were sealed under vacuum in a two compartment quartz tube and heated in stages up to 1000 K in a two-zone furnace until a complete reaction of the sulfur occured. The resulting compounds were then transformed into single crystals by mineralization. Their lattice parameters were determined by precision X-ray diffractometry and were found to be equal to a = 553.26(3) pm and a = 554.37(3) pm respectively. The compounds, of cubic

rock salt structure type at ambient pressure, do not show any crystallographic phase transition in the domain of investigation. This result was not expected as previous studies of ThS showed a transformation to a hexagonal structure beginning at around 23 GPa and US underwent a rhombohedral distortion at 12 GPa.

From the pressure-volume relationship, we determined bulk moduli of 92 and 105 GPa with pressure derivatives of 4.6 and 5.7 for NpS and PuS respectively.

At ambient pressure, the observed diffraction spectra (Figs. 1.19 and 1.20) show the characteristic diffraction pattern of the NaCl structure type (space group: Fm3m). Upon compression the samples showed a continuous decrease of interplanar distances and a broadening of the diffraction peaks was observed. All high pressure diffraction spectra could be indexed according to the NaCl-type structure over the entire pressure range. This result is in agreement with the optical reflectivity studies where no indication of phase transitions up to 45 GPa could be found [1].

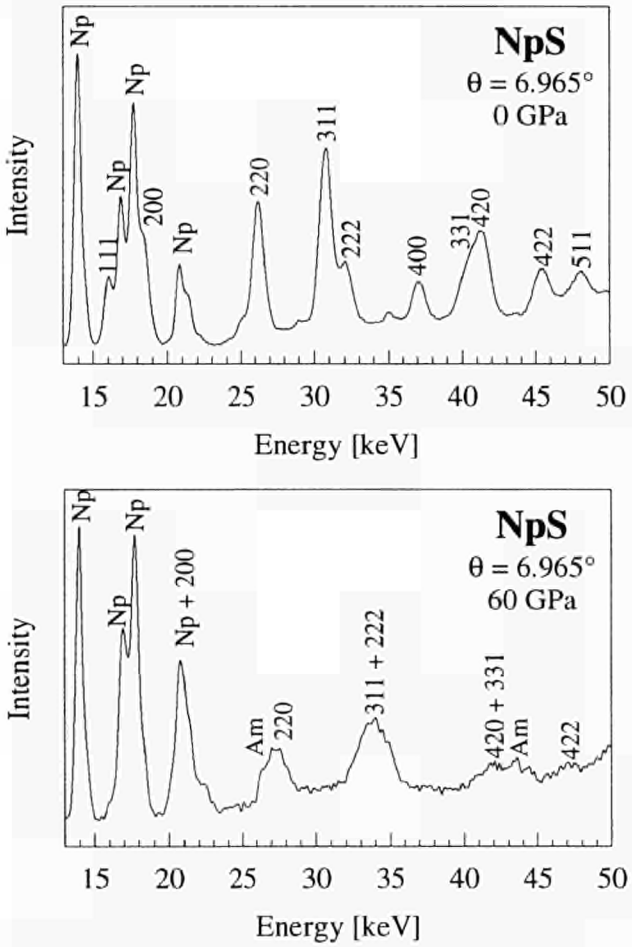

Fig. 1.19 Diffraction spectra of NpS at low and high pressure.

1.4.4 Study of Cm/Bk alloys under pressure at ORNL

Samples of curium/berkelium alloys were prepared and their behaviour under high pressure studied by energy dispersive X-ray diffraction. The samples of the Cm/Bk alloys were freshly prepared by R.G. Haire of ORNL to minimize the in-growth of Cf due to decay of the Bk. Two alloy compositions were prepared of approximately

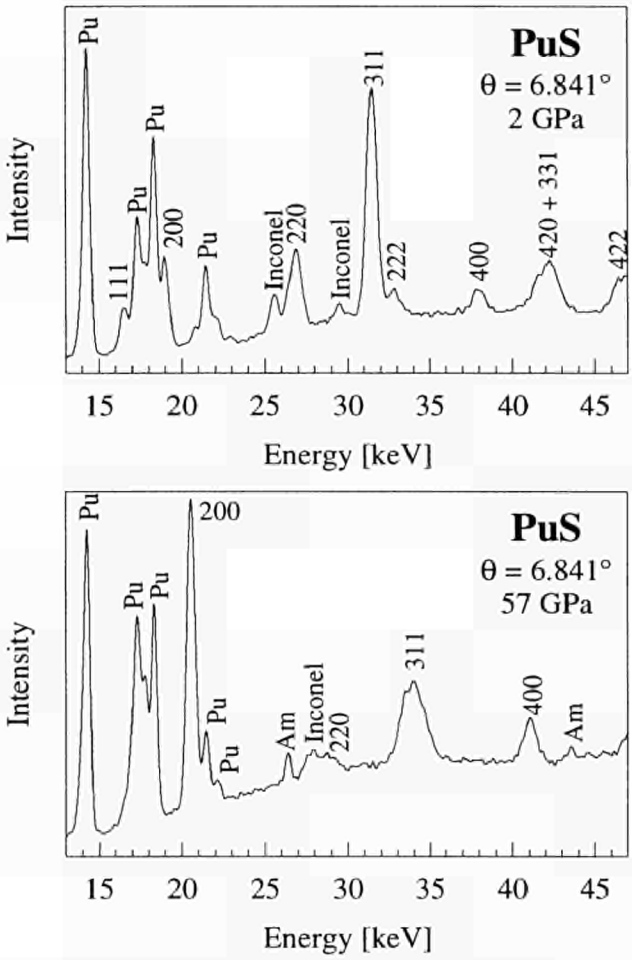

Fig. 1.20 Diffraction spectra of PuS at low and high pressure.

70% Cm 30% Bk and 46% Cm 54% Bk. The exact ratios of the two elements will be determined later by other techniques including measuring the in-growth of Cf to back-calculate the original percentage of Bk. Both samples were successfully loaded in the Holzapfel type pressure cell specially made for ORNL and studied under pressure up to 53 GPa which is normally the maximum pressure which can be attained with this type of cell without too great a risk of diamond breakage. Using the rotating anode generator at 55 kV and 60 mA the fine focus setting enabled us to collect reasonable spectra in 2 to 3 hours as compared to 8 to 12 hours using a normal sealed X-ray tube. For the 70% Cm alloy the original dhcp structure transformed to an fcc type at 12 GPa and to a third phase at about 35 GPa which is identical to that found in Am. For the 54% Bk sample dhcp – fcc occurred at 8 GPa and fcc – third phase at 24 GPa. The fourth phase of Am (alpha-uranium) which is stable above 18 GPa was not observed in either sample up to the maximum pressure of 53 GPa.

The sequence of phase transitions can be seen in Fig. 1.21 which follow:

In Fig. 1.22 it can be seen that the third phase of the Cm/Bk alloy is identical to that observed in our latest studies with Am (possibly alpha-2 Ce type).

References

[1] C. Abraham, U. Benedict, J.-C. Spirlet; Physica B **222** (1996) 52

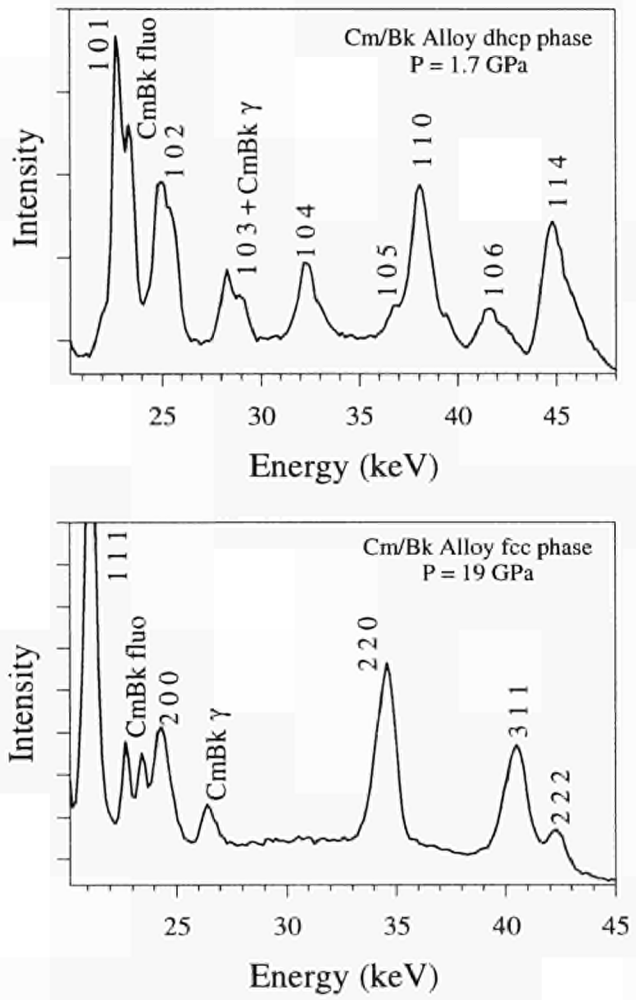

Fig. 1.21 Phase Change (dhcp to fcc) in Cm/Bk alloys.

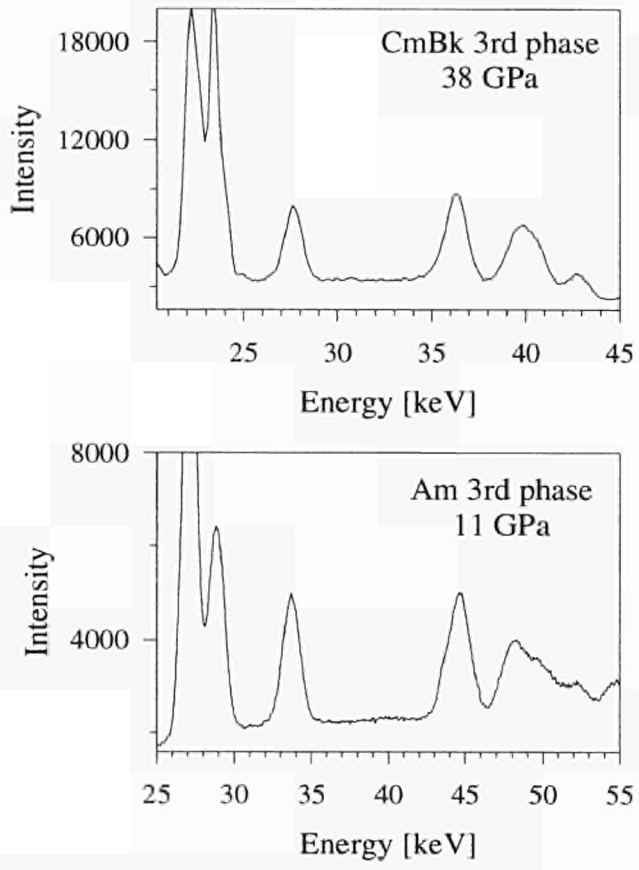

Fig. 1.22 Third phase observed with both Cm/Bk and Am.

1.5 Scattering Studies

Neutron experiments were performed this year at the Institut Laue-Langevin (ILL, Grenoble), Risø (Denmark), and at the ISIS (UK) spallation source. One of the themes emphasized here is to look at materials containing both actinides and transition-metal atoms. Possible applications of such systems are as permanent magnets (based on the large anisotropy of actinides) and in magnetic recording (because of the large Kerr effect observed in actinides).

We have continued X-ray magnetic scattering experiments at both the NSLS (at Brookhaven National Lab., USA) and the ESRF (in Grenoble).The NSLS experiments on surface magnetism are featured as a ITU highlight, and discussed at the front of this Annual Report. We will discuss here our efforts on the actinide rock salt compounds at the NSLS and experiments on a single crystal of MFe_4Al_8 (M=Dy) at the ESRF.

1.5.1 Neutron studies of magnetic configurations

A number of experiments have been performed on single crystals with the MFe_4Al_8 structure, where M = rare earth or actinide. The purpose of these has been to understand the interaction between the M and Fe sublattices. Although we have examined compounds with M = Dy, Lu, Y, and Ho, we shall confine our attention here to M = U, which is one of the most interesting of these compounds. Previous work on this compound was unable to establish either the magnetic configuration or whether the uranium atoms carried a magnetic moment. A series of neutron experiments, including the use of polarized neutrons on a single crystal, which was made in ITU, have solved this problem. We show in Fig. 1.23 the magnetic configuration of the U and Fe moments in the unit cell.

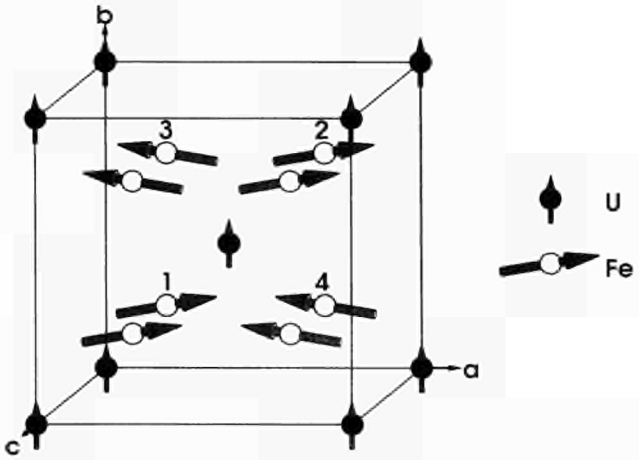

Fig. 1.23 One domain of the magnetic structure of UFe_4Al_8 as derived from the analysis of the polarized-neutron data. The solid points are the uranium atoms, with the open points the Fe atoms, the Al atoms are not shown. The sizes of the arrows is an indication of the sizes of the moments. The U atoms are at the origin and body-centered position of the unit cell, and the Fe atoms are at the positions (1/4, 1/4, 1/4) and all combinations.

Note the unusual "canting" of the Fe sublattice and the small "ferromagnetic" component of the U moments. The results of many previous experiments with other techniques, such as Mössbauer, magnetization, and

magneto-resistance, can be better understood with this proposed model. One interesting question is what distinguishes the configuration in Fig. 1.23 from that with the Fe moments 1 and 3 interchanged. In fact an analysis of the symmetry at the Fe site shows (Fig. 1.24) that the angle ϕ explained in the figure caption is defined by the local arrangements of the Al atoms around the Fe atom. An examination with neutrons of the local site susceptibility has shown that the anisotropy in the compound arises almost exclusively from the actinide site, which is expected, and this keeps all the moments confined to the ab plane of the tetragonal structure. The exchange path U – Fe – U is sufficiently strong that both the U and Fe sublattices develop their magnetic moments at the same T_N. This is not the case for the M = rare-earth compounds, in which the lack of any direct f – Fe 3d hybridization results in the rare-earth sublattice ordering at a much lower temperature than the Fe sublattice.

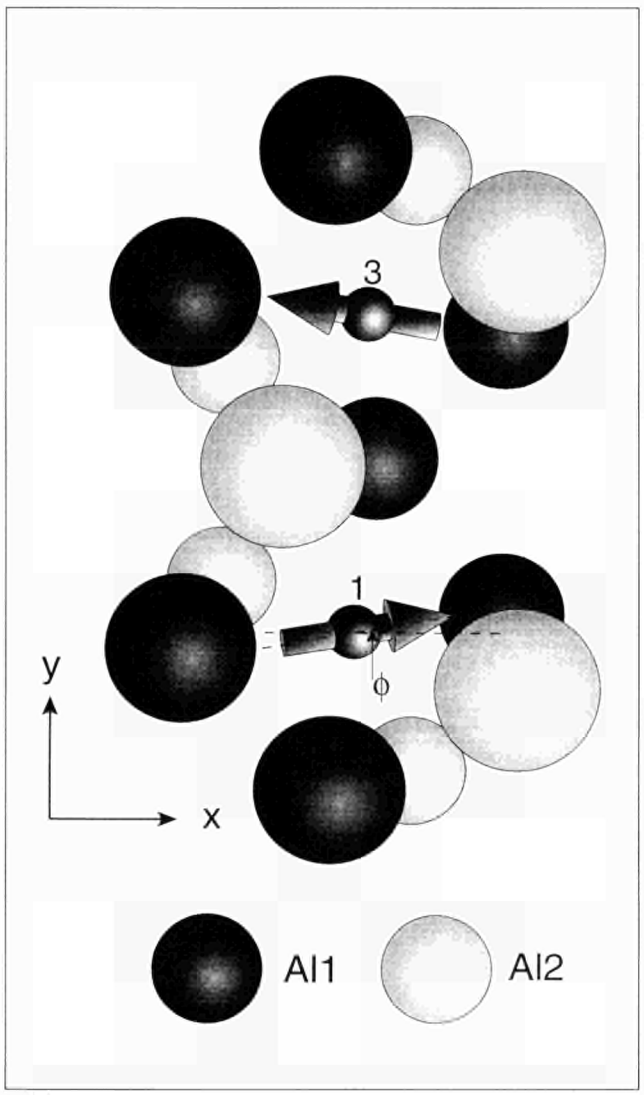

Fig. 1.24 Schematic drawing to show the arrangement of aluminum atoms around the Fe atoms in UFe_4Al_8. Note that Fe #1 and #3 are equivalent only when the spins rotate from ø in Fe #1 to (180-ø) at Fe #3. Note that ø=0° would signify no interaction between the two sublattices, experimentally ø=13° with H=0, but as the field is applied in the b direction the moments of the Fe sublattice turn towards the applied field, so that by H=4.6T the angle ø=25°.

1.5.2 Neutron experiments on multilayers

This has become an active field on account of the potential applications of transition-metal multilayers that exhibit the giant magneto-resistance effect and can be made with perpendicular anisotropy. We believe multilayers containing actinides will have a number of interesting properties, and that those containing uranium might even find some applications. The reason for this relates to the strongly hybridizing properties of the 5f electrons, and their intrinsic orbital moment, and hence their substantial conribution to the intrinsic anisotropy. With this in view we have started a programme in this field. Our first experiments have been on UAs/Co multilayers that we obtained from IBM Research, Yorktown Heights, USA. These have been characterized with X-ray reflectivity to get the atomic arrangement, and we show in Fig. 1.25 the neutron reflectivity from the multilayer containing 12 biplanes of [20 Å Co/ 80 Å of amorphous UAs] on top of a 200 Å Co buffer. The difference in the reflectivity for the two neutron spin states can be used to establish the magnetic profile of the multilayer, and confirms that at low temperature the uranium atoms carry a small magnetic moment, as proposed from the Kerr rotation measurements [1]. Collaborative efforts with PSI – Switzerland and the University of Liverpool, UK, are to continue on these materials. We have already prepared high-quality Ce/Fe multilayers.

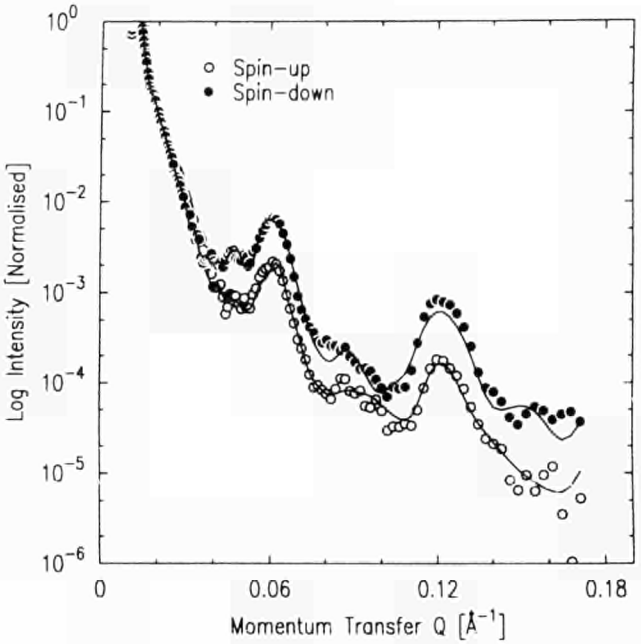

Fig. 1.25 Neutron reflectivity taken with polarized neutrons at the ISIS spallation source on a multilayer with 12 repeats of [80 Å amorphous UAs/ 20 Å Co]. The peaks arise from the biplanar structure of the multilayer and show that the interfaces are relatively smooth. The difference in the signal for the two neutron spin states (spin up being parallel to the magnetic field) can be fit to a model (solid lines) to give the detailed magnetic profile of the multilayer.

1.5.3 Neutron inelastic scattering

Experiments this year were performed on single crystals of UPd_2Al_3, UGa_3, and UFe_2. We will describe here the new results on the itinerant ferromagnet UFe_2 and

these are shown in Fig. 1.26. Previously [2], we had characterized the spin-wave response (experimental points in the figure) up to 7 meV. The use of one of the high-intensity triple-axis spectrometers at the ILL allowed this to be extended to ~20 meV. The previously measured quadratic behaviour, shown as a dashed line in the figure, is followed up to about 10 meV, but above this energy a strong interaction appears with another mode. This is indicated schematically by the contours of equal intensity, showing a broad mode around 14 meV, which then narrows, and by 18 meV the spin wave is again well defined.

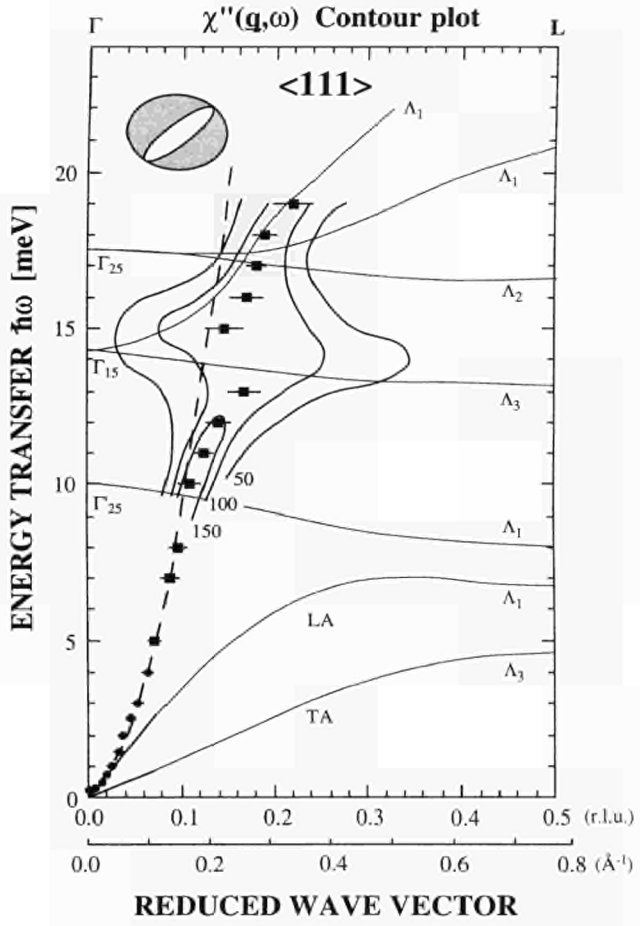

Fig. 1.26 The dispersion curve of the Fe spin wave (experimental points) as deduced at 100 K in a recent experiment at the ILL. The quadratic relationship (dashed curve) at low q is valid to 10 meV, but deviates considerable above that energy. The strong interaction of the Fe spin-wave with another mode around 14 meV is shown by contours of equal intensity. The resolution function is shown in the upper left-hand corner. The phonon dispersion curves are shown as thin solid lines.

There could be a number of possible reasons for the mode interaction in UFe_2 at ~14 meV. One possibility is the Fe spin wave interacting with a phonon, possibly that of Γ_{15} symmetry as shown in the figure. It is significant, however, that this interaction has not been seen in the rare-earth Fe_2 compounds, which have similar phonon modes. The second possibility is that it interacts with the mode from the uranium moments, which up to now has not been observed. Yet a third possibility is that the interaction is with the Stoner continuum from the conduction electrons. Further analysis and experiments will be needed to decide; but it is clear that our understanding of the sublattice interactions in UFe_2 is far from complete.

References

[1] P. Fumagalli, T.S. Plackett, D. Weller, T.R. McGuire, R.J. Gambino; Phys. Rev. Lett. **70** (1993) 230

[2] L. Paolasini, G.H. Lander, S.M. Shapiro, R. Caciuffo, B. Lebech, L.-P. Regnault, B. Roessli, J.-M. Fournier; Europhys. Lett. **34** (1996) 459; Phys. Rev. B 54 (1996) 7222

1.5.4 Resonant X-ray magnetic scattering of actinides

We continued this year with our studies of the NaCl-type actinide compounds by examining NpS, PuBi, and a second sample of PuSb at the NSLS (Brookhaven) synchrotron. The resonant scattering experiments involve a scattering with the photon beam tuned to the energy of the M_4 absorption edge of the respective actinide. Performing these experiments at the M_4 of uranium are now almost standard, and a great amount of information is available about the magnetism. Examples from our work are on USb-UTe solid solutions [1], and the surface magnetic scattering mentioned above [2]. We extended this to NpAs [3], and in 1996 performed a successful experiment on NpS. However, since these experiments are performed at the energy of the absorption edge, the penetration of the beam is much reduced. We show in Fig. 1.27 the intensity of a Bragg peak (from the charge scattering) from three different materials containing the first 3 actinide nuclides.

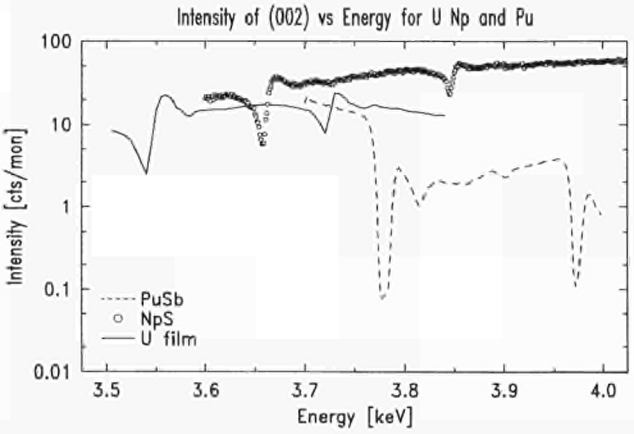

Fig. 1.27 Variation in the intensity of the charge Bragg peaks of three materials containing U, Np , and Pu nuclides as a function of energy in the vicinity of the actinide M absorption edges. The sharp minima correspond to the M absorption edges of the different nuclei, followed by EXAFS-like oscillations. Notice that the intensity at the Pu edges is more reduced than at the U or Np edges.

The strong reductions in intensity are at the absorption edges. Notice that the reductions in the case of Pu M edges are much greater than the others. It is this strong reduction at the Pu M edge that has prevented us succeeding with observing *magnetic* scattering from Pu compounds, despite 3 different samples of PuSb and PuBi being examined. One easy explanation would be that the Pu M edges are different in strength from that of U and Np. Since little experimental work has been reported yet on these edges (the majority of studies in

absorption spectroscopy are done on the L edges, which are at higher energy), we cannot exclude this possibility, although there would seem to be no reason why the atomic physics would change between Np and Pu. A more likely explanation is that the surfaces of these Pu crystals are covered with either an amorphous layer, or a thin oxide layer. This would have to be ~0.2 μm to give the observed effect. A further possibility is that the growth of this layer may be promoted preferentially at the surface by the radioactivity. Since ^{239}Pu has an activity some 100 times greater than ^{237}Np, this argument might account for the difference between Np and Pu samples, which otherwise have many similar properties.

1.5.5 Studies of X-ray resonant effects

A major question in the field on resonant magnetic scattering, which was discovered about 10 years ago, is whether any "solid-state", rather than just atomic, physics can be extracted from the observations. M-edge studies in the actinides have so far not been performed with sufficient resolution, and appear to reflect predominately the atomic nature of the transition from a 3d core electron promoted to a "localized-like" 5f orbit. Not until recently at the ESRF has there been a spectrometer capable of measuring at the actinide L edges (17 to 23 keV) so we have been doing some test experiments on rare-earth edges, which lie in the convenient energy range of 6 – 9 keV.

In particular, at the ESRF we have examined a single crystal of $DyFe_4Al_8$. This is isostructural with UFe_4Al_8 discussed in Sec. 1.5.1 The material orders magnetically at T_N = 170 K with a cycloidal magnetic structure. Initially, only the Fe moments order, with the Dy moments ordering at a much lower temperature of ~25 K. In Fig. 1.28 we show the intensity of the two magnetic satellites measured at the Dy L_3 edge as a function of temperature.

The transitions involve promotions of a Dy 2p core electron to the partially filled 5d shell, and are thus sensitive to the occupation of the 5d shell. When the Dy 4f moments decrease in intensity (abruptly near 20 K) there is a sharp reduction of the intensity at the L_3 edge, *but it does not go to zero*. This may be interpreted as a measure of the polarized 5d moment. When the large Dy 4f moments disorder, most of the 5d polarization also disappears, but some of it is induced by the interaction between the Dy 5d shell and the (polarized) Fe 3d electrons. Indeed, the figure shows that the 5d polarization disappears only at T_N when the Fe 3d moments become disordered. This is the first direct measurement of the rare-earth 5d polarization being coupled to the Fe sublattice, and is important for understanding the magnetic interactions in these and similar compounds. A further interesting point is illustrated in the insert of the figure. This shows the intensity of the magnetic reflection as a function of energy for two different temperatures. We see a change in both the position (by about 1.5 eV) and the breadth of the resonance, depending on whether the 4f are long-range ordered (12 K) or disordered (75 K). These changes may be related to the position and mixing of the 5d band states in the solid, and would thus represent information about the solid-state physics of the material. For example, the breadth of the resonance is related to the core-hole lifetime. Experiments are planned on both this material and others containing rare-earths and actinides to further explore what information can be obtained by examining the scattering at the resonant energies.

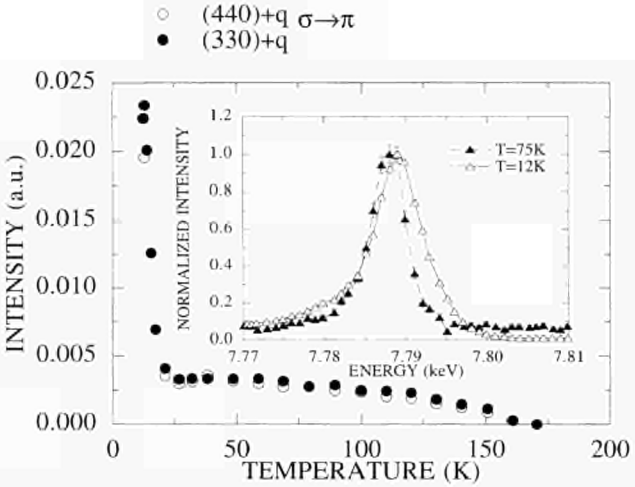

*Fig. 1.28 Temperature dependence of the [330]+**q** (closed circles) and [440]+**q** (open circles) intensities as measured at the Dy L_3 edge in the σ → π polarization channel from the single crystal of $DyFe_4Al_8$. The inset shows the energy dependence of the [440]+**q** satellite at T=12 K (open triangles) and T=75 K (closed triangles). The lines are Lorentzian fits. The energy resolution of the instrument (ID20 at the ESRF) is about 2 eV in this energy range.*

References

[1] W.J. Nuttall, S. Langridge, W.G. Stirling, G.H. Lander, B. Lebech, O. Vogt; Phys. Rev. B **52** (1995) 4409

[2] G.M. Watson, D. Gibbs, G.H. Lander, B.D. Gaulin, L.E. Berman, Hj. Matzke, W. Ellis; Phys. Rev. Lett. **77** (1996) 751

[3] S. Langridge, W.G. Stirling, G.H. Lander, J. Rebizant; Physical Review B **49** (1994) 12010-21; Phys. Rev. B **49** (1994) 12022

1.6 Theory: Optical Properties and Chemical Bonding in US, UN and UC

In the quest for materials with highly specialized properties, it is of crucial importance that models are developed which select the few parameters that are primarily responsibile for the physical characteristics of the material. We have calculated the dielectric function, reflectivity and electron energy loss for the NaCl-type uranium compounds UC, UN and US and established the relationship between the optical properties and chemical bonding in these compounds.

The change in the nature of the chemical bond from more ionic in US to more covalent in UC may be seen from comparison of the number of states per unit energy (or state densities) for UC, UN and US (Fig.1.29). The valence bands of the more ionic sulphide lie 4-8 eV below the Fermi energy and there is an intrinsic gap

between the valence and conduction bands of about 2 eV. The valence band contains mostly anion-p electrons with a 5f admixture in the valence band and corresponding anion-p admixture in the conduction bands. In UN the valence band has moved 1.5 eV higher in energy, lying 2-6 eV below the Fermi energy and the gap has become a pseudo-gap as the state density never becomes zero. The uranium-5f admixture in the valence band and corresponding anion-p admixture in the conduction bands has increased. In UC, if they did not hybridize, the anion p and uranium 5f bands would overlap completely but strong hybridization pushes the anion-p derived valence band down so that it lies from 0 to 5 eV below the Fermi energy. The uranium-5f derived conduction bands are correspondingly pushed above the Fermi energy. The bands close to the Fermi energy are heavily hybridized anion-p and uranium 5f states and the gap has disappeared.

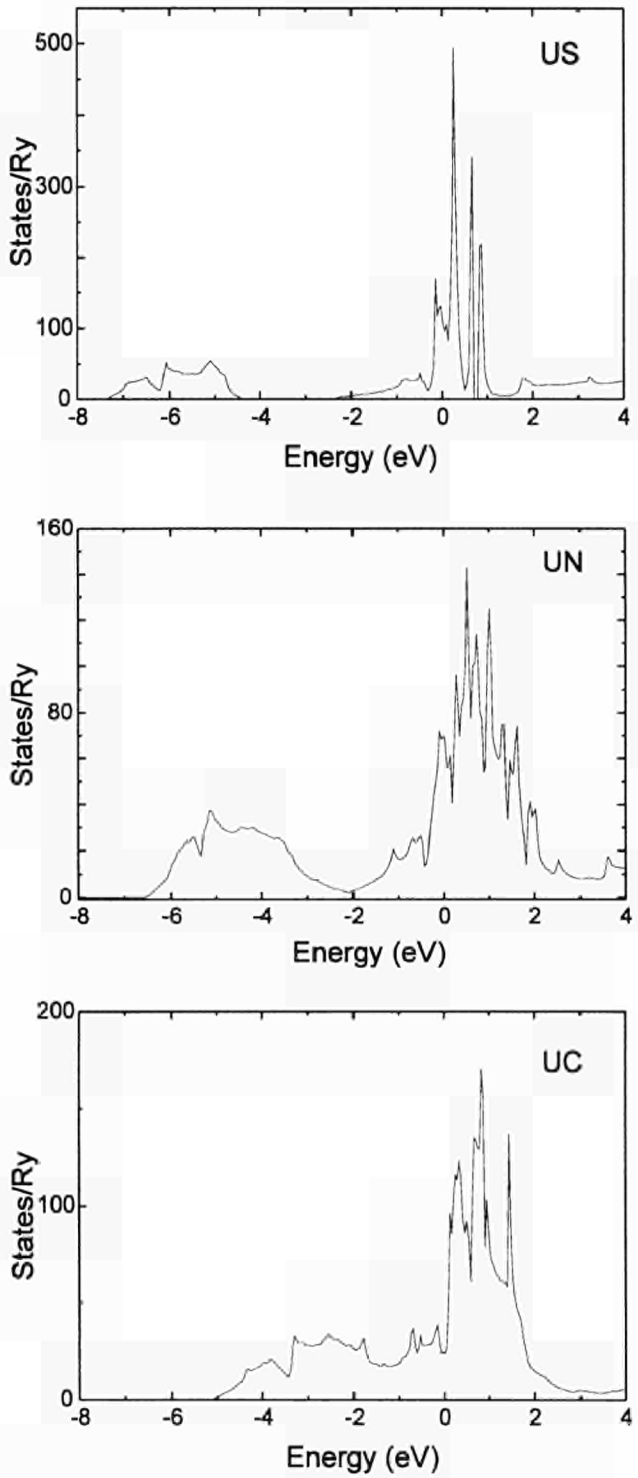

Fig. 1.29 The calculated state densities of US, UN and UC. The Fermi energy is at the zero of energy.

There are several bands crossing the Fermi energy in all three compounds which leads to low frequency interband absorption in addition to the zero frequency Drude response. The real part of the interband absorption should peak at low energies of less than 1 eV. The state density at energies of more than 2 eV above the Fermi energy decreases rapidly with increasing energy and, as the photon energy is increased, the absorption due to transitions from bands at the Fermi energy decreases rapidly. In addition the state density on the low energy side of the Fermi energy decreases rapidly with decreasing binding energy due to the pseudo-gap in the nitrides and the gap in the oxides and the absorption decreases strongly in the 2-3 eV range. This effect should be strongest for the sulphide and minimal for the carbide. At higher photon energies transitions from the valence to conduction bands should dominate the response and absorption should be relatively strong.

In Fig 1.30 we have plotted the calculated reflectivity and energy loss function for the range 0 to 12 eV. The results are in good agreement with measurements where they exist [1]. The complex Drude intraband conductivity dominates in the low energy region below 1 eV. The low energy 5f-d and d-5f interband transitions are centred at about 0.5 eV. With increasing photon energy the number of possible transitions to states above the Fermi energy is reduced by the absence of initial states in the gap. Above the gap energy, with increasing photon energy, the number of transitions from the valence to conduction bands increases rapidly and the imaginary part of the dielectric constant increases. The real part of the interband dielectric constant at low photon energies is dominated by contributions from valence to conduction band transitions which have a larger energy (about 5 eV) than the photons. The interband contribution to the dielectric constant, unlike the Drude contribution, is therefore positive and changes sign only when the photon energy is greater than that of the bulk of these transitions. Fig. 1.29 shows that this energy should be about 5-8 eV in US and UN. In fact Fig. 1.29 shows that the interband optical properties of US and UN should be fairly represented by two resonances: firstly a small and narrow resonance centred at about 0.5 eV arising from low energy transitions close to the Fermi energy; and secondly a larger, broader resonance centred at about 5 eV arising from valence to conduction band transitions. The pseudo-gap ensures a separation of the two resonances. In UC the high energy resonance is much broader with the result that the Drude and interband parts of the real part of the dielectric constant cancel at lower energy.

The interesting optical properties then arise from the addition of a third resonance, the Drude contribution,

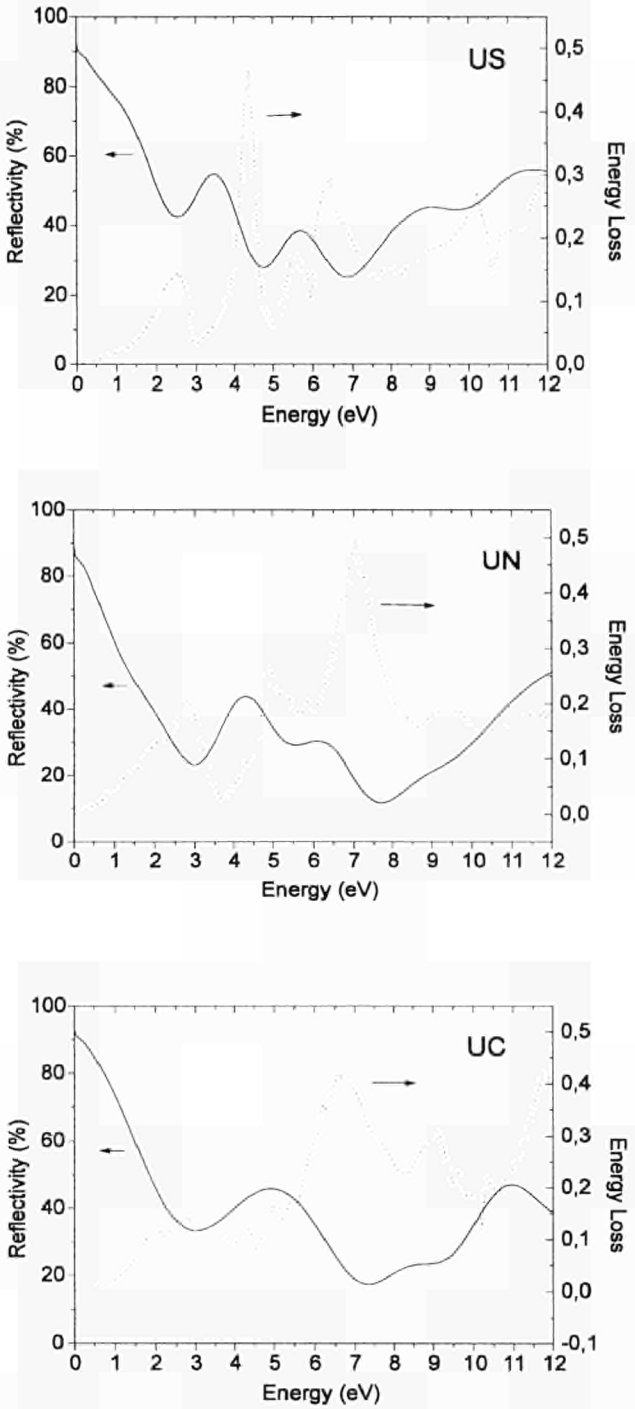

Fig. 1.30 The calculated reflectivity and energy loss functions of US, UN and UC.

at zero energy. The Drude contribution dominates completely up to 2 eV and it completely determines the low energy reflectivity. The real part of the dielectric constant is negative and the reflectivity high. The rise in reflectivity above 3 eV is due to interband transitions and up to 5 eV the real part of the interband dielectric constant is positive. The depth of the dip in the reflectivity about 3 eV is determined by how low the interband contribution to the imaginary part of the dielectric constant is when the Drude and interband contributions to the real part of the dielectric constant cancel. This in turn is determined by the pseudo-gap. There is a real gap in the sulphide and the reflectivity has a deeper minimum than in the nitride since the separation between valence and conduction bands is larger.

The plasma resonance, which appears as a peak in the energy loss function (Fig. 1.30), occurs when the real part of the dielectric constant is zero provided that the imaginary part is small. The plasma resonance in the sulphide at 4.5 eV is due to the low value of the imaginary part of the dielectric constant arising from the valence conduction electron band gap. In the nitride the plasma resonance is heavily damped. In both cases it is plasma resonance of the conduction electrons shielded by the valence bands which polarize by interband transitions to the conduction bands. In UC there is, due to the position of the Fermi level and the strong p-d hybridization, no clear separation between the low and high energy resonances. The plasma resonance of the conduction electrons is overdamped due to shielding by valence to conduction band transitions.

In conclusion, we have been able to show that the main features of the optical properties of the compounds studied can be explained in simple terms. A complete calculation is in good agreement with experiment.

References

[1] J. Schoenes; in 'Handbook of the Physics and Chemistry of the Actinides', eds. A.J. Freeman and G.H. Lander, North Holland Physics Publishing (Elvesier Science Publishing Co.), Amsterdam, Vol.1 (1984) p.341; ISBN: 0-444-86903-4

1.7 Radioimmunotherapy

^{213}Bi labelled anti-CD33 antibodies for therapy of myeloid leukemias: preclinical and first clinical evaluation

The preclinical tests on the use of ^{213}Bi-immunotherapy to treat acute myelogeneous leukemia were completed in the Memorial Sloan Kettering Cancer Center in New York. At the end of 1996, clinical trials were started by treating the first two patients. On request of the hospital and dependent upon the availability of a patient in a more or less stable situation, a ^{213}Bi generator is sent from ITU to the US (Fig. 1.31). The special requirements related to the stability under transport and the safe processing of such a generator at the hospital were solved by ITU researchers. They developed both the transport mechanism (a quartz ampoule in which the ^{225}Ac is fixed as a chloride in colloid-free form) and a dissolution, elution and purification procedure, allowing the ^{213}Bi to be extracted in the hospital, directly before the coupling to the relevant antibody (HuM195 in this case) and before the injection of the radioimmunoconjugate into the patient [1,2].

A novel α-particle emitting construct of the anti-CD33 monoclonal antibody, HuM195, has been designed and evaluated for the clinical treatment of myeloid leukemias. HuM195 is a recombinant CDR grafted humanized anti-CD33 construct and it has been chemically modified by appending up to ten cyclohexylbenzyl DTPA (CHX-A-DTPA) chelates per antibody [3]. The

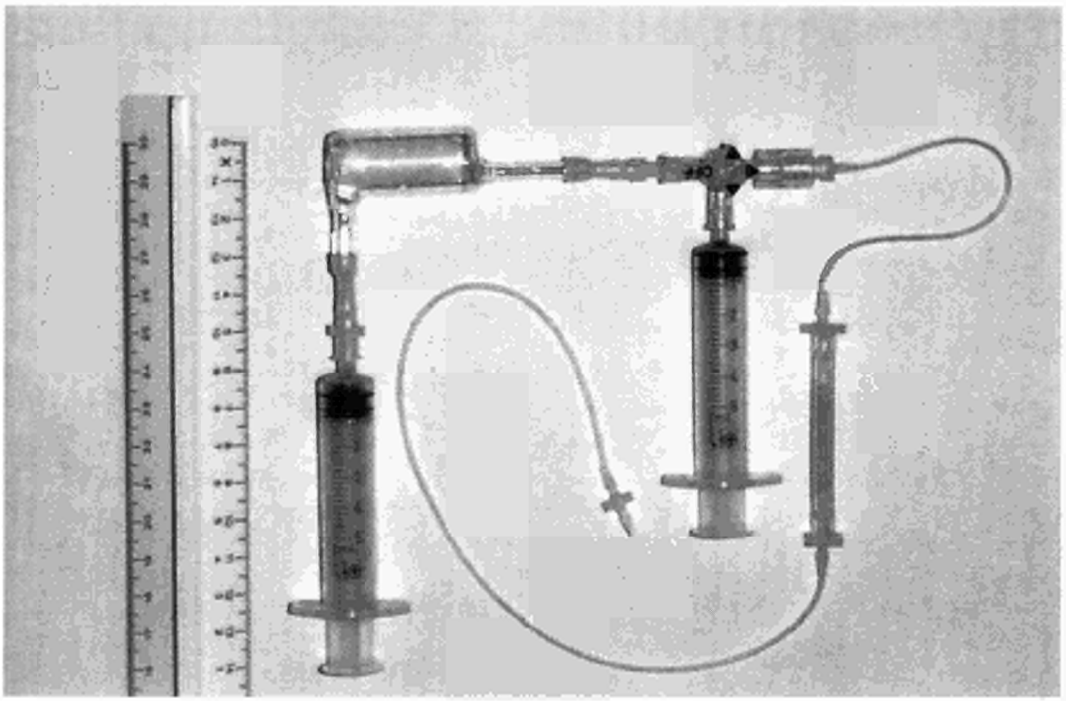

Fig. 1.31 ^{213}Bi-generator

alpha emitting radio-nuclide used is ^{213}Bi [4]. The alpha particles have a range of 10-80 μm and are 100-1000 times more cytotoxic than the β-particle emitted by ^{131}I.

A generator system has been constructed that allows as much as 25 mCi of ^{213}Bi to be eluted from the generator every 3-4 hours for antibody labelling over a thirty-day period. CHX-A-DTPA-HuM195 labelling efficiencies for eight different reactions carried out under similar conditions had an average incorporation yield of ^{213}Bi of 89% ± 3% within 20 minutes at ambient temperature. The radiolabelled antibody is purified from low molecular weight impurities by standard size exclusion techniques. The average % activity recovered after purification is 75% ± 8%. The average purity of the radiolabelled antibody constructs is 98% ± 2%. In addition, pulse height multi-channel analysis of the purified radiolabelled antibody solutions has not detected any ^{225}Ac radioisotope in the final product resulting from generator breakthrough. The average specific activity of the (^{213}Bi)-CHX-A-DTPA-HuM195 after reaction and purification is 8.5 ± 1.4 Ci/g.

The immunoreactivity as determined by Affinity Thin Layer Chromatography [5] was 80% to 95% and found to be independent of specific activity. The radiolabelled HuM195 is rapidly internalized into HL60 leukemia cells in a time-dependent manner ranging from 50% at 1 hour to 65% at 24 hours. The labelled construct was found to be stable for at least 2 days in vitro in the presence of human serum at 37 °C with only a 3.5% loss of bismuth (using ^{205}Bi/^{206}Bi) from the constructs over a 48 hour period. Studies in normal Balb/c mice indicate that there was no uptake or loss of bismuth to mouse tissues, which do not express CD33, or to the kidney, which has affinity for free bismuth metal. Mice injected with doses of (^{213}Bi)CHX-A-DTPA-HuM195 (0.5 to 20 mCi/kg) showed no effects of toxicity, but at 70 mCi/kg, two of three mice died within two weeks and a third mouse showed significant reductions in white blood cell counts. HL60 leukemia cell cytotoxicity assays showed dose- and specific activity-dependent killing. The radiolabelled HuM195 was 10-fold more potent against a CD33+ cell line vs. a CD33- cell line.

Clinical evaluation of (^{213}Bi) CHX-A-DTPA-HuM195 in humans is underway. The first patients treated received four doses of ^{213}Bi labeled HuM195; renal and liver functions are being monitored as are white blood cell and platelet counts. Additionally, imaging data and dosimetry modelling are currently evaluated. The drug is behaving as predicted from the preclinical data. No acute side-effects were observed and a significant anti-leukaemia effect was shown.

References

[1] R. Molinet, W. Janssens, C. Apostolidis, L. Koch, "Production of ^{225}Ac and ^{213}Bi for alpha-therapy", Extended abstract H-P2, NRC4, St. Malo, September 8 to 13, 1996.

[2] L. Koch, C. Apostolidis, R. Molinet, W. Janssens, J. Van Geel, "^{213}Bi for alpha-immuno-cancer therapy", RRAI 96, Abstract, page 67 Radioisotope and radiation application in industry and environment, Berlin, October 20 to 23 1996

[3] T.N. Nikula, M.R. McDevitt, C.Wu, R.W. Kozak, K. Garmestani, M.W. Brechbiel, M.J. Curcio, C.G. Pippin, L. Tiffany-Jones, R.D. Finn, M.W. Geerlings, C. Apostolidis, R. Molinet, O.A. Gansow, D.A. Scheinberg; "Alpha Particle Emitting Bismuth Cyclohexylbenzyl DTPA Constructs of Recombinant Humanized Anti-CD33 Antibodies for Therapy of Myeloid Leukemias" Submitted for publication.

[4] D.A. Weber, K.F. Eckerman, L.T. Dillman, J.C. Ryman in MIRD: Radionuclid Data and Decay Schemes, The Society of Nuclear Medicine, Inc. 1989.

[5] Zamora, K. Sass, A.S. Cardillo, C.R. Lambert, P. Budd, M.J. Marek, and B.A. Rhodes, "Affinity Thin-Layer Chromatography Test of the Immunoreactive Fraction of Radiolabeled Antibodies" Biotechniques **16**(2) (1994) 306.

2. Safety of Nuclear Fuels

Introduction

The work to investigate the safety of LWR nuclear fuels (including MOX fuel) at very high burn-up continued along the lines defined in the workschedules. Major emphasis was placed on four major areas:

- structural investigations and basic studies on simulated very high burn-up fuels, up to 200 GWd/tM were examined and compared with real high burn-up fuel to better understand the RIM effect formation processes.
- studies of high temperature properties of nuclear fuels including fission gas release and source term measurements.
- continuation of fuel performance code development for high burn-up fuel.
- determination of specific heat of UO_2 with burn-up of 3 and 8 a/o (SIMFUEL).

In addition, a new fabrication technique for the production of targets for transmutation and incineration experiments was successfully tested.

As in previous years, important results were obtained, evaluated and published within the reporting period.

2.1 Structural Investigations and Basic Studies on High Burn-up Fuel

2.1.1 Phase characterization of simulated high burn-up UO_2 fuel

The aim of this work is the study of the influence of the fission products concentration on the homogeneity range of the U_4O_9-type phase in the system U-FP-O that occur with increasing burn-up and increasingly oxidising conditions. The widening of this range at increasing burnups is assumed to be responsible for the observed delayed oxidation kinetics of spent fuels at low temperatures. On the other hand, the variation of the lattice constant of the fluorite phase, as well as the composition modification of the segregated phases, will be studied up to large dopant concentrations. The latter data are needed to characterize the structural modifications of the fuel at high burnups, specially at the pellet periphery of UO_2 fuels (outer rim) [1] and in the Pu-agglomerates of LWR MOX fuels.

The KORIGEN code was used to calculate the fission products inventories at the different burnups. For this purpose, 19 elements were considered, representing all major fission products except the volatile elements. In the present study, Pu was replaced by Ce, and Am and Cm by La. Thus, the selected dopants (Ce, La, Rb, Sr, Y, Zr, Mo, Ru, Rh, Pd, Ag, Ba, Pr, Nd, Sm, Eu) were added to fine UO_2 powder in the form of high purity oxides, using high energy planetary ball milling to achieve a good homogenisation and micronization of the mixture [2]. Pre-reaction treatment (to drive off volatile components and improve subsequent sintering properties) was done for 1 week at 1000 °C under air atmosphere. After granulation, stoichiometric pellets were produced by cold pressing and sintering under Ar-8% H_2 atmosphere at 1650 °C during 8 hours.

Fig. 2.1 shows the lattice parameter variation of UO_2 with the simulated burn-up in the range 0-200 GWd/tM (experimental data from the present work cover the range 100-200 GWd/tM with seven simulated fuel samples). In Fig. 2.1, also previous experimental data in the range 0-100 GWd/tM are given [3-6], as well as the limiting values calculated by the Vegard's law (ideal solution), considering 25% and 100% solubility of Zr [7]. As suggested by the curve, a stagnation in the lattice contraction seems to appear above 100 GWd/tM. The dependence of these data on sintering time and the real composition of the matrix is presently under study. In addition, samples with different O/M ratios at constant burn-up are being characterized by X-ray diffraction, in order to determine the limits of existence of the UO_{2+x} and U_4O_9-type phase fields as function of fission product concentration.

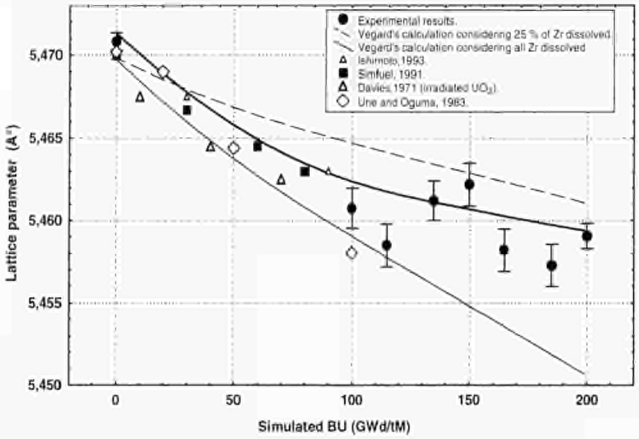

Fig. 2.1 Lattice parameter as a function of the simulated burn-up.

References

[1] J. Spino, K. Vennix, M. Coquerelle; Detailed characterization of the rim microstructure in PWR fuels in the burn-up range 40-67 GWd/tM; J. Nucl. Mater. **231** (1996) 179-190

[2] D. Warin, M. Bauer, M. Seiss, R. Lorenzelli; Mechanisms of dry ball milling in MOX fabrication. IAEA Technical Committee Meeting on Recycling of Plutonium and Uranium in Water Reactor Fuel. Newby Bridge, Windermere, U.K. 3-7 July 1995 (to be published)

[3] J.H. Davies, F.T. Ewart; The chemical effects composition changes in irradiated oxide fuel materials; J. Nucl. Mater. **41** (1971) 143-155

[4] P.G. Lucuta , B.J. Palmer, Hj. Matzke, I.J. Hastings; Preparation and characterization of Simfuel: Simulated CANDU high-burn-up nuclear fuel. Second national conference of CANDU, 1-5 Oct. 1989, Toronto, INIS-mf-13767 p. 132-146

[5] S. Ishimoto, M. Hirai , K. Ito, Y. Korei; Effects of soluble fission products on thermal conductivities of nuclear fuel pellets; J. Nucl. Sci. Techn. **31** (1994) 796-802

[6] U. Une, M. Oguma; Oxygen potential of UO2fuel simulating high burn-up; J. Nucl. Sci. Techn. **20** (1983) 844-851
[7] H. Kleykamp; The solubility of selected fission products in UO_2 and $(U,Pu)O_2$; J. Nucl. Mater. **206** (1993) 82-86

2.1.2 Formation of ion tracks in UO_2 induced by fast heavy ions

The slowing down of high energy heavy ions, i.e. fission products, is the main process for heat production in nuclear fuels of fission reactors. These energetic heavy ions create point defects and defect clusters along their path. Above a certain threshold of local energy deposition, tracks are formed which may be directly visible in Transmission Electron Microscopy (TEM). As shown in previous reports (TUAR-94, p. 37; TUAR-95, p. 72), heavy ions of high energy obtained from large accelerators can be used to investigate track formation in UO_2, thus avoiding the difficulty of large radiation fields as they are formed during reactor irradiation. Different ions (e.g. I, Cd, Sn, Xe and U) of different energy (72 to 2713 MeV) and hence different energy losses (29 to 60 keV/nm) were used to produce visible tracks, and the technique of cross-sectional TEM was developed and applied to UO_2, as described in TUAR-94 and TUAR-95.

In the reporting period, the first cross-sectional TEM ever made on UO_2 was successfully performed. Fig. 2.2 shows an example of the power of the technique.

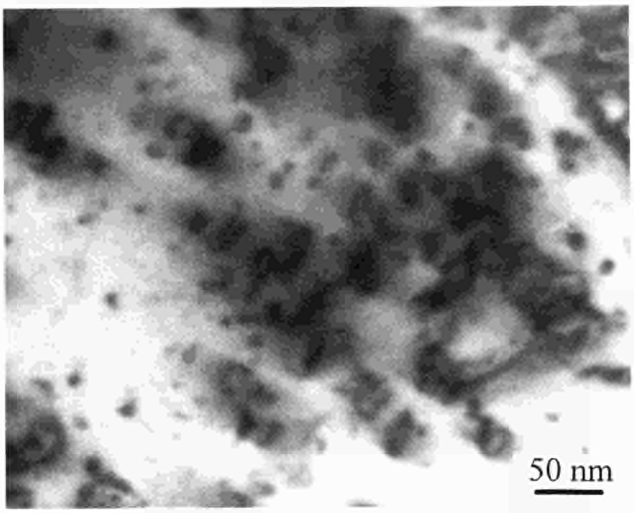

Fig. 2.2 Cross sectional transmission electron micrograph of ion-irradiated UO_2. The figure shows details of damage formation at a depth of 25 mm beneath the specimen surface.

The figure shows details (e.g. loop formation) of a thin area 25 μm below the surface onto which Cd ions of 1050 MeV energy were implanted. In the area shown, the remaining ion energy was 280 MeV. Note that in normal TEM either only the first ~ 0.1 μm at the surface or a poorly defined shallow depth of ~ 0.1 μm thickness can be analysed, whereas with the cross sectional microscopy available now a large depth interval of many μm can be examined on one specimen. Evaluation of these results have begun and the results will be reported in the next TUAR. In addition, more ion irradiated UO_2 specimens were investigated in conventional TEM, and a new thermal spike model was used to describe the track sizes, using known thermodynamic data of UO_2 and taking into account energy loss and velocity of the ions. First results were presented at an international conference in May 1996 [1].

The model used to calculate the radii of the observed tracks was that of Toulemonde et al. [2]. This model assumes that the energetic ions transfer their energy in a first step to the target electrons, and then to the lattice via electron-phonon interactions which may cause heating of the lattice. It is assumed that the effects of the electron-phonon coupling can be described by the parameter λ, the mean diffusion length of the energy deposited on the electrons [3]. Fig. 2.3 shows that the experimentally measured track radii are in good agreement with those calculated for a value of λ = 6 nm.

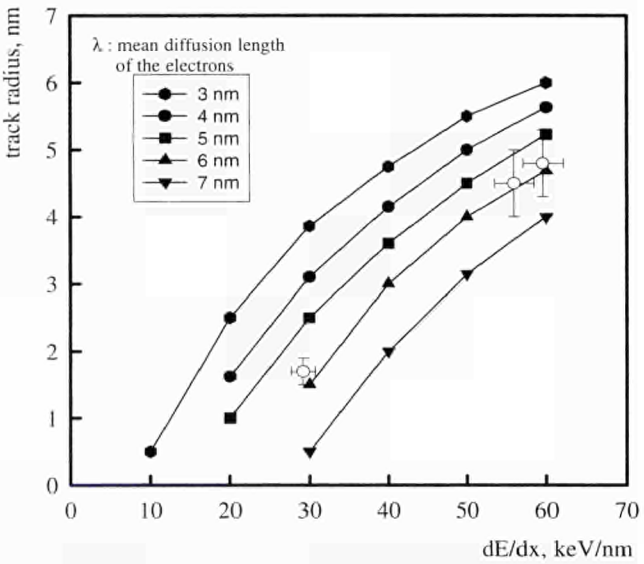

Fig. 2.3 Track radius vs. energy loss for UO_2, calculated with the model of Toulemonde et al. [2]. The lines and the full symbols correspond to different values of the mean diffusion length of the energy deposited on the electrons, while the open dots with error bars are the experimental data points.

This result can be used to calculate local lattice temperatures along the ion track as a function of time and radial distance from the ion path for UO_2 and given ions

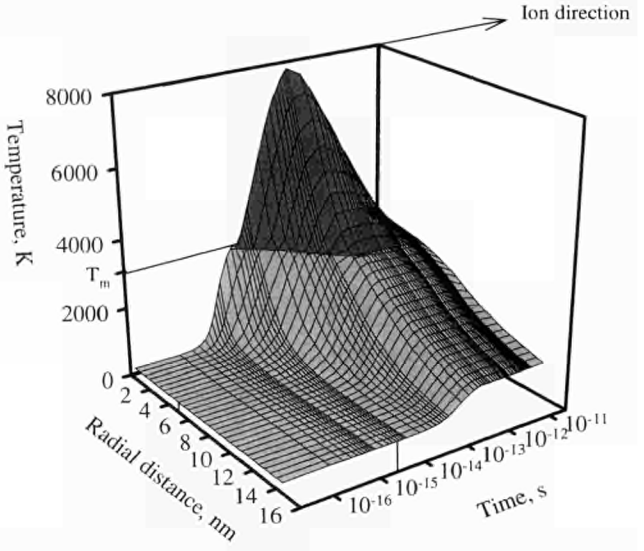

Fig. 2.4 Calculated evolution of the UO_2 radial temperature distribution along a track in UO_2 as a function of time. The calculations are for 11.4 MeV/u U ions in the first nm of the target, i.e. dE/dx_e = 60 keV/nm with λ = 6 nm.

of given energy. Fig. 2.4 shows the results for the track of a U-ion of 11.4 MeV/u displaying a large electronic energy loss of dE/dx_e = 60 keV/nm.

The peak temperature of the spike increases to its maximum value within a very short time of ~ 10^{-13} s and then it decreases and the spike broadens as a result of heat conduction. A similar calculation for 173 MeV Xe ions with dE/dx_e = 29.1 keV/nm also shows a good correlation between measured and calculated track radii, demonstrating, at least for the values of dE/dx studied here, that this model can be successfully applied to UO_2.

References

[1] T. Wiss, Hj. Matzke, C. Trautmann, M. Toulemonde, S. Klaumünzer; Nucl. Instr. and Meth. B **122** (1997) 583.
[2] M. Toulemonde, E. Paumier, C. Dufour; Rad. Eff. Sol. **126** (1993) 205.
[3] M. Toulemonde, J.M. Costantini, C. Dufour, A. Meftah, E. Paumier, F. Studer; Nucl. Instr. and Meth. B **116** (1996) 37.

2.1.3 Further observations on OCOM MOX Fuel: microstructure in the vicinity of the pellet rim and fuel-cladding interaction

The investigation of the in-pile behaviour of OCOM MOX fuel continued during 1996. The work carried out in the reporting period was mainly concerned with four questions.

1. Is the transformation of the MOX agglomerate microstructure similar to the microstructure changes seen at the surface of UO_2 fuel at high burn-up, and is the same mechanism involved?
2. Second, does the swelling of the MOX agglomerates at the pellet rim hinder cladding creep-down and increase fuel-cladding mechanical interaction?
3. Do the MOX agglomerates increase the oxidation rate of the cladding and if so is the oxide layer on the cladding inner surface in MOX fuel rods significantly thicker than in UO_2 fuel rods?
4. Since the burn-up in MOX fuel is concentrated in the Pu-rich agglomerates, does the high burn-up structure (rim effect) in the UO_2 matrix form at a higher pellet burn-up than in UO_2 fuel?

The study was carried out using mainly Quantimet, SEM and EPMA results from the same two MOX fuel segments previously used in the investigation of the effects of fuel inhomogeneity on fission gas and caesium release levels (see TUSR-95, p. 75). One segment contained OCOM 15 fuel; the other OCOM 30 fuel. Both segments were irradiated to a burn-up of about 44 GWd/tM under normal PWR conditions in the KWO reactor at Obrigheim in Germany.

It was confirmed that the MOX agglomerates in the outer low temperature region of OCOM fuel share several common features with the high burn-up structure at the rim of conventional UO_2 fuel. These common features include a small grain size, a high density of small faceted pores and strong xenon depletion (see Tab. 2.1).

Tab. 2.1 Similarities between MOX agglomerates and the high burn-up structure at the rim of conventional UO_2 fuel.

Characteristic	MOX agglomerate (OCOM 30)	High burn-up structure in UO_2 fuel
Mean grain size (μm)	1.5 ± 0.7 a)	0.3 ± 0.2 b)
Porosity (%)	20 - 30	15 - 17 b)
Pore size (μm)	1.3 - 1.5	1.1 - 1.2 b)
Xe retention (w/o)	≤ 0.5	~ 0.25 c)
Cs retention (w/o)	~ 100	~ 100 d)

The data for Xe and Cs retention are from EPMA measurements; i.e., they refer not to the concentration retained in the structure as a whole, but in the UO_2 or mixed oxide lattice.
a) Measured on a agglomerate at a magnification of 1100X using the linear intercept method.
b) J. Spino et al., ref. [1]
c) K. Lassmann et al., ref. [2]
d) C. Walker et al., ref. [3]

Such similarities are taken as a powerful indication that in both cases the mechanism producing the characteristic microstructure is the same. This mechanism is identified as recrystallisation, probably induced by the accumulation of irradiation damage, and an attendant increase in the strain energy in the lattice [4]. Further, it was found that the magnitude of cladding creepdown and the level of fuel-cladding mechanical interaction in OCOM fuel is not significantly different to that found in conventional UO_2 fuel. Although surface MOX agglomerates protrude into the gap they do not noticeably retard cladding creepdown.

OCOM fuel pellets undergo similar dimensional changes to UO_2 fuel pellets. The swelling of surface agglomerates is small compared with the fuel pellet diameter (Fig. 2.5).

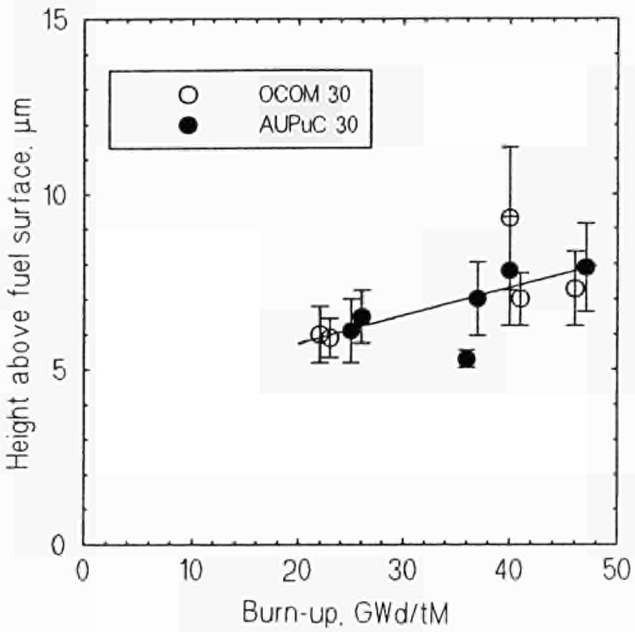

Fig. 2.5 Growth of surface MOX agglomerates into the gap under conditions of weak fuel-cladding mechanical interaction.

Moreover, it appears that when hard fuel matrix-cladding contact occurs, the contracting cladding is able to push the swollen agglomerates back into the fuel (see Fig. 2.6).

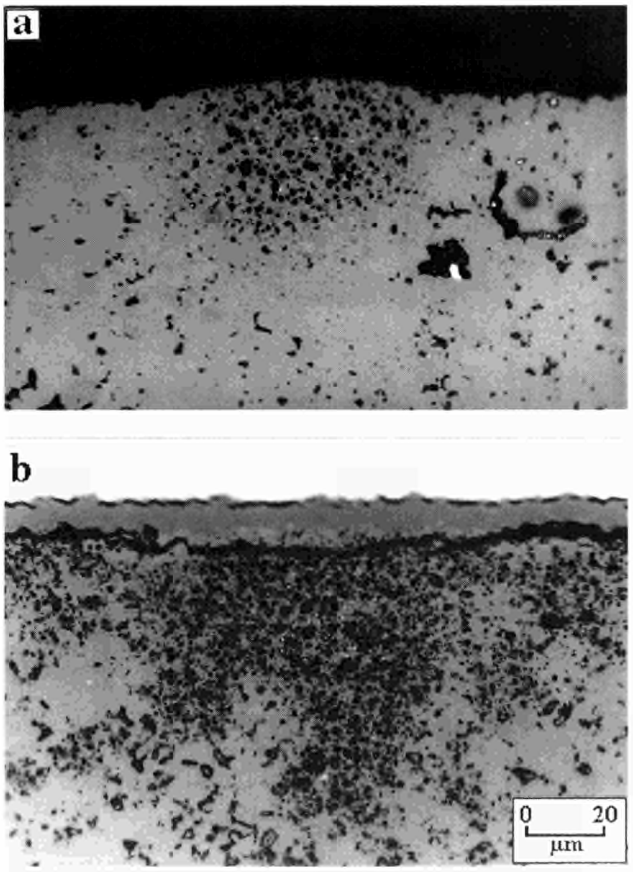

Fig. 2.6 Optical micrographs showing MOX agglomerates at the surface of OCOM pellets.
a) at a burn-up of 21.0 GWd/tM; b) at 44.5 GWd/tM. At the lower burn-up the MOX agglomerate distends into the gap, whereas at the higher burn-up it has been pressed into the fuel.

It was also established that the mean thickness of the oxide layer on the inner cladding surface in OCOM fuel rods does not differ significantly from that found in conventional UO_2 fuel rods of similar design. Nevertheless, it would appear that the oxide is thicker at points where contact with surface MOX agglomerates had occurred (see Fig. 2.7).

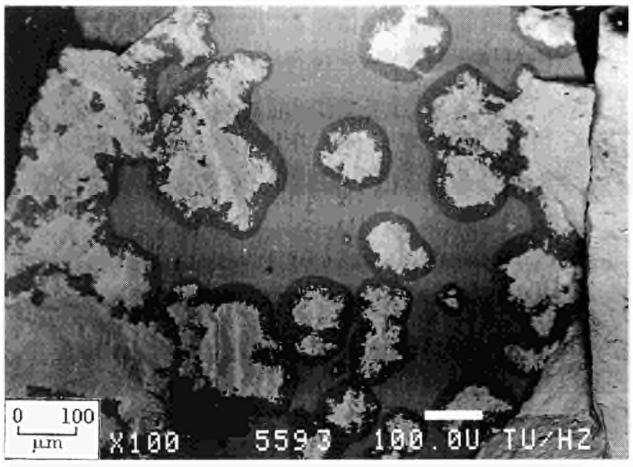

Fig. 2.7 SEM micrograph showing marks on the cladding inner surface caused by raised MOX agglomerates on the fuel pellet surface. OCOM 30 fuel rod. Pellet burn-up 44.5 GWd/tM.

Increased oxidation of the zircaloy cladding takes place at such locations, because the MOX agglomerates which have a high burn-up are more oxidising than the surrounding UO_2 matrix.

As to the formation of the high burn-up structure in the UO_2 matrix of OCOM fuel, it is judged that this will form once the threshold burn-up is exceeded. As in conventional UO_2 fuel this presumably lies in the range 60 to 80 GWd/tM [2,5]. Accordingly, it is the magnitude of the local burn-up at the pellet rim that determines whether the high burn-up structure forms. This in turn, is mainly governed by the amount of fissile material in the UO_2 matrix; that is, by the level of uranium enrichment and by the amount of MOX fuel scrap added during pellet fabrication. In conventional UO_2 fuel, a local burn-up of around 60 GWd/tM is normally obtained at the fuel rim when the pellet burn-up reaches about 45 GWd/tM. Limiting the MOX scrap addition will delay the formation of the high burn-up structure.

References

[1] J. Spino, C. Vennix, M. Coquerelle; J. Nucl. Mater. **231** (1996) 179
[2] K. Lassman, C.T. Walker, J. van de Laar and F. Lindström; J. Nucl. Mater. **226** (1995) 1
[3] C.T. Walker, W. Goll, T. Matsumura; J. Nucl. Mater **228** (1996) 8
[4] K. Nogita, K. Une; J. Nucl. Mater. **226** (1995) 302
[5] T. Kamayema, T. Matsumura and M. Kinoshita, Proc. Int. Topical Meeting on LWR Fuel Performance: Fuel for the 90's, Avignon, France, 1991, Vol. 2 p. 620

2.2 Studies of High Temperature Properties of Nuclear Fuels

2.2.1 LAF-2: A project for simultaneous measurement of heat capacity and thermal diffusivity up to very high temperatures

Introduction

In the previous annual report (TUAR-95, p. 90) we reported the results of a feasibility study for an experiment in which a sample, in the form of a thin disk, is heated up to high temperatures by two continuous-wave (CW) laser beams impinging onto the two basal surfaces. An additional short laser pulse of low intensity is then applied on the "front" surface of the disk, and the resulting thermal perturbation is recorded by measuring the transient temperature on both the front and back surface. The aim of the experiment is to deduce, from the temperature pulse analysis both the phenomenological heat transport coefficient (diffusivity) and the specific heat.

It should be mentioned that such a measurement was envisaged soon after the "temperature-flash" technique was introduced in 1961. Through the progress of laser technology and fast pyrometry, the flash-method became more and more precise and reliable. Nevertheless, for nearly three decades, the extension of this technique to calorimetric measurements was considered as unpracticable.

Only at the end of the 80's in the Institute of Technology of the Jet Propulsion Laboratory, Pasadena [1], was a flash-method successfully applied, using a xenon lamp, for heat capacity measurements up to 1300 K. The method was, however, based on a comparative empirical procedure, using POCO AXM-5Q graphite as a standard; moreover, the sample had to be sputtered with graphite in order to ensure the same energy absorbivity as in the standard. The weak point of this method was the sensitivity of the measurements to the sample positioning within the light beam.

In 1990, in the National Laboratory of Metrology of Ibaraki (Japan) [2], a feasibility study was positively concluded, in which a "Laser-Flash" device was used to measure heat capacity. Again, a comparative method was chosen, whereby, thanks to the homogeneity of the laser beam used, the standard sample was now permanently mounted in a separate holder, in order to avoid position misadjustments. In this set-up the standard sample was essentially acting as a simple reference calorimeter.

It should be noted that in both cases an essential limitation of the applied methods is set by the heat losses, which may be different in the standard and in the measured sample, and cause large systematic errors. A correction is to a certain extent possible. It requires, however, a rather complicated mathematical procedure which practically annuls the advantages offered by the simplicity of the comparative method.

This was the state of the art when our project started in March 1996.

The new setup

The constructed apparatus is shown in Figs. 2.8a,b.

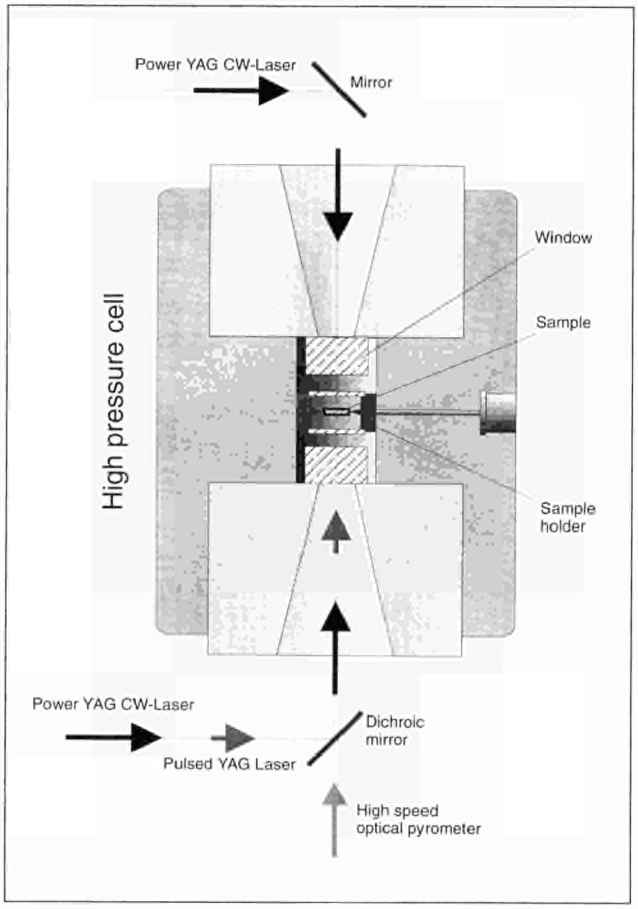

Fig. 2.8b The new CLASH autoclave.

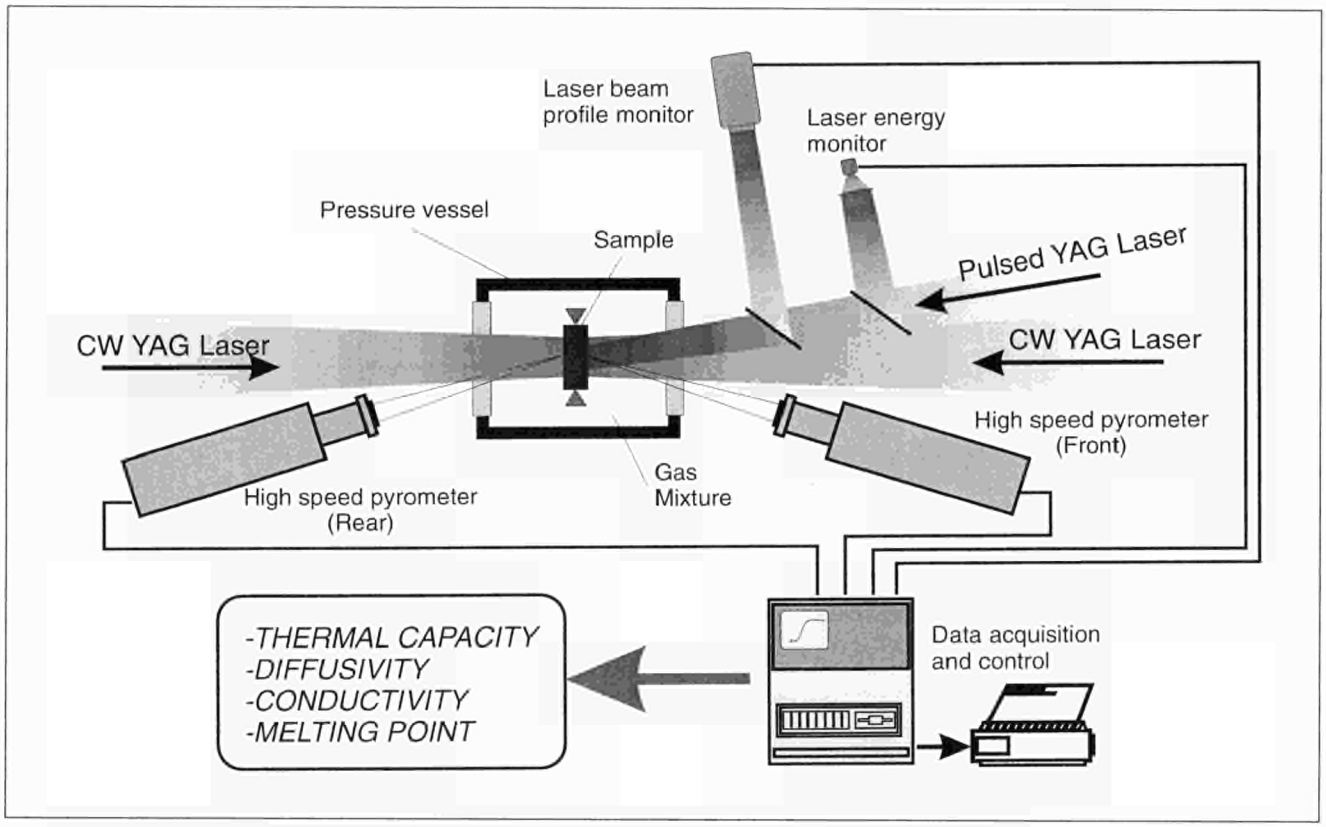

Fig. 2.8a Scheme of the CLASH setup for the measurement of the heat capacity at very high temperatures.

The sample, in the form of a disk of 5 mm diameter and approximately 0.5 mm thickness, is held by a three-pin mounting in a small autoclave. Two opposing CW Nd-YAG laser beams (of 300 W total power) heat the two faces of the sample up to the pre-established conditioning temperature. This is detected and recorded on the front face of the disk by a rapid and very precise pyrometer (with risetime of the order of 10 μs and sensitivity of better than 0.1 K).

Thanks to the almost flat radial profile of the two laser beams (Fig. 2.9), and to their stability in time, a homogeneous and constant sample temperature can be achieved within a few tens of seconds.

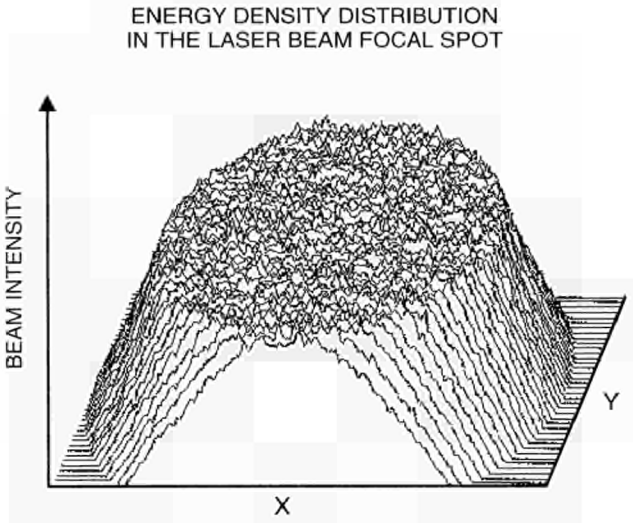

Fig. 2.9 Spatial power distribution of the CLASH probe-laser. The central region of the beam with almost constant specific power is used for the pulse.

A temperature pulse is then applied on the front face of the sample with another YAG laser. This pulse is normally of 1-2 ms duration, with a deposited energy of the order of less than 0.5 J. This laser beam has also an almost constant radial profile, so that the produced perturbation is very homogeneous.

The front-face temperature pulse is detected above the existing thermal radiation background by the above mentioned pyrometer with a time resolution sufficient to provide several thousand measurements during the onset and decay of the flash perturbation.

In addition, a second high-speed pyrometer views the rear face of the sample with a small field stop aperture (0.3 mm diameter), pointing at the central area of the specimen surface. The off-set of this pyrometer is previously compensated for the background temperature signal in order to detect the arrival of the thermal perturbation on the rear face of the sample with the best achievable accuracy (0.05 K).

The front- and rear-temperatures, the compensated rear-surface perturbation, and the laser energy, are recorded by a 12-bit/four channels transient digitiser, and then transmitted to a computer interface.

Parallel to the transient temperature measurement, the power of the pulsed laser beam is measured and recorded as a function of time. The integrated energy is measured by a photodetector, to which a precisely pre-fixed fraction of the laser beam impinging on the sample is sent through a partially reflecting mirror. The photodetector was previously calibrated with a calorimeter. The surface power absorbed by the sample during the pulse is then calculated from the (measured) optical absorbivity of the sample at the wavelength of the Nd-YAG laser.

Model and analytical procedure

Given the measured temperature pulse, both the thermal diffusivity, a, and the heat capacity of the sample, C_p, can be evaluated from an appropriate function of time, t, and spatial co-ordinates, r and z, which realistically describes the examined pulse. Since the measured values of a and C_p are related to the primary empirical data through a theoretical model, the quality of the final results depends both on the measurement accuracy of the transient temperature and on the confidence limits of the model.

The assumed theoretical expression of the temperature evolution in the sample corresponds to the general integral of the diffusion equation of a surface temperature perturbation into a disk, under the following restrictions:

- The applied pulse, as well as the geometrical and physical properties of the sample are axially symmetrical.
- The sample heat losses from the two basal surfaces are purely radiative.
- The heat losses from the lateral surface are either radiative or conductive, and are in both cases homogeneous.

On the other side, important features are allowed and correctly taken into account:

- The laser pulse may have an arbitrary length, with intensity evolving with time.
- The (cylindrical) radial profile of the laser beam is arbitrary.
- The Biot numbers, which represent the ratio of the heat radiated into vacuum to that diffusing into the sample, may be different on the front and on the rear surface.
- The ratio of the sample and the laser beam diameter is arbitrary.

The expression of the temperature function T=T(t,r,z) in the sample and, in particular on the front and rear surfaces is rather complicated but can be evaluated numerically with sufficient precision. This function depends on parameters which represent the applied perturbation and the sample properties. The former are provided by experimental measurements. The latter can be reduced to a set of five quantities whose magnitude *a priori* is to be considered as unknown, these are:

1. Thermal diffusivity of the sample
2. Heat capacity
3. Front surface Biot number
4. Rear surface Biot number
5. Lateral Biot number

The analysis applied consists of a least-squares minimisation of the difference between the calculated and measured temperatures, by a simultaneous optimisation of the above mentioned parameters.

Though theoretically feasible, the difficulty of such a numerical procedure is evident. In fact, the effectiveness of the multi-parameter fitting is in our case secured by the following conditions or prerequisites:

- First, the two parameters, a and C_p, are mathematically by far more influential than the Biot numbers and the effective laser spot radius.
- Second, the accuracy of the temperature measurements in the reported set-up is very high, and a large number of experimental points are available.
- Third, the Biot numbers (parameters 3,4 and 5) are correlated, at least theoretically, so that in cases where the two previous conditions do not suffice to obtain a significant determination of all of them, these relationships can be used to reduce the number of unknowns from a maximum of five to a minimum of three.

Finally, a comprehensive error analysis enables one to establish confidence levels of the fitted parameters, in particular of a and C_p.

The method, applied to various refractory materials up to temperatures above 3000 K, proved to be very powerful and accurate. An example is reported in the following section.

Heat capacity measurement of POCO graphite

Heat capacity test-measurements were performed on POCO AXM-5Q graphite samples – a recommended standard material. The results of a single shot fitting are reported in Fig. 2.10.

The resulting parameters, reported in the legend, show that the accuracy is excellent, being approximately 1% and 3% for the thermal diffusivity and heat capacity respectively, and 5% for the heat losses. To these errors one must add the uncertainty of the effective specimen thickness and that related to the evaluation of the input energy from the independent measurements of laser energy, time and space profiles of the laser beam, and sample absorbivity. These errors are larger than the fitting error, and are mainly responsible for the observed scatter of the results.

The measured heat capacity and thermal conductivity from 1800 to 3200 K are shown in Figs. 2.11a-c.

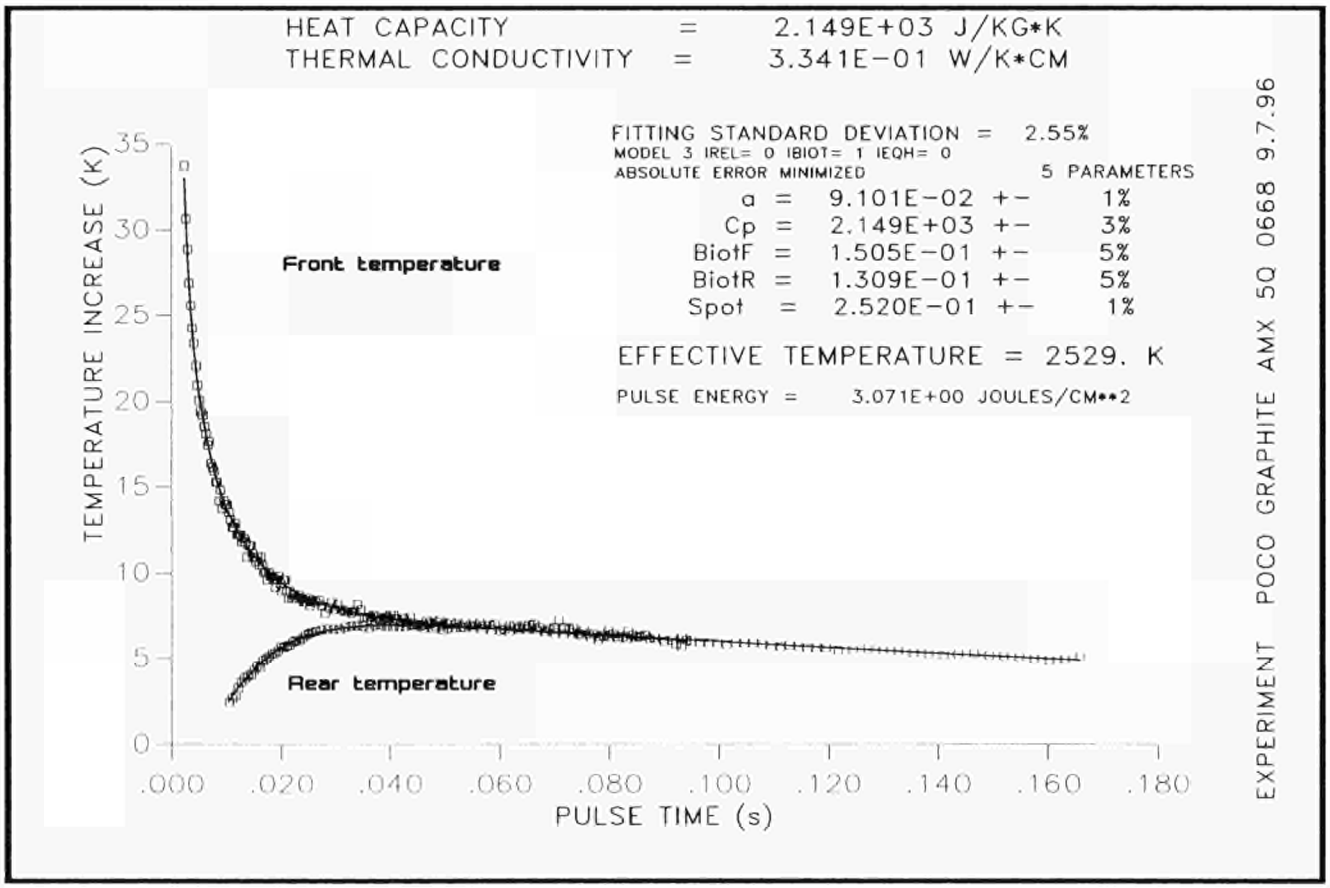

Fig. 2.10 Recorded temperature on the rear and front surfaces of the disk, and fitting curve calculated from the theoretical model. The fitting parameters are listed in the legend.

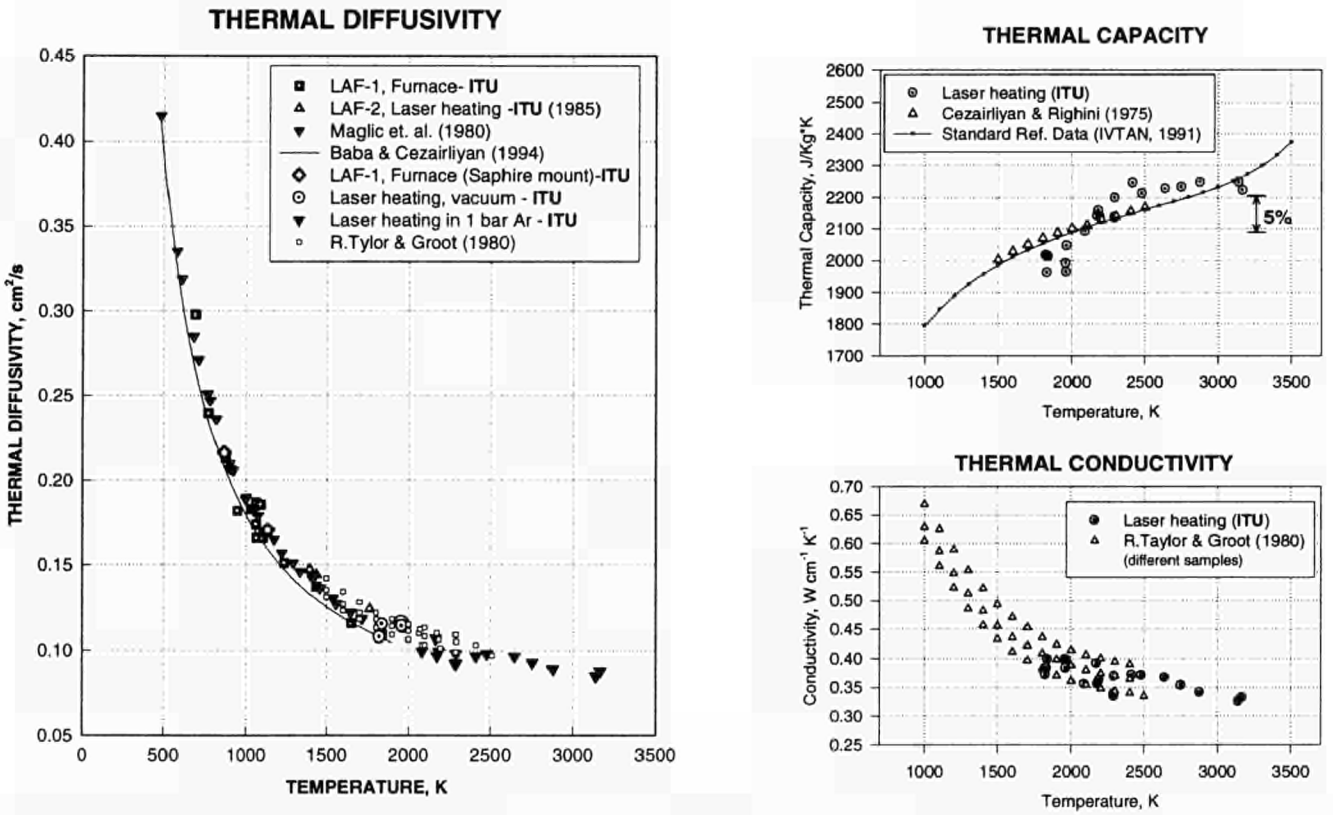

Fig. 2.11a-c Thermal diffusivity, thermal capacity and thermal conductivity of standard POCO AMX-5Q graphite measured with the CLASH setup.

The recommended heat capacity versus temperature curves [3,4] provide the "best values" obtained from selected datasets (for this reason these points are well aligned on the respective spline functions). The conductivity data by Taylor and Groot [5] are given for three different samples, whereby each dataset was separately smoothed. Therefore, the dispersion of these points represents the effective accuracy of the data.

On the other side, the points corresponding to our measurements refer to direct, single measurements. It can be seen that these measurements fall within the uncertainty band of the recommended values.

Other tests have been also carried out with urania samples, whose heat capacity is sufficiently well defined up to 2500 K. The results of these tests, which are not reported here, were also very satisfactory.

References

[1] J.W. Vandersande, A. Zoltan, C. Wood; Int. J. Thermophys. **10** (1989) 251-257

[2] T. Baba; Proc. of the 11th Japan Symposium on Thermophysical Properties, Tokyo, Nov. 6-8, 1990, p. 449-452

[3] A. Cezairliyan, F. Righini; Rev. Int. Hautes Temp. Refract. **12** (1971) 124-131

[4] G.A. Bergman et al., State Bureau of Standard Reference Data, GSSSD 25-90, USSR Committee for Quality of Products, Moscow (1991)

[5] R. Taylor, H. Groot; High Temp.- High Pressures **12** (1980) 147-160

2.2.2 Fission product effusion from high burnup LWR fuel

The study of effusion and release of fission products (FP) from irradiated fuel heated in a Knudsen Cell continued. KWU fuel, irradiated in an LWR up to 67.000 MWd/tHM (1567full-power days) was analysed (rod AF-D2).

These measurements provide a direct evidence on the limits of FP retention in case of in-pile temperature excursions, as well as indications on the state of the FP in the fuel at end-of-life.

In TUAR-95 the results of FP effusion measurements on a similar fuel (KWU-10B2, irradiated to ≈60 GWd/tHM) were reported in detail, and the main characteristic features of the observed FP release stages were discussed. At that time, the samples mounted in the Knudsen Cell were rudimentarily obtained from a fuel rod cross section in the form of rather large (1-2 mm) broken chips. This time one pellet was extracted from the fuel pin, and dry-milled on a micrometric bench. Samples in the form of a coarse powder were finally obtained from the periphery (excluding the rim) and the centre of the pellet, respectively, and mounted in different tungsten cells internally clad with ThO_2.

The samples were submitted to isochronal annealings up to 2300 K, and the effusing vapours measured by mass spectrometry. Almost all fission products and fuel constituents were progressively vapourised and detected until exhaustion.

Results

Stoichiometry

The sample stoichiometry was evaluated from the ratios of the partial pressures of the uranium-bearing species (Fig. 2.12), detectable above 1750 K. At this temperature the samples were effectively stoichiometric but a tendency to reduction was observed at higher temperatures.

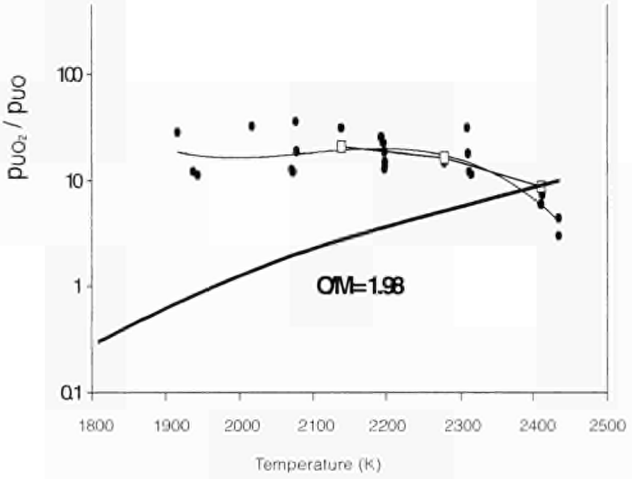

Fig. 2.12 Variation of the ratio p_{UO_2}/p_{UO} of the fuel as a function of the absolute temperature, T.

Tellurium-Iodine-Xenon-Caesium-Barium

The release of this important FP radionuclide chain was investigated. Effusion of these elements from the Knudsen cell takes place in three stages: a low-temperature stage (I) involving grain boundary diffusion and restructuring, an intermediate stage (II) in the range 1600-2000 K dominated by bulk diffusion, and a high-temperature stage in which effusion is governed only by evaporation (see TUAR-95, p. 95). The analysis of the measured effusion rate, in conjunction with that of diffusion in the bulk of the sample [1] enables the typical parameters of each stage to be obtained for all the detected nuclides, although only stage III can be interpreted in terms of the equilibrium vapour pressure of the measured species.

Some relevant new effects were observed :

a) Less volatile and chemically reactive elements like Ba exhibit the same fractional release curve as in the, previously examined, low burnup fuel of BR3 (se TUAR-94, p. 75). Xenon and caesium, however, show a much more pronounced fractional release, F(T), at low temperatures (Fig. 2.13).

For instance, in stage I, F (1500 K) for ^{136}Xe was of the order of 0.1 to 0.4, against 0.01 measured in the BR3 fuel. This effect is typical for LWR fuels. Therefore, in the simplest diffusion/release models (which predict independence of function F=F(T) on burnup) the diffusion enthalpy is often empirically reduced with increasing burnup to account for the enhancement of F. Yet, in our measurements the diffusion enthalpy in the high burnup samples remains quite high (100 kcal/mole in stage II and approximately 45 kcal/mole in stage I), indicating that the energy barrier of the elementary

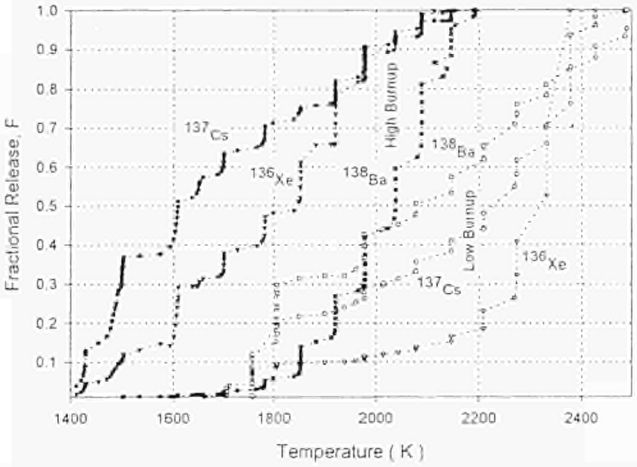

Fig. 2.13 Fractional release of ^{138}Ba, ^{137}Cs and ^{136}Xe as a function of temperature for high burnup KWU fuel and low burnup BR3fuel (open symbols).

atomic jumps is not greatly affected by the irradiation. Therefore, the effect of burnup on F(T) is likely caused by an increase of the entropy factor (e.g. by the presence of a higher concentration of defects). It is finally worth noting that the burnup enhancement is maximum for rare gas, less marked for caesium, and almost negligible for barium. This confirms that the last element, though rather mobile in UO_2 (at low burnups it is released at lower temperatures than xenon), displays a well defined vaporisation rate which is likely due to formation of stable BaO (T_m=2246 K), whose equilibrium partial pressure at 1700 K (p_{BaO}=4.10^{-6} bar) corresponds indeed to our detection limit.

b) Comparing the release in the peripheral and central samples (Fig. 2.14a,b) one can see that in the former, caesium and xenon have a more pronounced stage I, with a completion fractional release value approximately five times larger than in the latter.

   The difference in release of barium is less important, stage I involving only 1% of the barium inventory, the massive release starting only at temperature above 1600 K.

c) The release of xenon in the central sample exhibits at low temperature (1500 K) a peak composed of the sole ^{131}Xe isotope (Fig. 2.15), whilst in the release stages at higher temperatures all the other isotopes are present with the expected compositions. The absence of a gross rare-gas release at this stage is also confirmed by the measured rate of β-activity (mostly due to ^{85}Kr) of the exhausting gases. The preferential release of this isotope is, however, not observed in the peripheral sample.

In fact, ^{131}Xe has as parent nuclide ^{131}I, whose half-life (8 d) is sufficiently long to enable this iodine isotope to freely diffuse to the grain boundaries before decaying into xenon. This is confirmed by the presence of a release peak of the long-lived ^{129}I at the same temperature. Therefore, it can be inferred that during irradiation, in the central pellet region, iodine was to a large extent segregated at the grain boundaries.

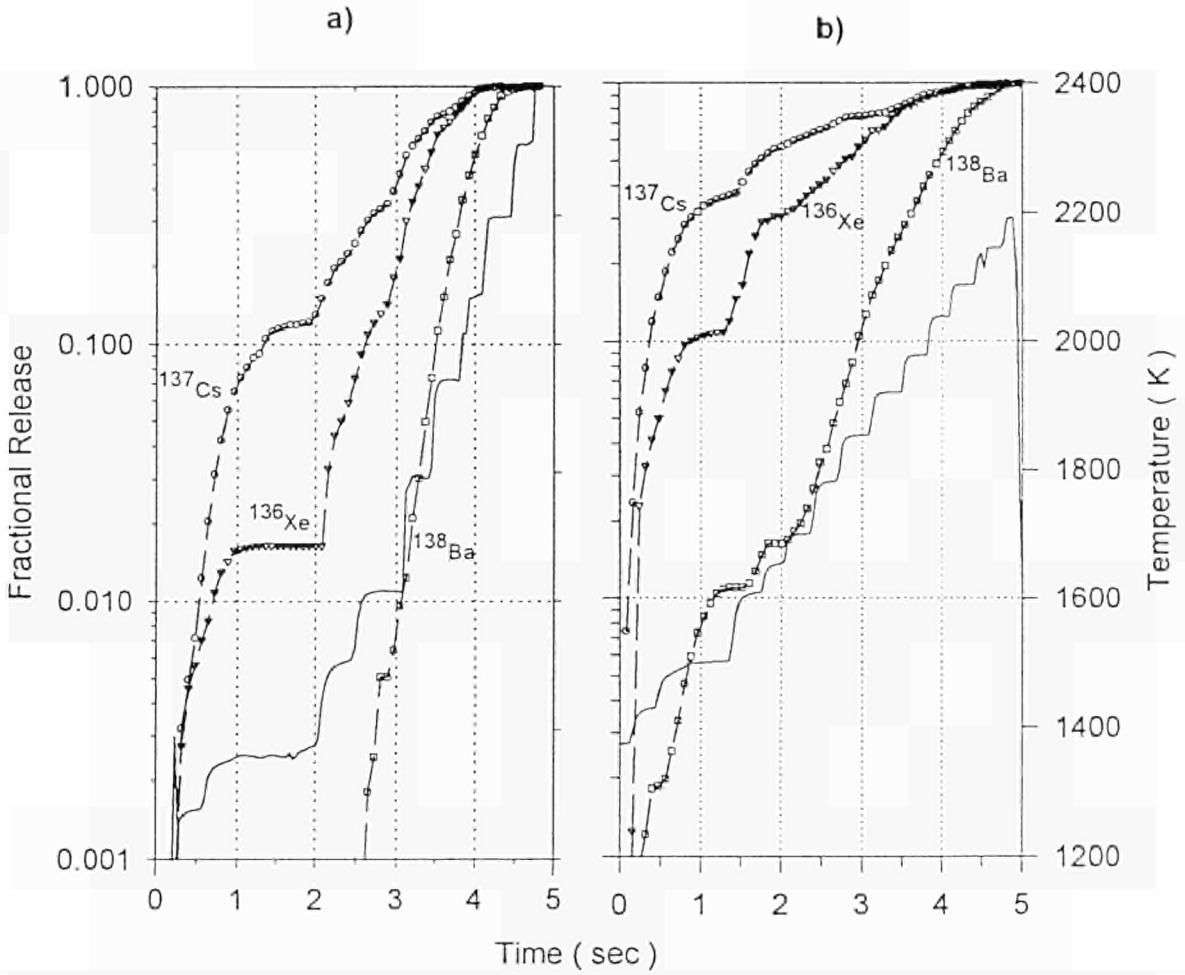

Fig. 2.14a,b Comparison of the fractional release of ^{138}Ba, ^{137}Cs and ^{136}Xe as a function of temperature for a peripheral (a) and a central (b) sample of a high burnup KWU fuel.

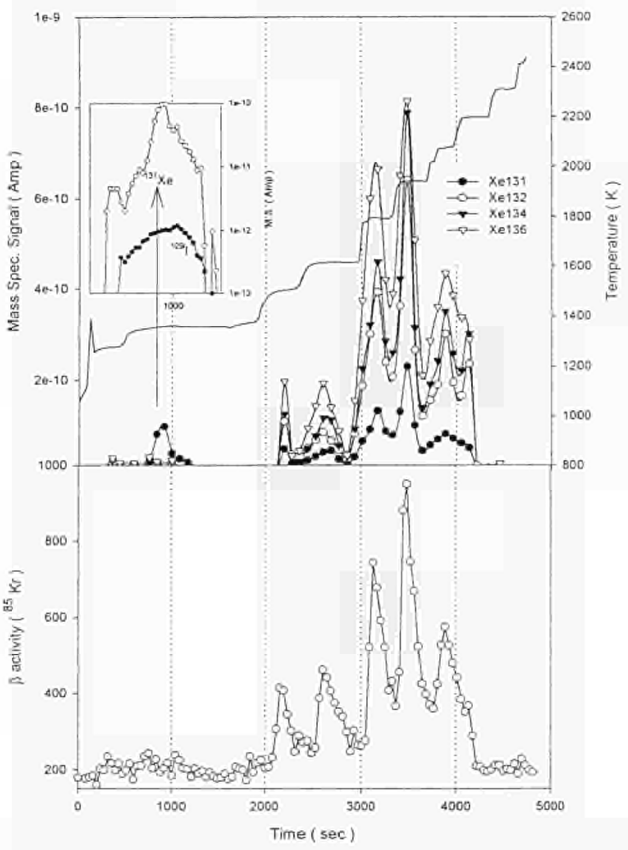

Fig. 2.15 Release of xenon measured by Mass Spectrometry and of ^{85}Kr measured by beta counting; comparison of the low temperature effusion peak of ^{131}Xe with ^{129}I, for a KWU sample from the central region of fuel.

It should be noted that in the peripheral pellet region, the release of both ^{129}I and ^{127}I (Fig. 2.16) exhibits also a two-stage mechanism, with a low temperature peak at 1500 K ; but in this region ^{131}Xe, formed from intragranular decay of iodine, is trapped by point defects, and hence is obliged to follow the same diffusion route as the other xenon isotopes.

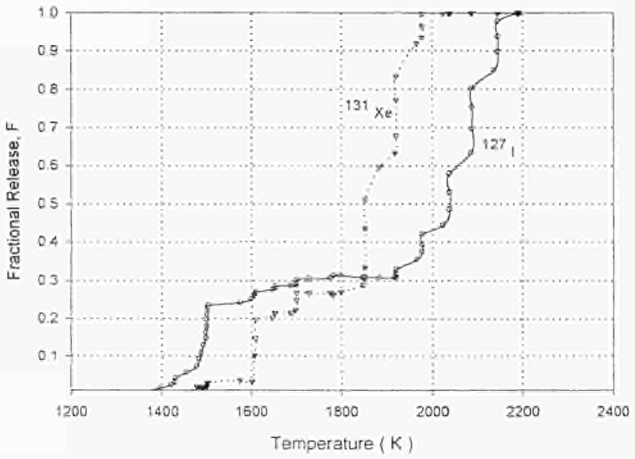

Fig. 2.16 Fractional Release of ^{127}I and ^{131}Xe as a function of temperature for a high burnup KWU fuel.

d) As for the possible presence of CsI, a correlation between caesium and iodine release was not found.

Negative evidence was also provided by the absence, both in the central and peripheral samples, of particular effects at 1670 K, the dissociation temperature of CsI.

Release of caesium becomes detectable at temperatures above 1400 K and comes almost to completion below 2050 K, the onset temperature of stage III. As mentioned above, the release is more rapid in the peripheral than in the central pellet region – the respective fractional release curves are shown in Fig. 2.14.

On the other hand, the second massive iodine release occurs at much higher temperatures during stage III, involving, probably, atoms which have been trapped in the intragranular bubbles formed during annealing.

A complete analysis of all measured effusion rates and of their mutual relations, dealing with approximately 50 nuclides, is being carried out based on various comparative schemes, using databases as well as an adequate statistical analysis. The work is in progress for further measurements and physical interpretation of the data

References

[1] F. Capone, J.-P. Hiernaut, M. Martellenghi, C. Ronchi; "Mass Spectrometric Measurements of Fission product Effusion from Irradiated LWR Fuel", Nucl. Sc. & Eng. **124** (1996) 436-454

2.3 The Fuel Performance Code TRANSURANUS

Introduction

TRANSURANUS is a computer program for the thermal and mechanical analysis of fuel rods in nuclear reactors which has been developed at the Institute [1]. It is fully described in the literature and has been outlined in previous Annual Reports. The code is in use in several European organisations, both in research and private industry. In 1996, the TRANSURANUS code and the related know-how was released to eight Eastern Countries (Armenia, Bulgaria, Czech Republic, Hungary, Poland, Romania, Slovak Republic and Ukraine) within the Regional Technical Co-operation Project RER/4/012 of the IAEA. One further contract was signed within the PHARE Programme with the Czech Republic.

Verification work

Extensive verification work was done in 1996. Here, only the verification work of the TRANSURANUS WWER version is outlined.

Validation of TRANSURANUS against WWER data

WWER reactors are PWR's of Russian origin and design. The fuel for these reactors, 440 MW or 1000 MW units, has special features compared to LWR fuel. The cladding material and the centre hole in the pellets are the most outstanding differences influencing the behaviour of individual rods. The conditions in WWER-440 reactors, coolant temperature (312 °C max.) and pressure (12.5 MPa) are not as severe as in Western PWR's. In WWER-1000 reactors, however, the conditions do not differ significantly from the corresponding ones in 1000 MW PWR's.

Some earlier predictions of the in-pile behaviour of WWER -type fuel rods by the TRANSURANUS code have been reported [2]. After these preliminary trials several data cases on experimental and power reactor WWER fuel were made available through the OECD/NEA data base. The evaluation of the performance of TRANSURANUS in calculating these cases is an important step in the development of a specific WWER version. The first results of the currently on-going validation work against these data have been obtained.

The data from the so-called SOFIT-programme included fuel centre temperature measurements from eight experimental rodlets of WWER type. Detailed pre-characterization data and irradiation histories of these rodlets were available. Rods with small (~150 μm), medium (~200 μm) and large (~270 μm) pellet – cladding gap width were involved. The gap sizes were within the specification tolerances of WWER-440fuel. The fuel density was characteristic of sintered WWER pellets (96–97% of T.D.). Also the other rod parameters, except the rod length, corresponded to the ones encountered in power reactor WWER rods.

Power histories

The irradiation of the rods lasted 160 days in the SOFIT-1.1 and 78 days in the SOFIT-1.3 experiment. The maximum linear heat rates varied between 34 and 45 kW/m. Due to the relatively short irradiation time the maximum local burnup was only about 16 GWd/tU. The assembly power was determined calorimetrically by measuring the coolant mass flow rate and the temperature increase in the flow channel. The axial power profile in SOFIT-1.1 experiment was measured by axially positioned neutron detectors, but for SOFIT-1.3 it was only approximated. The experience from SOFIT-1.1 showed that the shape of the axial power distribution under the conditions prevailing in the research reactor changed within quite short time intervals. The obvious uncertainty in the determination of the local linear heat rating of the SOFIT-1.3 rods was the reason for excluding those temperature data from the evaluation.

Models used

WWER specific pellet and cladding material properties, and models were utilised in the calculations whenever available and incorporated into TRANSURANUS. A correlation of fuel thermal conductivity developed for WWER fuel was used, although it was practically similar to many Western LWR correlations. Elastic modulus and Poisson ratio of WWER cladding material were also applied. A WWER specific correlation, obtained from the literature and programmed into the code, was used for cladding creep. Otherwise, standard Transuranus

models were used. A new relocation model was used to give better heat rate and burnup dependency at the beginning of the irradiation.

Results

The results of the thermal analysis for the very first rise to power have been reported in [3]. Some peculiarities in the coolant conditions during the heating made the interpretation of the data difficult, but in general the code was able to reproduce the measured temperature versus linear heat behaviour reliably. This is seen clearly in Fig. 2.17, where the calculated temperatures are plotted in terms of the measured ones.

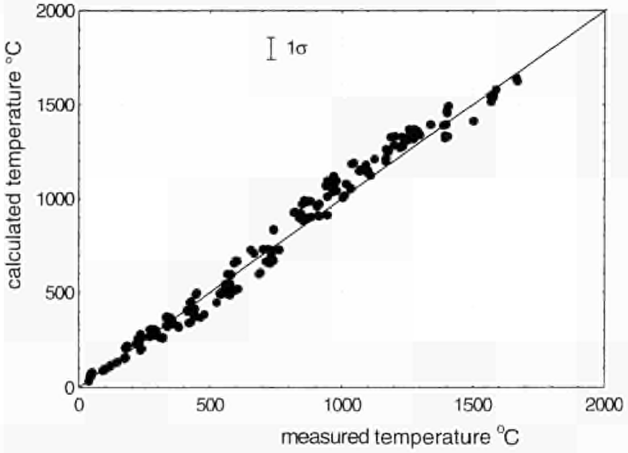

Fig. 2.17 Calculated versus measured temperatures of SOFIT-1.1 rods at the first rise to power (6 rods).

The verification of TRANSURANUS against the long term irradiation data from SOFIT experiments have also been published [4]. Because of thermocouples failed the available temperature data are in most cases limited to burnups below 10 GWd/tU. Nevertheless, valuable information was gained on the current performance of the code in predicting WWER fuel behaviour. The maximum fuel centre temperatures were in, or a little above, the range for typical LWR fuel (1200–1500 °C depending on gap size and heat rating). The feedback effect of the fission gas release on the fuel temperatures was insignificant, since the relatively low burnups did not allow a large amount of gas to be released and, in addition, the helium pre-pressurisation of the rods acted as a barrier against strong feedback. The calculated long term temperatures versus the measured ones are plotted in Fig. 2.18. Statistical analysis showed that the obtained deviation between the calculated and measured temperatures can be explained by assuming reasonable tolerances for a few important input parameters.

Future development

The current activities in improving the performance of TRANSURANUS to predict the behaviour of WWER fuel include evaluation of cladding creep down, fission gas release and clad axial swelling. These studies are carried out in co-operation with the Institute for Nuclear Research and Nuclear Energy in Bulgaria within the frame of the PHARE 92-94 programme. Data from high

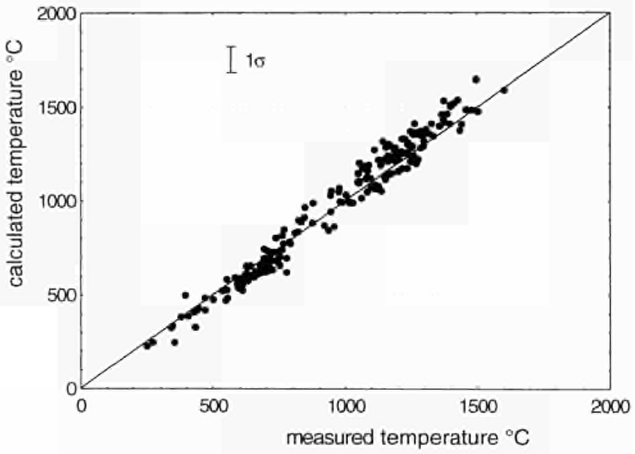

Fig. 2.18 Calculated versus measured temperatures of base irradiation of SOFIT-1.1 rods (data from 8 hours to 160 days).

burnup WWER-440 rods irradiated in power reactors will be used to develop and verify WWER fuel and cladding specific models. The effect of the high burnup structure on the fuel performance during normal operation and transients will be evaluated.

References

[1] K. Lassmann; J. Nucl. Mater. **188** (1992) 295-302

[2] S. Stefanova, M. Vitkova, V. Simeonova, G. Passage, M. Manolova, Z. Haralampieva, A. Scheglov, V. Proselkov, K. Lassmann; Proceedings of the international seminar:'WWER Reactors Fuel Performance, Modelling and Experimental Support', held in St. Constantine, Varna, Bulgaria, 7–11 November 1994

[3] P. Lösönen; Institute for Transuranium Elements, Technical Note K0296185, April 1996

[4] P. Lösönen; IAEA/OECD Data Base Training Meeting in Halden, Norway, 25–27 September 1996

2.4 Specific Heat of UO_2-based SIMFUEL

Introduction

Reliable thermophysical data of UO_2 fuel are required for normal reactor operating conditions and for reactor safety assessments. The specific heat of UO_2 is important in certain accident scenarios: e.g., fuel-coolant interactions, post-accident heat removal and loss-of-coolant accidents, for which the ability to store heat can be critical. In the case of an excursion, the specific heat directly affects the fuel behaviour and determines the temperatures attained during the excursion, and therefore the Doppler feedback. Specific heat is also needed to convert thermal diffusivity to thermal conductivity, the former being commonly measured in out-of-pile tests, as was done in our earlier work on SIMFUEL [1-3].

The specific heat and enthalpy of UO_2 have been published in different papers and these data were critically reviewed 10 years ago by Hyland and Ohse [4]. However, that review does not treat the effect of fission-product buildup and deviation from stoichiometry on the heat capacity of irradiated fuel. There are several papers by Naito, Matsui and coworkers [5-9] reporting specific

heat measurements on UO_2 doped with the rare earths Gd, La and Eu, or with Sc, Nb or Ti. These authors used direct-heating pulse calorimetry. In their latest paper [10], they report specific-heat values for a Simfuel-like material, representing 10 a/o burnup. All their results showed an anomalous increase in specific heat that decreased with impurity content. Such an increase (e.g., by up to 25% at 1400 K), was not found in SIMFUEL [1] or in $(U,Gd)O_2$ [11] for the temperatures reported by the Nagoya group. Also, recent measurements of C_p on irradiated high burnup fuel samples did not show any anomalous increase [12].

Experimental

Unirradiated UO_2 and SIMFUEL samples with equivalent burnups of 3 and 8 a/o were measured using a NETZSCH DSC 404 calorimeter. Specimens were annealed in reducing and slightly oxidizing conditions, to achieve various deviations from stoichiometry prior to the C_p measurements. Tab. 2.2 lists the designation of the specimens, the annealing conditions, and the measured deviation from stoichiometry.

Tab. 2.2 Experimental conditions for sample preparation and designation of the specimens. The measured deviations from stoichiometry are also given.

Sample ID	Equivalent Burnup (a/o)	Annealing Conditions			ΔG_{O_2} (kJ/mol)	Measured O/U-ratio
		atmosphere	temp.	time		
000	0 a/o ($UO_{2.00}$)	4% H_2/Ar	1500 °C	2 hrs	-540	2.000
005	0 a/o ($UO_{2.04}$)	CO_2/CO=99/1	1220 °C	2 hrs	-205	2.035
010	0 a/o ($UO_{2.08}$)	CO_2/CO=99/1	1380 °C	2 hrs	-160	2.084
300	3 a/o SIMFUEL	4% H_2/Ar	1500 °C	2 hrs	-540	1.997
310	3 a/o SIMFUEL	CO_2/CO=99/1	1380 °C	2 hrs	-160	2.071
800	8 a/o SIMFUEL	4% H_2/Ar	1500 °C	2 hrs	-540	1.995
805	8 a/o SIMFUEL	CO_2/CO=99/1	1220 °C	2 hrs	-205	2.026
810	8 a/o SIMFUEL	CO_2/CO=99/1	1380 °C	2 hrs	-160	2.067

* The SIMFUEL specimens are indicated as e.g. $3S_{2.07}$ which stands for 3 a/o SIMFUEL oxidized to a ratio of O/M = 2.071, where M = U plus the metallic fission products which are in solid solution.

The O/M-ratios given in Tab. 2.2 use as metal, M, the sum of uranium and of the dissolved metallic fission products in the fluorite lattice.

The specific heat measurements were made at a heating rate of 20 °C/min in a high-purity argon (99.999% pure with an oxygen scrubber in the gas supply line) atmosphere with a flow rate of 50 ml/min. To avoid oxidation by trapped oxygen, the instrument was evacuated with a standard roughing pump and backfilled several times with argon prior to the tests. Baseline measurements (no sample) and measurements with sapphire (as reference) necessary to compute the specific heat values from the raw data were performed under conditions identical to those that were used for the test specimens. Specific heats were calculated using the standard ratio method. Data were acquired in 25 °C increments between 100 and 1400 °C.

Results and Discussion

In general, the results show a small increase in the specific heat with burnup and deviation from stoichiometry for each temperature when compared with UO_2. The results are plotted as a function of temperature for the various burnups and deviations from stoichiometry in Fig. 2.19 (eight plots grouped by increasing oxygen content (see Tab. 2.2).

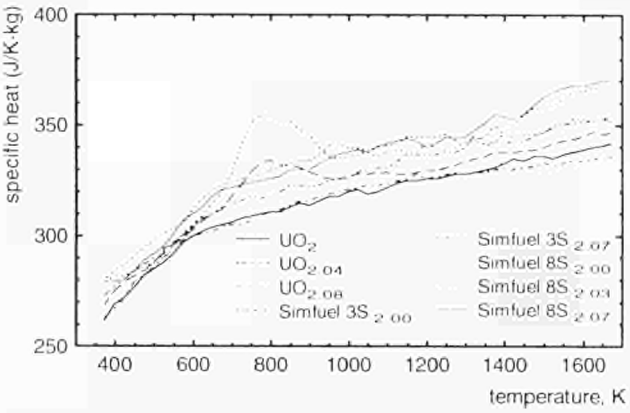

Fig. 2.19 Specific heat of UO_2 and SIMFUEL preannealed at three different oxygen potentials (see Tab. 2.2) as a function of temperature. The results are bundled within about 10% variation.

The specific heat of hyperstoichiometric UO_{2+x} is slightly higher than the values measured for UO_2. Between 400 and 600 °C, the specific heats of hyperstoichiometric $UO_{2.035}$ and $UO_{2.084}$ show a hump, which was confirmed in second runs on both samples of hyperstoichiometric UO_{2+x}, the ones for $UO_{2.035}$ being shown in Fig. 2.20.

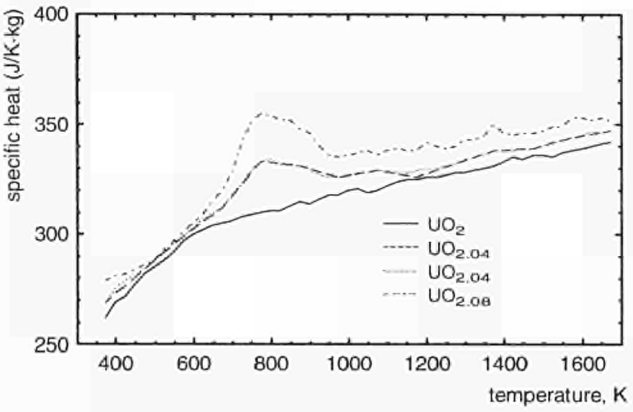

Fig. 2.20 Specific heat of hyperstoichiometric $UO_{2.035}$ (duplicate runs) and $UO_{2.084}$ showing an endothermic behaviour between 400 and 700 °C caused by the U_4O_9 dissolution.

We attribute this hump to the dissolution of the U_4O_9 phase into UO_{2+x} fluorite lattice, which occurs at temperatures above 400 °C. The U_4O_9 phase precipitated in hyperstoichiometric UO_{2+x} during sample preparation; X-ray diffraction at room temperature showed it as broad, low intensity reflections toward lower Bragg angles. X-ray diffraction of SIMFUEL samples annealed under the same conditions did not exhibit the U_4O_9 formation; consequently, their specific heat dependence on temperature did not show a protuberance between 400 and 600 °C .

All SIMFUEL specimens (except for samples $3S_{2.00}$ and $8S_{2.00}$ annealed in reducing conditions) showed an increase in specific heat with increasing temperature, and had the same trend as UO_2. The increase was most pronounced below 600 °C . However, the two SIMFUEL samples annealed in reducing conditions ($3S_{2.00}$ and $8S_{2.00}$) showed a different trend at temperatures above 900 °C ; the specific heat did not increase significantly with increasing temperature. Consequently, the C_p values of these samples were lower than those of UO_2 above ~ 1200 °C. This behaviour suggests a slight oxidation process. Such an oxidation is possible since a few ppm oxygen are probably present in the test gas and the samples were initially slightly hypostoichiometric (see Tab. 2.2).

The SIMFUEL results indicate that the burnup effect caused by fission products (except gases and volatiles) is rather small. This is in agreement with calculations performed for SIMFUEL using the Neumann-Kopp rule [13]. The anomaly in the T-dependence for UO_2 containing impurities or fission products reported by Naito, Matsui and coworkers were not observed in our study. The results have been reported at the Int. Symp. on Thermodynamics of Nuclear Materials in August 1996 [14].

Conclusions

In summary, the specific heat measurements on UO_2 and SIMFUEL have shown:

- the specific heat of SIMFUEL has a similar temperature dependence to UO_2
- the specific heat increases slightly with the burnup as predicted by the Kopp-Neumann rule.
- higher oxygen contents increase the specific heat, but only slightly.
- the anomaly reported in the literature does not exist in SIMFUEL.

References

[1] P. G. Lucuta, Hj. Matzke, R.A. Verrall, H.A. Tasman; J. Nucl. Mater **188** (1992) 198
[2] P.G. Lucuta, Hj. Matzke, R.A. Verrall; J. Nucl. Mater. **223** (1995) 51
[3] P.G. Lucuta, Hj. Matzke, I. Hastings; J. Nucl. Mater. **232** (1996) 166
[4] G.J. Hyland, R.W. Ohse; J. Nucl. Mater. **140** (1986) 149
[5] H. Inaba, K. Naito, M. Oguma; J. Nucl. Mater. **149** (1987) 341
[6] T. Matsui, Y. Arita, K. Naito; J. Radioanal. Nucl. Chem. **143** (1991) 149
[7] T. Matsui, Y. Arita, K. Naito; Solid State Ionics **49** (1991) 195
[8] T. Matsui, T. Kawase, K. Naito; J. Nucl. Mater. **186** (1992) 254
[9] T. Matsui, Y. Arita, K. Naito; J. Nucl. Mater. **188** (1992) 205
[10] K. Naito, J. Nucl. Mater. **167** (1989) 30
[11] Y. Takahashi, M. Asou; J. Nucl. Mater. **201** (1993) 108
[12] T.L. Shaw, J.C. Carrol, R.A. Gomme; presented at Enlarged Halden Program Group Meeting, Loen, Norway, May 19-29, 1996, report F 3.1
[13] H.A. Tasman, ITU Technical Note K 0290137 (1990), cited in ref. [1]
[14] Hj. Matzke, P.G. Lucuta, R.A. Verrall, J. Henderson; J. Nucl. Mater., special issue proceedings STNM 96, Osaka, in press

2.5 Development of Advanced Fuel Fabrication Techniques

Infiltration of highly radioactive materials

Three possible fabrication routes for the production of transmutation and incineration targets contained in an inert matrix are summarized in Fig. 2.21. The main handicap of traditional fabrication methods lies in the handling of fine powders. This is difficult to automate and results in a build-up of radioactive dusts, which can ultimately lead to an undesired increase in exposure of the operating personnel to harmful radiation.

Sol-gel coprocessing avoids some of the disadvantages associated with conventional powder blending methods. Though it can be automated effectively, all fabrication steps must be made within the glove boxes. Furthermore, the chemistry involved in the droplet to particle conversion step is not always readily adaptable to all types of matrix materials which are currently being considered for the fabrication of the targets.

Infiltration of a liquid, solution or a melt into a solid porous material is another process by which composite materials can be fabricated [1-4]. This process has the advantage that matrices with a low radioactivity or zero activity can be fabricated and formed into the required shape in an unshielded facility. The matrix material is then introduced into the shielded glove box and immersed in a solution (or melt) of the infiltrant in a controlled way. The resulting material is treated, thermally or otherwise, to convert the infiltrant into the desired chemical form, and sintered to produce the product pellets. The number of fabrication steps involving handling of highly radioactive material is significantly less than in either the powder mixing or sol-gel processes, and unnecessary high exposure levels to the operating personnel can be avoided. Furthermore, the radioactive wastes produced in the process are negligible.

In this case porous spinel ($MgAl_2O_4$) pellets were fabricated by cold pressing of the powder outside of gloveboxes. Following calcination at 650 °C, they were introduced into the glove box and immersed in an americium solution with an Am content of circa 400 g/l. Following their removal from solution, the infiltrated americium nitrate was converted to the oxide by thermal (700 °C) treatment. After sintering at 1600 °C for 6 hours, the pellets contained 7.7 w/o americium and their densities were 96-97% of the theoretical value.

Radiation dose rates of the samples were measured by positioning one end of each pellet against the inside of the 8 mm thick plexiglass wall of the glove box and a detector on the outside. "Contact" measurements of the activity were made using a thermoluminescence dosimeter (TLD) in the form of a film while measurements at a distance of 60 mm from the sample were made using a Geiger type Panoramic 470A detector. The results obtained for pellets of spinel and UO_2 containing americium are shown in Tab. 2.3. Although the quantity of americium present in each sample is similar, the

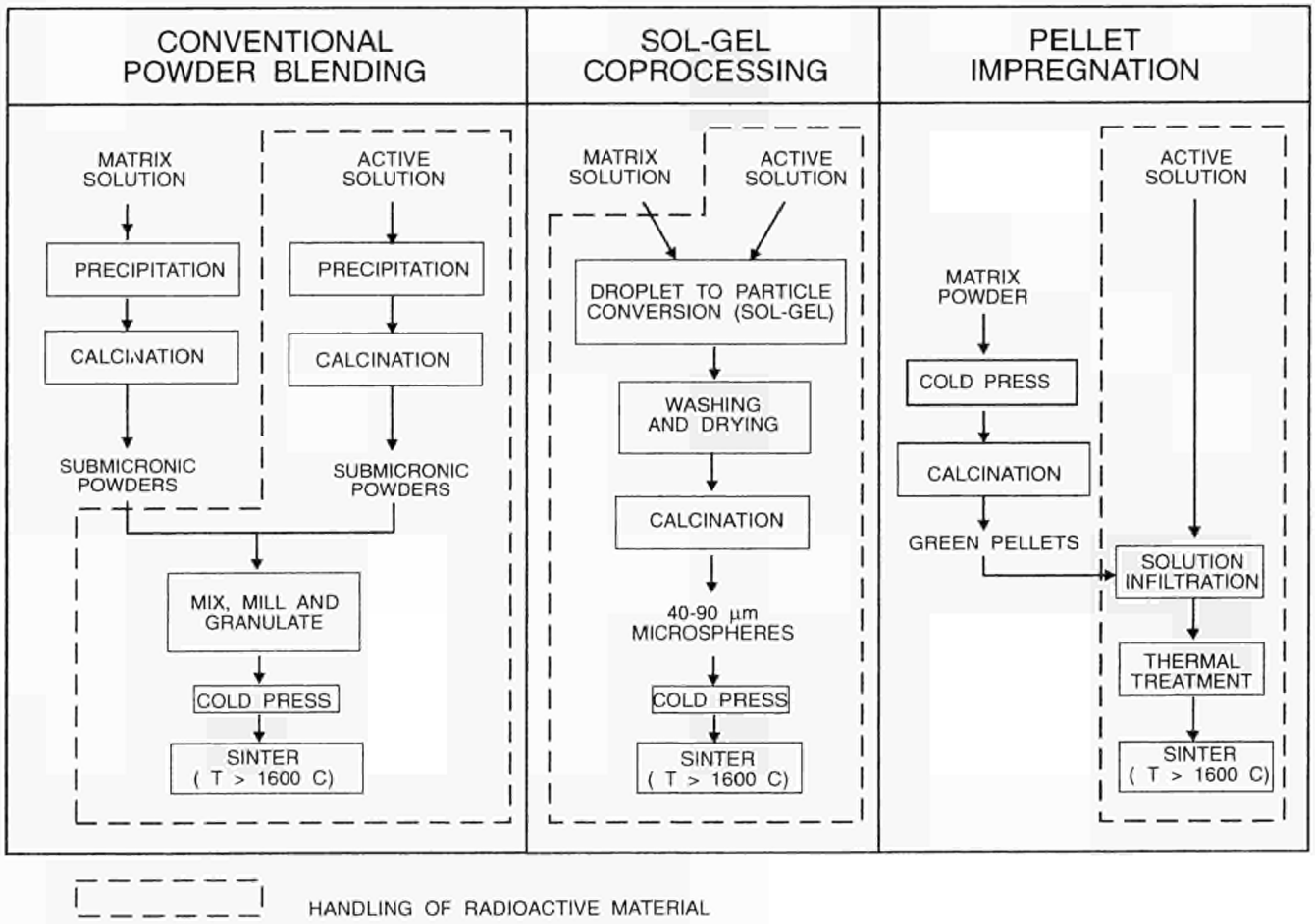

Fig. 2.21 Comparison of the steps involved in three fabrication routes for the production of highly radioactive targets for transmutation and incineration of actinides and fission products.

dose rate of the spinel-Am pellet is far higher than the U-Am pellet. This effect is directly attributable to the lower absorption of the gamma rays (59.5 keV), emitted on decay of the americium, by spinel compared to uranium.

Tab. 2.3 Radiation dose rate measurements of spinel and UO_2 pellets containing americium.

Sample*	Pellet weight (mg)	Am weight (mg)	dose rate (contact) (µSv/hr)	dose rate (Panoramic detector)# (µSv/hr)
7.7 w/o Am in AmO_2 - Spinel	610	47	158000	1800
$(Am_{0.06}U_{0.94})O_2$	700	42	27000	260

* All samples were in the form of pellets with diameter of 5.3 mm and heights varying between 3.3 and 7.4 mm.
# Due to its housing, a contact measurement made with the Panoramic detector gives a measurement in effect at 60 mm distance from the contact point of the housing.

The distribution of americium within the targets was determined by a auto-radiography measurements (see Fig. 2.22) taken from polished faces of sectioned pellets. The uniform nature of the α auto-radiograph indicates that the americium is relatively evenly distributed throughout the pellet. Other measurements using X-ray radiography (see Highlights 1996 in this report) have also confirmed this result.

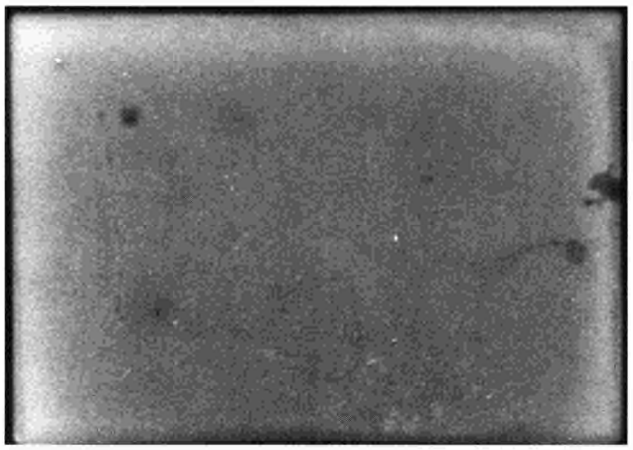

Fig. 2.22 Alpha autoradiograph (x 10) of an axially sectioned spinel pellet containing 7.7 w/o Am fabricated by the infiltration technique.

Optical micrographs of these samples indicate that the americium particles within the spinel matrix have a diameter of less than 2-3 µm. This is significantly smaller than that obtained in other samples prepared by pressing mixtures of powders.

Conclusions

The fabrication of highly radioactive targets for transmutation and incineration of long lived toxic isotopes by infiltration of radioactive materials (in short INRAM) offers many advantages. The number of fabrication steps involving highly radioactive materials are minimised; those remaining can be automated or made remotely. The infiltrant needs only be present in liquid form, i.e. it could be transferred directly from the reprocessing plant for fabrication into targets without conversion into solid form.

Further investigations to establish process data for the fabrication of materials, with tailored microstructures and infiltrant distributions, from a variety of matrices and infiltrants (Pu solutions, etc.) are underway. This process has already been used to fabricate AmO_2-spinel targets for two fuel pins (EFTTRA-T4 – see chapter 8.2) which have been sent to HFR – Petten for irradiation.

References

[1] V.J Michaud, L.M. Compton, A. Mortensen; Metall. Mater. Trans. **25A** (1994) 2145
[2] W.B. Hillig; J. Am. Ceram. Soc. **71** (1988) 96
[3] S.J. Glass, D.J. Green; Adv. Ceram. Mater. **2** (1987) 129
[4] M.D. Sachs, S.D. Vora; J. Am. Ceram. Soc. **71** (1988) 245

3. Mitigation of Long Lived Actinides and Fission Products

Introduction

The Institute continued its' work in the area of partitioning and transmutation (P + T) of minor actinides and long lived fission products.

A major prerequisite for a successful P + T strategy is the develoment of an effective chemical separation technology. In the report on the recovery of minor actinides from irradiated SUPERFACT fuels, the status of the development in this area, in particular for the separation of actinides from lanthanides, is described.

Of similar importance is the development of advanced fabrication technologies for fuels containing minor actinides. Progress on fabrication of targets for the transmutation of technetium and americium including inert matrices is presented in chapter 3.2.

The report on the Minor Actinide Laboratory shows, that considerable progress was achieved in the definition of the goals and extension of this laboratory. Studies to select suitable materials for inert matrices continued. Materials investigated include spinel, zircon, cerium-phosphate, cerium dioxide, silicon carbide and silicon nitride.

Some high burn-up nitrides were examined for their suitability for the incinceration of plutonium.

Finally a brief status report is provided on the TRABANT irradiation experiment.

3.1 Reprocessing of Irradiated Transmutation Fuel Targets

The feasibility of recovering actinides from irradiated SUPERFACT $(U_{0.6}Np_{0.2}Am_{0.2})O_2$ fuel for further recycling and transmutation has been demonstrated (TUAR-95, p. 104). Extraction chromatography with diamylamylphosphonate is a suitable technique to separate the main bulk elements U and Pu [1].

Almost complete recovery of the actinides Am, Cm, (An) together with the lanthanide fission products (Ln), was achieved in a continuous extraction process by means of trialkyl phosphine oxide using a battery of 12 centrifugal extractors [2].

If Am and Cm have to be recycled, a Ln/An separation is necessary for transmutation target fabrication in order to avoid negative effects of Ln in the fabrication process and in a FBR reactor. Neither in metal alloys nor in mixed oxides do Lns form solid solutions. They segregate in separate phases with the tendency to grow under thermal treatment. Because of their chemical nature, An tend to concentrate in these phases, leading to an unacceptable non-uniform heat distribution in the fuel matrix under irradiation. Therefore in case of a heterogeneous fuel concept, with Am and/or Cm concentrations of up to 20%, a Ln/An separation factor of about 30 would be needed [3].

Results

Dissolution

The fuel pin (about 100 g) was cut in segments of 3 cm length (about 5.4 mm in diameter) and dissolved in 400 ml 7 M HNO_3 at 95 °C for 5 h. The progress of the dissolution process is continuously monitored by spectrophotometry. The dissolver solution is pumped through a photometer cell connected to the instrument (CARY 17D) by means of optical fibres, allowing the U concentration to be constantly measured. After cooling to room temperature, the dissolver solution is clarified by filtration (1 and 0.2 μm) and centrifugation. The composition of the clarified dissolver feed solution was determined by TIMS and ICP-MS. Tab. 3.1 shows the actinide content in the dissolver solution .

Tab. 3.1 Actinide content in the dissolver solution dtermined by TIMS.

actinide	content g/l
Np	42.0
U	170.6
Pu	33.7
Am	44.2
Cm	0.5

For each of the 4fuels irradiated in the frame of the SUPERFACT experiment, the weight of the residue was determined (Fig. 3.1).

Fig. 3.1 shows, that the residue amounts measured for the 2 SUPERFACT pins with low MA content are in agreement with PWR and LWR fuels, whereas a higher MA content leads to larger residue amounts relative to the burn-up reached.

Representative aliquots of the residues were dissolved in a mixture of $HCl/HNO_3/HF$ (9/1/0.04) at 180 °C for 16 h in autoclaves and analysed by ICP-MS. Even for the fuels with high MA content, no significant amounts of actinides were found.

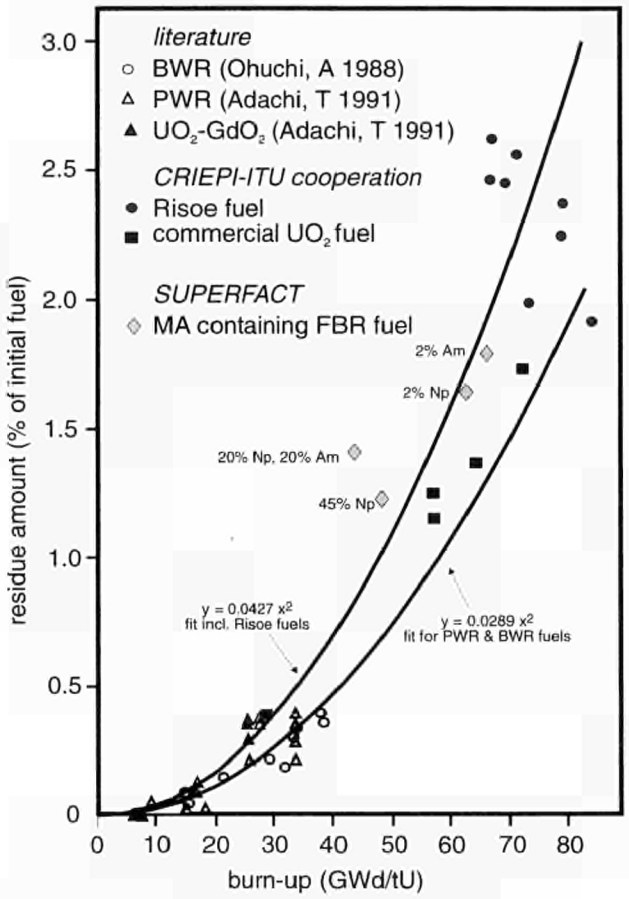

Fig. 3.1 Amount of residue as a function of burn-up.

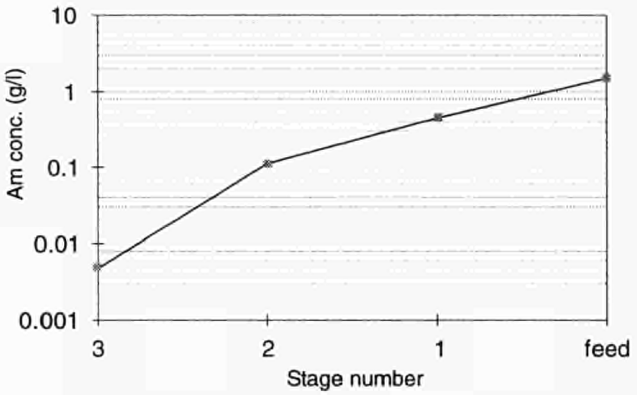

extraction stage	1	2	3
An/Ln separation factor	4.9	3.2	2.1

Fig. 3.2 Concentration profile of Am and An/Ln separation factors in a 3 step extraction process by means of dithiophosphonic acid.

An/Ln separation

Ln/An separation is carried out in a separate process by means of CYANEX 301 (a dithiophosphonic acid from CYTEC Industries) [4]. The Ln/An fraction obtained from the above mentioned partitioning process is about 5.5 M in HNO_3 and has therefore to be denitrated by means of formic acid. The denitrated solution (pH 3), containing ca. 300 mg of Am, 3 mg of Cm and 350 mg of Ln is then mixed with 0.5 M CYANEX / 0.5 M TBP in dodecane. The extractant is used without further purification. Fig. 3.2 shows the concentration profile of Am in a 3-step extraction and the corresponding An/Ln separation factors.

After only 3 extraction steps, the Am concentration in the feed has decreased by more than 2 orders of magnitude and an An /Ln separation factor >30 has been reached. Thus an An fraction containing less than 5% of Ln has been obtained. Such a product can then be reintroduced as such to the transmutation fuel cycle, e.g. the target fabrication.

References

[1] J.-P. Glatz, C. Song, L. Koch, H. Bokelund, X.M. He; Hot Tests of the TRPO Process for the Removal of TRU Elements from HLLW, Int. Conf. on Evaluation of Emerging Nuclear Fuel Cycle Systems, Proc. GLOBAL 1995, p. 548, September 11-14, 1995, Versailles, France,

[2] C. Song, J.-P. Glatz, X. He, H. Bokelund, L. Koch; Actinide Partitioning by Means of the TRPO Process, Proc. of the Fourth Int. Conf. on Nuclear Fuel Reprocessing and Waste Management, "RECOD '94", April 24-28, 1994, London, UK

[3] L. Koch, G. Nicolaou; Comparison of Possible Partitioning and Transmutation Schemes when Added to the Existing Nuclear Fuel Cycle, Proc. Technical Committee Meeting on Safety and Environmental Aspects of Partitioning and Transmutation of Actinides, IAEA 29.11–2. 12. 1993

[4] G.D. Jarvinen, R.E. Barrans Jr., N. C. Schroeder, K. L. Wade, M.M. Jones, B.F. Smith, J.L. Mills, G. Howard, H. Freiser, S. Muralidharan; Proc. of the ACS symposium on *f* Elements Separations, March 13-17, 1994, San Diego, Ca., eds. K.L. Nash, S.R. Choppin; Plenum Press p. 43, 1995, ISBN: 0306450704

3.2 Fabrication of Targets for the Transmutation of Technetium and Americium

The international EFTTRA collaboration (CEA, ECN, EDF, FZK, IAM, ITU) is concerned with the study of the transmutation of Tc-99 (metal) and the development of materials (inert matrices) for the transmutation of americium.

Technetium

The examination at ECN of a metallic technetium target after irradiation in HFR (EFTTRA-T1 experiment) showed that the burn-up was about 6.4% and that no swelling of the rods had occurred [1]. Some of the irradiated samples have been sent to ITU and CEA for comparative examination; the results from the three laboratories are being discussed and interpreted together, and a detailed report is under preparation. The observations at ITU and CEA confirm the results obtained at ECN, i.e. the irradiation had no significant effect on the structure of the material, and no swelling was detected. This good behaviour of technetium metal is being investigated further for higher burn-ups. For this purpose two technetium rods have been re-packed at ECN for a re-irradiation in the HFR. This irradiation (EFTTRA-T2) was started in February 1996 and will last for about 500 full power days during which a burn-up of more than 20% will be achieved.

The concentration distribution of Ru along the radius of the sample was determined at the ITU by EMPA (Electron MicroProbe Analysis). It showed the same sharp decrease as for the ECN sample, from about 13% at the surface, down to 8% at 0.1 mm depth and 6% at 1 mm depth (diameter of the samples: 4.8 mm). The value obtained at the surface of the sample is slightly below the ECN value. This could be due to the very steep slope of the concentration curve near the surface, or to the orientation of the sample. No significant variation of the Ru concentration was found along the axis of the samples. The PIE observations are in excellent agreement with the results of detailed KENO Monte Carlo calculations, as performed at ECN [2].

The irradiation of three other Tc target capsules is planned in the fast reactor Phénix (EFTTRA-F2). Depending on the schedule of the Phénix reactor, the irradiation should start in 1997. The samples will be placed in the radial blanket of the reactor, in a thermalized neutron flux, with CaH_2 as moderator. The experiment aims at a transmutation of 15%.

Inert matrices

The heterogeneous recycling of Am requires that transmutation targets, with a high percentage of americium (10 to 40%), be fabricated, irradiated, and reprocessed. The choice of a suitable inert matrix depends on its thermodynamic, physico-chemical, and mechanical properties, and on its behaviour under irradiation or during cooling.

Preliminary studies are being made in the laboratory, for a first selection of matrices. Techniques have to be developed for the fabrication of these materials. If reprocessing by the Purex process is envisaged, the solubility of the matrix in nitric acid, possibly after crushing of the material, is an important factor. Once the targets have been fabricated, a range of parameters have to be measured. The ideal matrix material should have high thermal conductivity and melting point, low creep and swelling values, low activation coefficient, low neutron absorption, and should not react with the cladding or the coolant. Radiation damage can be studied out-of-pile, by ion implantation. For the study of the behaviour of the candidate matrices under irradiation, several experiments are planned. UO_2 may be added to the samples, to simulate the presence of americium oxide. The EFTTRA-T2 experiment, already mentioned above, also includes the irradiation in HFR of samples of Al_2O_3, YAG ($Y_3Al_5O_{12}$) and spinel ($MgAl_2O_4$). A shorter, parallel irradiation of these matrices and a sample of CeO_2, was started at the same time in HFR (EFTTRA-T2bis), and should give a quick indication of the behaviour of the matrices in a high thermal neutron flux environment.

The start of the EFTTRA-T3 experiment, with a selection of inert matrices containing UO_2, 20% enriched in U-235, is planned for 1997.

Americium targets

The same preliminary studies on fabrication techniques, properties, and reprocessing behaviour, have to be made with the matrix material containing americium. First investigations were made on the AmO_2-MgO system [3] and are being continued with AmO_2-spinel.

The irradiation in HFR of a sample of americium oxide embedded in a spinel matrix, the EFTTRA-T4 experiment (described in chapter 8.3), is now under way. Samples with 11 w/o Am were produced by an infiltration procedure, developed within ITU's research programme. The fuel pins have been under irradiation at HFR Petten since September 1996. The duration will be about 400full power days, with a fluence of the order of $4x10^{26}$ m^{-2}. According to calculations, the actinide content in the sample is expected to be reduced by 35% [4,5].

References

[1] R.J.M. Konings, W.M.P. Franken, R. Conrad, J.-F. Gueugnon, J.-C. Spirlet; Transmutation of technetium and iodine – Irradiation tests in the frame of the EFTTRA cooperation, Nucl. Technol. **117** (1997) 293-298

[2] J.L. Kloosterman, J.A. Hendriks, R.J.M. Konings; Transmutation of technetium in the Petten HFR: a comparison of measurement and calculation, 4th NEA International Information Exchange Meeting on Actinide and Fission Product Partitioning and Transmutation, Mito, Japan, September 11-13, 1996

[3] S. Casalta, K. Richter, C. Prunier; A study of AmO_2-MgO system for americium target transmutation in fast reactors, in GLOBAL'95, International Conference on Evaluation of Emerging Nuclear Fuel Cycle Systems, Versailles, September 11-14, 1995, p. 1725

[4] J.L. Kloosterman; Incentives for transmutation of americium in thermal reactors, report ECN-R–94-022 (1994)

[5] W.J.M. de Kruijf; Calculational study on irradiation of americium fuel samples in the Petten High Flux Reactor, report ECN-R–94-027 (1995)

3.3 Extension of the Minor Actinide Laboratory

Introduction

In parallel to the discussions with external partners concerning the future use of the Minor Actinides (MA) laboratory facilities at ITU, the possibility of limiting the costs of the planned extension of the laboratory was investigated. Currently a laboratory equipped with "water-shielded cells" is at our disposal. This laboratory consists of a row of 5 large glove boxes equipped with manipulators and with sufficient additional shielding against neutrons and gamma-rays; this is the main constituent of the present MA laboratory.

The existing laboratory is used for chemistry. In addition to purification of Am and Cm (metals), chemical preparation of the starting solutions is performed there. The sol-gel equipment for preparation of beads has also been installed in the MA laboratory. Up to now, the calcination of the sol-gel beads, as well as the pellet and fuel pin preparation, are carried out in standard glove boxes. Due to the increased amount of minor actinides to be handled in the future, this will no longer be possible.

The original proposal for an extension of the MA laboratory (TUAR-94, p. 71), was flexible but expensive: it

required the installation of a complete pellet and pin fabrication chain in a new caisson in wing G. At the other extreme, a fast and economical solution could be based on making maximum use of the existing facilities, mainly the hot cells in wing B. Most of the fabrication, including the sintering of the fuel pellets, could be done there, but this solution had to be discarded for its lack of flexibility. Meanwhile, an intermediate solution was proposed, combining economy and flexibility, with a limited extension of water-shielded cell equipment. Considering the considerable advantages of the water cells over the hot cells (i.e. easier intervention in the cells from the back side, through gloves, and easier exchange of equipment by replacing the whole glove box behind the protecting wall), this intermediate solution was finally adopted. It seemed also advisable to group the "dry" operations (pellet pressing and sintering) in one place (wing F).

Description of the selected approach

In the selected approach, the sol-gel material will be fabricated and calcinated in one laboratory. The operations originally planned for the 8 boxes of the dedicated caisson will be shared between two laboratories and the hot cells of wing B:

- The weighing, and possibly mixing, of the material prepared by sol-gel, will be done in an existing cell equipped with a calcination furnace.
- Pressing of the pellets will be performed in a new cell. After pressing, the pellets must be controlled and sorted out.
- For the sintering of the pellets under controlled atmosphere, a furnace will also be installed in a cell in the new laboratory.
- For the machining of the pellets, if necessary, a centerless grinding machine is foreseen.
- The control and characterisation of the pellets, as well as the preparation for the filling of the pins, will be done in the hot cells in wing B.
- With some adaptations, the existing equipment in a hot cell could be used for pin filling and welding. The unit is presently used for the re-fabrication of pins after PIE, for reprocessing; the cladding and the plug are made of zircalloy. For the welding of stainless steel pins, a new electrode is needed, and tests have to be done. The pin end control will also be done in wing B.
- Finally, the scrap waste will be conditioned in wing B.

It should pointed out that the selected approach can be considered as a test for the remote fabrication chain needed in the future for the nuclear industry.

Conclusion

In conclusion, budget limitations and time constraints inevitably led to a modification of the original proposal. The choice of the above "intermediate" solution, should allow the fulfilment of commitment of fabrication of Am containing pins for the ACTINEAU experiment.

The following actions have been launched for 1997:

- installation of a calcination furnace;
- installation of a water wall;
- ordering of a press for installation;
- ordering and installation of a sintering furnace;
- adaptation of a welding device.

This extension of the MA laboratory at ITU should be completed in the course of 1998.

3.4 Inert Matrices for Transmutation of Minor Actinides

Work to identify stable inert matrices, and to discard unstable matrix materials (started as a project between ITU and Electricité de France, TUAR 94, p. 210; TUAR 95, p. 200) was continued. The results obtained will be presented at a forthcoming international conference [1]. An inert matrix should fulfil a number of criteria: proven fabrication procedures, thermal and mechanical properties as good as – or preferably better than – those of UO_2, compatibility with clad and coolant, small neutron absorption cross sections and good radiation stability. The materials studied in the reporting period were spinel $MgAl_2O_4$, zircon $ZrSiO_4$, monazite $CePO_4$, CeO_2, SiC and Si_3N_4. Radiation stability was tested in two ways: matrices containing Am-241 subjected to α-decay damage were stored at ambient temperature and the lattice parameters were measured at 2 months intervals. Other samples were irradiated with a fission product (I-ions of 72 MeV energy) at Chalk River, AECL, Canada to investigate fission damage. In parallel work, physical properties of importance for reactor irradiation were measured.

In the following, some typical examples of this work are given. Fig. 3.3 shows measurements of thermal properties (specific heat C_p and thermal diffusivity α) of CeO_2 and CeO_{2-x}.

Despite the lower density of the CeO_2, its thermal conductivity $\lambda = \rho \cdot \alpha \cdot C_p$ (ρ = density) is very similar to that of UO_2. However, oxygen potential measurements (see Fig. 3.4) show that it is difficult to keep CeO_2 stoichiometric at elevated temperatures. Its oxygen potential is high, which could create problems with inner clad corrosion. If CeO_{2-x} is used as matrix, its thermal properties deteriorate as shown in Fig. 3.3. CeO_2 has the advantage of showing a high solubility for PuO_2 but its thermal behaviour needs careful optimization to be acceptable.

Another important aspect is radiation stability. The inert matrix is subjected to α-decay damage from the moment of its fabrication, and it is subjected to fission damage and neutron damage during its utilization in nuclear reactors. Some potential matrices have to be discarded because of their poor stability under irradiation, a typical example being Al_2O_3 which is easily turned amorphous [2,3]. Fig. 3.5 shows the behaviour of Al_2O_3 under the impact of fission (iodine ions at fission energy). The irradiated area "pops out" of the sample because of very high swelling rates. Simultaneously,

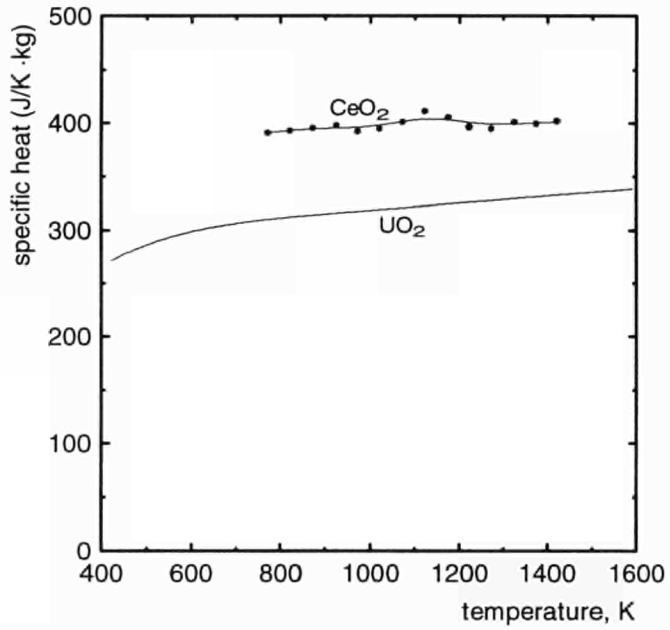

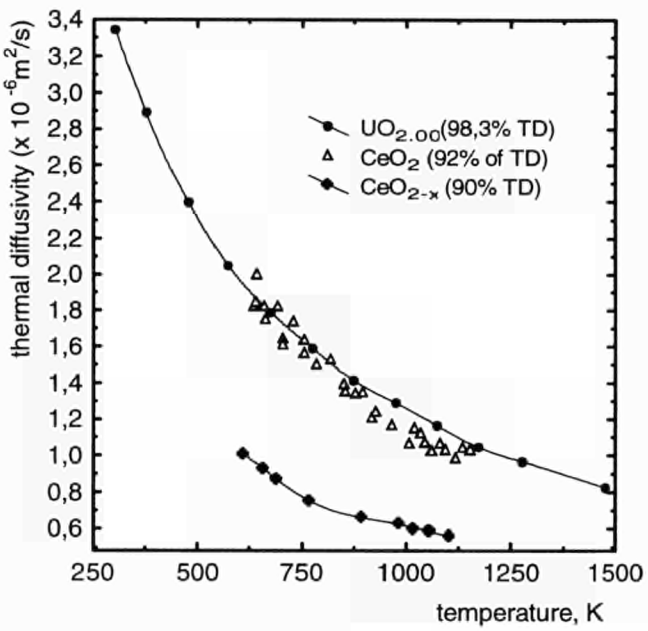

Fig. 3.3 Specific heat and thermal diffusivity of CeO_2 and CeO_{2-x} as inert matrix, compared to UO_2.

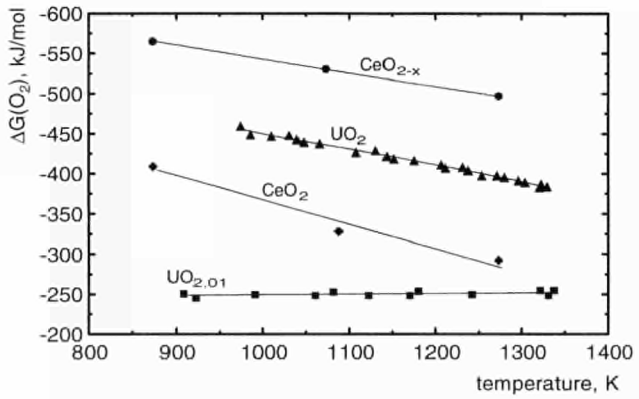

Fig. 3.4 Oxygen potential of CeO_2 and CeO_{2-x} compared to UO_2 and $UO_{2.01}$.

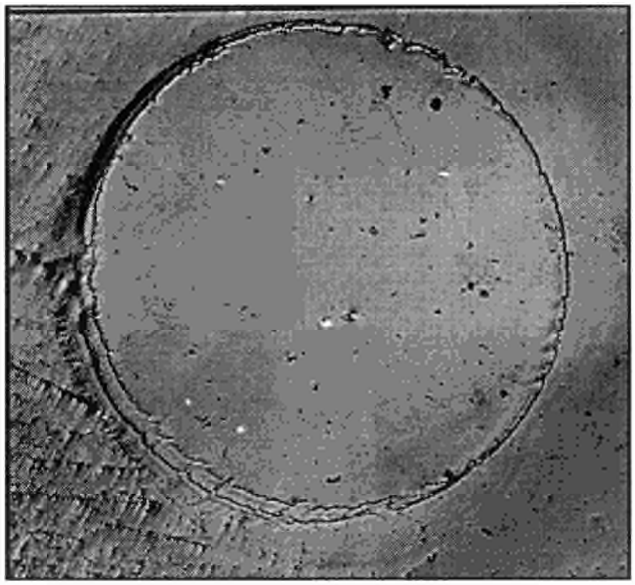

Fig. 3.5 Swelling of Al_2O_3 due to irradiation with iodine ions of fission energy ($1x10^{17}$ I-ions/cm², 72 MeV, 150 °C).

Al_2O_3 becomes amorphous thus changing not only its volume but also many other important properties.

Al_2O_3 was therefore discarded as inert matrix. Fig. 3.6. shows rather unexpected results for spinel $MgAl_2O_4$: this material is known to be very stable against neutron irradiation, but Fig. 3.6 shows that it swells significantly under the impact of fission products. Separate measurements (Rutherford backscattering/channeling with 2 MeV He-ions) and X-ray techniques (θ, 2 θ, and Ω scans) show that spinel does not become amorphous, but rather undergoes polygonization, i.e. very small polycrystalline grains are formed, as in the rim structure of UO_2.

These few examples show that the selection of a suitable inert matrix for transmutation of minor actinides necessitates further R&D work.

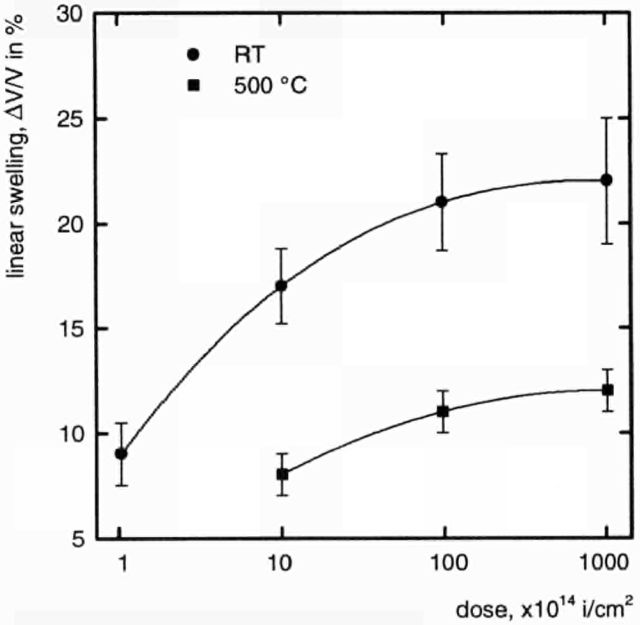

Fig. 3.6 Swelling of spinel $MgAl_2O_4$ due to irradiation with iodine ions of fission energy at two temperatures.

References

[1] M. Burghartz, Hj. Matzke, C. Léger, G. Vambenepe, M. Rome; Inert Matrices for the Transmutation of Actinides: Structure and Thermal Properties of Ceramic Materials, to be presented at ACTINIDES 97, Baden-Baden (1997)
[2] Hj. Matzke, J.L. Whitton; Can. J. Phys. **44** (1966) 995
[3] Hj. Matzke; Nucl. Instrum. Methods in Phys. Research **B116** (1996) 121

3.5 Investigation of High Burn-up Nitrides as Candidate Fuel for Incineration of Plutonium

Nitrides are reconsidered as a possible fuel for incineration of plutonium in fast reactors, as for example in the CAPRA project, because of their good compatibility with sodium and with the PUREX process.

The goal of the present study is to examine and understand the structural behaviour, chemical properties, fission gas retention, of (U,Pu)N produced in the Institute [TUAR-92, p. 56-57, TUAR-94, p. 62] irradiated to a burn-up > 20 a/o in the HFR reactor in Petten (NL). Details on the POMPEI irradiation concept are published elsewhere [TUAR-92, p. 56-57; TUAR-94, p. 62]. The instrumented capsule contained nine (U,Pu)N pellets of 1.5 mm thickness by 9 mm in diameter and also three Tc-Ru alloys of the same size, individually encapsulated in small stainless steel capsules. For the present study, γ-scanning and γ-spectroscopy, optical microscopy, electron microprobe analysis (EMPA) and scanning electron microscopy (SEM) were used.

Irradiation data

Details of pellet burn-up and centre-line fuel temperature calculated by HFR Petten [1] are shown in Tab. 3.2.

Tab. 3.2 Irradiation temperatures and burn-up of U,PuN fuel. Irradiation time: 5745 hours.

Pellet Nr.	Type	In pile outer capsule surface temp. (°C)	Average center line calcul. temp. (°C)	Total burn-up (a/o)
1	UPuN	502	1180	23.98
2	Tc (100% Tc)	408	430	7.13
3	UPuN	546	1220	25.86
4	UPuN	547	1250	26.67
5	UPuN	576	1290	26.94
6	UPuN	594	1325	26.94
7	UPuN	594	1325	26.94
8	UPuN	561	1320	26.40
9	UPuN	618	1320	25.59
10	Tc/Ru (50% Tc)	438	450	7.05
11	Tc/Ru (20% Tc)	506	450	6.82
12	UPuN	651	1310	22.63

Post irradiation data

Axial cross-sections were prepared for metallographic and ceramographic examinations (Fig. 3.7). Preliminary ceramography results from pellet no. 1 are summarized below:

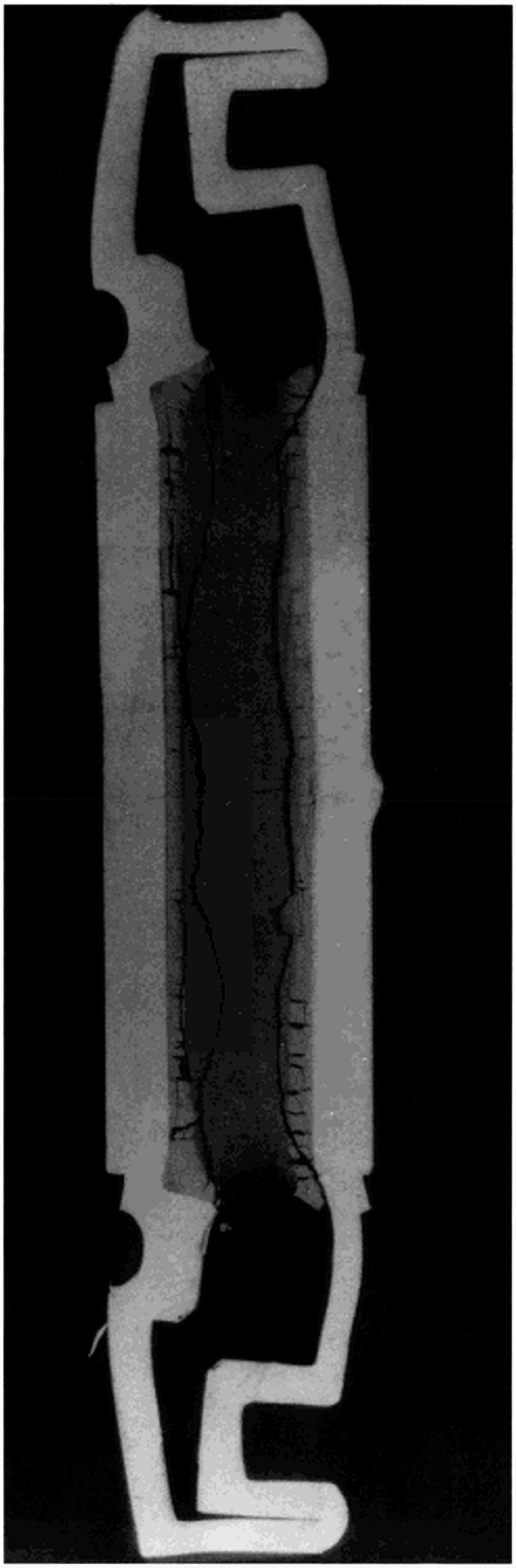

Fig. 3.7. Macroscopic overview of the pellet in axial cross-section. Note the different crack patterns lenghtwise and radially. Magnification: 13.65X.

a) Fuel restructuring

Three distinct zones are observed from the pellet-capsule interface towards the pellet centre:

- reaction zone of 30 μm in average thickness, formed lengthwise at the top and bottom of the pellet-capsule interface (Fig. 3.8).

The absence of grain boundaries after ion etching could be due to the amorphous or microcrystalline nature of the zone.

- Poreless zone of 50 μm average thickness and an average grain size of 10 μm (Fig. 3.8).
- Porous zone of approximately 1300 μm thickness. Pore size and density varied axially along the major heat flow direction. Pore sizes vary from submicron to a few microns from the top to the centre of the pellet. Fig 3.9 shows a representative centre location.

Fig. 3.8 The reaction zone at the top centre of the pellet. Grain strucuture could not be revealed by cathodic etching. Magnification: 500X.

b) Mechanical behaviour

The presence of cracks at the pellet-stainless steel interface and along the central part of the pellet with high porosity concentration indicates a high compression stress (Fig. 3.7).

c) Swelling

The estimation of the change in the geometrical shape of the pellet revealed a $\Delta V/V$ volume change of the order of 29%.

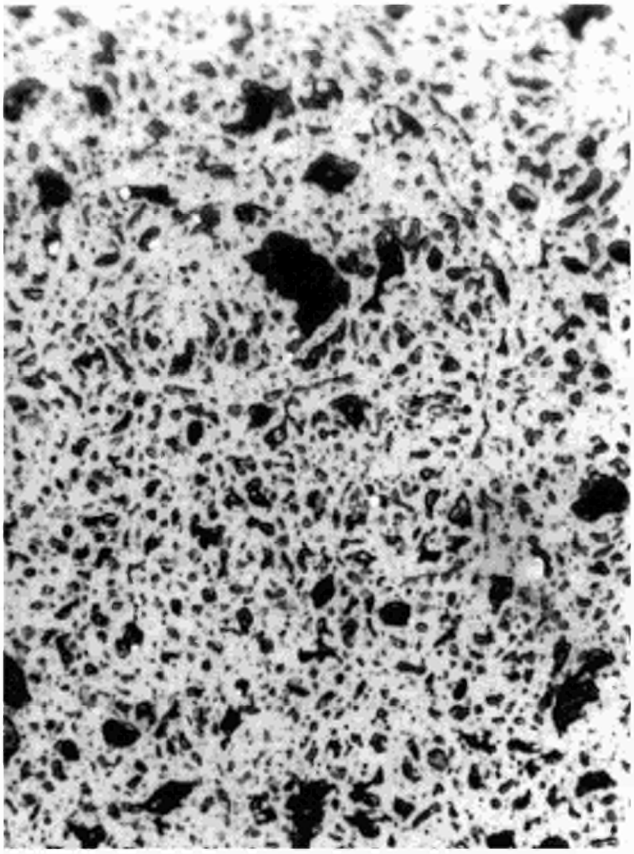

Fig. 3.9 Porosity at the centre of the pellet. Very large pores are most probably due to the loss of grains during polishing. Magnification: 1100X.

Preliminary conclusions

The above preliminary results indicate:

- The abrupt change of porosity concentration as temperature increases confirms the existence of a critical fuel temperature (T_c) at which swelling accelerates.
- Mechanical deformation and occurence of intergranular cracking indicates a stress corrosion mechanism in the stainless steel capsule that could affect its tightness.

Future prospects

- More precise information on the pore size/density distribution will be gained by means of image analysis.
- EMPA could also be used in order to check the burn-up values calculated by HFR Petten (Tab. 3.1), and to evaluate the Xe, Cs retention in the fuel. A further objective of the EMPA examinations will be the determination of a potential interaction between the stainless steel and the UPuN.

References

[1] R.L. Moss, JRC Petten; personal communication

3.6 CAPRA-TRABANT Irradiation Experiment

The irradiation experiment TRABANT (TRAnsmutation and Burning of ActiNides in Triox) [TUAR-95, p. 106] is being executed within the framework of the trilateral (ITU, FZK and CEA) collaboration CAPRA (Consommation Accrue de Plutonium dans les RApides). In this experiment three fuel pins containing Pu and Np within U and Ce matrices were fabricated [1] and have been under irradiation in HFR-Petten since December 1995.

The pin with the $(U_{0.55}Pu_{0.45})O_{2-x}$ fuel showed an unexpected increase in temperature at 7 a/o burn-up. The irradiation was continued up to 10 a/o.

For the pin with the plutonium-cerium oxide fuel $(Pu_{0.43}Ce_{0.57})O_{2-x}$ also an increase in temperature was observed at 3 a/o burn-up. A neutron radiograph performed at 5 a/o burn-up indicates a melting of the fuel. This could be explained by the lower thermal conductivity of the substoichiometric fuel.

These two fuel pins have been removed from the reactor for destructive and non-destructive examination. Replacement fuel pins will be fabricated and inserted in the reactor during 1997. The irradiation of the remaining pin, containing a $(U_{0.55}Pu_{0.40}Np_{0.05})O_{2-x}$ fuel, is being continued. A burn-up of 7 a/o has now been reached without any abnormal behaviour.

4. Spent Fuel Characterization in View of Long Term Storage

Introduction

Intermediate and subsequent long term storage of unreprocessed fuel is an option followed by some Member States of the European Union.

The Institute has therefore carried out work in this area with the objectives

(a) to characterize the spent fuel behaviour under long term storage conditions,

(b) to develop instrumentation to determine the actinide inventory of spent fuel,

(c) to determine the evolution of the radiotoxicity as a function of time, and

(d) to investigate the corrosion and leaching behaviour of spent fuel under realistic conditions.

The major advantage of the Institute is that such work can be carried out on real spent fuel under hot cell conditions. During 1996 work continued along the following main lines:

- electrochemical studies of UO_2 corrosion, dissolution and leaching
- low temperature oxidation of fuel fragments
- improvement of a shielded X-ray goniometer
- dissolution behaviour of spent UO_2 and MOX fuel as a function of the oxidation state
- determination of spent fuel inventory
- leaching behaviour of spent fuel in simulated granitic water
- interaction of fuel with structural materials and
- non-destructive assay of spent fuel

4.1 Characterization of Spent Fuel

4.1.1 Study of UO_2 corrosion by electrochemical techniques

The aim of this project is to understand the mechanisms of irradiated UO_2 dissolution or alterations in aqueous solutions to obtain a better knowledge of leach rates that occur in fuel repositories.

In the last few years, remarkable results have been obtained from electrochemical experiments carried out with spent fuel electrodes in different aqueous solutions. In the case of specimens embedded in resin, under normal air pressure and polished down to 1 μm, it was found that during the measurement the current and/or the potential response of the system under investigation was very noisy. Smooth and undisturbed signals were obtained, after reimpregnating under vacuum and repolishing the samples. This behaviour was found while performing cyclic voltammetry or during long term corrosion potential measurements. Investigations of the corrosion potential dependency on oxygen concentration showed in the case of non-porous single crystal UO_2 sample a direct linear relation, whereas with a sintered porous UO_2 a hysteresis was obtained (attributed to the time necessary for O_2 to diffuse out of the pores). These results indicate that the fuel structure and also grain boundary effects play an important role for the dissolution of spent fuel, especially if the higher dose rate in cracks and pores of irradiated fuel, i.e. stronger radiolysis effects at these sites, is taken into account.

To elucidate dissolution at grain boundaries, experiments were carried out in a newly constructed microcell which needs only 3 ml volume of electrolyte. The working and auxiliary electrode are plane parallel with a separation of approximately 10 mm with the tip of the reference electrode positioned between them. The aim of the microcell was to minimise the electrolyte volume, and to obtain fission products that are leached out from irradiated fuel in a more concentrated form. Initial tests were carried out with non-irradiated UO_2 pellets in 3 w/o Na_2CO_3 solution at 25 °C. Under galvanostatic control, current densities ranging from 20 to 85 μA/cm² were applied for 2 h. Afterwards, the solutions were analysed by ICP-MS and the specimens were examined optically. Comparing the results from solution analysis and flowing charge, good agreement is obtained if one assumes $UO_{2.33}$ is dissolved. This means the surface of the specimen was slightly oxidised by air. From quantitative image analysis, a porosity increase from 10% (20 μA/cm²) to 42% (85 μA/cm²) mainly due to grain boundary attack and intra-granular etch pits (round shaped) was found. At 40 μA/cm² the onset was mainly observed at grain boundaries. Therefore, a current density of 30 μA/cm² was chosen to investigate high enrichment (8.6% ^{235}U) high burn-up (53 GWd/tU) fuel. ICP-MS analysis of the electrolyte solution shows an increase of Cs and Ba compared with theoretically predicted values from KORIGEN indicating grain boundary attack. The Mo content matches with the prediction which is an indication of intragranular attack. This behaviour is confirmed by image analysis. The SEM micrograph (Fig. 4.1) of the specimen shows in the middle a vertical crack. On the right hand side of this crack, both attacked grain boundaries and elongated intragranular pits are visible. The left side remains non-attacked due to electrical disconnection from the other two thirds of the sample. Adjusting the surface area in electrical contact the applied current

density rises to approximately 50 μA/cm². This resulted in an increased porosity of 35% area fraction and matches very well with the value expected from the non-irradiated UO_2 testing.

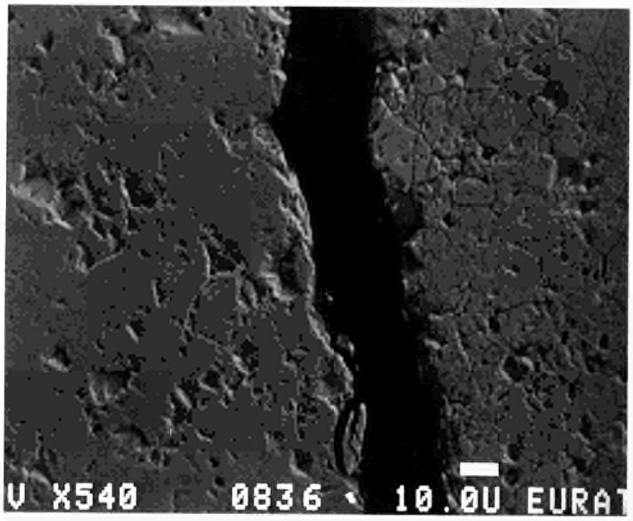

Fig. 4.1 View of electrode at central crack: etched grain boundaries and intragranular attack on right hand side, no grain boundary etching evident on left hand side (540x).

Cyclic voltammography offers the possibility to study redox reactions at electrodes. In the case of UO_2 and irradiated fuels, it is difficult to interpret the obtained voltammograms because the high ohmic resistance of these materials leads to a large distortion of the curves. Therefore a method was developed to prepare UO_2 samples with a low bulk resistance. Several metals (Cu, Ti, Ta, Zr, Au) were coated with a thin UO_2 layer (1-2 μm thickness) and tested electrochemically. UO_2-coated gold electrodes behave best because gold is electrochemically nearly inert in the potential range of interest in aqueous solution. A first series of experiments were carried out with UO_2-coated gold electrodes in 95% saturated NaCl solution. It was found that after an initial UO_2 dissolution at anodic potentials higher than 400 mV_{SHE}, redox reactions of U species can be detected at the electrode under non-stirred conditions. The corresponding redox peaks were missing in strongly stirred solution. In the case of first non-stirred dissolution and second detection of redox peaks in stirred solution, the height of the oxidation and reduction peaks decreased but it was not possible to remove them completely. This means that after dissolution in salt brine U species may adsorb at the UO_2 examined surface and can also precipitate to cover the electrode with higher oxidised species.

First long term experiments were started with sintered PuO_2 electrodes at 25 °C in 0.1 M NaCl solution. The measured corrosion potential dropped from initial anodic potentials down into the cathodic range and reached after 300h, -200 mV_{SHE}. The trend to even more cathodic potentials was observed. Also in the case of irradiated MOX fuel (SCA programme) corrosion potentials were in the cathodic range. This may indicate an influence of PuO_2 as a potentially cathodic phase on the electrochemical behaviour of MOX fuels.

The preliminary conclusions show that

1) Electrochemical methods can be applied to examine irradiated fuel, despite the difficulties due to the high resistance of UO_2.

2) Irradiated fuel has considerable differences in comparison with pure UO_2 . The potential trace shows considerable noise; this can be due to either the localised dissolution at active sites such as pores and grain boundaries, probably with the fission product accummulations and/or to radiolysis of water by the fuel.

3) The irradiated fuel appears to show more anodic (active) behaviour than pure UO_2 with higher corrosion rates.

4) PuO_2 has quite a different behaviour and its influence in MOX fuel in aqeous solutions in being investigated.

4.1.2 Oxidation of irradiated UO_2 at low temperatures

Long term oxidation experiments of spent fuel fragments have been continued in the autoclave installed in a hot-cell (TUAR-94, p. 96). The results obtained to date, concerning the weight gain of irradiated (U,Pu)O_2 samples after exposure to air at 268 °C and for a time interval of up to 2000 h, are given in Fig. 4.2. They confirm a significantly different behavior in the oxidation rate between MOX and UO_2 spent fuel (TUAR-95, p. 129).

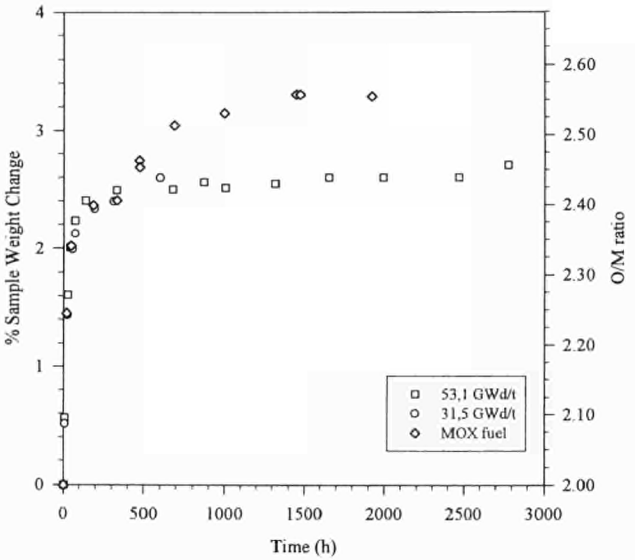

Fig. 4.2 Oxidation of spent fuel fragments in dry air at 268 °C.

Contrary to the UO_2 fuel samples, MOX samples are after 800 h partially and after 2000 h completely powdered, due to the formation of a less dense oxidation product, probably U_3O_8. Characterization of this oxidation product will be performed by XRD analysis in a lead shielded glove-box (TUAR-95, p. 130).

Fig. 4.3 shows also the experimental data for UO_2 fuels with burn-ups of 53.1 and 31.5 GWd/tM respectively.

The oxidation mechanism is well represented in the micrographs of Fig. 4.2. It can be seen that the oxidation of the irradiated UO_2 proceeds by rapid formation of a new phase (probably U_4O_9) along the grain boundaries, reaching completion after 530 h and remaining stable up to at least 3000 h at 268 °C. Similar results have been reported in the literature [1-3].

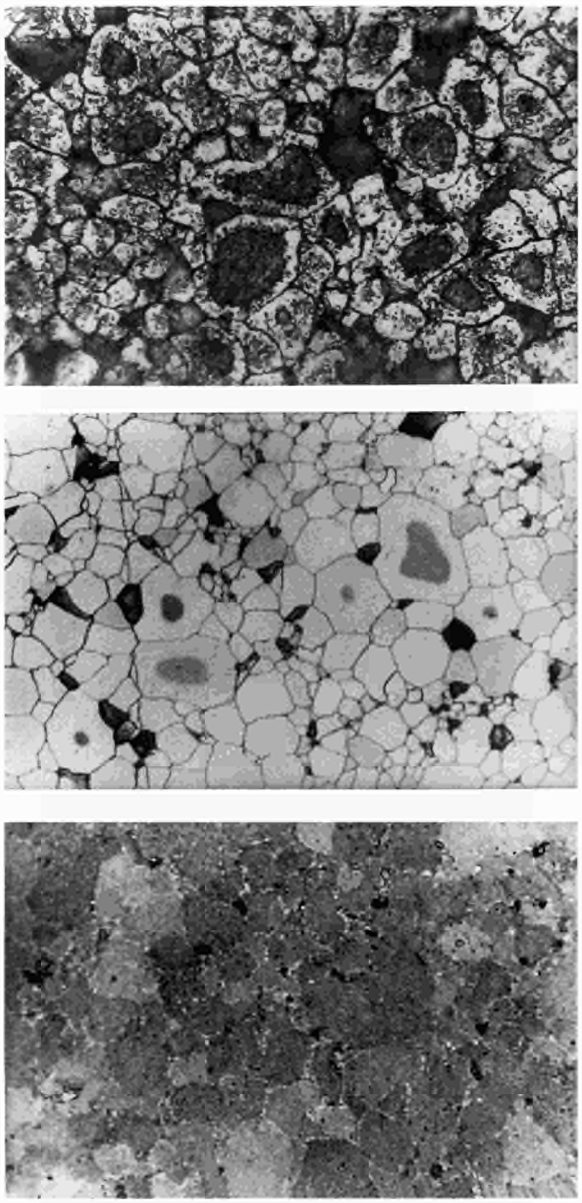

Fig. 4.3 Internal rapid oxidation of irradiated UO_2 during exposure in dry air at 268 °C.
a) after 41 h, bulk O/M = 2.346 ; b) after 48 h, bulk O/M = 2.389 and c) after 530 h, complete oxidation to U_4O_9, bulk O/M = 2.440.

References

[1] R.E. Einziger, L.E. Thomas, H.C. Buchanan, R.B.Stout; J. Nucl. Mater. **190** (1992) 53-60
[2] L.E. Thomas, R.E. Einziger, H.C. Buchanan; J. Nucl. Mater. **201** (1993) 310-319
[3] K.M. Wasywich, Third IAEA RCM on BEFAST-III, Paris, October 16-20, (1995)

4.1.3 Further developments of the lead shielded X-ray goniometer

Improvements to the X-ray goniometer installed in the lead shielded box (TUAR-95, p 130) concerned:

- Optimization of the calibration method used for accurate determination of lattice parameters. In this respect, a complete and statistically reliable calibration curve of the peak shift correction versus the observed diffraction angle was constructed by repeated measurements with various internal standard materials [1, 2].
- A series of measurements with UO_{2+x} with simulated fission products has been performed to determine the influence of burnup (fission product concentration) on the lattice parameter of UO_2 fuels (see chapter 2.1.1).
- Much effort was dedicated to the development of a new collimating technique for XRD microanalysis. The X-ray beam, with 10 μm thickness, emerges parallel in contrast to the focussed beams in monocapillary or multilayer mirror collimators [3-6]. Although the investigation is continued, our first collimator has already shown good performance in preliminary high resolution measurements. In a test, a Zircaloy-4 tube sample oxidized in the LOCA Quenching Facility at IMF I (FZK) was analyzed with our micro-XRD system, in order to detect structural modifications inside the oxide phase (200 μm thick) formed at the outer phase of the tube. The sample was scanned with the micro X-ray beam at space intervals of 30 μm. The obtained spectra, as well as a representation of the interface analyzed, are shown at the beginning of this report (see Highlights 1996). The equipment was indeed able to identify the evolution of the different oxide phases formed across the Zircaloy/ZrO_2 interface. Also, from the peak shifting of the Zr_α reflections within the Zircaloy-phase, it is possible to anticipate some oxygen gradient within the metal phase (α-Zr(O)). The spatial evolution of the different phases formed across the Zircaloy/ZrO_2 interface can be estimated by the intensity variations of the representative Bragg reflections of each phase, as function of the scanning step.

References

[1] H. Toraya, M. Kitamura; J. Appl. Cryst. **23** (1990) 282-285
[2] H. Toraya, W. Parrish; Advances in X-Ray Analysis **35** (1992) 431-438
[3] D.H. Bilderback; D.J. Thiel; Rev. Sci. Instrum. **66** (1995) 2059-2063
[4] D.H. Bilderback; S.A. Hoffman, D.J.Thiel; Science **263** (1994) 201-203
[5] D.J. Thiel, D.H. Bilderback, A. Lewis; Rev. Sci. Instrum. **64** (1993) 2872-2878
[6] A.G. Michette; Optical Systems for Soft X-Rays, Plenum Press, New York and London, 1986

4.1.4 Influence of the oxidation state of spent UO_2 on the dissolution behaviour of UO_2 and MOX spent fuel

The present work was initiated to investigate the influence of the oxidation state of spent UO_2 on the dissolution behaviour of LWR and MOX spent fuel. The study has as a main goal the evaluation of the consequences of a possible fuel oxidation resulting from contact of the spent fuel with air and groundwater when a fuel cladding failure occurs during storage.

Experimental

The samples used in the present study were pieces of UO_2 (53.1 GWd/t) and MOX (38.8 GWd/t) spent fuels, previously oxidised to various oxidation states in flowing dry air at 270 °C (TUAR-95, p. 129).

The leaching tests were performed in de-ionised water and air atmosphere at the room temperature of the hot cell (about 25 °C). The surface/volume ratio (S/V) was approximately $2m^{-1}$, considering the specimen as a sphere. The actinides and fisson product concentrations in the leachate were determined by ICP-MS.

Results

The leaching results obtained for the main fission products and actinides are represented as a fraction of inventory, i.e. the ratio between the amount measured in the leachate and the content of the corresponding element in the fuel, obtained from KORIGEN code calculations.

Fig. 4.4 shows the uranium fractional release for oxidized UO_2 LWR spent fuel as a function of time and 4 different O/M ratios. A high dissolution rate at the beginning, the so called instantaneous release [1] decreases to a very low value after 30 days ($<10^{-7}$ g cm^{-2} d^{-1}). For the two fuels with higher O/M ratios belonging to the stable zone of U_4O_{9+x}, (TUAR-95, p. 128-130), the instantaneous release is about one order of magnitude higher than for the less oxidised fuel samples, where the oxidation process does apparently not affect the leaching behaviour.

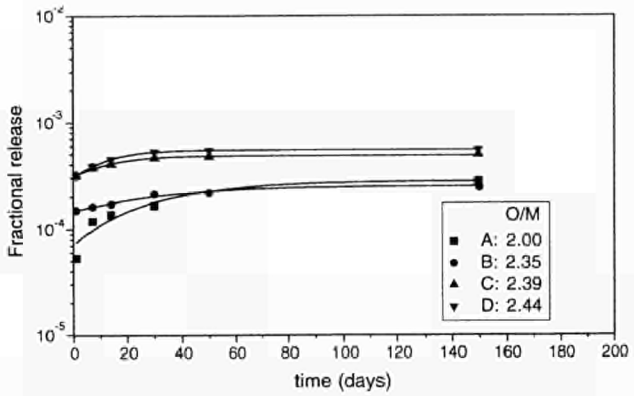

Fig. 4.4 LWR fuel. Cumulative fractional release for uranium -238 as a function of contact time.

For the MOX fuel the instantaneous fractional release of uranium is two orders of magnitude higher than the UO_2 spent fuel at higher O/M ratio (Fig. 4.5).

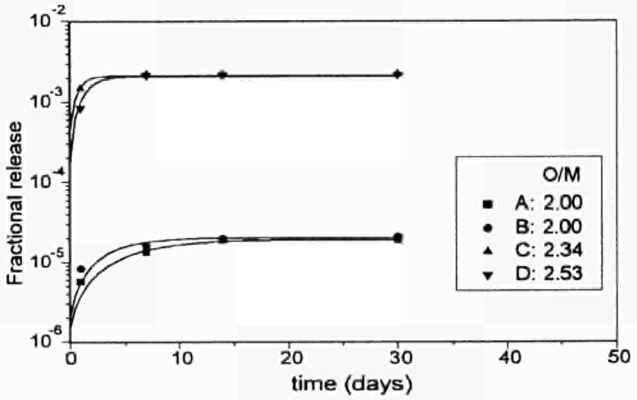

Fig. 4.5 MOX fuel. Cumulative fractional release for uranium -238 as a function of contact time.

In order to compare the dissolution behaviour of the different fission products and actinides, the fractional release for each element was normalised to the uranium release. These normalised fractional release values for UO_2 and MOX fuel, corresponding to the highest O/M ratio are shown in Fig. 4.6 and 4.7.

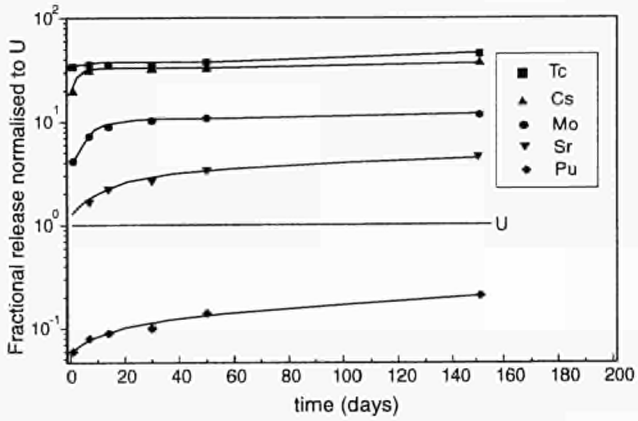

Fig 4.6 LWR fuel. Fraction release normalised to uranium for O/M = 2.44.

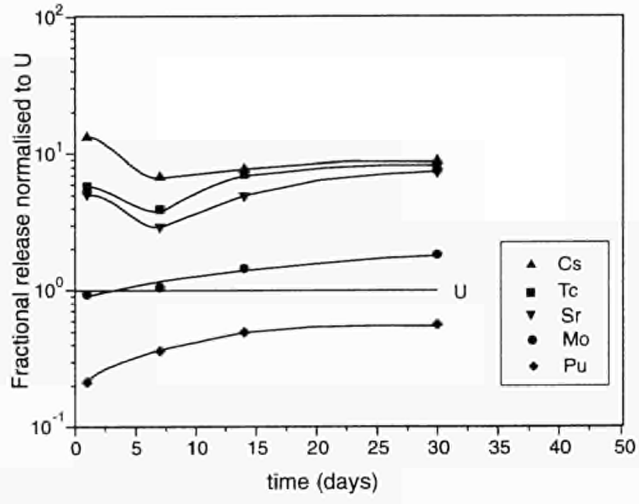

Fig 4.7 MOX fuel. Fraction release normalised to uranium for O/M = 2.53.

For both fuels the normalized fractional release of Pu is lower than 1, due to the known lower solubility of Pu compared to actinides. The increased fractional release of all fission products in comparison to U (up to 100 times) can be mainly attributed to three effects:

- preferential leaching at the level of the grain boundaries which contain higher concentrations of fission products,
- a higher intrinsic solubility of some fission products like caesium,
- redox sensitivity of some fission products such as Tc or Mo.

Discussion

The presence of an accelerated dissolution during the first leaching phase can be attributed to two potential causes. The first is a mechanism proceeding at preferential sites such as grain boundaries and pores [3], TUAR-94, p. 85. The second reason is, that the high O/M specimens have higher dissolution rates. In this case the presence of U_3O_8 at the grain boundary surface [4] or $UO_3 \cdot x\ H_2O$ at the surface can be expected and would enhance the dissolution rate. Unfortunately characterisation of the specimens by X-ray diffraction or by microstructure analysis is not yet completed. This will be carried out in the near future and should allow a better understanding of the dissolution mechanism.

References

[1] R.S. Forsyth, L.O. Werme; J. Nucl. Mater. **190** (1992) 3.
[2] J. de Pablo, I. Casas, J. Gimenez, V. Marti, M.E. Torrero; J. Nucl. Mater. **232** (1996) 138-45
[3] D. Bottomley, D. Wegen, M. Coquerelle; J. Nucl. Mater. **238** (1996) 23-37
[4] S. Sunder, N.H. Miller; J. Nucl. Mater. **231** (1996) 121-130

4.1.5 Complete spent fuel inventory after dissolution in a salt melt

Previous studies (TUAR-95, p. 141) showed that salt melt dissolution of irradiated fuel in a sealed capsule is a suitable method to determine the complete inventory of elements retained in the fuel. This method includes the quantification of volatile fission products such as Xe, Kr, He, ^3H, I (and possibly Br).

A possible application of this analytical method is the determination of the fission gas retained in spent fuel [1,2]. From the local burn-up the local fission gas release can be calculated. These data are of great interest in view of the fission gas release on the behaviour of high burn-up UO_2 fuel [3,4]. A further application of this development is the correlation between the local fission gas release and the corresponding radial fuel restructuring. The present study aims at a better understanding of the process of the fission gas release as a function of fuel temperature. A prerequisite condition for this is the ability to machine irradiated fuel pellets in order to isolate a definite part of fuel characterised by a specific fuel restructuring.

The goals of this study are i) to quantify elements not possible to analyse by EPMA (Kr, I, and He), ii) to confirm results of EPMA (Xe, Cs), iii) to have a complementary method to minor structure analysis and to help understand the behaviour of UO_2 and MOX fuel irradiated to high burn-up.

Experimental

Fuel rod sections were cut from a UO_2 fuel rod irradiated in a power reactor to a burn-up of 80 GWd/t. These fuel rod sections were machined by progressive retrieval of the fuel from the centre of the fuel pellet in order to dissolve fuel sections representative of:

- the fuel pellet as a whole
- structure at the periphery of the fuel pellet (outer rim, $0.92 \leq r/r_0 \leq 1$)
- the fuel zone including the outer rim and the transition zone ($0.54 \leq r/r_0 \leq 1$)

Thus one can determine the average inventory for three different radial areas. The dissolution procedures for the salt mixture and the remaining residues as well as the procedure for the gas measurements are described in TUAR-95, p. 141.

Results

The experimental values of the quantitative analyses of Kr and Xe in a full UO_2 fuel disk (80 GWd/t) were compared to those obtained from the KORIGEN code (Tab. 4.1).

Tab. 4.1 Amounts of Kr and Xe in a full disk compared with the values obtained from the KORIGEN code for UO_2 fuel at a burn-up of 80 GWd/t. Also shown are the results of released gas analysis.

Gas	Experimental [1] (g/tUO_2)	KORIGEN (g/tUO_2)	Filling gas analysis (g/tUO_2)
Kr 82	12	3.5	
Kr 83	28	46	7.4
Kr 84	191	271	35
Kr 85	23	47	5.6
Kr 86	262	376	50
Kr total	525	743	98
Xe 130	46	59	
Xe 131	313	540	72
Xe 132	2255	3330	328
Xe 134	2668	3720	382
Xe 136	4502	6230	603
Xe total	9784	13880	1384
Xe/Kr	19	19	14

1) in the absence of ICP-MS determination of U and Pu in the salt melts, these values have been obtained from weight estimation. This is of course not precise, and the results are be considered as preliminary. The values will be recalculated when more accurate data for U and Pu are available.

The variation between duplicated samples lies within 15%, while the total amounts of Xe and Kr detected (not including the release to the plenum) are by about 30% lower than those predicted by the KORIGEN code.

It should however be pointed out that the burn-up of 80 GWd/t is beyond the code's usual range of application.

The average release ratio calculated from the filling gas analysis is 14-15% which is an indication that gas is released from the fuel pellet mainly by diffusion mechanism. The present specimen located in a peak power position should display a higher release ratio because the two outer ends of the fuel rod (ca. 25% of the total fuel stack length) have a lower linear power and a strongly reduced fission gas release. Therefore a higher gas release could be expected in the specimen measured.

The Xe/Kr ratio of the gas retained in the fuel is in agreement with the predicted value. The lower value determined in the plenum may indicate that atomic diffusion is the determining mechanism, which favours the release of Kr having a smaller ionic radius

Fig. 4.8 shows the average w/o for Xe in the three different disks segments at higher burn up (full segment and segments with holes up to r/r_0=0.54 and r/r_0=0.92, respectively). The distribution for Kr (not shown in Fig. 4.8) shows a similar variation but has a lower magnitude.

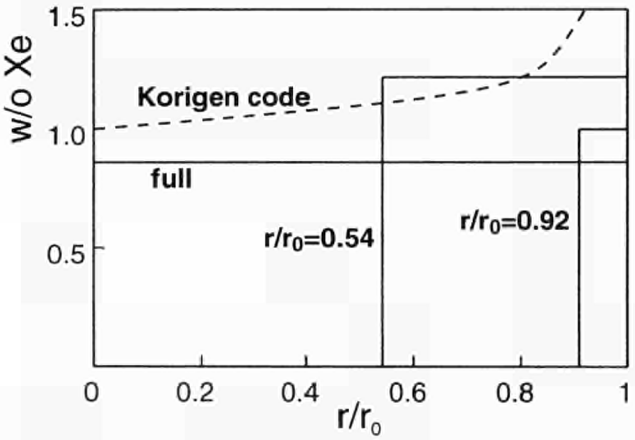

Fig. 4.8 The amount of Xe (w/o), for the three different segments, in a UO_2 fuel with a burn-up of approx. 80 GWd/t. The dashed line represents the amount of Xe formed at 83 GWd/t [4].

The quantification of Xe and Kr release has to be referred to the U and Pu content of each sample obtained by ICP-MS. Unfortunately ICP-MS results show that only up to 5% of the fuel in the nitrate salt mixture is brought into solution even after using excessive amount of concentrated nitric acid and this will cause an uncertainty in the values for Xe. Although the above procedure to dissolve and determine the total inventory of irradiated UO_2 and MOX fuel was successfuly applied (see TUAR-95, p. 141), the reason for the current difficulties is not yet known. A possible explanation is that some Zr of the zircaloy capsule may have dissolved in the caustic salt and formed (U,Zr) oxide that is not easily dissolved in nitric acid. A further dissolution with a mixture of concentrated HCl/HNO_3/HF (9/1/0.04) solution will be undertaken. An alternative capsule material such as stainless steel or copper, now envisaged, may avoid these problems in the future [5].

Futher tests are foreseen in order to investigate further the mechanisms of fission gas release, and to quantify more precisely the inventory of the different samples analysed.

References

[1] A Guidebook to Nuclear Reactors, A.V. Nero Jr., University of California Press (1979)

[2] Nuclear Chemistry, G.R. Choppin, J. Rydberg, Pergammon Press (1980)

[3] R. Manzel, M. Coquerelle, M.R. Billaux, Proceedings of the ANS Topical Meeting on Light Water Reactor Fuel Performance, West Palm Beach, F.L., USA, April 17-21, 1994, p. 335

[4] R. Manzel, M. Coquerelle, ANS International Topical Meeting on LWR Fuel Performance, Portland, USA, March 1997, to be published.

[5] Proc. of the First Inf. Meeting on the TM1-2 Accident, S. Langer, W. Young, (1985) p. 195

4.1.6 Leaching of SIMFUEL and irradiated fuel in simulated granitic water

Introduction

Previous work (TUAR-95, p. 133-139 and [1]) dealt with the static leaching behaviour of SIMFUEL with different burnup compositions at 200 °C under anaerobic conditions in granitic water in the presence of granite monoliths. During the reporting period leaching experiments under static conditions have been performed on SIMFUEL with 3 a/o simulated burnup and, in parallel, on irradiated UO_2 fuel with a burn-up of about 43.3 GWd/tM. The experimental conditions were, as much as possible, identical: room temperature, granitic water and ambient air atmosphere. The influence of the presence of granite monoliths was also studied. The results were compared to the earlier data for SIMFUEL and UO_2 (TUAR-95, p. 133-139, TUAR-92, p. 90-93) and for irradiated fuel [2]. The constraints on the experimental conditions, aimed at simulating a granitic repository for the final storage of spent fuel, were mostly dictated by the difficulties in performing such tests in a hot cell. The aim of these experiments was also to compare the behaviour of SIMFUEL with that of irradiated fuel under the same test conditions. In this respect, one has to keep in mind that results from leaching experiments using irradiated fuel samples do not correspond directly to the conditions in a repository several hundred years after the final disposal of such fuel, because at that time the α-radiation field will be dominating; the relatively fresh fuel available nowadays, however, is characterized by an additional strong γ-radiation field, which has significant effects on the dissolution behaviour of the fuel [3].

Experimental

Four leaching times were selected: 1 d, 10 d, 30 d, and 60 d. For each leaching time, three glass bottles of 40 cm^3 volume were used as leaching vessels: the first loaded with fuel (SIMFUEL or irradiated fuel) + granitic water; the second loaded with fuel + granitic water + a granite cylinder; the third (blank test) loaded with

granitic water + a granite cylinder. The blank tests were performed to evaluate the contribution of the granite monolith to the measured amounts of fission products and uranium released in the leachate and in the rinse solutions (both U and the fission products of the SIMFUEL were present, mostly as impurities, in the granite [1]). For each test, 15 ml of leachate were used. The compositions of SIMFUEL, granite, and granitic water are given in TUAR-95, p 133-139. The tests with SIMFUEL were carried out at ambient lab. temperature of 23±2 °C; those with irradiated fuel were performed in a hot cell, at ambient hot cell temperature of 25±2 °C. The blank tests were performed both in the lab and in the hot cell. A new fuel sample was used for each test. The irradiated fuel pieces were from a LWR pin. They had irregular shapes, with weights ranging between 0.165 g and 0.610 g. All the SIMFUEL specimens had cylindrical shape, with approximately the same weight (~1.1 g) and dimensions (1.2 cm diameter, ~0.09 cm thickness). From the geometry measurements, a specific surface area of ~1.5 cm^2g^{-1} was calculated. In the case of SIMFUEL tests, the S_{fuel}/V_{sol} ratio was ~0.175 cm^{-1}. The granite cylinders had a diameter of 1.6 cm, a thickness of ~1.4 cm, and an average weight of 7.1±0.4 g. No significant loss of leachate from the vessels was detected at the end of the tests. The leaching vessels used for the tests with the SIMFUEL were inspected in order to locate and remove possible fragments broken off the edges of the specimen during leaching. Subsequently, all the containers and the granite cylinders were rinsed *separately* with 20 ml of 1N HNO_3 for 60 minutes at room temperature. All leachates and all rinse solutions were analyzed using ICP-MS (Perkin-Elmer ELAN 5000). The SIMFUEL specimens were weighed and observed under an optical microscope. The SIMFUEL surface was analyzed using Scanning Electron Microscopy (SEM). Other measurements, such as Electron-Probe Micro-Analysis (EPMA), X-ray Photoelectron Spectroscopy (XPS), Rutherford Backscattering Spectrometry (RBS), helium resonance scattering, and Elastic Recoil Detection Analysis (ERDA) are currently in progress, or will be used to characterize the leached surfaces [4].

Results

SIMFUEL

In general, the results of the ICP-MS did not show an unequivocal increase of the amount of dissolved nuclides with increasing leaching time under the present experimental conditions, indicating early saturation. The data for the leachates and for the rinse solutions can be qualitatively summarized as follows: Ru, Rh, and Pd were not detected in any solution; Y, Zr, La, Ce, and Nd, which are present in the 60 to 400 ppm level [1] in the granite used, were found only in the granite rinse solutions, and were therefore attributed to acid dissolution of granite. Tab. 4.2 summarizes the measured concentration data for Sr, Mo, Ba, and U. These were the only elements detected in the leachates.

Qualitatively, the results of this set of experiments, performed at room temperature in air, were similar to the results of the leaching experiments at 200 °C under anaerobic conditions reported previously [1] (TUAR-95, p. 133-139). In particular, Mo was present, mostly in large amounts, only in the SIMFUEL leachates. By comparing the results for the leachates of SIMFUEL + granite with those for the SIMFUEL alone, no clear difference was evident in the case of Mo. This, together with

Tab. 4.2 Summary of the ICP-MS data for the leaching experiments of SIMFUEL. The values are in ppb, with a precision of about ±5%.

Element, leaching time	Leachates (ppb)			Rinse leaching vessels (ppb)			Rinse granite cylinders (ppb)	
	SIMFUEL only	SIMF. + granite	granite only	SIMFUEL only	SIMF. + granite	granite only	SIMF. + granite	granite only
Sr 1d	0	173	0	11	1	2	94	51
10d	123	0	0	5	1	1	36	30
30d	346	0	0	5	2	4	84	59
60d	11	0	0	2	2	1	51	30
Mo 1d	101	63	0	0	0	0	0	0
10d	82	82	0	0	0	0	0	0
30d	220	151	0	0	0	0	0	0
60d	145	151	0	0	0	0	0	0
Ba 1d	142	312	0	80	18	62	347	169
10d	632	53	0	151	45	53	329	223
30d	1006	9	0	71	45	53	419	312
60d	445	53	0	89	53	36	374	214
U 1d	3	17	9	3	1	2	371	293
10d	9	12	0	18	1	0	195	226
30d	25	25	19	30	1	2	319	133
60d	15	78	18	4	4	1	474	191

the absence of Mo in the blank test leachate and in the rinses of the leaching vessels or of the cylinders, suggests that the granite has no detectable influence on the dissolution behaviour of Mo, and that sorption phenomena do not play a significant role for this element. Another similarity was with the previous results that Sr was detected in the leachate of SIMFUEL + granite tests only after the shortest leaching time. In the SIMFUEL + granite solutions (both leachate and rinses) the concentrations of Sr and Mo were generally higher in the present set of experiments performed in air, despite the lower temperature. In the case of U the values measured in the leachates were similar or occasionally higher in the high temperature tests, while the opposite was observed for the rinse solution values. For Sr and Ba, the concentrations in the leachate of SIMFUEL alone were significantly higher than those of SIMFUEL + granite after all leaching times, except after the shortest one. This may suggest that, after leaching in presence of granite for times longer than 1 day the Sr and Ba released by the SIMFUEL were removed from the solution by reprecipitation onto the SIMFUEL and/or by sorption onto the granite surface. The removal was only partial for Ba, while no Sr was detected in the leachate of SIMFUEL + granite after 10, 30 or 60 days of leaching. The ICP-MS results for the blank test leachates show that no fission products were detected. This indicates that the granite monoliths did not contribute to the total amount of fission products released in the leachate. On the contrary, by considering -only qualitatively, due to the unavoidable scatter of the data caused by the many components of the granite surface- the concentration values for the acid rinses of the granite cylinders, in almost all cases the values for the cylinder which had been leached together with the SIMFUEL were higher than the corresponding ones for the cylinder which had been leached alone in the blank test. This would indicate that part of the amount of fission products dissolved from the granite by the rinse procedure was first leached from the SIMFUEL and then sorbed onto the granite surface during the leaching test. In addition, the concentration values from the acid rinse solutions of the leaching vessels which had contained the SIMFUEL alone were generally larger than the other vessel rinses. In most cases the concentration of fission products found in the rinse solutions of the vessels was on the order either of a few ppb or negligible (i.e. < 1 ppb), with the exception of Ba, which was found in amounts ≥ 10 ppb in all vessel rinses. The concentrations of U measured in the leachates were similar to values reported in literature for leaching of SIMFUEL in granitic groundwater at room temperature under anoxic conditions [5]. The present data showed higher concentrations in the leachates of SIMFUEL + granite than in the leachates of SIMFUEL only. Part of the difference could be attributed to a contribution of the granite cylinder to the total released amount of SIMFUEL + granite (see the data for the blank test leachates in Tab. 4.2). Moreover, the amounts of U measured in the rinse of the vessels indicated that, at least after 10 d and 30 d of leaching, more U is sorbed onto the walls of the vessel when leaching SIMFUEL alone.

Irradiated fuel

The ICP-MS results for the leaching tests of irradiated fuel, like those for SIMFUEL, did not show evidence of a clear effect of leaching time. Also, Ru, Rh, and Pd were not detected in any solution. Y, Zr, La, Ce, and Nd were detected in non-negligible amounts in the fuel leachates, but were not detected in almost all the vessel rinse solutions and found in large amounts in the rinse of the granite cylinders. The ICP-MS data for U and some relevant fission products are summarized in Tab. 4.3.

^{98}Mo and ^{99}Tc were present essentially only in the fuel leachates. This behaviour was qualitatively similar to that of Mo from the SIMFUEL tests. A direct comparison between irradiated fuel and SIMFUEL results for Sr is not appropriate because ^{90}Zr interferes on the granite rinse data (this is why the values in column 8 are in parenthesis in Tab. 4.3), and also because of the difference of the inventories in the two cases (in the particular SIMFUEL used for these experiments, Sr simulates also Cs; it is therefore present in a fraction ~3 times higher than the calculated inventory of ^{90}Sr in the irradiated fuel). The ^{90}Zr interference did not affect the results for the leachates, since nothing with atomic mass 90 was detected in the blank test leachate (and also in the SIMFUEL leachate solutions). Ba, like in the SIMFUEL leaching tests, was found in all solutions except the blank test leachate. Its concentration values were small in all fuel leachates and vessel rinse solutions, and large in most of the granite rinses. ^{133}Cs was also measured in all solutions. ^{239}Pu was essentially found only in the fuel leachates in non-negligible amounts. The ratio of Pu/U concentrations in the leachates was consistent with congruent dissolution of the fuel matrix. U, differently from the SIMFUEL tests, was found in large concentrations in the fuel leachates and in some of the rinses, and in small or non-negligible amounts in the blank tests.

The concentrations of U measured in the leachates are similar to values reported in literature for leaching of irradiated fuel at room temperature in synthetic groundwater in air [6]. In presence of granite the concentration of U in the fuel leachate after 1 d, 10 d, and 30 d was lower by a factor of ~2, while after 60 d the amount of U was higher by a factor of ~4. The contribution of the granite cylinders to the quantities measured in the leachates was one order of magnitude smaller than that of the fuel (see blank test leachate in Tab. 4.3). For Mo and Tc, no effect due to the presence of granite is evident, similarly to what was observed for Mo in the results of SIMFUEL leaching. Also in the case of Ba there is no evidence of an effect due to the granite. For the other fission products, the measured concentrations are too small to determine a clear pattern. The irradiated fuel pieces had masses ranging between 15% and 55% the average mass of a SIMFUEL sample. Therefore, it is useful to consider the results also in terms of Fraction of Inventory in the Aqueous Phase (FIAP). Fig. 4.9 illustrates the FIAP data for U in the leachates of irradiated fuel and SIMFUEL with and without the granite cylinders.

Tab. 4.3 Summary of the ICP-MS data for the leaching experiments of irradiated fuel. The values are in ppb, with a precision of about ±5%.

Nuclide, leaching time	Leachates (ppb)			Rinse leaching vessels (ppb)			Rinse granite cylinders (ppb)	
	Fuel only	Fuel + granite	granite only	Fuel only	Fuel + granite	granite only	Fuel + granite	granite only
^{90}Sr 1d	4	5	-	0	0	-	(22)	-
10d	5	2	-	0	0	-	(28)	-
30d	2	0	-	0	0	-	(35)	-
60d	3	5	-	0	0	-	(106)	-
^{98}Mo 1d	4	6	0	0	0	0	1	1
10d	7	7	0	1	0	1	1	0
30d	2	3	0	0	0	0	6	0
60d	4	3	0	0	0	0	0	0
^{99}Tc 1d	6	3	-	0	0	-	0	-
10d	8	7	-	0	0	-	1	-
30d	5	5	-	1	1	-	0	-
60d	4	4	-	0	0	-	0	-
^{127}I 1d	2	2	0	1	1	1	1	1
10d	15	14	0	0	0	0	0	0
30d	10	13	0	2	2	0	1	0
60d	1	2	1	1	1	0	1	1
^{133}Cs 1d	198	185	1	7	8	0	1	0
10d	271	137	2	8	5	0	51	1
30d	67	13	0	3	1	0	15	1
60d	39	135	1	7	2	0	20	1
^{138}Ba 1d	12	27	0	12	7	12	95	89
10d	93	3	0	40	40	23	211	227
30d	43	62	0	24	35	30	120	119
60d	1	42	4	101	57	51	206	64
^{238}U 1d	617	354	8	48	132	28	43	33
10d	754	331	9	175	105	25	559	50
30d	609	156	28	26	34	2	116	49
60d	203	990	82	112	22	2	83	35
^{239}Pu 1d	3	2	-	0	1	-	0	-
10d	5	3	-	1	1	-	0	-
30d	2	2	-	0	1	-	0	-
60d	1	2	-	1	0	-	0	-

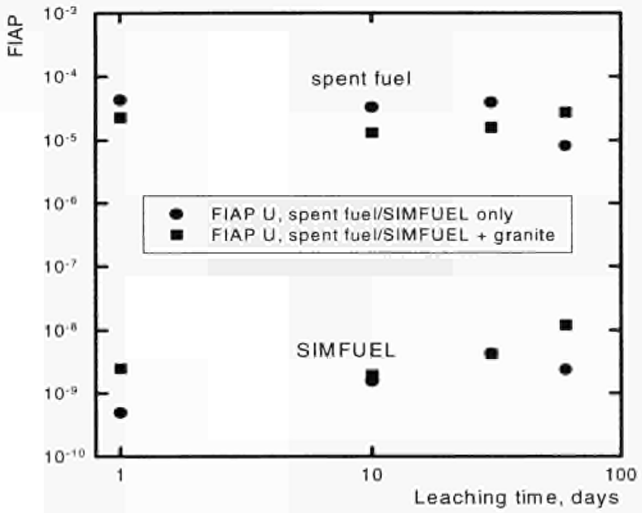

Fig. 4.9 FIAP of U in the leachates of irradiated fuel and SIMFUEL with and without granite. The estimated error on the data points plotted is about 10%, which corresponds to error bars smaller than the plotted symbols.

The FIAP values for irradiated fuel are approximately 4 orders of magnitude higher than those for SIMFUEL. A small fraction of this difference can be due to different surface areas, but most of it has to be attributed to the effect of radiolysis, which enhances U solubility by increasing the oxidation state of U ions. Fig. 4.10 shows the FIAP data for Sr and Mo. For better clarity, only the results of the tests without granite are reported in the figure. Also in this case the FIAP values for the irradiated fuel are higher than those for the SIMFUEL, although the difference, mostly within one to two orders of magnitude, is smaller than for U. This is expected, since the radiolysis-enhanced solubility effect is less important for these fission products than for U.

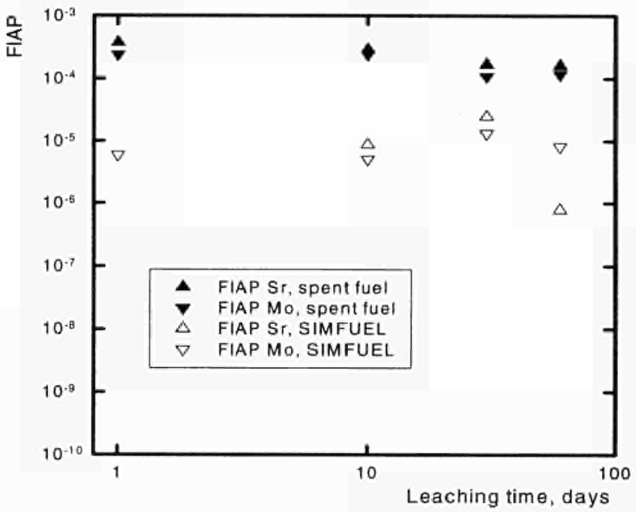

Fig. 4.10 FIAP of Sr and Mo in the leachates of irradiated fuel and SIMFUEL. For better clarity, only the data of the tests without granite monoliths are reported. The estimated error on the data points plotted is about 10%.

Conclusions

This work provides direct comparison of the leaching behaviour of SIMFUEL and spent fuel under specified conditions (static leaching, room temperature, ambient air, granitic water, with and without the presence of granite monoliths) as identical as possible. Many similarities for the two types of fuel were observed for the elements where radiolysis effects are not expected. In the case of U, the fractions leached from the irradiated fuel were dramatically higher than those leached from the SIMFUEL. This clearly implies a strong radiolysis effect. Additional work is currently ongoing to further study the effects of effects of γ- and α- radiolysis on the fuel dissolution and to characterize the surfaces of the leached samples, and will be included in future reports.

References

[1] V.V. Rondinella, Hj. Matzke; J. Nucl. Mater. **238** (1996) 44
[2] J.P. Glatz, E.H. Toscano, G. Pagliosa, A. Nicholl; J. Nucl. Mater. **223** (1995) 84
[3] A. Loida, B. Grambow, H. Geckeis, P. Dressler; Mater. Res. Soc. Symp. Proc. **353** (1995) 577
[4] Hj. Matzke; Surface Interface Analysis **22** (1994) 472
[5] K. Ollila; J. Nucl. Mater. **190** (1992) 70
[6] R.S. Forsyth, L.O. Werme; J. Nucl. Mater. **190** (1992) 3

4.2 Interaction of Nuclear Fuel with Structural Materials

The objective of this work is to examine the interaction of reactor structural materials and nuclear fuel during reactor accidents. It is a complementary study to the analysis carried out on PHEBUS materials and will contribute to a better understanding of reactor degradation. The main materials are Zircaloy-4 cladding, Ag-15 In-5 Cd (AIC) PWR absorber material, 304 L stainless steel absorber cladding material, and Inconel 718 (Ni-based alloy) for springs and spacer grids. These materials have been tested along with natural UO_2 by dilatometric and differential thermal analysis techniques in either combination of 2 materials (a stack of 2 cylinders) or three materials (a stack of 2 cylinders with a central disc of a 3rd material). The first series of experiments (see TUAR-94, p. 102-109) lead to the conclusion that the Ni-Zr and Fe-Zr interactions were the most important for the degradation between stainless steel, Inconel and Zircaloy. Current experiments attempt to assess:

1) the effect of contact pressure between the cylindrical samples on interaction temperature,
2) the effect of contact geometry on the interaction, and
3) the effect of the Zircaloy alpha-beta transition on the interaction. The results are summarized in Tab. 4.4.

Tab. 4.4 Materials interactions.

Materials (*top → bottom*)	Experiment	$T_{interaction}$	$T_{max.}$	Interaction DTA peak (μV) Dilatometer depth (μm)	Comment
A) Contact Weight Dilatometry					
Zry/ss 304	extra weight (4.2 g)	1090°C	1100°C	18 μm	thin 2-phase interaction zone
Zry/ss 304	no extra weight	1060°C	1100°C	20 - 30 μm	more attack of 304 than Zry
B) Contact geometry DTA					
V2A cone/Zry-4 cylinder		1350°C ↑ 1250°C ↓		weak (- 15 μV) moderate (- 20 μV)	unstable from 1200°C on rising (liquefaction?)
Zry-4 cone/V2A cylinder		1280°C ↓		strong (- 30 μV)	unstable from 1300°C upwards
In 718 cone/Zry-4 cylinder		1180°C ↑ 1320°C ↓		weak (- 10 μV) strong (- 50 μV)	– very sharp interaction
Zry-4 cone/In 718 cylinder		1320°C ↑ 1160°C ↓		strong (- 200 μV) weak (- 30 μV)	very sharp interaction
C) α - β transition temperature dilatometry					
In 718/Zry-4		980°C 1020°C	to 1200°C (10°C mn^{-1})	α → β strong liquefaction at 1020°C	–
In 718/Zry-4		880°C 970°C	to 900°C @ 10°C mn^{-1} then to 1000°C @ 0.6°C mn^{-1}	α → β strong liquefaction at 970°C	–
304 ss/Zry-4		880°C 1075°C	to 900°C @ 10 °C mn^{-1} then to 1100°C @ 0.6°C mn^{-1}	α → β strong liquefaction at 1075°C	–

Contact pressure

The contact weight is normally 3 g: additional ZrO_2 weights were made to raise the contact weight to 7.2 g, for the 304 stainless-Zry couple. Despite a doubling of the weight the interaction temperature was slightly higher (1060 °C vs 1030 °C). Thus there is no significant difference with direct contact weight.

Contact geometry

The effect of contact geometry was examined using a cone in contact at its pointed end with a plane disc so that there was a point of high contact pressure, as well as a greater supply of one sample (disc material) compared to the other (cone material). The stainless steel/Zircaloy and Inconel 718/Zircaloy couples were tested in both geometries by differential thermal analysis (DTA).V2A, the German equivalent of the American stainless steel 304L was used; composition ranges are similar except for a slight difference in carbon content: 304C has 0.03 a/o C while V2A has 0.06 a/o C). The results are given under B) in Tab. 4.4.

These showed some differences with geometry. For the Zircaloy/Inconel system, a larger Inconel supply gives a rapid reaction with the Zircaloy at ~ 1320 °C releasing more heat than vice versa (see Fig. 4.11).

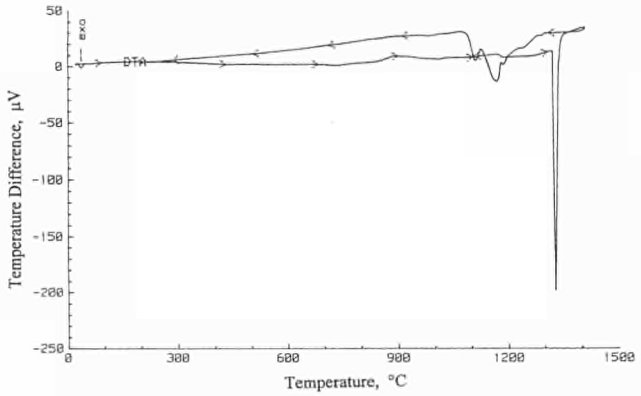

Fig. 4.11 Differential Thermal Analysis graph of a point contact of Zircaloy with Inconel 718 (i.e. inverted Zry cone on a Inconel 718 disc) where Inconel 718 supply to the interacting zone is greater. The graph shows a very large and sharp heat release at 1320 °C.

Given that Inconel is a nickel-based alloy and its behaviour can be interpreted in terms of Ni interactions, then this implies the heat release at 1320 °C is due to the Ni-rich Zr alloy (e. g. Ni_7Zr_2), a second peak on cooldown at 1160–1200 °C may due to NiZr eutectic solidification (see Fig. 4.12).

In the Zircaloy/stainless steel system the small difference between the two configurations implied that larger Zircaloy supply reacts faster with stainless steel than vice versa. Assuming that stainless steel is Fe-based, then it implies that the peak at 1350 °C is due to a Zr-rich Fe alloy, however, the chosen temperature is in fact close to the Fe-10% Zr eutectic at 1340 °C. The peak on cooldown at 1260 °C is puzzling as this is no reaction around this temperature for Fe-Zr system and may represent a Ni-Zr or a (Fe, Ni)-Zr interaction. This suggests

Fig. 4.12 Micrograph of the interface between Zircaloy-4 and Inconel 718 composed of 2 phases (probably Zr-rich and Ni,Fe-rich intermetallics). The proportion of these phases also varies across the interaction zone.

that stainless steel may not always easily be equated to Fe in its interaction behaviour unlike the comparison between Inconel 718 and Ni. The metallography indicates, as has the previous work, that it is Zircaloy that loses its solid form most quickly (see Fig. 4.13).

Moreover, examination of the phase diagram shows that the liquidus temperatures of Zr drop rapidly as it is diluted with upto 20 a/o Fe or Ni. The Ni-Zr liquidus/solidus temperatures are, in any event, approx. 100–150 °C lower than the corresponding Fe-Zr alloys for a wide range of compositions. By contrast, the Cr-Zr alloys have relatively high liquidus temperatures (see TUAR-95, p. 147). Thus the most critical stage appears to be that of the diffusion of Ni or Fe into the Zircaloy reducing the liquidus temperature and with exothermic formation of intermetallics that can accelerate the Zircaloy liquefaction. This occurs at approximately 1100 °C and is probably initiated by the Ni-Zr interaction. This confirms work from the previous year (TUAR-95, p. 152).

The effect of the alpha-beta transition

The next stage was to examine the Zircaloy alpha-beta transition effect on the interaction of a 2 disc Inconel 718 or 304 ss/Zircaloy-4 couple. This used dilatometric measurements on this couple while heating in 3 different profiles.

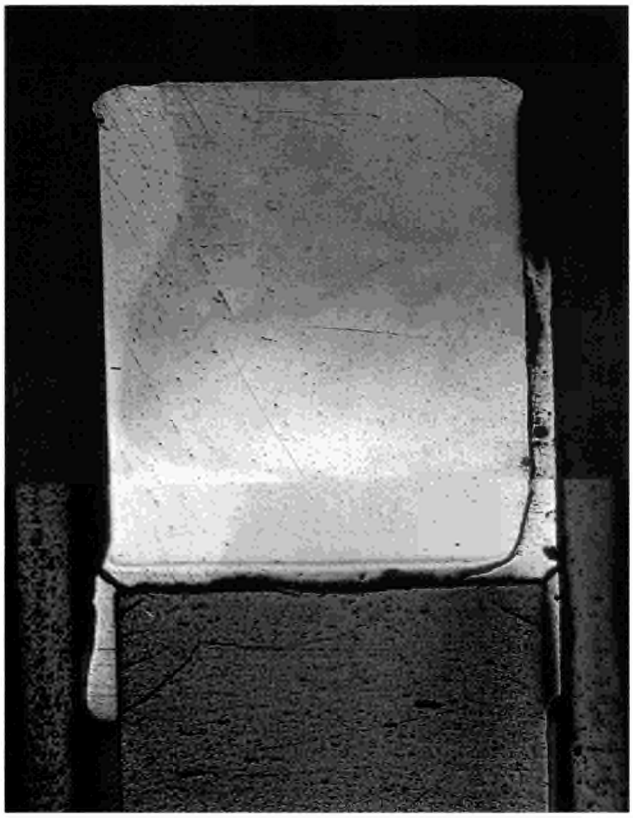

Fig. 4.13 Metallography of a dilatometry test for the interaction of a 3 material combination UO_2/Zircaloy/IN 718 rising to 1100 °C under argon atmosphere. The central Zircaloy disc has completely liquefied and flowed away compared with only slight attack of the upper Inconel cylinder. Attack of this Zr-rich phase on the UO_2 cylinder has not yet commenced.

1) In 718/Zry-4 directly to 1200 °C at 10 °C min^{-1}

2) In 718/Zry-4 to 900 °C at 10 °C min^{-1}, thereafter slowly at 0.6 °C min^{-1} to 1000 °C

3) 304 ss/Zry-4 to 900 °C at 10 °C min^{-1}, thereafter slowly at 0.6 °C min^{-1} to 1100 °C

In 1) at 980 °C the hexagonal alpha-Zr converted to body centred cubic beta-Zr and soon at 1020 °C (4 min. later) a rapid liquefaction had started.

In tests 2) and 3) the alpha-beta transition initiated the interaction at 880 °C and is, in view of the lower temperature gradient, probably closer to the real value for the transition. The interaction accelerates away at 970 °C in the second (In 718/Zry-4) test and 1075 °C in the third (304 ss/Zry-4) test. Despite the 100 °C difference in temperature, it is clear that the Ni-Zr or Fe-Zr reactions can be dominating shortly after the $\alpha \rightarrow \beta$ transition from 1000–1070 °C onward. These samples are currently awaiting metallographic examination.

Concluding remarks

1. The effect of contact weight is negligible on the extent of interaction between 304 ss and Zircaloy.

2. Geometry tests indicate that Ni-Zr is the more reactive interaction than Fe-Zr, and thus In 718/Zry reaction is quicker than the 304 ss/Zry reaction. Phase diagrams show how at the Zr-rich end of both Fe-Zr and Ni-Zr systems, the Zr alloy melting point is greatly reduced (to approx. 1000 °C with 15 w/o Ni or Fe content).

   Metallography of both In 718/Zry and 304 ss/Zry interactions also confirms how the Zircaloy undergoes the greatest liquefaction (see TUAR 94 p. 152).

3. The $\alpha \rightarrow \beta$ Zircaloy dilatometry shows clear sample deformation shortly after the $\alpha \rightarrow \beta$ transition, and this plays a role in the interaction between stainless steel/Inconel 718 and Zircaloy. Possibly by improving contact between the metals or disrupting any oxide films on the surface (enabling better interdiffusion) as well as weakening the Zircaloy.

Future work

Similar slow heat up rate experiments will be carried out with the 304 stainless (or German equivalent V2A)-Zircaloy couple. The effect of preoxidation or oxide films on the effective interaction temperature will also be examined. Further work will then investigate the kinetics of one interaction (e. g. Zry/In 718) with time.

4.3 Non-Destructive Assay of Spent Fuel

The possibility of using a CdTe detector for gamma spectroscopy of nuclear material has already been investigated at the Institute [1,2]. On the basis of these preliminary studies, a compact monitor was constructed and installed inside the hot-cell for gamma spectroscopy on high burn-up fuel, in the presence of intense gamma background. Gamma spectroscopy will eventually complement passive neutron assay in the characterization of spent fuel in terms of burn-up, cooling time and inventory [3].

A planar CdTe detector with 9 mm^2 sensitive area and 2 mm thickness was used. It operated without cooling at a voltage of 120 V. The amplifier used combined normal amplification and electronic pulse processing (Charge Loss Corrector, CLC) resulting in improved energy resolution and peak-to-noise ratio [4]. The detector was mounted in a compact cylindrical monitor made of lead [4] and installed inside the $\beta \rightarrow \gamma$ hot cell where spent nuclear fuel rods from PWR and BWR are stored. The fuel rod studied is held parallel to the top surface of the monitor and can be translated horizontally on its supporting stand for gamma scanning. The gamma radiation is collimated onto the CdTe detector through a tungsten bore hole collimator, of 1 mm in diameter, that is fitted into the lead shielding. The CdTe detector and preamplifier are connected by a LEMO connector to the electronic modules situated outside the hot cell, through a cable of 12 m length.

The performance of the detector inside the hot cell is illustrated through the gamma spectrum of spent nuclear fuel [46 GWd/t burn-up, 1.5 y cooling time] (Fig. 4.14).

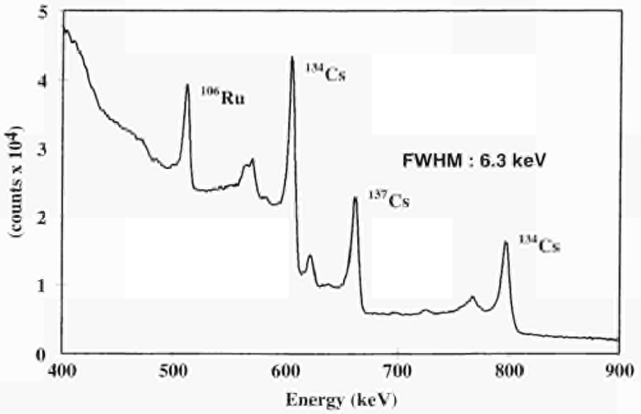

Fig. 4.14 Gamma spectrum of a spent nuclear fuel rod (Burn-up 46 GWd/t and 1.5 years cooling time).

Gamma rays from the fission products ^{134}Cs, ^{137}Cs and ^{106}Ru are observed in the spectrum. The 605 and 662 keV lines from ^{134}Cs and ^{137}Cs are well resolved; the 796 and 802 keV from ^{134}Cs form a doublet, which is also the case for the 512 keV of ^{106}Ru and 511 keV annihilation radiation. The energy resolution (FWHM) of 6.3 keV at 662 keV was obtained. The effectiveness of the collimator has been demonstrated, as well, in the scanning of a fuel rod where the gap between successive pellets is clearly visible.

References

[1] K. Abbas, G. Nicolaou, D. Pellottiero, P. Schwalbach, L. Koch; Nucl. Instr. and Meth. A **376** (1996) 248

[2] G. Nicolaou, K. Abbas, L. Koch; Proceedings 17th Annual Symposium on Safeguards and Nuclear Material Management, p. 519-521, Aachen, Germany, 9-11 May, 1995 (EUR 16290 EN)

[3] G. Nicolaou, K. Abbas, L. Koch; TOPSEAL '96 International Topical Meeting on Demonstrating the Practical Achievements of Nuclear Waste Management and Disposal, European Nuclear Society ECN, Stockholm, Sweden, 9-12 June, 1996

[4] K. Abbas, G. Nicolaou, L. Koch; Nucl. Instr. and Meth. A. (in press)

5. Safeguards Research and Development

Introduction

The Institute has used some of its institutional resources to perform research and development in areas not covered by the institutional support programme for DG I and DG XVII. The activities carried out concern essentially initial tests and the establishment of methods for environmental monitoring and improvements of methods for the determination of the origin or transfer routes of seized nuclear materials. In addition, a new miniature cadmium zinc telluride detector was tested for future safeguards applications.

A remote measurement system for uranium and plutonium in nuclear waste samples by laser ablation emission spectroscopy was further tested.

5.1 Analysis of Uranium Particles by Secondary Ion Mass Spectrometry (SIMS)

For the characterization of single particles in terms of their isotopic composition, SIMS has been carried out on several swipe samples. The instrument used, a Cameca IMS 6f installed at the beginning of 1996, has a double-focusing mass spectrometer which allows fast switching between masses giving the possibility to scan over the mass range of interest. In addition, it has microfocus ion sources (caesium and duoplasmatron with oxygen or argon gas) that can be used in either microscope or microprobe mode. With this instrument, small particles of actinides and other elements of interest can be identified and their isotopic ratio determined.

Particles of enriched uranium in swipe samples, collected during several field trials carried out in collaboration with the IAEA and/or the Euratom Safeguards Directorate (ESD), have been identified.

The method used for sample preparation involved the transfer of the material loaded on the swipe to special adhesive supports. A coating of 20 nm of carbon was added in order to avoid charging effects during the instrumental analysis.

A resolution of up to 10000 can be obtained, but for the measurement of the 235/238 isotope ratio, a resolution of 2000 was found to be sufficient. At this resolution flat top peaks are obtained which greatly improve the accuracy of the measurement. A sensitivity in the ng/g – pg/g range can be achieved by optimising certain instrumental parameters, such as the acquisition time.

An 8 keV primary O_2^+ beam with a current between 50 and 200 nA was used for the rastering. The complete sample surface was scanned by several rasters 150 x 150 μm square and the areas from which a uranium signal was obtained, were identified. From the ion map obtained, the uranium particle was pinpointed and the mass spectrum between mass 234 and 239 was recorded in order to measure the intensities of the two uranium isotopes. After decreasing the resolution to obtain flat top peaks and checking the mass calibration, the acquisition for the determination of the isotopic ratio was started.

The size of the particles in the first campaign was 1-10 μm.

5.2 Gamma ray Spectrometry of Nuclear Material using a CdZnTe Detector

The performance of a CdZnTe detector for gamma spectrometry on diverse nucler materials has been investigated.

A planar CdZnTe detector of 5 mm thickness and 100 mm^2 sensitive area was used in this work. The nuclear instrumentation comprised a high voltage unit (bias 1500V), a standard amplifier (Ortec 572) with shaping time of 0.5 μs and an ultra-high speed analog-to-digital converter (0.75 μs fixed conversion time for high resolution and count rate spectroscopy).

Gamma-ray spectrometry was performed on a UO_2 spent nuclear fuel pin, PuO_2 powder, MOX pellets and natural uranium solution. The studies on spent fuel were performed at the β-γ hot cell facilities where the fuel is stored. The cell wall was made of concrete with a thickness of 1 m. A collimator of lead and tungsten, 1.2 mm diameter, was incorporated into the wall allowing gamma-ray spectrometry of pins with a detector situated outside the cell. The powder and solution samples were analysed in contact with the CdZnTe detector.

Gamma spectrometry of standard radioactive sources has shown that the CdZnTe and CdTe detectors have comparable resolution, which is about a factor of 5 lower than that of a HPGe detector. However, the CdZnTe detector is by far inferior from the peak-to-valley ratio viewpoint. This is due to charges lost from recombining or trapping of the holes. A drastic decrease in efficiency occurs which is up to a factor of 1000 in the energy range of 100 to 700 keV. In the case of the HPGe detector, this factor is less than 10. The energy resolution varies from 5% to 2% in the above energy range. However, the peak-to-valley ratio is much higher at low energies (< 200 keV) indicating the suitability of the CdZnTe detector used at these energies, i.e., for uranium analysis.

A typical gamma-ray spectrum of uranium solution, obtained with the CdZnTe detector, for a counting period of 1800 s, is shown in Fig. 5.1. The corresponding spectrum with a HPGe detector is included for comparison.

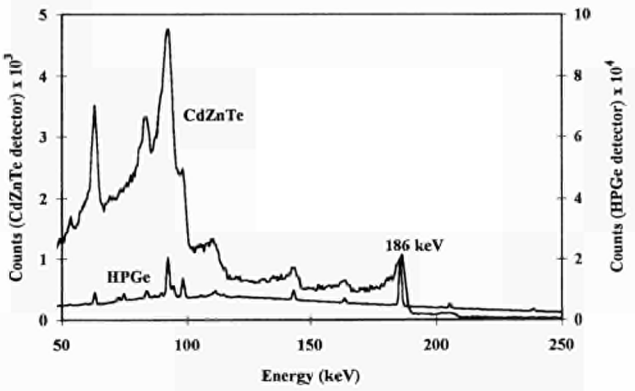

Fig. 5.1 Gamma ray spectra of uranium solution obtained with the HPGe detector and with the CdZnTe detector.

Each sample contained 5 ml solution in a Plexiglas container (2 cm x 4.5 cm x 1.2 cm). The gamma lines of ^{235}U at 186, 163 and 144 keV are well resolved by the CdZnTe detector. The measurement of the ^{235}U concentration is carried out by determining the 186 keV peak area. The plutonium in the MOX or PuO_2 samples could only be qualitatively identified. In the energy range between 500 and 800 keV, the poor spectra quality prevents any verification of the declared burn-up or cooling time of the spent fuel studied. Nevertheless, sufficient information is obtained to identify it as being spent fuel. It is evident that, on a qualitative basis, the different types of nuclear material analysed could be discriminated [1]. The small size, portability, ambient operation and performance, as demonstrated by this work, indicate that CdZnTe detectors are capable of preliminary in-situ identification of unknown nuclear material.

In this context, the development of a portable monitor comprising, besides gamma spectrometry, passive neutron assay is in progress.

References

[1] K. Abbas, G. Nicolaou, P. Schwalbach, L. Koch: Appl. Radiat. Isot. **47** (1996) 755

5.3 Remote Measurement of U and Pu in Nuclear Waste Samples by Laser Ablation-Optical Emission Spectroscopy (LA-OES)

Introduction

Optical emission spectroscopy (OES) of a plasma produced by laser ablation (LA) was shown to be a method which allows a direct measurement of U on a vitrified waste product (TUAR-95, p. 183). No sampling or additional sample preparation is required. The remote sensing technique allows the measurement of U concentration in real highly active waste glasses.

Pu measurements

The equipment installed at ITU in a glove-box was used to determine the Pu content in waste materials. Mixed $(U_{0.8}Pu_{0.2})O_2$ pellets were analysed in comparison to natural UO_2 and simulated waste glass containing 0.7% U. Fig. 5.2 shows the emission spectra obtained.

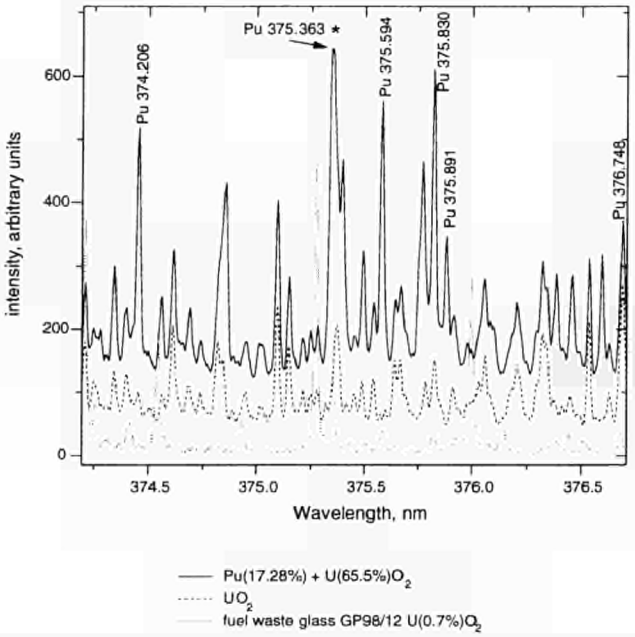

Fig. 5.2 OES spectra for different reference materials (detection 20 μs, delay time 5μs, 10 laser shots)

Fig. 5.2 shows, that the resonance line Pu(I) 375.363 interferes with U and Ti lines. The three other main Pu lines (Pu(I) 376.748, Pu(I) 375.594 and Pu(I) 374.206) are, however almost free of any interference. A good reproducibility of the laser ablation was observed and a standard deviation of 3% could be determined.

U isotopics by Laser Induced Fluorescence

Several modifications and improvements of the experimental set-up (Ar flushed cell, diode lasers for fluorescence excitement and several improvements in the optics) were needed to measure the isotopic composition of U. Fig. 5.3 shows the intensity of ^{238}U and ^{235}U at different currents of the diode lasers measured on a pellet of natural UO_2.

Due to the odd number of nucleons, ^{238}U shows a hyperfine structure in contrast to ^{238}U (Fig. 5.2). Because of a non-linear response of the detector (charged coupled device (CCD) camera), the ratio of the fluorescence signals measured for the two isotopes by peak integration is lower than the isotopic ratio. A correction factor of 1.9 was determined in the present case.

Future work is needed to confirm this factor and to demonstrate, that this value is constant over a large range of isotopic composition. Furthermore, improvements in the optics should bring down the detection limit to values around 1 ppm also in the case of Pu. As mentioned above several Pu lines seem to be very suitable to achieve this goal.

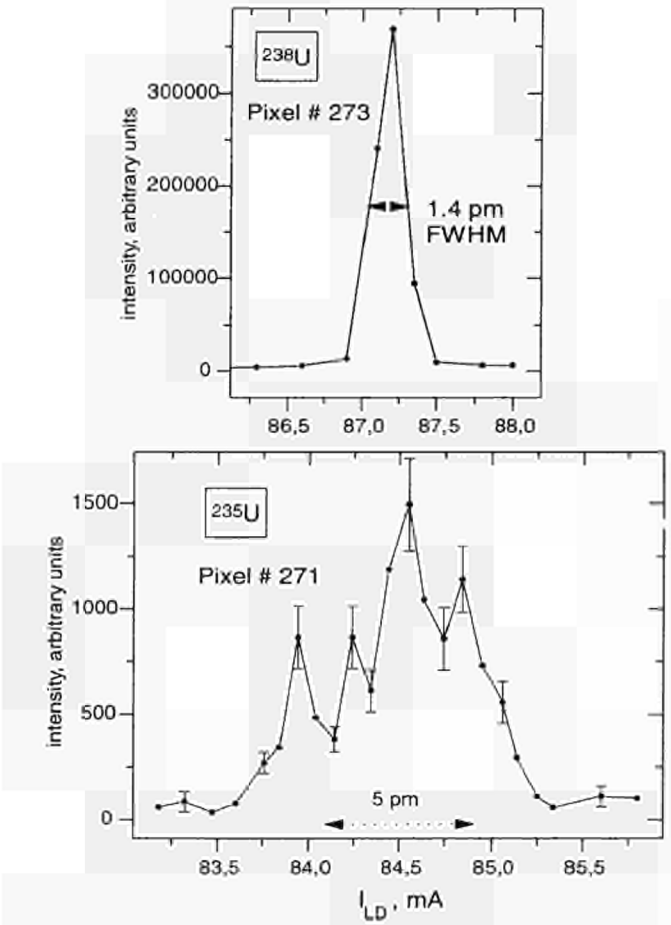

Fig. 5.3 Fluorescence spectra of ^{238}U and ^{235}U at different currents of the diode lasers measured on a pellet of natural UO_2.

B. Scientific and Technical Institutional Support Activities

6. Scientific and Technical Support to DG XVII

Introduction

The Institute continued to provide technical support to the Euratom Safeguards Directorate (ESD), DG XVII-E, in the form of analytical measurements for safeguards verification purposes, development of analytical techniques and training. The efforts concentrated on the following areas:

- Design and setting up of on-site laboratories at the reprocessing facilities in Sellafield (United Kingdom) and La Hague (France).

  Considerable effort was spent on the development, manufacture and testing of equipment in the Institute's pre-on-site laboratory (pre-OSL); training of the inspector analysts, implementation of a quality assurance system and preparation of the necessary documentation for the On-Site Laboratory (OSL) in Sellafield.

  The design of the Laboratoire sur Site (LSS) at La Hague is well underway.

- In-field measurement activities, where the ITU analysts perform measurements on safeguards samples on site using permanently installed equipment or mobile instrumentation.

- Analysis of safeguards samples that are transported from nuclear facilities to the Institute. In the framework of the European Commission's Safeguards Analytical Measurements (ECSAM) also consultation on analytical techniques is provided. Furthermore, analysis of seized nuclear material is performed.

- Development and improvement of analytical techniques aiming at effective and efficient safeguards measurements has been performed, and a nuclear material databank is being set up.

6.1 Pre-On-Site Laboratory at ITU (pre-OSL)

The Institute's pre-OSL (see TUAR-95, p. 171) has been set up for training personnel for their future work at the On-Site Laboratory Sellafield (OSL). It allows the testing of the different prototype boxes, their analytical equipment and the communication software for the future OSL. It serves also for performing analyses of radioactive samples sent to the Institute by the Euratom Safeguards Directorate (ESD).

Prototype boxes

Two new boxes, the *Product box* and the *COMPUCEA box* have been installed in the pre-OSL.

Product box

The original concept of housing in one box the Non-Destructive Assay Techniques (NDA), such as the Neutron Coincidence Counting (NCC), the Product K-Edge Densitometry (PKED), and the High Resolution Gamma Spectrometry (HRGS) and also Density Measurement, Microwave Dissolution and Potentiometric Titration had to be modified for several reasons:

- background interferences with the NCC technique during neutron counting. An additional shielding with high density polyethylene did not solve this problem
- the space required for the robotized titration left insufficient room for operating the NDA equipment under routine conditions
- the reliability of the robot did not meet pre-OSL requirements. As the hardware could not be improved, the robot was exchanged for a new XP-type. However, some minor problems still need to be investigated
- need for simultaneous measurement of uranium and plutonium in the PKED.

The new concept for both the pre-OSL and the OSL assembly foresees the analysis of product samples in two separate boxes. One box will house the microwave dissolution and the robotized titrators for plutonium and uranium while the second box will contain the instrumentation for NDA techniques including a microwave oven for dissolution of solid sample material.

The PKED, as it had initially been installed in the product box, could not discriminate between uranium und plutonium. In order to enable the simultaneous determination of U and Pu, the PKED needed to be modified.

The PKED design was extended with a detector to determine the uranium/plutonium ratio. The new set-up allows the accurate determination of the Pu concentration in Pu solutions in the presence of uranium and enables the measurement of dissolved MOX samples.

COMPUCEA box

This box consists of the instrument for COMbined Product-Uranium Concentration and Enrichment Assay (COMPUCEA), the microwave oven for dissolution and a densitometer to measure the sample density. COMPUCEA is a combination of two methods, K-edge densitometry and high resolution gamma spectroscopy. The modules, as now installed in the box, have been thoroughly tested. During gamma spectrometry measurements, a microphonic effect was observed giving rise to low energy signals. As a concequence, the box was separated from the detector with low density insulating material and the microphonic effect could be reduced to an acceptable level.

Training of operators

Training of the inspector analysts started in 1995. The introduction to the nuclear fuel cycle and the different analytical methods, given in form of lectures and workshops, has been completed in 1996 while practical training in the pre-OSL to simulate future OSL operations is continuing. Teams of four analysts work on a weekly shift. Each is responsible for a specified analytical technique i.e. NDA, Titration, Robot and Mass spectrometry. Communication between the teams, at present, is achieved by the use of a data management program and also by handover meetings on a weekly basis. A logbook system has been arranged which provides detailed information about equipment, maintenance, events and status of the samples.

Since under routine working conditions in Sellafield, the successive working teams will not be able to pass over information directly, a computerized ITU Analysis Management System (TAMS) is being set up to guarantee necessary communication and information.

Laboratory manual, quality assurance, working instructions and analytical procedures

ITU is putting effort into the implementation of a quality assurance system in compliance with ISO 9001.

OSL operation will be based on a Laboratory Manual covering all aspects of operation. It contains the working instructions (WI) and analytical procedures (VA). The working instructions describe the execution of a specific activity in detail (for example: dissolution of uranium oxide) while the analytical procedures are of a more general nature and describe the complete sample treatment within the Nuclear Chemistry unit from material reception to the release of the final results. The procedures refer, wherever possible, to the working instructions. Their format is in compliance with specific rules at ITU and will be adapted to conform with BNFL working practice and local on-site rules.

Development of the ITU Analysis Management System (TAMS)

Following the strategy of harmonised software used for analysis for the Euratom Safeguards Directorate (ESD) and the future On Site Laboratory, the development of TAMS was started this year. In order to avoid developing and running different programs on even more different platforms (i.e., operating systems and programming languages) with resulting problems like complex user-machine and machine-machine interfaces, it was decided to restructure and rewrite the major part of the analysis software. As described earlier [1] many modules and programs for operating individual measurement instruments were realized in C++ running on PC's under OS/2. The TAMS interacts with all these programs and compiles the measurement results. The data are then combined (where necessary) and prepared for transfer to ESD.

The TAMS program is foreseen to replace the programs currently running on the central VAX computer since extensive tests revealed that the VG-LIMS mentioned in [1] did not meet our specific needs without excessive programming effort. TAMS accepts the measurement results from the different analysis methods and makes final calculations and prepares the reports for the customer (ESD-Luxembourg). A preliminary version of the program has been installed at the end of the year and is presently being tested. It is foreseen that a first version will be ready in March 1997.

The major differences between TAMS and its predecessor ('ANALYSE' on the VAX) are:

- Data are presented in a format that can be read by the Euratom Destructive Analysis Management system (EDAM), which is being used by ESD-Luxembourg.
- The implementation of the newly introduced quality assurance policy in the Institute.
- Measurement data are subject to consistency checks. Quality control measures are fully integrated in TAMS.

Updates to 'PREP':

The 'PREP' program (which was introduced in [1]) has been extended with three new features:

1. The possibility to print bar code labels (for sample identification).
2. Density measurements with the PAAR DMA48 densitometer.
3. Interface to the COMPUCEA software.

The bar codes can be printed for all dissolutions and dilutions made using the system. These can then be glued to the bottle for reading with a bar code reader.

In the density measurement, data is read from the PAAR DMA48 via a serial interface. It allows the user to calibrate the machine and measure the reference (water) and the samples. Thereafter, calibrations and samples measurements can be performed.

'PRCO': manual 'PREP' for the 'mobile'-COMPUCEA

To avoid the creation of two different versions of the COMPUCEA software, the PRCO program was created. This program is basically a simplified combination of the expert system (for sample initialization) and 'PREP' (for dissolution and density data).

The program allows the user to initialize samples, perform dissolutions, make dilutions automatically and enter the density values manually. There is no connection to a densitometer because the mobile COMPUCEA uses a hand-held densitometer which has no serial output. The interface to COMPUCEA is in this case exactly the same as that for 'PREP'.

Quality control for Thermal Ionization Mass Spectrometry (TIMS) and Isotope Dilution Mass Spectrometry (IDMS) Measurements

The ESD samples that require TIMS or IDMS measurements are chemically prepared in the Isotope Dilution Analysis (IDA) box by the robot. A turret accommodating the samples is then transferred to the mass spectrometer for measurement. In order to apply quality control on these samples, a well known reference solution is subjected to the same procedure as the samples. The selected quality control material has a similar composition (chemically and isotopically) as the samples and is treated in the same way by the robot.

The 'IDA' program has been improved in order to give the analysts the tools to perform this quality control. A database was created where the data provided by the analytical runs are held and regularly updated. The most important information stored in this database is the link between quality control (QC) material and samples done in the same run. Once the samples on the turret are measured, the data is requested from the central data system. This data consists of the measured isotopic abundance ratios as determined by mass spectrometry for all the samples done in the run and all the previous measurements of the standards used in this run. For plutonium QC samples, the ratios are decay-corrected to the appropriate reference date. These data plotted on various QC charts according to the different measurement instruments and types of measurement, allow the analyst to decide whether to accept or reject a measurement.

Titration analysis management

The application, rewritten in C++ for a PC running under OS/2 last year (TUAR-95, p. 78), has been installed in the laboratory for final testing.

The programs have been upgraded and modified to take into account the demands of the operators and new requirements of the analyst. In particular, changes have been introduced due to the development of TAMS and the numerical procedures have been finalized to include the quality control criteria.

As a result of the introduction of TAMS the interfaces to the other programs (i.e. the Expert system, IDA, MS) have also been adapted accordingly.

Developments for Pu element assay by neutron coincidence counting (NCC)

Passive NCC will be applied as the prime method for Pu element assay in gram-sized solid samples at both OSLs in Sellafield and the LSS La Hague. To cover the complete range of different sample types due for analysis in those laboratories, further studies were pursued to establish the neutron coincidence response of the small sample neutron counter (OSL counter) for MOX materials.

In order to find an optimum calibration approach, and to limit the necessary number of certified reference materials, the main differences between the counter's

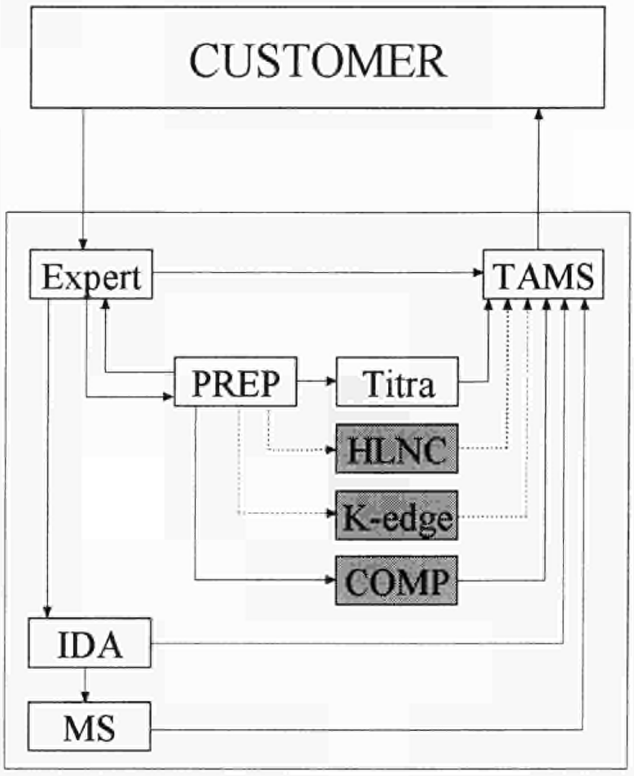

Fig. 6.1 Schematic view of data flow between the different programs.

response to MOX and PuO_2 have to be understood. Measurements with the OSL counter and related data analyses thus covered the following three basic types of samples:

- PuO_2 powders (continued from 1995)
- MOX powders
- MOX pellets.

A uniform NCC response for all types of samples should result in a narrow band of data points in a representation as shown in Fig. 6.2 (ratio of 'Reals' rate, R, to m_{240eff} versus m_{240eff}).

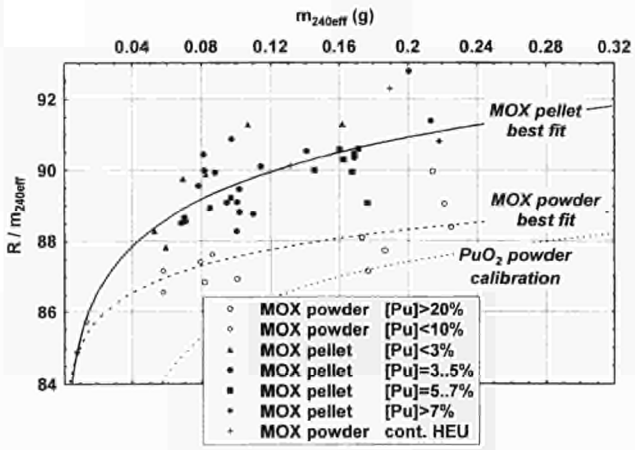

Fig. 6.2 Overview of available NCC response data[1]) for MOX pellets (full points) and MOX powders (open points). Pu concentration ranges are marked with different symbols. Data from special MOX powder samples containing highly enriched uranium are identified with crosses and not included in the fits. Individual data points for PuO_2 powder samples are not shown.

[1]) Ratio of Reals (R) to Pu-240 equivalent weight (m_{240eff}) plotted as a function of m_{240eff}

In reality, different response functions are observed for the different types of sample material. Fig. 6.2 illustrates that the measured data for MOX powders and pellets indeed separate into two groups, which in turn, also differ from the previously established calibration for PuO_2-powder samples. The available data for the two types of MOX samples still show significant scatter. The use of preliminary calibration coefficients from the best-fit curves result in standard deviations of typically 1%. About half of this uncertainty may still be due to various sample parameter effects, which cannot yet be quantified.

Future measurements will be done with a new polyethylene shielding around the neutron counter to reduce the single neutron ("Totals") background by a factor of 4. This will eventually allow one to compare the "Totals multiplication correction" analysis [2] (which helps to bypass the use of different calibration functions for different materials for large samples) with alternative approaches (see e.g. [3]) as well as with a procedure based on "known multiplication" inferred from the isotopic composition [4]. In this context, systematic studies will investigate a more detailed dependence of the response on parameters such as:

- sample geometry
- (alpha,n)-content
- Pu-fissile content (given by a ^{239}Pu effective mass [3])
- Pu element concentration

The final goal is to combine 2-3 major calibration curves with minor correction terms. For the same purpose systematic Monte Carlo calculations taking into account the complete detailed geometry of sample and counter will be performed.

Hybrid product K-edge densitometer

The initial product K-edge densitometer set-up designed for the OSL, which combines K-edge densitometry and passive gamma spectrometry for the element and isotopic analysis of Pu product solutions, has been expanded to allow for additional K-XRF measurements.

This added option will be utilised to improve further and to enlarge the measurement capabilites of the instrument in the following areas:

- Determination of minor actinide concentrations in support of K-edge densitometry.
- Pu element concentration measurement in dissolved PuO_2 samples spiked with an internal uranium standard.
- U- and Pu-concentration measurements on MOX pellets (the feasibility of this application still needs to be evaluated).

The layout of the modified set-up, now referred to as 'Hybrid Product K-Edge Densitometer' (Hybrid PKED), is shown in Fig. 6.3. The new set-up also incorporates a beam monitor for improved performance in those applications, where the XRF analysis will be employed as a stand-alone technique for direct concentration measurements.

References

[1] TUAR-95, EUR 16368, p. 178-179

[2] N. Ensslin; "A Simple Self-Multiplication Correction for In-Plant Use", Proceedings of the 7th Annual ESARDA Symposium on Safeguards and Nuclear Materials Management, 1985, p. 233-238

[3] Ming-Shih Lu, Th. Teichmann; Proceedings of the 14th Annual ESARDA Meeting on Safeguards and Nuclear Materials Management, 1992, p. 247-251

[4] H.O. Menlove, R. Abedin-Zadeh, R. Zhu; "The Analyses of Neutron Coincidence Data to Verify Both Spontaneous-Fission and Fissionable Isotopes", Los Alamos National Laboratory, LA-11639-MS, August 1989

6.2 Progress of the 'On-site Laboratory' (OSL), Sellafield

The BNFL Engineering Department (Risley), started to build the infrastructure of the laboratory and by the end of 1996 the rooms appear to be ready to accept the equipment to be delivered by ITU. The Institute was involved in design discussions and most of the non-compliancies have been resolved.

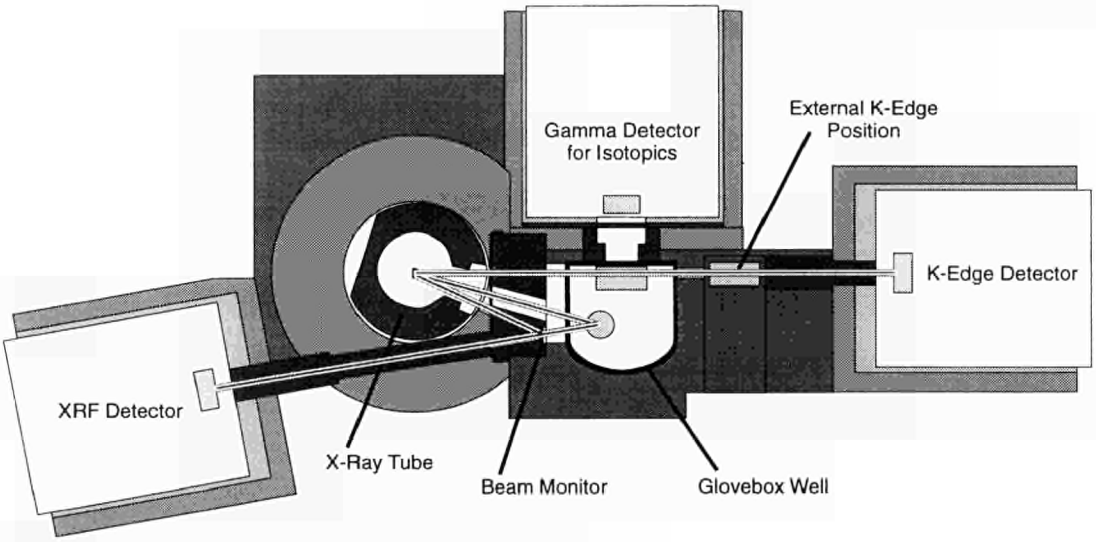

Fig. 6.3 Layout of the Hybrid-Product K-edge Densitometer.

ITU put the emphasis on:

- construction and assembly of the analytical equipment, glove-boxes and training of the staff
- preparation of the equipment for transport, installation and testing at BNFL (site B229)
- preparation for integration of the OSL into the BNFL management structure

Quality assurance

The QA system, as described in detail in TUAR-95, p. 180, was subject to further implementation. Some of the twenty one project procedures needed change to reflect better daily working conditions.

The software design plan for the robot software was drawn up and discussed with our QA consultant from NNC Ltd., Risley. Test and inspection plans were worked out for all relevant pieces of equipment. Glove-box testing was carried out by the guidance of Inspection and Test Plans (ITPs).

Procedures and working instructions were drafted, reviewed and approved. They cover all analytical and operational activities in the pre-OSL and the OSL. Currently, they reflect the situation of the pre-OSL at ITU. In the light of experience of the installation, testing and commissioning of the OSL they will be modified and extended to fit the situation of the OSL.

Purchase and construction of glove-boxes

The purchase of the material such as boxes and analytical equipment, started in 1995, continued this year.

The OSL equipment assembly was started early this year as well as testing of components. In total, 9 boxes were conctructed in compliance with the Design Plan established in the frame of quality assurance for the OSL project. Drawings were subject to approval by NNC Ltd., Risley, to assure compliance with the codes and standards called for in the Design Concept and the Pre-Construction Safety Report (PCSR). For important equipment such as glove-boxes, mass spectrometers, K-edge desitometer and the COMPUCEA instrument, ITPs have been established. Those ITPs demanded by the QA, shall cover the different test activities including the glove-boxes. Though the boxes will not be used in the Institute but on-site by ITU personnel, they will be subject to approval by the Institute's glove-box committee. It is of fundamental importance to demonstrate that the boxes do meet the safety standard of ITU. Additionally they must be in compliance with the PCSR.

Transport

The transport of the ITU equipment (boxes, instrumentation) has been planned to take place at the end of February 1997. The mass spectrometers to be shipped to the OSL have been thoroughly decontaminated, dismounted, have been cleared for release and have transport certificates. They are awaiting measurement for tailored shock absorbing pallets for the transport.

Installation/testing – training and health and safety plan

A "Contractor's Health and Safety Plan for Installation" was drafted by ITU and provides a comprehensive guideline for conventional safety throughout the installation to be performed by ITU at Sellafield Site. The document is rather detailed and requires in-depth knowledge of the UK Health and Safety at Work Regulations, especially the Construction and Design Management Regulations. A similar plan will be written by the Resident Engineer at BNFL for ITU testing activities.

In-depth safety-related training is not required for ITU staff or their contractors, however for health and safety reasons BNFL requests that the on-site staff have a short course by the Safety Training Officer in the presence of the BNFL Safety Manager. In order to obtain a site pass and film-badge for the active area of B229 and the surroundings, each ITU member of OSL must undergo the 'Contractor's Classified Person's Course'.

More stringent training requirements are stipulated by BNFL for testing activities starting after the installation phase. A detailed plan as well as the contents of certain courses are still being negotiated and discussed with BNFL.

Integration into BNFL infrastructure

The structure of BNFL differs to some extent from ITU's organization. The OSL must be in compliance with both systems. To assure harmonization, e.g., discussions between BNFL and ITU took place on topics such as accountability for fissile material, QA for operation, managerial functions in the OSL and subsequent additional training for the inspector analysts.

6.3 Progress of the 'Laboratoire Sur Site' (LSS), La Hague

The LSS project is being executed on schedule and the calls for tender for the infrastructure (ventilation, electricity, supplies, etc.) and the glove-boxes have been prepared by the engineering company Société Générale pour les Techniques Nouvelles (SGN), based on the analytical scheme and input data provided by ESD and ITU. The first part of the design/management contract will be accomplished at the end of January 1997. At this time the offers will be presented to ESD for the preparation of the purchase orders. The purchasing of analytical instrumentation by ESD will also start next year.

After approval of all purchasing orders, SGN will implement the building phase of the project, which is scheduled to be completed within 23 months. Therefore, the earliest date for the hand-over of the LSS to ITU is estimated to be at the beginning of 1999.

The training of ITU inspector analysts has been defined in compliance with the specific rules used at the Cogema La Hague plant, particularly for the work with tele-manipulators.

Design modifications:

- As a large number of samples (input-, process-, URP-UCD-, and QA-samples) have to be analysed with the three Hybrid K-edge systems installed in the hot-cells, two of these instruments will be equipped with a sample changer.
- The sample changer was developed and designed by ITU in view of the limited manpower available on-site and of the large number of samples to be measured by the Hybrid K-edge instruments.
- To avoid corrosion problems in the liquid waste piping system in the presence of the HF used for the dissolution of the PuO_2, the product box will be disconnected from the overall laboratory effluent waste stream. The fluoride containing waste solution will be collected separately and transferred manually to Cogema for further treatment. For the same reason it is not possible to send an aliquot of the dissolved PuO_2 to the hot-cell via the pneumatic transfer system for an additional XRF measurement in the Hybrid K-edge instrument. Hence the design of the PuO_2 chain was modified in order to take up its own Hybrid K-edge system.
- The large number of samples to be analysed by mass spectrometry requires the installation of two instruments and two robotized boxes for the chemical preparation of the samples. This was demonstrated by careful calculations and thorough considerations of the average workload.

Some technical problems remain to be solved:

- Preparation of the input samples for IDMS measurements: To comply with the permitted operator dose level at the working place, which will be in force at La Hague and which will apply to the isotope dilution analysis (IDA) glove-box, measures have to be taken for a drastic reduction of the dose rate per sample. This can be achieved either by applying a dilution factor of 20000 for dissolved input samples instead of 1000 as assumed up to now, or by a separation of the (γ-active) fission products in the hot cell prior to transferring the sample to the IDA box. Further tests on alternative analytical methods based on ion-exchange have to be performed to overcome this problem.
- The accuracy or precision of the density measurement on input solutions in hot-cells has been defined by ESD. Investigations on the choice of the system and extraction chromatography performed and the possiblity of modification for operation in a hot-cell (nuclearisation) are evaluated.

6.4 On-Site Verification Activities

Inspector analysts from the Institute travel regularly to La Hague and Sellafield to carry out routine verification measurements on input solutions (dissolved spent fuel) with the Hybrid K-edge instruments installed at both sites. During the weekly missions to La Hague, more than 600 input samples from UP3 and UP2-800 have been measured over the last year, bringing up the total number of measurements done, including those to be carried out for instrument control, to more than 1000 (see Tab. 6.1)

Tab. 6.1 Evolution of the number of samples measured by the Hybrid K-Edge at La Hague

Year	Number of input samples	Number of measurements (total)	Effective working days	Measurements per day (average)
1989	15	33	11	3.00
1990	107	234	66	3.55
1991	175	317	98	3.24
1992	199	335	85	3.94
1993	305	435	104	4.18
1994	407	597	109	5.48
1995	573	917	144	6.37
1996	647	1096	156	7.03

At Sellafield, where the THORP plant was not yet fully operational and where ITU support was limited to one week per month, about 50 samples had to be measured. However, considerable effort was spent on instrument maintenance, repair and modernisation.

Support to ESD was provided for the installation and commissioning of a new Hybrid K-edge apparatus at the Dounreay reprocessing plant. This work was completed by the middle of the year with an extended calibration for the larger range of sample types encountered in the on-site verification measurements at this facility.

Significant effort has been invested into the preparation of stable reference solutions required for instrument control measurements in the in-field K-edge systems. Previous stability problems were overcome by welding reference solutions into a new type of leak-tight stainless steel cuvette. A set of this type of reference sample has been fabricated at ITU and commissioned to the Hybrid K-edge instruments at La Hague, Sellafield and Dounreay.

6.5 European Commission's Safeguards Analytical Measurements (ECSAM): In Field Verification Measurements

Analysis of Pu bearing materials

In the framework of the European Commission's Safeguards Analytical Measurements (ECSAM), the analytical measurements for safeguards verification purposes were conducted as far as possible under pre-OSL working conditions. In addition to the analytical codes routinely requested and in view of further testing, training and performance evaluation, all Pu bearing materials were analyzed by the OSL-counter prior to dissolution for the routine destructive analysis. The paired comparison of measurement results from neutron-gamma counting and potentiometric titration – thermal ion mass spectrometry (TIMS) respectively,

were performed to allow accurate corrections to be made for variations in the neutron counter response. The ^{241}Am content was measured by gamma spectrometry using MGA, which has now become the adopted method for ^{241}Am analysis.

Physical inventory verification

On special request from the Euratom Safeguards Directorate (ESD) Luxembourg, analytical support has been given for physical inventory verification. The determination of the uranium content and the ^{235}U abundance in mainly low-enriched uranium samples were conducted using the mobile COMPUCEA equipment. During the course of seven campaigns 184 samples were analyzed.

Analysis of spent fuel using the large size dried spikes

Comparative measurements were carried out at ITU in order to examine the possibility to use the Large Size Dried Spikes (LSD) for spiking of reprocessing input solutions. Samples of spent fuel solution were aliquoted and spiked in parallel with the LSD and with a $^{233}U/^{244}Pu$ spike mixture after appropriate dilution. The investigation aimed at quantifying the repeatability and reproducibility of the two spiking techniques and the detection of random and systematic differences between them and finally at the validation of the LSD for application in the OSL and LSS.

A spent fuel solution, showing a U/Pu ratio of about 150 and a ^{239}Pu isotope abundance of about 72%, corresponding to an LWR fuel of moderate burn-up and a well characterized U/Pu mixture used as quality control sample were treated under, as closely as possible, real working conditions. Therefore the preparation of dilutions or the LSD spiking were performed in the hot-cell facilities, the sample conditioning was performed using the robotized procedure as applied to ECSAM samples or in the OSL.

The measurement results showed improved repeatabilities and reproducibilities of the LSD spiking technique. This might be explained by the introduction of additional error sources in the "conventional" spiking method mainly caused by necessary dilution manipulations and weighings in the hot-cells.

6.6 Development of a Relational Database for Seized Nuclear Materials

A considerable amount of information has been accumulated in the course of the analysis of seized nuclear material at ITU Karlsruhe. It includes administrative as well as analytical data related to the individual cases. It was decided to systematize all information in a relational database in order to make efficient use of the data for possible future cases. For assuring maximum integrity and consistency, the ORACLE™ relational database management system was installed at ITU. It allows introduction of a confidentiality structure, flexible development as well as eventual migration to different operating systems. ORACLE™ also opens the possibility to develop modules for interaction with data management systems used at ESD Luxembourg.

The database design had to cover the following data types:

- general information about the case (e.g., circumstances under which the material was seized)
- morphological description of seized objects
- types of samples taken and analytical techniques used
- element and isotope composition of the sample (if available)
- data on the sample microstructure (e.g., grain and pore size distributions)

On the basis of ORACLE™ a simple relational table system (Tab. 6.2) has been implemented. The "case"-table can also contain information about the origin of the material. This permits one to include analogous entries about samples of known or partially identified origin and allows steady improvement and scalability of the database.

The system is currently being extended to relations with ORACLE Book™ documents, containing in-depth information from long texts, drawings or graphs, which cannot be categorized into tables. In the first phase of development all data on sample microstructure will fall into this category.

In addition, data stored in the system have been used for case studies of the technology-specific database which allows to identify missing analytical data and to recommend further measurements for characterization of the seized nuclear material.

Tab. 6.2 Simplified structure of tables in the sample-specific database.

Primary Key	Main Parameters
Case	case and incident description
Object (+ Case)	macroscopic geometry (e.g. dimensions, weight, density)
Sample (+ Object + Case)	form, analysis method
Element (+ Sample + Object + Case)	name, quantity, error
Isotope (+ Element + Sample + Object + Case)	name, quantity, error

6.7 Participation in a Field Trial for High Precision Trace Analyses

The Institute participated, at the end of 1995, in a field trial of High Precision Trace Analysis (HPTA) applications for safeguards applications in collaboration with the Euratom Safeguards Directorate (ESD). This test was carried out inside the Urenco centrifuge enrichment facility in Gronau, Germany. During the campaign swipe samples were collected in 15 locations.

The samples gathered in this field trial were analysed in the Institute using Secondary Ion Mass Spectrometry for their content of enriched uranium particles and isotopic composition.

The Institute also participated in the field trials organised by ESD in the Capenhurst enrichment plant and in the field trial at the hot-cell facilities in Rossendorf, Germany.

7. Scientific and Technical Support to DG I

Introduction

In order to support the policy of the European Union concerning non-proliferation, Directorate General I of the European Commission is sponsoring scientific/technical support of the Institute to the International Atomic Energy Agency (IAEA).

In the framework of this support several activities related to the development and implementation of analytical techniques are carried out. These tasks deal mainly with the determination of actinides in samples of different matrices, taking advantage of the expertise, equipment and specific measurement instrumentation available at ITU.

7.1 Participation in Field Trial of Environmental Monitoring and Analysis

In September 1995, the Institute participated in a field trial inside the Urenco centrifuge enrichment facility at Capenhurst, UK. The samples were taken on behalf of the Euratom Safeguards Directorate (ESD) and the IAEA. The first field trial of sampling of swipes outside and inside hot-cell facilities was carried out in May 1995 at the research centre in Rossendorf, Germany. ESD and the IAEA invited the Institute to join them in this campaign.

ARTINA (Analysis of Radioisotope Traces for Identification of Nuclear Activities) Laboratory

In 1996 the clean lab ARTINA (TUAR-94, p. 171; TUAR-95, p. 188) became operative. The swipe samples collected during the campaigns in Gronau and Capenhurst and those collected outside of the hot-cells in Rossendorf, have been handled and prepared here for instrumental analysis by secondary ion mass spectrometry. A micro-digestion system for the dissolution and leaching of environmental samples has also been installed and tested. This system, working in a robotized way, avoids cross-contaminations during the preparation of samples for bulk analysis.

7.2 Determination of Pu in Highly Active Liquid Waste

Samples of HALW were supplied to ITU by the IAEA. The samples had been spiked with ^{233}U and ^{244}Pu by the IAEA. As the Pu content of the samples is extremely low (a sample typically contains 5–20 ng of Pu), a chemical separation procedure needed to be developed that was capable of dealing with the minute quantities of U and Pu and the excess of fission products. The method uses anion exchange resin for the separation and relies on HBr for the elution step. The latter is corrosive to gloveboxes and therefore its use has to be limited to a strict minimum. Tests were carried out to possibly measure Cm in the presence of the fission products. The feasibility of these measurements would allow to reduce the consumption of HBr considerably. Comparison with TIMS measurements will be difficult, as the amount of Pu contained in a sample only slightly exceeds the amount required for a single filament loading. Separations will be optimized once ICP-MS results become available. After that TIMS measurements can be performed (early 1997).

7.3 Determination of ^{244}Cm in Spent Fuel Solution

The experiments aim at the validation of IC-ICP-MS (Ion Chromatography – Inductively Coupled Plasma – Mass Spectrometry) as analytical technique for the determination of ^{244}Cm in spent fuel solution. Dried samples of spent fuel solution were received at ITU in the middle of 1996. Samples had been spiked with U and Pu (large size dried spike) by the IAEA. A sample typically consisted of 500 μg U and 2 - 7 μg Pu.

Samples were dissolved and a ^{248}Cm spike was added. Subsamples were taken for IC-ICP-MS and TIMS (Thermal Ionization Mass Spectrometry) measurements, respectively. The TIMS aliquot was then subjected to chemical separation of fission products/uranium/plutonium/curium, as needed prior to TIMS measurements. The separation is based on ion-exchange; at the lower end of the column an alpha detector indicates the individual fractions. The elution of the U and Pu fraction could be clearly identified using this technique. The Cm fraction, however, showed no measurable alpha activity, due to the (expectedly) low concentration of Cm in the samples. U and Pu fractions were measured by TIMS. This technique could not be applied to Cm.

The second subsample will be subjected to measurements by ICP-MS which is coupled to Ion Chromatography (for separation of the individual actinide elements). Measurements on the remaining samples will be continued in 1997.

C. Competitive Activities under the Framework Programme

8. Shared Cost Actions

Introduction

In order to strengthen European cooperation in R&D and to further enhance competitiveness, the 4th Framework Programme of the European Commission permits the participation of the Institute in calls for tender under the different shared cost action (SCA) programmes.

In line with its mission, the Institute has limited its participation to the Nuclear Fission Safety. Progress in the various projects is reported below.

8.1 New Partitioning Techniques

The programme on new partitioning techniques – NEWPART – for the recovery of minor actinides from HLLW has three main objectives:

- extraction from highly concentrated HNO_3 feed solutions,
- no generation of secondary wastes, i.e., to use organic molecules made exclusively of Carbon, Hydrogen, Oxygen and Nitrogen (CHON principle), which can be completely converted into non-toxic gases after use,
- easy recovery from the organic solvent without solid phase formation.

The reference DIAMEX process using dimethyldibutyltetradecylmalonamide (DMDBTDMA) will be used to extract minor actinides (An) together with lanthanides (Ln) from HLLW. Variations on the DIAMEX processes using new diamide molecules will be tested. An An/Ln separation will be carried out by means of tripyridinetriazine derivatives (TPTZ).

Fundamental tests on extraction thermodynamics, kinetics and mechanisms, molecular modelling, synthesis and structural determinations will be treated in several partner laboratories. They will also be mainly responsible for the process development including cold tests. ITU will be in charge of integral counter current tests with real HLLW in centrifugal extractors.

Since signing the contract in July 1996 progress in the "NEWPART" project has been limited. This is also the case for ITU which relies on preliminary development work for other partners. First real tests are supposed to start around mid-1997. To date, small equipment modifications have been carried out, mainly involving the extension of the extraction battery from 12 to 16 stages. A set of 4 extractors has been set up for cold tests using lanthanides in order to determine extraction parameters of the centrifuges (stage efficiency). Those will be used by the DIAMEX computer code developed in CEA Marcoule to define the optimal operation conditions (O/A ratio, number of extractions, scrubbing and back-extraction stages), to be used in the hot verification tests mentioned above.

8.2 Joint EFTTRA Experiment on Transmutation of Americium

The goal of the international EFTTRA collaboration is the investigation of the feasibility of transmutation and incineration of long lived isotopes in nuclear facilities. Within the general EFTTRA collaboration, the specific irradiation experiment EFTTRA-T4 is being supported through a shared cost action of the Framework Programme on Nuclear Fission Safety. The participants are: CEA Cadarache, EdF Paris & Lyon, FZK Karlsruhe, ECN Petten, JRC-IAM Petten and JRC-ITU Karlsruhe.

This irradiation experiment required the fabrication of targets containing circa 10 w/o americium in an inert spinel ($MgAl_2O_4$) matrix. These targets were prepared in ITU by the INRAM process. In this case, an americium nitrate solution was infiltrated into pre-formed porous spinel pellets. After sintering, the pellet diameters and heights were 5.4 mm and 7.0 mm respectively, and their densities were 96-97% of the theoretical value.

Gravimetric analysis, before infiltration and after thermal treatment and sintering of the impregnated pellets, showed that they contained 11.2±0.3 w/o americium. In addition, the Am content was determined by gamma spectroscopy, calibrated by a control measurement on a pellet containing 8.0 w/o Am in spinel, which was fabricated by conventional powder mixing, blending, pressing and sintering procedures. Comparison of results obtained by gamma spectroscopy and by gravimetric analysis (see Tab. 8.1) shows good agreement between the measurements.

Tab. 8.1 Measurements of the americium content in sintered Am-spinel pellets fabricated by the infiltration technique.

Sample	Weight (g)	Am-Content (w/o) (Gamma spectroscopy)*	Am Content (w/o) (Gravimetric analysis)
1	0.603	11.1	9.7
2	0.622	11.1	11.4
3	0.627	10.9	11.2
4	0.630	11.1	11.6
5	0.629	12.4	12.2
6	0.630	11.5	11.0
7	0.619	11.3	11.5
8	0.631	11.5	11.9

* referenced to the measurement of a pellet containing 8.0% Am which was fabricated by pressing a mixture of Am and spinel powders

These pellets were then loaded and welded into two target capsules, the main details of which are given in Fig. 8.1.

The fuel column (Am-spinel pellets) is 70 mm long and is terminated at each end by a spinel pellet, with length, l = 5 mm, a HfO_2 pellet (l = 6 mm) and a stainless steel pellet (l = 17 mm). The radiation dose rates (see Tab. 8.2) at various distances from the pin measured using a thermoluminescence dosimeter (TLD) and with a Geiger type Panoramic 470A detector are given in Tab. 8.2.

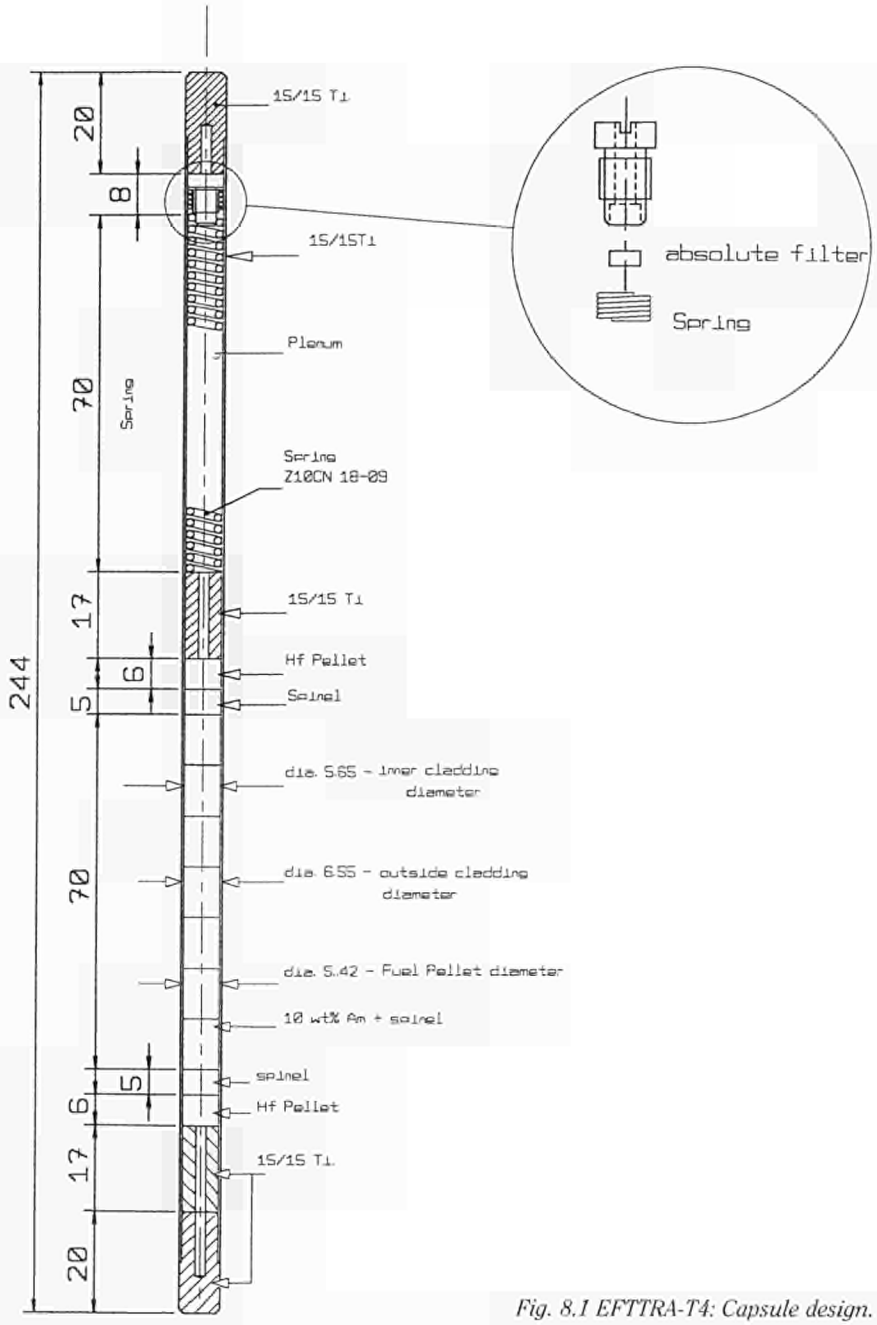

Fig. 8.1 EFTTRA-T4: Capsule design.

Tab. 8.2 Radiation dose rate measurements on Am-spinel fuel pins (all values in µSv/h).

Fuel pin	EFTTRA T4/1			EFTTRA T4/2		
measurement conditions	1	2	3	1	2	3
TLD *						
contact	368000			164000 #	140	
200 mm	5068			4750	20	
Panoramic detector						
contact (= 6 mm)	20000	100	25	20000		20
200 mm	1500	15		1600		
500 mm	200	4		200		
1000 mm	100			80		

* Thermoluminescence detector
\# Variation of contact position during measurement

Measurement conditions
1: Fuel pin without protection
2: Fuel pin with steel protection tube
(outer diameter = 20 mm, wall 6.5 mm thick)
3: Fuel pin with steel protection tube
(outer diameter = 20 mm, wall 6.5 mm thick) and 3 mm Pb

The irradiation of the fuel pins in HFR-Petten was started in September 1996 and will be continued for 400full power days. Following completion of the irradiation, these fuel pins will be returned to ITU for post irradiation examination.

8.3 Supporting Nuclear Data for Advanced MOX Fuel

Chemical analysis is being carried out on targets of actinides (^{232}Th....^{244}Cm in amounts of about 1 mg) and some fission products (e.g. ^{137}Cs, ^{106}Ru, ^{139}La in amounts of about 1 µg) which had been irradiated in the KNK II fast reactor.

The purpose of these irradiation experiments is the determination of integral cross-sections and fission yields of the various actinides and fission products irradiated and hence, the verification of neutron physics calculations.

The study involves the determination of the isotopic composition of the fresh and irradiated targets by destructive analysis. Composition measurements (actinides and fission products) will be performed using a range of mass and energy spectroscopy techniques. Furthermore, destructive analyses of multiple foil flux monitors will be performed in order to determine the local neutron flux density spectra. The resulting composition information will provide the means for verification of nuclear data through appropriate neutronic calculations.

8.4 Source Term for Performance Assessment of Spent Fuel

This is a shared cost action supported from Brussels DG-XII and co-ordinated by FZK-INE. ITU is involved in three tasks.

1) Leach testing on spent fuels with different porosity content.
2) Leach testing of defective rodlets of irradiated fuel.
3) Electrochemical measurements on irradiated fuel.

In the first sub-programme, a Hg picnometer has been adapted and installed in a hot cell; calibration and testing of samples will be carried out next year.

In the second sub-programme, 10 cm long rodlets of three irradiated UO_2 fuels of burn-ups of 30-54 GWd/tU have been cut. Stainless steel end caps have been welded on and then defects cut in the cladding. Five UO_2 rodlets have one set of 3x1 mm holes in the middle of the rod, while one rodlet has 2 sets of 3x1 mm holes; one at the top end and one at the bottom end. The rodlets with one set of defects are placed in autoclaves fully filled with groundwater so that fuel will be in contact with water. The double defected fuel rod will be in a half-filled autoclave such that one set of holes will be immersed while the other set will be exposed to water vapour only. The leach testing of these samples has commenced in simulated granitic groundwater at 95 °C for upto 100 days. Intermediate leachate samples will be taken at 30 and 60 days (and the leachate volume made up with fresh solution) for ICP-MS analyses.

In the third subprogramme, the electrochemical testing of irradiated fuel, electrodes from the same three UO_2 irradiated fuels (burn-up range: 30-54 GWd/tU) and a MOX fuel (burn-up: 20 GWd/tU) have been prepared. This has involved a more complicated polishing technique on one side for better contact to the electrode stub before embedding and polishing on the opposite side down to 1 μm diamond. This pre-polishing enables a better contact with the electrode brass stub and reduces the chances of short-circuiting of the UO_2 fuel via excess adhesive. Adaption of the heating plate has also been carried out for the testing of the electrodes in the two solutions (simulated granitic ground water and 95% saturation NaCl brine) at 60 °C.

The long term potential monitoring (up to 1000 h) of the three UO_2 and MOX fuels in 95% saturation NaCl brine at 25 °C in neutral pH has been carried out and has shown that MOX has a lower (more base) rest potential than the UO_2 fuels and different evolution in its E_{corr} value. Among the UO_2 fuels the highest burnup fuel shows the highest (most anodic) E_{corr} value. Optical microscopy of the high burn-up UO_2 fuel after 1000 h in 95% NaCl reveals considerable localised attack of the fuel surface. Often areas around larger pits or cracks are only slightly attacked. This may be due to the anodic pit or crack surface making the surrounding area cathodic and hence protecting it from attack.

8.5 Revaporization Tests on PHEBUS Fission Product Deposits

Thermal resuspension of fission products is a possible mechanism of material transfer in the primary circuit during a severe reactor accident. Within the frame of our work the release mechanism of such materials was investigated experimentally in two ways:

- Small-scale simulation studies of deposition and subsequent release of inactive caesium hydroxide on stainless steel coupons were performed, since this compound is predicted to be among the fission products that would dominate in the event of a severe accident.
- Samples taken from the vertical line of the PHEBUS FP FPT0 test were used in order to obtain qualitative and quantitative information on deposition and release phenomena on realistic samples.

Small scale simulation studies

The deposition and subsequent resuspension of caesium from stainless steel have been studied using Knudsen Cell mass spectrometry. Coupons of a 1.4301 stainless steel were reacted with caesium hydroxide vapour over the temperature range 200-1000 °C in an argon atmosphere. The coupon's surface examination and the reaction products' identification were carried out using SEM/EDAX and XRD techniques. The XRD analysis has given, in this case, very limited information. Since the XPS technique can give more detailed chemical information on the nature of the oxide phases we have already planned to perform such measurements in combination with depth profiles obtained by argon-ion bombardment. Although the Knudsen Cell measurements are not yet completed, it can be noted that:

- In the argon-caesium hydroxide atmosphere and at higher temperatures, a duplex oxide structure was formed on the stainless steel consisting of outer iron-rich scales covering a chromium-rich oxide layer.
- The caesium deposit stability on these materials increases with temperature.
- The deposition velocity of caesium on these materials increases at high temperature.

Studies with PHEBUS FP FPT0 samples

In this part we study the resuspension and subsequent deposition on stainless steel of the PHEBUS-FPT0 circuit deposit. Samples taken from the vertical line (samples 1^{bis}) were used.

Previous SEM/EDAX analysis of the deposit from this area indicates that some of the main components are Re, Ag, In, followed by U, Zr,W and Fe, Ni, Cr. ICP-MS analysis showed that fission products such as Cs were also present. The Knudsen cell re-vaporisation study showed release of In and Ag as the temperature rose above 700 °C. This release was completed as the temperature reached 1000 °C. Remarkably, no Cs was detected.

For the coupon's preparation a stainless steel tube was used. The Phebus sample and the stainless steel coupons were placed in fixed positions. He and $N_2/2\%H_2$ were used as carrier gases (flow rate 30 cm^3 s^{-1}). The temperature at the position of the Phebus sample was 1020 °C, while along the coupons there was a temperature gradient down to approx. 500 °C. The duration of each experiment was 240 min (heating rate 16.6 °C/min). The stainless steel coupons and the Phebus sample will be characterized with SEM/EDAX, XPS, XRD and other analytical techniques. For the release studies of these coupons, Knudsen cell mass spectrometry will be used.

The results of these examinations are expected to be useful since the consequences in the environment in the case of severe reactor accidents depend on the identities, stabilities and volatilities of compounds which appear in the PHEBUS-circuit deposit.

The above mentioned techniques will be also applied to the following PHEBUS FP FPT1 samples.

8.6. IABAT – Impact of Accelerator Based Technologies on Nuclear Fission Safety

The objective of the IABAT project is to assess the possibilities of accelerator driven hybrid reactor systems (ADS) from the point of view of safe energy production, minimum waste production and transmutation capabilities. In particular,

- to perform system studies on the accelerator driven hybrid reactor
- to assess accelerator technology
- to study the radiotoxicity of the fuel cycle for ADS and non-proliferation aspects
- to provide basic data

Success in this field could lead to practically unlimited sources of nuclear energy in a form acceptable to the general public.

Our task is to investigate the radiotoxicity and non-proliferation characteristics of ADS. In the present reporting period the calculational protocol for multiple irradiation and recycling has been established using ORIGEN2 [1]. Cross section data used were those for a fast lead cooled system [2]. Waste resulting from 10^{th} cycle spent fuel (1 cycle is 5 years irradiation plus 1 year cooling time) from a fast thorium fuelled ADS has been characterised. Actinide reprocessing losses were taken to be 1% of the core inventory at the end of each cycle. Ingestion radiotoxicity of this waste has been calculated for cooling times up to 10^6 years after discharge.

8.7. Thorium Cycles as a Nuclear Waste Management Option

The objective of this project is to investigate the use of thorium as fertile material in nuclear reactors with a view to reducing the amounts of long lived products in mining residues as well as those produced in reactors. The study will be of a generic nature with results applicable to various reactor types including PWR's, fast reactors, and accelerator driven systems. The work content consists of an assessment of all major aspects of thorium fuel cycles, taking into account the improved scientific knowledge and technological developments since the 70's. In particular, the study will cover

- radiological aspects of mining
- (re)fabrication aspects of thorium based cycles including various additive fissile components
- assessment of PWR with reduced actinide production based on thorium fuel
- assessment of PWR as thorium based TRU burner
- assessment of fast reactors with thorium fuel
- assessment of one particular ADS using thorium
- assessment of reprocessing
- residual risks of long term disposal
- technical aspects of non-proliferation

Our task at the Institute is to investigate this latter aspect i.e. technical aspects of non-proliferation of thorium cycles. In the reporting period the relevant nuclides for the thorium cycles have been identified. The uranium isotope vector for a thorium based fast reactor at a burnup of 100 GWd/t i.e. **U**(Fast, 100 GWd/t) has been calculated using the ORIGEN2 [1] code (pure Th^{232} is irradiated for five years in a fast neutron flux of $4x10^{15}$ cm^{-2} s^{-1} to obtain the compositions for the uranium isotopes). The cross section data used were those given by Rubbia et al. [2] for a fast lead cooled system.

The neutron multiplication factor (k_∞) for individual and mixtures of nuclides has been obtained. In particular, the neutron multiplication factor for the uranium isotope composition resulting from thorium irradiation to 100GWd/t in a fast reactor, i.e. for the isotope vector **U**(Fast, 100 GWd/t), has been evaluated.

References

[1] A. G. Croff; Nucl. Tech. **62** (1983) 335
[2] C. Rubbia, et al.; CERN report CERN/AT/95-53(ET), 12 Dec. 1995

9. Competitive Support Activities

Introduction

In the framework of technology transfer, Directorate General XIII of the European Commission is supporting cooperative activities between research Institutes and industrial partners on a competitive basis. Such support is given in particular to inventions (patents) originating from the Institute and having a high potential for industrial applications.

9.1 Enhanced Gas Cleaning by Infra-Sonic Agglomeration

Present status of the activity

On the basis of the positive results obtained on agglomeration and deposition of aerosols by infrasound [1] a new project aiming at the transfer of this technology to industry was accepted for funding under the Competitive Support Activities Programme administrated by DGXIII-D [2]. This project, entitled "Enhanced gas cleaning by infra-sonic agglomeration and deposition", involves two industrial partners. Infrasonik AB (Stockholm, Sweden) provided the design for an optimised infrasound chamber, and special parts of the equipment such as the infrasonic pulsator. Apparatebau Rothemühle (Wenden, Germany) built the infrasonic source, which is currently being installed in a by-pass at the Bayernwerk oil fired power plant near Ingolstadt.

The source, which is 8 meters long, and operates in the 25-30 Hz range, has been tested already in the workshops of Apparatebau Rothemühle. At the exit of the pulsator, a pressure up to 28 kPa (i.e. 186 dB) could be reached. Initial agglomeration and deposition tests were made in the acoustic cavity, without gas flow through the installation. Although it should be borne in mind that these tests were made on an aerosol whose size distribution is not the same as that expected at the industrial site in Ingolstadt, a positive effect could be observed and the cavity was cleared within 3 s.

The test of the source under laboratory and industrial conditions is scheduled for the beginning of 1997. The dependence of the agglomeration and deposition rates on the acoustic energy in the cavity will be evaluated along with the influence of turbulence generated by means of grids located in the oscillating flow.

Future activities

If the results described above are sufficiently promising, a demonstration project could be envisaged.

Furthermore, contacts with industrial European companies and with IAM (Instituto de Acústica de Madrid) have been established in view of building an international project on acoustic agglomeration of aerosols. The aim is to combine the know-how accumulated by the JRC and these organisations, to establish the viability of this process for the treatment of industrial effluent and process gases.

References

[1] EUR 16152 EN (TUAR-94), p. 155
[2] EUR 16368 EN (TUAR-95), p. 195

D. Competitive Activities outside the Framework Programme

10. Third Party Work

Introduction

In the following, a short summary of some of the work performed for third parties is given. Reporting is short and selective due to the commercial character of the work performed. For the Institute, such type of work is beneficial for essentially three reasons:

a) it shows the relevance and competence of the Institute for such work within the nuclear fuel cycle;

b) it increases the know-how of the Institute in areas of industrial applications, where access to material and data would otherwise not be possible;

c) last but not least it provides some financial income which is highly welcome to maintain a functional and safe nuclear infrastructure at the Institute.

10.1 Post-Irradiation Examination of Pressurised and Boiling Water Reactor Fuel Rods

In the framework of the contract with Siemens AG – Bereich Energieerzeugung (KWU), non-destructive and destructive examinations of power reactor fuel rods were carried out. The work performed and described in the last five annual reports [1] has continued. A list of types and number of examinations carried out on different fuel rods in 1996 is given in Tabl. 10.1.

Six fuel rods from the reactor Gösgen (KKGg) and nine fuel rods from the reactor Neckarwestheim (GKN) were transferred to ITU. The goal of the examinations is to provide experimental evidence of the good behaviour of the fuel rod at very high burn-up (up to about 100 GWd/t). The oxidation process and the amount of hydrogen pick-up by the cladding are some of the focal points of the studies.

In addition, four segments, previously refabricated in the Institute hot-cells, were received back for examination. The refabricated segments were irradiated in the Petten reactor, either ramped up to a high linear power or submitted to a power cycling experiment. The amount and isotopic composition of the gas released, the examination of Pellet Cladding Mechanical Interaction (PCMI) effects and the influence of power cycling, are some of the goals of the post-irradiation examinations.

12 capsules containing fuel rod segments were encapsulated and shipped back to the Gösgen reactor pool. Moreover, 6 refabricated segments from BWR reactor type fuel rods, were sent to the Petten reactor to be ramped.

References

[1] EUR 14493 (TUAR-91), p. 199; EUR 15154 (TUAR-92), p. 199; EUR 15741 (TUAR-93), p. 227; EUR 16152 (TUAR-94), p. 205, EUR 16368 (TUAR-95), p. 199.

Tab. 10.1 Number and types of examination carried out on different fuels rods.

Experiment / Type of Analysis	MTS-6	Arlane	KKGg-PCA2	KPP-1	KKK-1	Transp.GE	KKGg-IX	GKN-II-3	KWW-IASCC	AUTOCLAVE	KKGg-X	B-Segm.	CREEP	TOTAL
Vis.examination				5					8			4		17
Fuel rod length												6		6
Profilometry			4	2					3					9
Defects (cladding)			1	2				9	3					15
Oxide layer thick.				2				9						11
Gamma Scan.				2			1				2	1		6
Fission Gas Anal.				2								2		4
Free volume det°.				2								2		4
Metallography				3			14			2		2		21
Ceramography				1			5					2		8
Burn-up det°.							1							1
Isotopic Anal.		2												2
Density					8		3							11
H2-Determin.	10						10							20
SEM-Cladding									3					3
TEM-cladding				2			2			1				5
Weighing	3,5													3,5
ICP-MS							3							3
Refabrication				6										6
Creep Tests													6	6
Microhardness test				1						2				3
Special Studies (GE)						1								1

10.2 Development of a Closed-End Burst- and Creep-Test for Irradiated Cladding Materials

This test apparatus has been developed for the hot cells and for the future work to be carried out under contract with Siemens-KWU. The mechanical properties of highly irradiated materials are of great importance especially the creep phenomena occuring under biaxial stresses from operation, as well as in storage conditions due to internal gas pressure and residual heat. These latter influences need to be quantified for the licensing authorities.

A device, able to operate under remote handling conditions, has been developed to evaluate the mechanical properties of closed-end samples, taken from irradiated cladding materials, by performing burst- or long-term creep-tests. The system is based on the internal pressurisation of a cylindrical sample.

The equipment was designed for samples (normally 10.75 mm in diameter) up to 150 mm in length which, taking into consideration the grip length, ensures an unsupported length of about 10 times the average outside diameter, as recommended in the ASTM – Norm B 353.

An electrical furnace, provided with three heating zones and an internal double wall lining containing caesium, allows homogeneous heating of the sample to the test temperature, minimising the temperature gradient along the sample.

A data acquisition system provides simultaneous recording of the specimen pressure as measured by a transducer located near to the sample. The oil volume input to the specimens obtained from the piston travel with a potentiometric transducer and the temperature. At pre-set time intervals, the instantaneous values of pressure, temperature and piston displacement can be recorded during the whole test.

Three devices were developed in order to: 1) retrieve the fuel, 2) tighten the specimen grips and 3) measure the sample diameter before and after testing.

1) Based on a commercial drilling machine, able to hammer while drilling, a device was developed to retrieve the fuel from the segments of fuel rods irradiated in nuclear power plants. The device utilises a concrete drilling tool, fixed during the operation while the samples rotates. The system allows a smooth vertical displacement through counterweights which keep the sample in quasi-equilibrium during the drilling operation, permitting the operator to control and maintain the applied load at a minimum.

2) Mechanically attached end-fittings were used to seal the specimen. In order to screw the fittings to the specimen, a special device was developed on the basis of a commercial pneumatic wrench, able to perform a smooth tightening of the fittings, avoiding impacting or pulsing tightening cycles which could lead to the damage of the samples.

3) A displacement transducer has been mounted on a floating head to measure the relative movement of two knives which perform the measurements using, as reference, calibrated standards. The device is able to detect variations of ± 0.1 μm in the diameter. The same device permits the simultaneous measurement of the axial displacement (± 1 μm), allowing correlation of the diameter measured with the axial position on the sample.

CONCLUSIONS

A burst- and creep-test apparatus has been developed which has low stored energy, provides good control of the deformation through the oil volume pumping rate, produces a smooth pressure/volume curve and works reliably under remote-controlled conditions. Future work foresees the further testing of samples from 4 and 5 cycles LWR fuel rods. The influence of increasing radiation damage, oxide layer thickness and hydrogen pick-up will be studied.

10.3 Phebus fp Post-irradiation Examination (PIE)

The Phebus fission product (fp) project is financed by the French IPSN (Institut de Protection et Sureté Nucléaire), Cadarache with the participation of the European Commission. Four other countries (USA, Canada, Japan and Korea) have since joined. Its objective is to investigate severe accident scenarios in nuclear reactors, particularly the behaviour of fission products released into the primary circuit and containment. An analysis of the degraded bundle is also necessary for this purpose.

The bundle from the first Phebus test (FPTO) using trace-irradiated fuel was sectioned and 5 discs, chosen from the gamma tomography, were selected for metallographic analysis. ITU examined a disc sectioned at the lower level of the molten pool that had formed beneath the central cavity where the entire bundle had melted and/or collapsed. The aim was to determine the melt's composition and hence deduce the main degradation mechanism.

The low power optical microscopy revealed (see Fig. 10.1) a corium pool on the east side with an outer rim of columnar crystals, and a central zone of equiaxed grains. This shows the more rapid cooling (but not quenching) of the outer edge and the slow cooling of the centre. Approximately 20 thermocouple remnants were visible in the corium as opposed to an original number of 3 at this level. This indicates that many thermocouples had collapsed from above. On the west side of the bundle, which was not corium-filled, three badly degraded rods were evident along with an ultrasonic thermometer. The zircaloy cladding was completely oxidised from both sides or sometimes had interacted with melting fuel to produce a porous liquefied material.

Microprobe line scans of the outer corium and the surrounding ZrO_2 shroud revealed that interaction between the corium and the shroud had resulted in an interdiffusion of U and Zr to form a 1 mm thick interaction zone. The corium itself showed no Zr concentration gradient and was of uniform composition from the edge of the interaction zone outward into the corium. The thin outer CeO_2 layer of the shroud had been dispersed and cerium traces were found in uniform concentration in the melt along with Y from the Y_2O_3 stabiliser in the ZrO_2 shroud; some cerium had also diffused inward into the ZrO_2 shroud. Quantitative microprobe analysis indicates that the melt is approximately equiatomic (U, Zr)O_2 with traces of iron ($U_{0.51}Zr_{0.46}Fe_{0.03}O_{2\pm x}$). Powder samples from corium located 5 cm higher were examined at CEA Saclay by X-ray diffraction (XRD); these were interpreted as a highly deformed cubic fluorite lattice of (U, Zr)O_2. The small value for the lattice parameter (a) indicated approximately 45 to 50 a/o Zr present. XRD work on powder samples from this disc gave a similar pattern and supported this interpretation.

Metallographic examination also showed the corium to be principally a single phase material. Small amounts of second phases present at the grain boundaries were Fe, Cr, Ni-rich or W, rhenium containing oxidic material and resulted from dissolution of the stainless steel, Inconel components or the tungsten, W-Re thermocouples. Some bright metallic inclusions of Re-Ir (thermocouple remnants) were also visible. The distribution of these small secondary phases on the grain boundary imply that they were in solution and resulted from precipitation on cooling. Evidence of tungsten volatilization (probably as volatile oxides) was also seen in the damaged thermocouples. Although zircaloy can and very likely did attack the fuel from ~ 1800 °C onward, the uniformity of the melt composition and its full oxide stoichiometry as (U, Zr)O_2 imply that firstly, oxidation of the metallic liquefied material continued after liquefaction and secondly, the oxidic corium was mostly at 2500 °C (the melting point of this mixed oxide) and attack of the zirconia shroud indicates maximum temperatures in excess of 2700 °C.

ICP-MS analysis confirmed the microprobe analysis of the molten corium material as an approximately equiatomic (U, Zr)O_2 melt. No fission product Cs was found (although Cs-137 and Cs-134 are present in the residual solid fuel pieces outside the melt). Some silver was also evident in low and variable amounts in the melt (probably as metallic ex-solution precipitates). This analysis confirmed the composition of the oxide corium and also the pattern of fission products detected by other techniques.

10.4 Phebus fp Post-test Analysis (PTA)

ITU's participation in the Phebus fission product (fp) project also included post test analysis (PTA) of certain samples for fission product release (see section 10.3). The work on test samples from the first test of Phebus fp (FPT0) using trace-irradiated fuel was continued during 1996 under contract from IPSN (Institut de Protection et Sureté Nucléaire), Cadarache (France). The first samples were sedimentation coupons and granular beds from the cool (150 °C) horizontal line and the containment vessel simulating the primary circuit and the containment respectively.

The second batch of samples came from the vertical line section directly above the bundle. This was a Ni-based alloy Inconel 600 tube 50 mm to 35 mm diameter, which was maintained at 700 °C during the experiment. Samples were taken from the lower region (sample 1) and at the top of the vertical line or elbow (sample 5).

a) Lower vertical line

Gamma spectroscopy of a roughly 1 cm x 1 cm piece indicated the presence of Cs-127, Sb-125, Ru-106 and Nb-95, Zr-95 fission products (although Zr-95 can also be a zircaloy irradiation product) and also Ag-110 as an irradiation product from the Ag absorber.

A smooth surface was evident with particles embedded in it. These appeared to be Re-rich. The deposit had broken off in pieces to reveal a porous mixed Cr, Ni, Fe

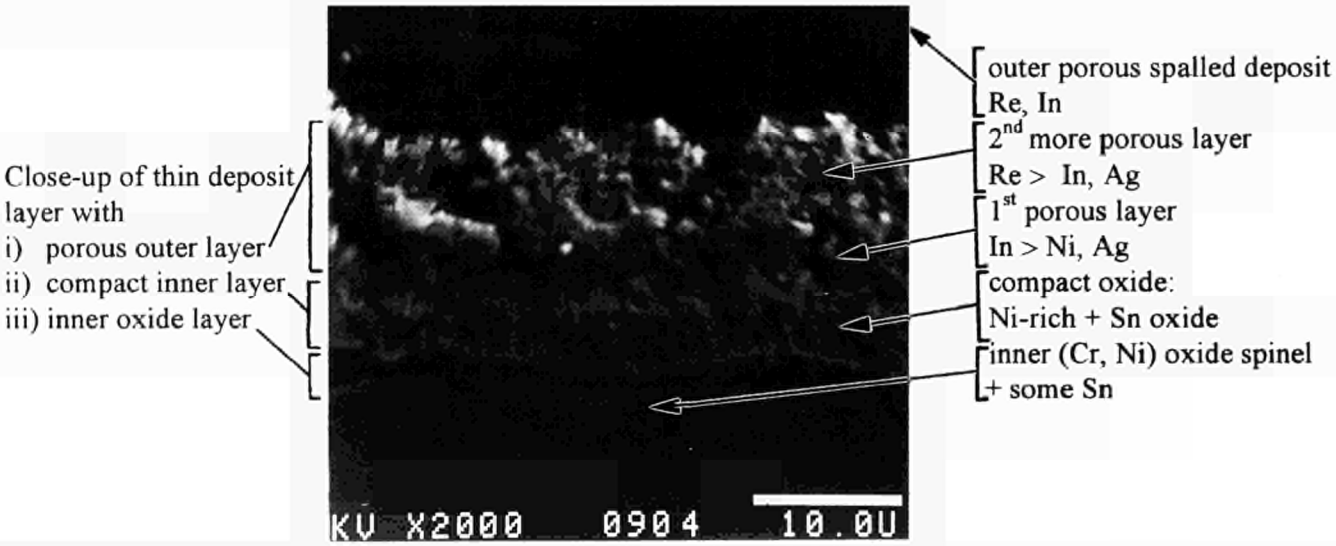

Fig. 10.1 Cross-section of the lower vertical line deposit showing the sequence of deposition. Sn, then Ag and In, then increasing Re. Increasing porosity towards the exterior indicates more aerosol agglomertion with time.

oxide. Analysis of the outer surface was difficult and this was apparently due to the inadvertent coating of the surface with resin while embedding the bundle.

A cross-sectionally mounted sample of the lower vertical line gives the sequence of elements released. It shows considerable Sn in the lower deposits (probably volatilised from the zircaloy cladding at approx. 1700 °C [1]) that appears to have been released very early (see Fig. 10.1).

Thereafter come In and less Ag from the Ag-15 In-5 Cd absorber rod (Cd was probably too volatile to condense at 700 °C) however with time and increasing temperature more Re was released (Re is richer in the outer oxide). The increasing porosity towards the outside indicates increasing particle agglomeration with time as vapour levels increased with increasing temperature and degradation. Re is very likely, in oxide form, to have volatilised at the bundle temperatures of 2000–2500 °C. These vapours appear to have condensed into particles and then agglomerated immediately along the vertical line. Tungsten appeared to be uniformly present in the deposit, indicating a more steady release with time.

b) Upper vertical line-elbow

horizontal arm

A thin black powdery deposit, unevenly distributed, was evident at low power optical microscopy, while SEM-EDX showed both fine granules and small crystallites in either cuboidal or needle-like forms (see Fig. 10.2).

The fine granules (< 0.1 μm diameter) appeared to be already agglomerated upon deposition. EDX analysis showed the cuboidal crystallites to be In-rich, while occasional larger blocky crystals were practically pure Re. The deposit was generally a In, W and Re mixture and given the low temperatures that prevailed compared to the Re and W melting points, they are presumed to be in the form of their more volatile oxides. Indium is also presumed to be in the form of its more volatile oxide. Silver is also present and is probably in metallic form.

vertical arm

The upper elbow showed a similar heterogeneous black powdery deposit although it was heavier, perhaps due to the greater turbulence in the bend. There were also considerable spheres visible in the deposit of approximately 10 μm diameter (see Fig. 10.3).

These appear to be frozen droplets of the liquid corium (fuel-cladding mixture) as they were an approximately equiatomic (U, Zr) oxide mixture ((U, Zr)O_2). They were covered with structural material crystallites and particles (In, Re, Ag, W and Fe, Cr, Ni) that appeared to have agglomerated or condensed on the sphere in flight and directly onto the surface of the bend. Cuboid, needle-like and granular geometries were present. Condensation of vapours and agglomeration of condensed or pre-existing particles appears to have been occurring during the whole flight along the vertical line.

The deposit at the elbow appeared to have approx. 3 a/o uranium content. This value was used along with the uranium values present in the other parts of the simulated circuit to estimate uranium release from the bundle during a severe degradation (approximately 0.5 w/o of the bundle content).

Reference

1] S.R. Mulparu, R.K. Rondeau, E.D. Lindquist; Trans. Amer. Nuc. Soc. **69** (1993) 313

Close-up showing
a large (Re-rich) crystal (2)
and fine agglomerated
particles (≤ 0.2 μm dia) making
up deposit (1)
4000 x

(1) Re 57 w/o (2) Re 64 w/o
In 24 w/o Ag 16 w/o
Ag 11 w/o In 8 w/o
W 4 w/o W 5 w/o

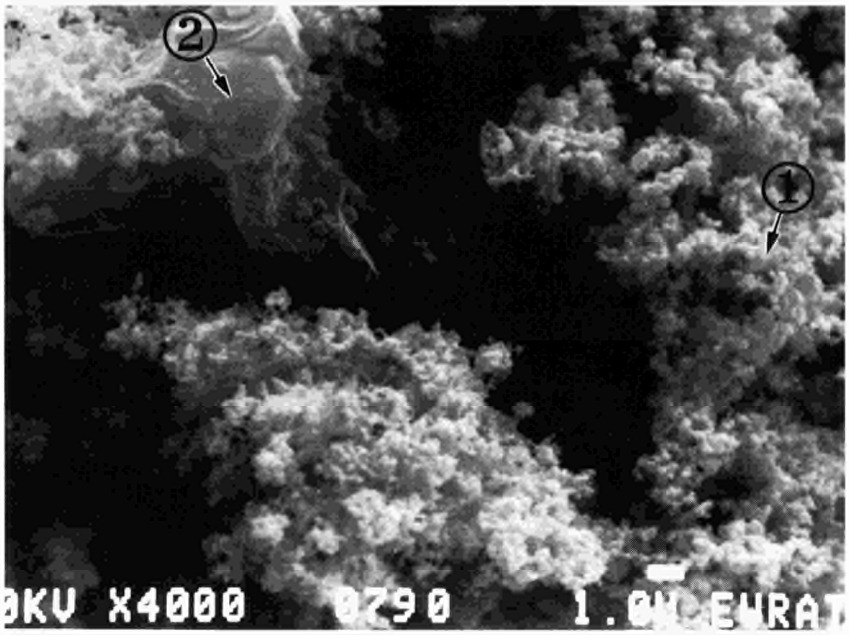

Fig. 10.2 SEM micrograph of the deposit on the vertical line elbow (horizontal end), showing a fine porous granular deposit containing Re, In, and W as well as Re-rich large crystallites.

View of clustered
U-Zr spheres (1)
with crystallites on their surfaces
2000 x

(1) U 48.3 w/o
Zr 30.0 w/o
Re 6.0 w/o
W 1.5 w/o
Cr 9.5 w/o
Ni, Fe 4.7 w/o

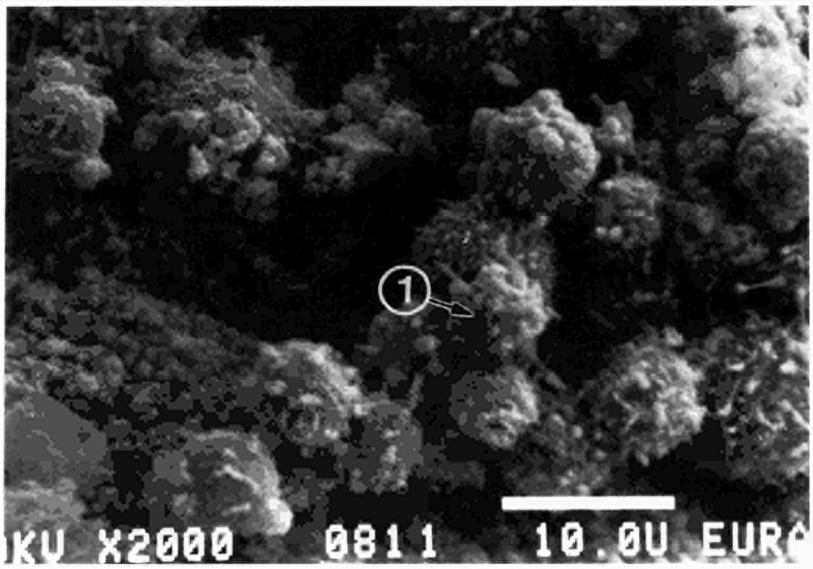

Fig. 10.3 Micrograph of the thicker deposit on the vertical arm showing a clump of frozen corium spheres covered with In-containing crystallites or Re, W and Ag-containing particles.

10.5 Spent Fuel Characterization for Interim Dry Storage

The project has been carried out under a contract with the Central Research Institute of the Electric Power Company (CRIEPI), Japan. The aim has been to characterize high burn-up UOX and MOX spent fuels in order to (a) assess their interim dry storage behaviour; and (b) obtain experimental data for the verification of computer codes used to evaluate the radiation source term for these fuels. Destructive and non-destructive analyses techniques have been used to characterize the fuel. The project began in 1993 and has continued through to the end of 1996.

The experimental items of the project can be grouped as: isotope analyses and radiation measurement for burn-up credit, radiation source measurement/distribution, fuel performance studies (cladding, pellet-cladding interface and fission gas data). Furthermore, fuel/assembly information (design, fabrication and irradiation history) were provided in order to simulate the fuel evolution during irradiation. During the last year of the programme the following studies were performed: chemical analyses of actinide and fission product content, EPMA, fission gas release during heat treatment (annealing test), microscopic studies (SEM, TEM) of annealed samples, mechanical properties of cladding, oxygen potential determination.

10.6 Characterization of Colloids in Dissolver Solutions of High Burn-up UO_2 Fuels

The residue obtained upon dissolution of spent fuel is mainly composed of coarse material which can easily be filtered from the dissolver solution, but it also contains fines, which remain suspended in the solution. The stability of this solid dispersed system depends on the particle size distribution, on the density of the solid particles and the electric charge at the surface. Upon reprocessing, these colloids can strongly disturb the extraction process. Thus the present study is carried out to characterize these materials especially with respect to their surface charge.

Two high burn-up UO_2 spent fuel samples were dissolved in 4 and 7 M HNO_3 respectively. After separation of the main residue by filtration at 0.2 μm, the colloids have to be separated from all the ionic species contained in the filtrate in order to measure the surface charge of the dispersed solid particles. A dialysis method, tested out on simulated solutions and also on a real sample, proved to be very efficient for this purpose.

The determination of the surface charge is carried out by titration with a standard N/1600 potassium polivinyl alcohol sulfate (PVSK) solution. A large number of test series were carried out with gold, platinum and iron colloids to determine the optimum experimental conditions. A successful titration of the real sample obtained as described above was carried out.

A systematic measurement of the two high burn-up UO_2 samples will be carried out in the beginning of 1997 including a chemical charaterization of all samples by ICP-MS. The final report will be ready by the end of 1997.

10.7 Characterization of Residues from Dissolution of High Burn-up UO_2 and MOX Fuels

The aim of this work carried out on hehalf of the Central Research Institute of the Electric Power Company, (CRIEPI) is to characterize residues obtained upon dissolution of high burn-up UO_2 and MOX spent fuels in order to assess their performance in the head end of the reprocessing process. A thorough character-

ization of the fuels by different destructive and non-destructive techniques has been carried out. The project began in 1994 and should be finished in April 1997.

The dissolution of the characterized fuel and residues is completed. An examination of the residues by optical and scanning electron microscopy has been completed in 1996. Burn-up, elemental and isotopic composition of the residues are determined and the interpretation of the results in comparison to the fuel data is done at present. The study will be completed by an EMPA examination of the fuel residues, scheduled for early 1997. The comparison of these data with the original fuel should allow to prepare a complete and detailed report by June 1997.

10.8 The RIM effect irradiation

The irradiation of the UO_2 based fuel disks fabricated in 1993 (TUAR-93, p. 227) in the OECD Halden reactor was terminated as planned in May 1996. The High Burnup Rim Project, HBRP, is managed by the Central Research Institute of Electric Power Industry, CRIEPI. Small UO_2 disks were irradiated at four temperatures (nominal 500, 700, 950, 1200 °C) to four burnups (nominal 55, 70, 85 and 100 GWd/t). In addition, two pressure capsules were used (0.3 and 14.0 MPa Ar), corresponding to about 30 MPa at the operating temperature. The released fission gases were analyzed during the irradiation to estimate variations in the S/V ratio.

The fuel rods and the pressure capsules were transported to ITU in December 1996. Post-irradiation examination will start in January 1997 to investigate the effect of the controlled parameters used (burnup, temperature, pressure and type of fuel) on polygonization (formation of the RIM structure). The irradiation results and analyses will be reported at an International Conference in March 1997 [1].

References

[1] M. Kinoshita, S. Kitajima, T. Kameyama, T. Matsumura, E. Kolstad, Hj. Matzke; ANS Int. Topical Meeting on LWR Fuel Performance: Going Beyond Current Burnup Limits, Portland, March 2-6, 1997

10.9 TRANSURANUS Training Course

21 participants from Armenia, Bulgaria, the Czech Republic, Hungary, Poland, Romania, the Slovak Republic and the Ukraine participated in a TRANSURANUS Training Course, held at the Institute from June 17-21, 1996. The course was a co-operative programme of the International Atomic Energy Agency (IAEA) and the European Commission. The participants were members of Central and East European regulatory bodies, atomic energy agencies and research institutions.

The objective of the TRANSURANUS Training Course was to make the participants familiar with the basic principles and the usage of the code. The participants received the TRANSURANUS code as source code together with the pre- and post-processor programs AXORDER, URPLOT and URSTAT as well as the TRANSURANUS handbook.

The training initiative was made possible through the engagement of the ITU Modelling Group in several IAEA projects and in the Commission's PHARE programme.

10.10 Reference Samples for In-Field K-Edge Densitometry

On request of the Euratom Safeguards Directorate (ESD) in Luxembourg, a new type of reference sample for the In-Field Hybrid K-edge instruments has been developed. These samples are required for the stability control of the measurement systems installed on the sites of La Hague (F), Sellafield (UK), Dounreay (UK) and ITU.

The final concept consisted of stainless steel capsules containing nitric acid solutions with and without uranium. These solutions were filled into the capsules which were welded and sealed by TIG welding. Problems arising during filling and welding were solved by a special design.

11 cuvettes were supplied:

- cuvettes with a uranium reference solution (uranyl nitrate solution with a concentration of 200 g U_{nat}/l)
- cuvettes containing 3 N HNO_3 solution
- empty spare cuvettes

11. Other Community Activities

Introduction

Apart from institutional support to the policy of the European Union, the Institute can participate in other Community activities. Examples are the European Commission´s technical assistance programmes to the Eastern countries, like the PHARE and TACIS programmes, or R&D cooperation in the framework of the INTAS programme (International Association for the Promotion of Cooperation with Scientists from the Independent States of the Former Soviet Union).

Another important area is the cooperation with the International Science and Technology Center (ISTC) in Moscow. The objective of this cooperation is to provide support and cooperation to projects financed inter alia by the European Union and which are performed by scientists from sensitive military installations in order to avoid a 'brain drain'.

Below is a short summary of projects, in which ITU is actively involved.

11.1 Phare Project 'Fuel Rod Modelling and Performance' (FERONIA)

This project is a co-operation between the Bulgarian Academy of Sciences, Institute of Nuclear Research and Nuclear Energy and ITU. The main activities are focused on the following areas:

1. Review of WWER fuel rod behaviour, materials properties and models.
2. Analysis of the PIN-micro code which has been used by Eastern Countries for the analysis of WWER fuel rod behaviour; comparisons with the TRANSURANUS code.
3. Detailed analysis of anisotropic cladding creep.

The first "Extended FERONIA Meeting" was held October 14-16 in Sofia, Bulgaria. The meeting was attended by about 25 experts from the Bulgarian Academy of Sciences, the Committee on the Use of Atomic Energy for Peaceful Purposes, the Kozloduy Nuclear Power Plant and ITU.

Details are given in Quarterly Reports which are available on request.

11.2 Investigation of the Environmental Impact of Spent Nuclear Fuel and Core Debris of the Destroyed CHERNOBYL-4 Unit

The investigation is aimed at defining the present conditions of the materials contained in the destroyed Chernobyl-IV reactor. Analyses will be carried out in the ITU laboratories both on remainder of fuel elements and on frozen lavas produced by the interaction of corium with concrete and structural materials (see Tab. 11.1).

Tab. 11.1 Materials of the Chernobyl IV destroyed Reactor to be analysed in the tacis project.

Type of specimen	Amount
spent UO_2 fuel ① (fuel element segment)	20-30 g
UO_2 fuel ②(pellet slightly irradiated)	20 g
lava-like FCM, brown ceramic ③	20-30 g
lava-like FCM, black ceramic	20-30 g
lava-like FCM, zebra ceramic	40 g

① The fuel will be cut from some twisted, but relatively undamaged fuel rods, which have been spotted in a reacheable reactor premise.
② To be analysed for comparative purposes.
③ FCM: fuel-containing material

The foreseen analytical methods are Knudsen vaporisation (Stage I) and laser heating (Stage II) with mass spectrometry of the vapours as well as detection of aerosols formed under simulated accident conditions (Stage III).

The apparatus for stage I was to a large extent available when the project was started. However, a new furnace with a device for rapid heating of the sample cell had to be constructed (Fig. 11.1). This is now ready, and will be mounted in the shielded glove-box when the Chernobyl samples arrive at ITU.

The time-of-flight (TOF) spectrometer which will be used in stage III, for the measurement of effusion under very rapid laser heating conditions, has been built according to an ad hoc design (Fig. 11.2) developed in our laboratory in collaboration with an external company, and will be delivered in April 1997.

Whilst the technical aspects of the project have been managed according to the initial time schedule, shipment of the samples from Chernobyl to Karlsruhe raised a number of problems which entailed a delay of more than one year. Finally an agreement was signed in Kiev between ISTC-Chernobyl, ITU, and Nuclear Cargo Co., envisaging shipment of the samples in April 1997.

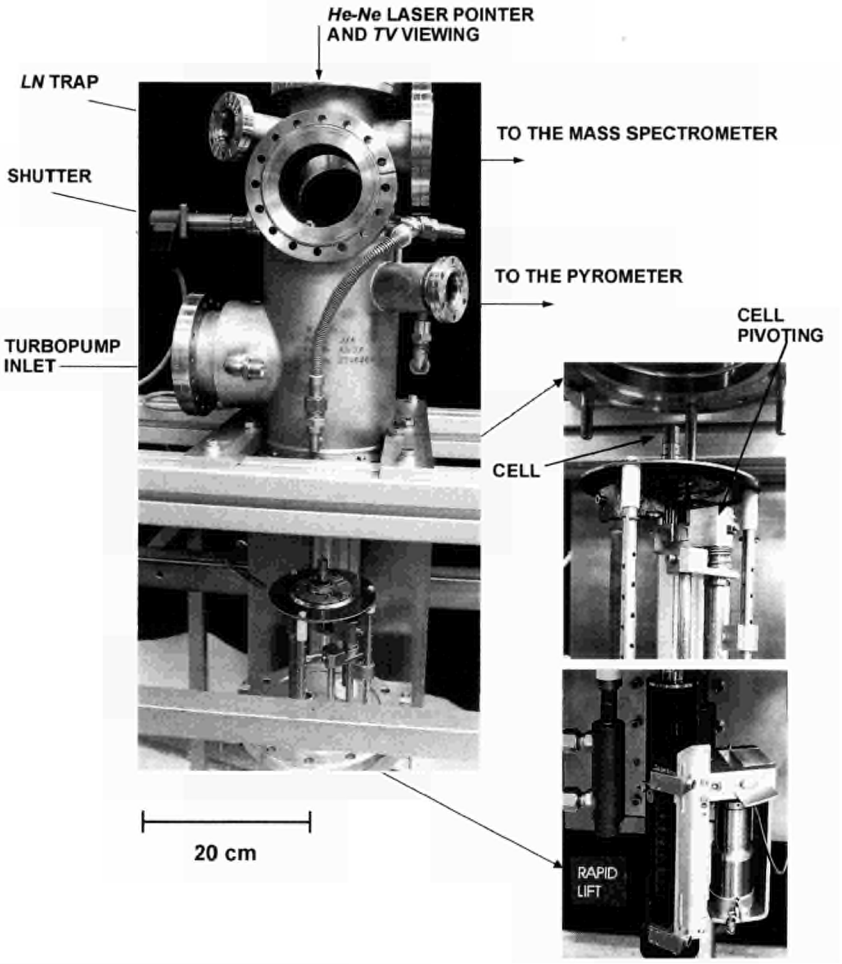

Fig. 11.1 New Knuden cell for the TACIS – Chernobyl Project.

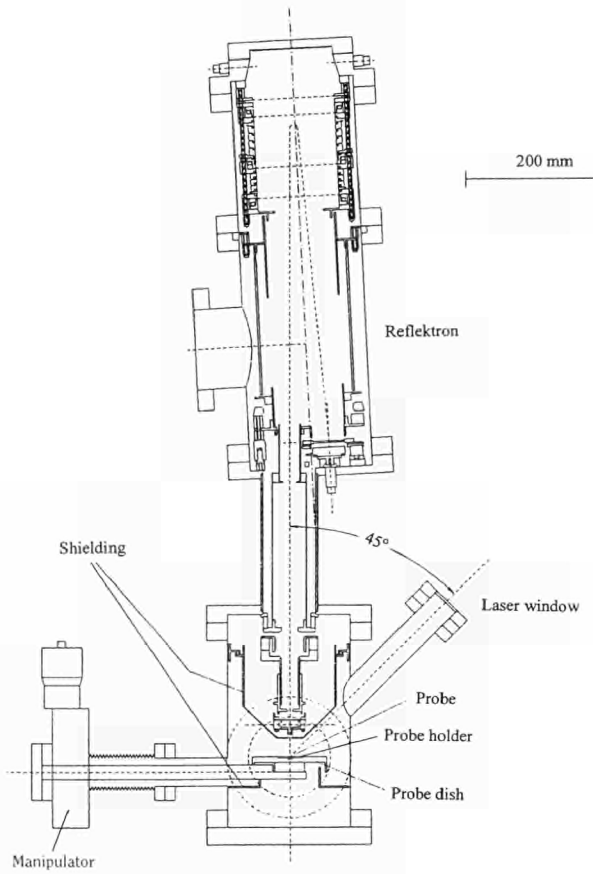

Fig. 11.2 Set-up of the time-of-flight spectrometer.

11.3 The Equation of State of UO_2 up to the Critical Point

A research project supported by INTAS (International Association for the promotion of cooperation with Scientists from the Independent States of the former Soviet Union) was started at the end of 1995 with the aim of improving the thermodynamic description of liquid UO_2 nuclear fuel at very high temperatures, in the range attained during the most severe hypothetical accidents. Specialists from IVTAN, Moscow (Russia), University of Warwick (United Kingdom), University of Odessa (Ukraine), TPI, Tashkent (Uzbekistan) and JRC-ITU (Germany) are working together on a joint experimental and theoretical programme.

The construction of the equation of state of liquid and gaseous uranium dioxide is a formidable problem which has been attacked in the last two decades by European and American teams. Despite the increasing complexity of the proposed models, the various approaches stumbled over two difficulties: first, the nature of the interatomic bonding in the liquid which is unknown and whose arbitrary assessement may compromise the validity of the model; second the non-congruency of the liquid and the equilibrium vapour, which requires a very complicated formalism, and is only applicable to certain types of models. Although the proposed models could normally be tuned to describe the available high temperature data, any extrapolation of primary quantities like density and pressure, or deductions of second order quantities like heat capacity or thermal expansion data remain very uncertain.

In the development of the new model, a more extended database was considered, including the recent heat capacity measurements in liquid UO_2 obtained at ITU, as well as revised thermochemical data of the vapour species.

The new approach [1] , based on Perturbed Hard Spheres (PHS), was chosen after considering the merits of the various models. The choice criterion was initially suggested by the flexibility of this model which is able to account for complex multi-component systems. However, corroboration of this choice was eventually provided by the theorem of Stillinger and Reiss (1960) [2,3] whose thesis may be expressed in simple words as follows:

"If order-disorder of a binary mixture of cations and anions is considered, the partition function formally corresponds to that of a fluid, all of whose particles are identical, and the effective potential is equal to the short-range interaction of the original core supplemented by attractive contributions which are of much shorter range than the original Coulomb interactions"

The importance of this formal equivalence is evident in treating a fluid like UO_2 where non-stoichiometric effects, and hence molecular clusters, have to be accounted for in a framework where, no doubt, ionic interactions play an essential role.

From one side, the virtual particle formalism obviously justifies the powerful PHS approach even in multi-component systems subjected to ionic interactions, yet, from the other side, this formalism entails the definition of an effective pseudopotential, whose physical interpretation is not free of ambiguity.

Most of the work in the reported period has been dedicated to the construction of realistic interaction potentials, by using available atomic and molecular parameters and to the study of their effects on the thermodynamic properties.

It has been demonstrated that some important features of liquid UO_2 may be reproduced by relatively simple models, however, the main difficulty still resides in the extension of the number of particle types in order to correctly describe non-congruent vaporisation. In this context, no experimental validation of the model seems to be possible, since no data are available on liquid and vapour compositions at very high temperatures. Several arguments concerning the consistency of the model predictions are being considered. For instance, calculations have demonstrated that non-congruent vaporisation has a strong impact not only on the critical parameters of the system, but also on its behaviour in the vicinity of the critical point. This provides important criteria for the selection of the model parameters.

At this stage of the the project, an equation of state of UO_{2+x} has been constructed, including 14 ionic and molecular clusters having distinct properties, and being submitted to all relevant types of mutual interactions. A computer programme has been also developed to validate the model and to perform thermodynamic calculations up to the critical point. A complete description of the model was published recently in a report with limited distribution [4].

References

[1] INTAS PROJECT 93-0066, "Construction of the Equation of State of Uranium Dioxide up to the Critical Point", Interim Report I (May 1996), Report ITU-K0296186.1

[2] F.A. Stillinger, J.G. Kirkwood, P.J. Wojtowicz; J. Chem. Phys. **32** (1960) 1837

[3] H. Reiss, S.W. Meyer, J. Katz; J. Chem. Phys. **35** (1961) 820

[4] INTAS PROJECT 93-0066, "Construction of the Equation of State of Uranium Dioxide up to the Critical Point", Interim Report II (December 1996), Report ITU-K0296186.2

11.4 Development of a Relational Database for Identification of Nuclear Material of Unknown Origin

During the last 6 years a number of serious events of illicit trafficking of nuclear materials has occurred in the European Union. In more than 20 cases the seized material has been analysed at ITU Karlsruhe, in order to characterize the material and to determine its origin and intended use. To perform this task efficiently, a comprehensive database, in connection with a retrieval system, is needed.

The main objectives of the nuclear material database system are:

- to guide the analyst by selection of appropriate techniques for proper characterization
- to reveal the origin and/or intended use of seized material

A database system for covering source-characteristic, but non-sensitive information has been installed on the same platform as the sample-specific database [see chapter 6.6], making use of the ORACLE™ relational database management system. However, the logical structures of both databases differ significantly. A simplified scheme of the source-characteristics database is given in Fig. 11.3.

Parameters can be divided into these groups:

1. Characteristic analysis parameters: e.g. fuel material, fuel form, pellet dimensions, initial enrichment, microstructure.
2. Query results concerning origin and intended use: reactor type, reactor unit, fuel cycle facility.
3. Auxiliary parameters for relating tables to each other: fuel type, fuel preproduct, reactor model, assembly model.
4. Reactor operation parameters needed for burnup calculations: reactor nominal power, moderator material, cladding material, linear heat generation rate, average burnup.

A typical retrieval operation will start from a comparison of analytical results with characteristic parameters (group 1). In the first phase, rough categories can already be excluded (e.g. CANDU reactors in the case of HEU fuel). By means of the auxiliary relations, remaining ambiguities can be identified and additional analysis steps may be recommended. Eventually, a sufficiently narrow circle of data belonging to group 2 will be left and will support the identification of origin and intended use. Studies for identification of simple cases have already been performed.

The prevailing fraction of development activities has been devoted to defining which parameters are indeed characteristic for individual fuel production processes and facilities. In this context a project on international co-operation between ITU and the All-Russia Research Institute of Inorganic Materials (VNIINM), Moscow has been launched, in the framework of which two guest scientists from VNIINM have visited ITU for 6 months each. Their expertise covers material data, specific for fuel fabrication, enrichment and reprocessing. More non-sensitive data for reactors situated within the EU have been accumulated from open literature as well as via direct contacts with fuel manufacturers. A first operational version of the database system has been set up, the data of which include power and prototype reactors working with U or MOX fuel.

Burnup calculations (ORIGEN) are being performed aimed at providing additional theoretical input to the database. For this purpose, new cross section libraries covering the sectors for which fresh fuel data are available, have been established using the SCALE software package. Together with experimental data, which are however very scarce, they will eventually give comprehensive characteristics for irradiated fuel.

Further developments will also include the implementation of histograms for microscopic parameters as grain or pore size distributions.

11.5 Safeguards Analytical Laboratories at Bochvar Institute, Moscow

In the framework of the Commission's TACIS programme (Technical Assistance to the Commonwealth of Independent States), also projects related to nuclear material control and accountancy are under consideration. Following the specific proposals from the summit of the EU in Essen 1994, ITU has taken the initiative for a project on the design and set-up of laboratories charged with:

1. the analysis of samples from the Russian nuclear fuel cycle, for accountancy or safeguards verification puposes,

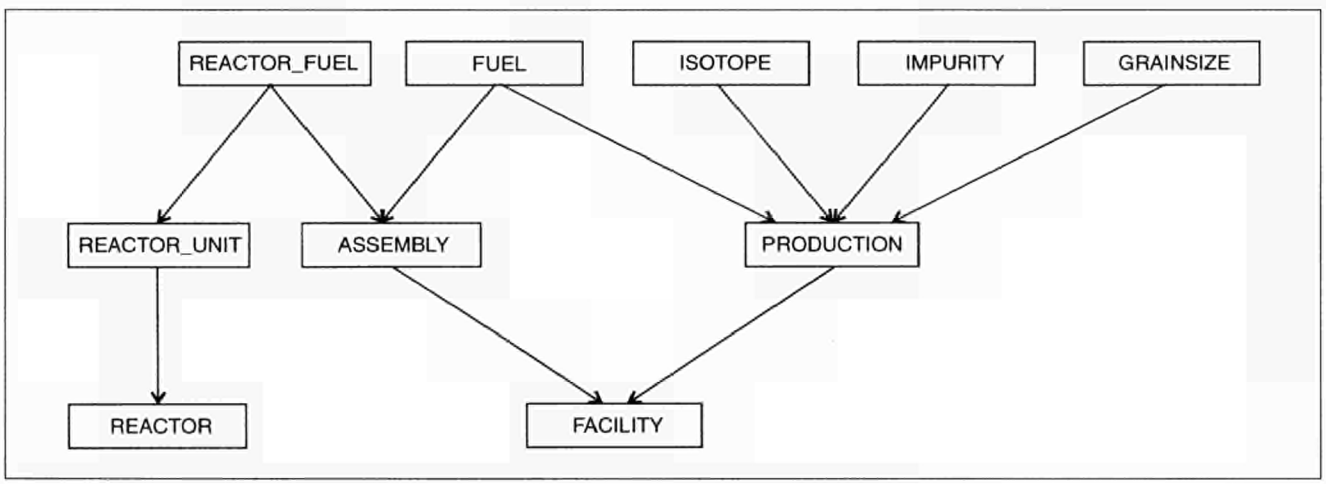

Fig. 11.3 Simplified scheme of relations used within the source-characteristics database.

2. the analysis of seized nuclear materials, in order to determine their origin or intended use,
3. the provision of metrological support in form of reference materials and independent quality control.

The technical responsibility for the latter lies with IRMM Geel. However, the project management and coordination for all three projects is with ITU.

In the reporting period a workshop was held at ITU with participants from the Bochvar – Institute, the Russian Federation Ministry of Atomic Energy (Minatom), the Russian Federation Safeguards Authority (GAN) and the Institute for Reference Materials and Measurements (IRMM).

The results were:

- definition of the basic technical parameters of each of the three laboratories
- instrumention required to execute the given tasks
- needs (Bochvar) and possibilities (ITU) for training
- work programme for 1997

12. Scientific Visitors and Scientific Fellows

35 graduate sectorial grantees from the following countries spent, in 1996, prolonged periods of time at the Institute. Four new doctoral grantees came from Spain, the Netherlands, France and Finland and four new post-doctoral grantees from Sweden (2), Finland and France.

Belgium	2	Italy	3
Finland	2	The Netherlands	3
France	8	Portugal	1
Germany	3	Spain	5
Greece	2	Sweden	3
Ireland	2	United Kingdom	1

Five doctoral grantees from the Institute have obtained their Ph. D. in 1996:

- *Luigi Paolasini*, 'Etudes par diffusion de neutrons des corrélations et des excitations magnétiques dans les composés intermétalliques UFe_2 et UPd_2Al_3', Université de Grenoble, February 1996.
- *Sylvie Casalta*, 'Etude des propriétés du système Am-O en vue de la transmutation de l'américium-241 en réacteur à neutrons rapides', Université d'Aix-Marseille I, April 1996.
- *Javier García Serrano*, 'Estudio de Productos de Fisión y Actínidos en Combustibles Nucleares Irradiados mediante la Técnica LA-ICP-MS (Ablación por Láser-Espectrometría de Masas con Fuente ICP), Universidad Complutense de Madrid, October 1996.
- *Arno Hiess*, 'Untersuchungen zur Konkurrenz der magnetischen Wechselwirkungen in elektronisch hochkorrelierten Metallen', Technische Hochschule Darmstadt, December 1996.
  Arno Hiess also received one of the 'Young Scientists' awards at the European Neutron Scattering Conference in Interlaken, Switzerland, October 1996, for his work.
- *Philippe Berton*, 'Analyse de la périphérie du combustible à fort taux de combustion: étude du monouranate de césium Cs_2UO_4', Université de Lyon, December 1996.

We also welcomed two consultants from Greece and Germany.

One 'Stagiaire Visitor' came from Japan. He was supported by his organisation of origin.

Four scientists from Russia stayed at the Institute: two of them coming from the Bochvar All-Russia Research Institute of Inorganic Materials, Moscow, in the frame of a cooperation with DG I, and two in the frame of a collaboration with the High Energy Density Research Center of the Russian Academy of Sciences, Moscow, and with the State Scientific Institute of Physics and Power Engineering, Obninsk, respectively.

13. Quality Management

During 1996 the Institute management decided to aim, in addition to certification according to ISO 9001, also for accreditation according to EN 45001. Accreditation distinguishes the holder as a recognized and competent measurement and test laboratory. The quality management system was further developed for customer related projects. Apart from the *quality representative* and the *quality manager* of the Institute, there were *quality mediators* nominated for each unit, which assist in implementing the system in their unit. For the *quality mediators* a two days training course was organized.

The quality manual 1 (in German language) was distributed during August to all collaborators of the Institute. A translation into English is in preparation. For the implementation of the manual into practice, a seminar was organized both in German and English, instructing the Institute's staff in the implications of the quality management system for everyday work.

In a first step the setting up of an inventory of the present state of the Institute's capacities and its project management was initiated. For immediate demands from customers (e.g. OSL-project) procedural and working instructions have been prepared.

A first QM-review meeting was convened in November to determine the state of setting up the actual inventory. In addition, two customer audits and three internal audits were carried out.

In 1997 the implementation of the QM-system reaches the phase of acquiring the target status according to the ISO and EN requirements. The certification and accreditation of some areas is planned for beginning of 1998.

Annexes

ANNEX I

Publications 1996

1. Conferences

Conference papers published in 1996 in journals or special conference proceedings volumes may appear also under paragraph 2 (Books and Periodicals)

1996 Winter Conference on Plasma Spectrometry
January 8-13, 1996, Fort Lauderdale, FL (USA)

Barrero Moreno, J.M., Betti, M., Garcia Alonso, J.L.
Determination of Trace Levels of Neptunium and Plutonium in the Presence of High Concentrations of Uranium by Ion Chromatography Inductively Coupled Plasma Mass Spectrometry
Proceedings Journal of Analytical Atomic Spectrometry

Betti, M.
Use of a Direct Current Glow Discharge Mass Spectrometer for the Chemical Characterization of Samples of Nuclear Concern
Proceedings Journal of Analytical Atomic Spectrometry 11 no. 9 (1996) 855-860

Betti, M., Lagerwaard, A.
Studies on Single Particles by Glow Discharge Mass Spectrometry

International Waste Management Conference (WM '96)
February 25-29, 1996, Tucson, AZ (USA)

Matzke, Hj., van Geel, J.
The Plutonium Issue: Materials Science Aspects of Going MOX and Alternative Solutions
Proceedings Radwaste Magazine 3 no. 2 (1996) 71-76

International Solvent Extraction Conference ISEC '96
March 19-23, 1996, Melbourne (Australia)

Song, C.L., Glatz, J.P., Koch, L., Bokelund, H., He, X.
A Mathematical Model for the Extraction of Am from HLLW by 30% TRPO and its Experimental Verification
Proceedings ISEC '96, eds. D.C. Shallcross, R. Paimin, L.M. Prvcic, Vol 1 (1996) 1355-1360

Symposium on the Centennial of the Discovery of Radioactivity
March 24-28, 1996, New Orleans, LA (USA)

Fuger, J.
One Third of a Century of Research at the Institute for Transuranium Elements

IAEA Research Coordination Meeting on Fuel Modelling at Extended Burnup (FUMEX)
April 1-5, 1996, Bombay (India)

Lassmann, K., Lösönen, P., van de Laar, J.
Overview of the TRANSURANUS Code-Version V1M1Y96

Lassmann, K., Lösönen, P.
The Thermal Analysis of the TRANSURANUS Code

Lassmann, K.
The Mechanical Analysis of the TRANSURANUS Code

Lassmann, K.
The Treatment of Fission Gas Release in the TRANSURANUS Code

Lassmann, K., Walker, C.T.
The TRANSURANUS Burnup Model TUBRNP

Lassmann, K.
Probabilistic Fuel Rod Analyses

26. Journées des Actinides
April 10-14, 1996, Szklarska Poreba (Poland)

Apostolidis, C., Kanellakopulos, B., Rebizant, J.
Hydrotris(1-pyrazolyl)borates of Trivalent Uranium, Neptunium and Plutonium

Brooks, M.S.S.
Calculated Equation of State and Magnetic Equation of State of UGa_3

Gomez Marin, E., Fournier, J.M., Spirlet, J.C., Rebizant, J.
High-Temperature Resistivity Measurements on Plutonium Monochalcogenides

Hiess, A., Langridge, S., Huth, M., Gibbs, Doon, Lander, G.H.
Resonant X-ray Scattering from a thin film of UPd_2Al_3

Ichas, V., Braithwaite, D., Spirlet, J.C., Rebizant, J., Benedict, U.
Np Monopnictides under High Pressure- Status Report

Higgins, E.J., Rebizant, J., Stalios, A.D., Walker, C.T., Wastin, F., Hynes, M.J.
Investigation of Actinide An_4T7X_3 phase

Pereira, L.C.K., Paixao, J.A., Bourdarot, F., Estrela, P., Rebizant, J., Godinho, M., Almeida, M., Spirlet, J.C.
Single-Crystal Magnetization and Neutron-Scattering Investigation of the Magnetic Structure of U_2Rh_2Sn

Pereira, L.C.J., Wastin, F., Kanellakopoulos, B., Rebizant, J., Spirlet, J.C.
Physical Properties of Transuranium 2:2:1 Intermetallic Compounds

Wastin, F., Bednarczyk, E., Rebizant, J., Sanchez, J.P.
Electrical Resistivity of $Np_4Ru_7Ge_6$

Watson, G., Gibbs, Doon, Lander, G.H., Gaulin, B.D., Matzke, Hj., Ellis, W.P.
X-ray Experiments on UO_2 Surfaces

International Workshop "Glass as a Waste Form and Vitrification Technology"
May 13-15, 1996, Washington, DC (USA)

Matzke, Hj.
Mechanical Properties of the Waste Form Glass

2nd Regional Workshop of the European Microbeam Analysis Soc. "Electron Probe Microanalysis of Materials Today"
May 19-22, 1996, Balatonfüred (Hungary)

Walker, C.T.
Electron Probe Microanalysis of Irradiated Nuclear Fuel

The Society of Nuclear Medicine 43rd Annual Meeting
June 3-6, 1996, Denver, CO (USA)

Faivre-Chauvet, A., Apostolidis, C., Mishra, A.K., Molinet, R., Thedrez, P., Wijdenes, J., Bataille, R., Chatal, J.F.
Optimal Conditions for Labeling Immunoconjugate (B-B4-CITC-DTPA) with Bismuth-213

2nd International Conference on Accelerator-Driven Transmutation Technologies and Applications
June 3-7, 1996, Kalmar (Sweden)

Magill, J., Peerani, P., van Geel, J., Landgren, A., Liljenzin, J.O.
Inherent Limitations in Toxicity Reduction Associated with Fast Energy Amplifiers

ENS Class 1 Topical Meeting on Research Facilities for the Future of Nuclear Energy
June 4-6, 1996, Brussels (Belgium)

Coquerelle, M.
Facilities for Post-Irradiation Analyses of High Burn-up Fuels
Proceedings of the Conference ENS

E-MRS Meeting
June 4-7, 1996, Strasbourg (France)

Wiss, T., Matzke, Hj., Trautmann, C., Toulemonde, M., Klaumünzer, S.
Radiation Damage in UO_2 by Swift Heavy Ions
Proceedings Nuclear Instruments and Methods in Physics Research B

International Topical Meeting on Radioactive Waste
June 9-12, 1996, Stockholm (Sweden)

Nicolaou, G., Abbas, K., Koch, L.
Simultaneous Passive Neutron Interrogation and Gamma Spectroscopy on Spent Nuclear Fuel
Proceedings TOPSEAL '96 Vol. 2 (1996) 79-82

Nuclear Material Accountancy and Control Training Course
July 1-5, 1996, Obninsk (Russia)

Mayer, K.
Verification Sample Analysis Activities

21. Rare-Earth Conference
July 7-12, 1996, Duluth, MN (USA)

Lander, G.H.
Studies of Magnetism with Photons
Proceedings J. Alloys and Compounds

SCES 96 Strongly Correlated Electron Conference
August 19-22, 1996, Zürich (Switzerland)

Hiess, A., Havela, L., Prokeš, K., Eccleston, R.S., Lander, G.H.
Magnetic Response Function in URhAl
Proceedings Phys. B Condens. Matter

Hiess, A., Zobkalo, I., Bonnet, M., Schweizer, J., Leliévre-Berna, E., Tasset, F., Isikawa, Y., Lander, G.H.
On the Magnetisation Density of CeNiSn
Proceedings Physica B

Zwirner, S., Waerenborgh, J.C., Wastin, F., Rebizant, J., Spirlet, J.C., Potzel, W., Kalvius, G.M.
Anisotropic Magnetic Coupling in $Np_xU_{1-x}Pd_2Al_3$, $Np_xU_{1-x}RU_2Si_2$
Proceedings Physica B

9. International Symposium Thermodynamic Nuclear Material
14. IUPAC Conference on Chemical Thermodynamics
August 25-30, 1996, Osaka (Japan)

Lucuta, P.G., Matzke, Hj., Cox, D.S.
Thermodynamic Behavior of SIMFUEL – Simulated High Burnup UO_2 Based Fuel

Matzke, Hj.
Polygonization and High Burnup Structure in Nuclear Fuels

Matzke, Hj., Lucuta, P.G., Verrall, R.A., Henderson, J.
Specific Heat of UO_2-Based SIMFUEL
Proceedings J. Nucl. Mat.

Merli, L., Lambert, B., Fuger, J.
Thermochemistry of Lanthanum, Neodymium, Samarium and Americium Trihydroxides and their Relation to the Corresponding Hydroxycarbonates
Proceedings J. Nucl. Mat.

Symposium on Magnetism in Metals
August 26-29, 1996, Copenhagen (Denmark)

Brooks, M.S.S.
Conduction Electrons in Magnetic Metals
Proceedings Royal Danish Academy of Science and Letters

Lander, G.H.
Magnetism in the Actinides
Proceedings Royal Danish Academy of Science and Letters

21. Annual Symposium of the Uranium Institute
September 4-6, 1996, London (United Kingdom)

van Geel, J., Matzke, Hj., Magill, J.
Bury or Burn Plutonium - The Next Nuclear Challenge
Proceedings of the Twenty-First Annual Symposium of the Uranium Institute
Uranium and Nuclear Energy: 1996, pp. 100-109; ISBN 0946777357

4th International Conference on Nuclear and Radiochemistry
September 8-13, 1996 St. Malo (France)

Fuger, J.
Thermodynamics of Inorganic Actinide Compounds Relevant to the Waste Disposal Problematics
NRC4 Extended Abstracts, eds. F. David, J.C. Krupa (1996) paper C-K

Glatz, J.P., Apostolidis, C., Molinet, R., Nicholl, A., Pagliosa, G., Römer, K., Bokelund, H., Koch, L.
Reprocessing of Irradiated Transmutation Fuel Targets
NRC4 Extended Abstracts, eds. F. David, J.C. Krupa (1996) paper G-O3

Jozefowicz, L.C., Schneider, H.G., Blohm-Hieber, U., Kloeckner, W.F., Koch, L.
Concept for an On Site Laboratory Facility to Analyse Samples at a Nuclear Reprocessing Plant
NRC4 Extended Abstracts, eds. F. David, J.C. Krupa (1996) paper G-P13

Koch, L.
Chemistry of the Nuclear Fuel Cycle
NRC4 Extended Abstracts eds. F. David, J.C. Krupa (1996) paper G-K

Molinet, R., Janssens, W., Apostolidis, C., Koch, L.
Production of ^{225}Ac and ^{213}Bi for Alpha-Therapy
NRC4 Extended Abstracts, eds. F. David, J.C. Krupa (1996) paper H-P2

Wastin, F., Pereira, L.C.J., Rebizant, J., Lander, G.H., Sanchez, J.P.
Transuranium Ternary Intermetallic Compounds: Review
NRC4 Extend Abstracts, eds. F. David, J.C. Krupa (1996) paper C-O8

Wellum, R., Kühn, H., Schneider, H.G., Rasmussen, G., Koch, L.
Age Determinations in Nuclear Forensic Analysis
NRC4 Extended Abstracts, eds. F. David, J.C. Krupa (1996) paper B-O2

European Aerosol Conference 1996
September 9-12, 1996, Delft (The Netherlands)

Capéran, Ph., Somers, J., Richter, K.
Interaction Between Different Sized Particles During Acoustic Agglomeration of Soil Droplets
J. Aerosol Sci. Vol. 27 Suppl. 1 (1996) S413-S414

TEMPMEKO '96
September 10-12, 1996, Turin (ITALY)

Halton, D., Heinz, W., Musella, M., Selfslag, R., Ronchi, C., Sheindlin, M.
Development of New Laser-Pulse Techniques for Thermophysical Properties Measurements of Refractory Ceramics

4th NEA International Information Exchange Meeting
September 11-13, 1996, Mito (Japan)

Babelot, J.F., Conrad, R., Gruppelaar, H., Mühling, G., Prunier, C., Salvatores, M., Vambenepe, G.
EFTTRA Irradiation Experiments for the Development of Fuels and Targets for Transmutation
Proceedings 4th NEA P&T Int. Information Exchange (OECD/NEA)

14. European Conference on Thermophysical Properties
September 15-18, 1996, Lyon (France)

Halton, D., Heinz, W., Selfslag, R., Musella, M., Ronchi, C., Sheindlin, M.
Progress in Laser-Flash Applications for Thermophysical Measurements

Network Conference "Ab initio calculation of complex processes in materials"
September 17-21, 1996, Schwäbisch Gmünd (Germany)

Brooks, M.S.S.
Theory of Interatomic Exchange Interactions in Transition Metal Intermetallic Compounds

Gasche, T., Brooks, M.S.S., Johansson, B.
Exchange Interactions in Gd and Cm: Conduction Electron Polarization and Ordering Temperature under Pressure

IAEA Regional Training Course on the Fuel Database
September 25-27, 1996 Halden (Norway)

Lassmann, K.
Adaption of the TRANSURANUS Code to WWER Fuel: Progress Made Since the First TRANSURANUS Training Course

Lösönen, P.
Verification of TRANSURANUS against Temperature Data from WWER Type Test Fuel Rods from SOFIT Experiments

1st European Conference on Neutron Scattering ECNS'96
October 8-11, 1996, Interlaken (Switzerland)

Hiess, A., Bonnet, M., Burlet, P., Ressouche, E., Sanchez, J.P., Boudarot, F., Waerenborgh, J.C., Zwirner, S., Wastin, F., Rebizant, J., Lander, G.H., Suard E., Smith J.L.
Magnetic Structures of $NpBe_{13}$ and $NpPd_2A_{13}$
Proceedings Physica B

Hiess, A., Boucherle, J.X., Givord, F., Schweizer, J. Lelièvre-Berna, E., Tasset, F., Gillon, B., Canfield, P.C.
Magnetization Density in the Intermediate Valence Compound $YbAl_3$
Proceedings Physica B

Mannix, D., Stirling, W.G., Brown, S., Haycook, P., Lander, G.H., Bucknall, D., Felcher, G.P., Tang, C.C., Plasket, T.
Polarised Neutron Reflectivity Measurements from a [UAs(80Å)/Co(20 Å)]*12 Multilayer
Proceedings Physica B

Marmeggi, J.C., Lander, G.H., Currat, R., Zeyen, C.M.E.
Soft Phonons and the Charge-Density Wave Transition in Alpha-Uranium
Proceedings Physica B

Paixao, J.A., Langridge, S., Sorensen, S. Aa., Lebech, B., Conçalves, A.P., Lander, G.H., Brown, P.J., Burlet, P., Talik, E.
Unusual Sublattice Interactions in Compounds with the $ThMn_{12}$ Structure
Proceedings Physica B

Paolasini, L., Lander, G.H., Shapiro, S.M., Caciuffo, R., Lebech, B., Regnault, L.P., Roessli, B., Fournier, J.M.
Enhanced Exchange in the itinerant Ferromagnet UFe_2

Extended PHARE FERONIA Meeting
October 14-16, 1996 Sofia (Bulgaria)

Lassmann, K.
Status of the PHARE FERONIA Project and Difficulties Encountered

10. Camus-Treffen, Cameca France/Geoforschungszentrum Potsdam
October 16-18, 1996, Potsdam (Germany)

Walker, C.T.
Electron Probe Microanalysis of Irradiated Nuclear Fuel

International Conference on Radioisotope and Radiation Application in Industry
October 20-23, 1996, Berlin (Germany)

Koch, L., Apostolidis, C., Molinet, R., Janssens, W., van Geel, J.
^{213}Bi for Alpha-Immuno-Cancer Therapy
Proceedings Nucleonica

Koch, L.
Nuclear Forensics in Enviromental Protection

10. Pacific Basin Nuclear Conference
October 20-25, 1996, Kobe (Japan)

Sasahara, A., Matsumura, T., Nicolaou, G., Glatz, J.P., Toscano, E., Walker, C.T.
Post Irradiation Examinations and Computational Analysis of High Burnup UOX and MOX Spent Fuels for Interim Dry Storage
Proceedings of the Conference

IAEA Technical Committee Meeting on Advances in Pellet Technology for Improved Performance at High Burnup
October 28-November 1, 1996 Tokyo (Japan)

Baron, D., Leclercq, S., Spino, J., Taheri, S.
Development of a Microindentation Technique to Determining the Fuel Mechanical Behaviour at High Burnup
Proceedings of the Conference

Spino, J., Coquerelle, M., Baron, D.
Microstructure and Fracture Toughness Characterization of Irradiated PWR Fuels in the Burnup Range 40-67 GWd/tM
Proceedings of the Conference

Spino, J.
State of the Technology Review on Fission Gas Release at High Burnups
Proceedings of the Conference

Tag der Seltenen Erden
December 5-7, 1996, Magdeburg (Germany)

Apostolidis, C., Kanellakopulos, B., Molinet, R., Rebizant, J., Dornberger, D.
Röntgenographische Einkristalluntersuchungen an Hydro-tris(1-pyrazolyl)boraten der dreiwertigen Lanthanoide: Von der Struktur zur Separation

Kanellakopulos, B., Apostolidis, C., Rebizant, J.
Systematische Untersuchungen an 1:1- und 1:2-Addukten von Lanthanoid-tris(cyclopentadienyl)-Verbindungen mit aliphatischen Nitrilen (Acetonitril, Propionitril)

2. Books and Periodicals

(including publications which had been submitted or presented at conferences in 1995 and which appeared in print in 1996)

Abbas, K., Nicolaou, G., Pellottiero, D., Schwalbach, P., Koch, L.
Gamma Spectrometry of Spent Nuclear Fuel using a Miniature CdTe Detector
Nucl. Instrum. Methods Phys. Res. Sect. A 376 (1996) 248-253

Abbas, K., Nicolaou, G., Schwalbach, P., Koch, L.
Gamma-Ray Spectrometry on Nuclear Material Using a CdZnTe Detector
Appl. Radiat. Isot. 47 no.8 (1996) 755-760

Abbas, K., Nicolaou, G.
In Situ Gamma Spectroscopy of Spent Nuclear Fuel Using a CdTe Detector
Nucl. Instrum. Methods 383, Iss 2-3 (1996) 601-604

Abraham, C., Benedict, U., Spirlet, J.C.
Optical Reflectivity of Neptunium and Plutonium Monochalcogenides under High Pressure
Physica B Condens. Matter 222 (1996) 52-60

Barrero Moreno, J.M., Garcia Alonso, J.I., Arbore, Ph., Nicolaou, G., Koch, L.
Characterization of Spent Nuclear Fuels by Ion Chromatography-Inductively Coupled Plasma Mass Spectrometry
J. Anal. At. Spectrom. 11 (1996) 929-935

Betti, M., Giannarelli, St., Onor, M.
Investigation of the Behaviour of Tellurium (IV) and Selenium (IV) in Ion-Exchange Chromatography
J. Chromatogr. (submitted)

Blank, H.
Hägg's Rule and Fast Solute Diffusion in Cubic Transition-Metal Phases
Philos. Mag. B 73 no. 5 (1996) 833-844

Blank, H.
Fast Diffusion in Dilute Binary Alloys and its Analysis Based on Hägg's Rule
J. Nucl. Mater. (submitted)

Bonfait, G., Godinho, M., Estrela, P., Goncalves, A.P., Almeida, M., Spirlet, J.C.
Giant-magnetoresistance Anomaly Associated with a Magnetization Process in UFe_4Al_8
Phys. Rev. B Condens. Matter 53 no. 2 (1996) R480-R483

Bottomley, P.D.W., Wegen, D.H., Coquerelle, M.
Construction of an Electrode for Irradiated UO_2 Fuel and Preliminary Results concerning its Use in Aqueous Solutions
J. Nucl. Mater. 238 no. 1 (1996) 23-37

Brooks, M.S.S., Johansson, B.
Spin-Orbit Interaction, Orbital Magnetism and Spectroscopic Properties
"Spin-Orbit Influenced Spectroscopies of Magnetic Solids" (eds. H. Ebert, G. Schütz) Springer-Verlag (1996) 211-228; ISBN 3-54060-843-5

Capone, F., Hiernaut, J.P., Martellenghi, M., Ronchi, C.
Mass Spectrometric Measurements of Fission Product Effusion from Irradiated Light Water Reactor Fuel
Nucl. Sci. Eng. 124 no. 3 (1996) 436-454

Cornelius, A.L., Schilling, J.S., Vogt, O., Mattenberger, K., Benedict, U.
High-presssure Susceptibility Studies on the Ferromagnetic
Uranium Monochalcogenides US, USe and UTe
J. Magn. Magn. Mater. 161 (1996) 169-176

De Ridder, D.J.A., Rebizant, J., Apostolidis, C., Kanellakopulos, B., Dornberger, E.
Bis(cyclooctatetraenyl)neptunium(IV)
Acta Crystallogr. C 52 Part 3 (1996) 597-600

De Ridder, D.J.A., Apostolidis, C., Rebizant, J., Kanellakopulos, B., Maier, R.
Tris(eta(5)-cyclopentadienyl)phenolatoneptunium(IV)
Acta Crystallogr. C52 (1996) 1436-1438

Delin, A., Oppeneer, P.M., Brooks, M.S.S., Kraft, Th., Wills, J.M., Johansson, B., Eriksson, O.
Optical Evidence of 4f-band Formation in CeN
Phys. Rev. Lett. (submitted)

Delin, A., Eriksson, O., Ahuja, R., Johansson, B., Brooks, M.S.S., Gasche, T., Auluck, S., Wills, J.M.
Optical Properties of the Group-IVB Refractory Metal Compounds
Phys. Rev. B Condens. Matter 54 no. 3 (1996) 1673-1681

Garcia-Alonso, J.I., Thoby, D., Giovannone, B., Koch, L.
Analysis of Long-Lived Radionuclides by ICP-MS
J. Radioanal. Nucl. Chem. 203 no. 1 (1996) 19-29

Gasche, T., Brooks, M.S.S., Johansson, B.
Calculated Magneto-optical Kerr Effect in Fe, Co, and Ni
Phys. Rev. B Condens. Matter 53 no. 1 (1996) 296-301

Gasche, T., Brooks, M.S.S., Johansson, B.
Calculated Optical Properties of Thorium, Protactinium, and Uranium Metals
Phys. Rev. B Condens. Matter 54 no. 4 (1996) 2446-2452

Glatz, J.P., Garcia Alonso, J.I., Kameyama, T., Koch, L., Pagliosa, G., Tsukada, T., Yokoyama, H.
Dissolution Behavior of Highly Burnt Fuel
J. Radioanal. Nucl. Chem. 203 no. 1 (1996) 11-18

Gomez Marin, E., Fournier, J.M., Spirlet, J.C., Wastin, F.
High-Temperature Resistivity Measurement Equipment for Actinide Metals and Compounds
J. Phys. Colloq. (submitted)

Gouder, T.
Electronic Structure of Uranium Overlayers on Magnesium and Aluminium
Surf. Sci. (submitted)

Hiess, A.,Bonnet, M., Burlet, P., Ressouche, E., Sanchez, J.P., Waerenborgh, J.C., Zwirner, S., Wastin, F., Rebizant, J., Lander, G.H., Smith, J.L.
On the Magnetic Interactions in Metal-Be_{13} Compounds
Phys. Rev. Lett. 77 no. 18 (1996) 3917-3920

Jeandey, C., Sanchez, J.P., Oddou, J.L., Rebizant, J., Spirlet, J.C., Wastin, F.
Mössbauer Study of the Intermetallic Compound $Np_4Ru_7Ge_6$
J. Phys. B Condens. Matter 8 (1996) 4259-4268

Koch, L.
Transuranium Elements
Ullmann's Encyclopedia of Industrial Chemistry Vol. A27 (1996) 167-177

Konings, R.J.M., Franken, W.M.P., Conrad, R., Gueugnon, J.F., Spirlet, J.C.
Transmutation of Technetium and Iodine – Irradiation Tests in the Frame of the EFTTRA Cooperation
Nucl. Technol. (submitted)

Langridge, S., Lander, G.H., Nuttall, W.J., Stirling, W.G., Bernhoeft, N., Stunault, A., Vettier, C., Grübel, G., Sutter,C., Mattenberger, K., Vogt, O.
Separation of the Spin and Orbital Moment in Antiferromagnetic UAs
Phys. Rev. B Condens. Matter (submitted)

Le Bihan, T., Heathman, S., Darracq, S., Abraham, H.C., Winand, J.M., Benedict, U
High Pressure X-ray Diffraction Studies of UX_3 (X = Al, Si, Ga, Ge, In, Sn)
High Temp. – High Pressures 27/28 (1996) 157-162

Lucuta, P.G., Matzke, Hj., Hastings, I.J.
A Pragmatic Approach to Modelling Thermal Conductivity of Irradiated UO_2 Fuel: Review and Recommendations
J. Nucl. Mater. 232 (1996) 166-180

Matzke, Hj., Wang, L.M.
High-Resolution Transmission Electron Microscopy of Ion Irradiated Uranium Oxide
J. Nucl. Mater. 231 (1996) 155-158

Matzke, Hj., Rigato, V.
Hydrogen Profiles at the Surface of Leached Synroc
J. Nucl. Mater. 231 no. 3 (1996) 260-263

Matzke, Hj.
Analysis of the Structure of Layers on UO_2 leached in H_2O
J. Nucl. Mater. 238 no. 1 (1996) 58-63

Matzke, Hj., Wiss, T.
TEM Studies on Track Formation in UO_2 Induced by Swift Heavy Ions
Annual Report 1995, GSI Darmstadt (1996) 126

Matzke, Hj.,Wiss, T.
Simulation of Fission Damage in UO_2 and Study of the Behavior of Xe in UO_2
Hahn-Meitner Institut, Annual Report 1995 (1996) 94

Morita, Y., Glatz, J.P., Kubota, M., Koch, L., Pagliosa, G., Roemer, K., Nicholl, A.
Actinide partitioning from HLW in a Continuous DIDPA Extraction Process by Means of Centrifugal Extractors
Solvent Extr. Ion Exch. 14 no. 3 (1996) 385-400

Nakotte, N., Purwanto, A., Robinson, R.A., Prokeš, K., de Châtel, P.F. et al, Pereira, L.C.J., Seret, A., Rebizant, J., Spirlet, J.C., Trouw, F.
Hybridization Effects in U_2T_2X Compounds: Magnetic Structures of U_2Rh_2Sn and U_2Ni_2In
Phys. Rev. B Condens. Matter 53 no. 6 (1996) 3263-3271

Nicoll, S., Matzke, Hj., Grimes, R.W., Catlow, C.R.A.
The Behaviour of Single Atoms of Mo in Urania
J. Nucl. Mater. (submitted)

Oppeneer, P.M., Brooks, M.S.S., Antonov, V.N., Kraft, T., Eschrig, H.
Band-theoretical Description of the Magneto-optical Spectra of UAsSe
Phys. Rev. B Condens. Matter 53 (1996) R10437-R10440

Paolasini, L., Lander, G.H., Shapiro, S.M., Caciuffo, R., Lebech, B., Regnault. L.P., Roessli, B., Fournier, J.M.
Enhanced Exchange in the Itinerant Ferromagnet UFe_2
Europhys. Lett. 34 (6) (1996) 459-464

Paolasini, L., Lander, G.H., Shapiro, S.M., Caciuffo, R., Lebech, B., Regnault, L.P., Roessli, B., Fournier, J.M.
Magnetic Excitations in the Itinerant Ferromagnet UFe_2
Phys. Rev. B Condens. Matter 54 no. 10 (1996) 7222-7232

Pereira, L.C.J., Paixao, J.A., Estrela, P., Godinho, M., Boudarot, F., Bonnet, M., Rebizant, J., Spirlet, J.C.
Almeida, M.
Single-Crystal Magnetization and Neutron-Scattering Investigation of the Magnetic Structure of U_2Rh_2Sn
J. Phys. B Condens. Matter 8 (1996) 11167-11179

Perry, S.C., Nuttall, W.J., Stirling, W.G., Lander, G.H., Vogt, O.
X-ray Scattering Study of the Two Magnetic Correlation Lengths in Uranium Antimonide
Phys. Rev. B Condens. Matter 54 no. 21 (1996) 15234-15237

Ray, I.L.F., Matzke, Hj., Thiele, H.A., Kinoshita, M.
An Electron Microscopy Study of the RIM Structure of a UO_2 Fuel with a high Burnup of 7.9% FIMA
J. Nucl. Mater. (submitted)

Ronchi, C., Hiernaut, J.P.
Experimental Measurement of Pre-Melting and Melting of Thorium Dioxide
J. Alloys Comp. 240 (1996) 179-185

Rondinella, V.V., Matzke, Hj.
Leaching of SIMFUEL in Simulated Granitic Water; Comparison to Results in Demineralized Water
J. Nucl. Mater. 238 no. 1 (1996) 44-57

Sato, N., Aso, N., Hirota, K., Komatsubuara, T., Endoh, Y., Shapiro, S.M., Lander, G.H., Kakurai, K.
Anisotropy and Two Length Scales in the Magnetic Critical Scattering in the Heavy-Fermion Superconductor UPd_2Al_3
Phys. Rev. B Condens. Matter 53 no. 21 (1996) 14043-14046

Severin, L., Brooks, M.S.S., Johansson, B.
Relationship between the Coulomb Integral U an the Stoner Parameter I – Reply
Phys. Rev. Lett. 76 no. 18 (1996) 3466-3467

Spino, J., Vennix, C., Coquerelle, M.
Detailed Characterisation of the Rim Microstructure in PWR Fuels in the Burn-up Range 40-67 GWd/tM.
J. Nucl. Mater. 231 no. 3 (1996) 179-190

Spirlet, M.R., Rebizant, J., Apostolidis, C., Dornberger, E., Kanellakopulos, B., Powietzka, B.
Oxo-Bridged Bimetallic Organouranium Complexes: The Crystal Structure of μ-Oxo-Bis Tris(Cyclopentadienyl) Uranium(IV)]
Polyhedron 15 (1996) 1503-1508

Turos, A., Falcone, R., Drigo, A., Sambo, A., Nowicki, L., Madi, N., Jagielsi, J., Matzke, Hj.
Structural Transformations in Leached Uranium Dioxide
Nucl. Instrum. Methods Phys. Res. B 118 (1996) 659-662

Vargoz, E., Link, P., Jaccard, D., Le Bihan, T., Heathman, S.
Is $CeCu_2$ a Pressure-Induced Heavy-Fermion Superconductor?
Phys. Rev. B Condens. Matter (submitted)

Walker, C.T., Goll, W., Matsumura, T.
Effect of Inhomogeneity on the Level of Fission Gas and Caesium Release from OCOM MOX Fuel during Irradiation
J. Nucl. Mater. 228 (1996) 8-17

Walker, C.T., Bagger, C., Mogensen, M.
Observations on the Release of Caesium from UO_2 Fuel
J. Nucl. Mater. 240 (1996) 32-42

Walker, C.T., Goll, W., Matsumura, T.
Further Observations on OCOM MOX Fuel: Microstructure in the Vicinity of the Pellet Rim and Fuel-Cladding Interaction
J. Nucl. Mater. (submitted)

Watson, G.M., Gaulin, B.D., Gibbs, Doon, Thurston, T.R., Simpson, P.J., Shapiro, S.M., Lander, G.H., Matzke, Hj., Wang, S., Dudley, M.
Origin of the Second Length Scale Found Above TN in UO_2
Phys. Rev. B Condens. Matter 53 (1996) 686-698

Watson, G.M., Gibbs, Doon, Lander, G.H., Gaulin, B.D., Berman, L.E., Matzke, Hj., Ellis, W.
X-Ray Scattering Study of the Magnetic Structure near the (001) Surface of UO_2
Phys. Rev. Lett. 77 no. 4 (1996) 751-754

Zwirner, S., Ichas, V., Braithwaite, D., Waerenborgh, J.C., Heathman, S., Potzel, W., Kalvius, G.M., Spirlet, J.C., Rebizant, J.
Magnetic Properties of $NpGa_3$ at High Pressures
Phys. Rev. B Condens. Matter 54 no. 17 (1996) 12283-12293

3. Reports

Schenkel, R., Richter, J., Pel, D., Wellum, R. (eds.)
Annual Report 1995 – Institute for Transuranium Elements
EUR 16368 EN (1996)

Casalta, S.
Etude des propriétés du système Am-O en vue de la transmutation de l'americium 241 en réacteur à neutrons rapides
EUR 16465 FR (1996)

Babelot, J.F., Gueugnon, J.F., McGinley, J., Richter, K., Spirlet, J.C.
Fabrication de 3 aiguilles Techr étium pour irradiation dans Phénix - Capsule ANTICORP 1
K0296188 (1996)

Fuchs, C., Fourcaudot, S., Richter, K.
MOX-Nuclear Reference Material for IRMM – Geel
K0296189 (1996)

Lösönen, P.
Verification of TRANSURANUS Code against Startup Data from SOFIT-1.1 Experiment (WWER-Fuel)
K0296185 (1996)

Ronchi, C.
Construction of the Equation of State of Uranium Dioxide up to the Critical Point
K0296186 (1996)

Richter, K., Gueugnon, J.F.
EFTTRA-T4 Irradiation Experiment in HFR Specification
K0296187 (1996)

4. Patents

Patent applications & proposals

Fuchs C., Fourcaudot S., Richter K., Somers J.
Verfahren zur Vorbereitung von Hochradioaktiven Stoffen für eine Transmutation und/oder Verbrennung
Deposition date/number: 19.03.96 / 88727, Reference: LU 2498

Capéran P., Somers J., Richter K.
Procédé et dispositif d'agglomération de particules dans un écoulement gazeux
Deposition date/number: 29.04.96 / 88751, Reference: LU 2497

Werner P., Spino J., Coquerelle M., Barn D.
Vorrichtung zur Materialprüfung mit einem Mikrostempel
Deposition date/number: 01.10.96 / 88821, Reference: LU 2512

Nicolaou G., Abbas K., Koch L.
A monitor for measuring both the gamma spectrum and neutrons emitted by spent nuclear fuel
Deposition date/number 15.10.96 / 96 116 506.5, Reference: EP 2515

Koch L., Janssens W., van Geel J., Dezeure F., Vanstraelen D.
Ex-corpare method for treating human blood cells
Deposition date/number: 15.11.96 / 96 118 377.9, Reference: EP 2519

Ronchi C., Cheindline M.
Multipurpose laser-flash startup for measurement of the thermal diffusivity under remote manipulation
Deposition date/number: 23.12.96 / 96 120 836.0; Reference: EP 2464

Nicolaou G., Abbas K., Koch L.
A monitor for the in situ gamma spectroscopy of irradiated nuclear fuel rods and assemblies using a CdTe detector
PP 2502 (19.03.96)

Annex II

Collaborations with External Organizations

ARGENTINA

CNEA Buenos Aires: Diffusion in solids (F. Dyment)

ARMENIA

Armenian Nuclear Regulatory Authority, Yerevan: TRANSURANUS fuel pin code development (A. Martirossian)

AUSTRIA

International Atomic Energy Agency (IAEA), Vienna: Evaluation and automation of techniques for safeguards analysis (K. Lessmon); *Safeguards Directorate:* Environmental analysis (K. Serena); *SAL:* EURATOM Support Programme (S. Deron); TRANSURANUS fuel pin code development (M. Samiei)

Technical University of Vienna: Resistivity of alloys and high-pressure effects (E. Gratz)

BELGIUM

Société Belge pour l'Industrie Nucléaire, Brussels: Post irradiation examinations (S. Pilate, M. van den Borck, M. Lippens, J. Basselier, D. Haas)

University of Leuven: Xe-implantation (H. Pattyn)

University of Liège: Single crystal growth, X-ray diffraction, and analysis (J.F. Desreux, L. Martinot, M.R. Spirlet)

BULGARIA

Committee on the Use of Atomic Energy for Peace, Sofia: TRANSURANUS fuel pin code development (P. Ardenska)

Institute of Nuclear Research and Nuclear Energy, Bulgarian Academy of Science, Sofia: Fuel rod modelling and performance, FERONIA (Y. Stamenov, S. Stefanova)

CANADA

AECL
Chalk River: Gas release, SIMFUEL production and property studies (I. Hastings, P. Lucuta, R. Verrall); Behaviour of Rb and Cs in SIMFUEL (W. Hocking)

CZECH REPUBLIC

Nuclear Research Institute Rez plc, Rez: TRANSURANUS fuel pin code development (F. Pazdera)

State Office for Nuclear Safety, Prague: TRANSURANUS fuel pin code development (P. Krs)

University of Prague: Magnetic and electrical measurements (V. Sechovsky, L. Havela); Gas release measurements (V. Balek)

DENMARK

Risø National Laboratory: Neutron scattering (B. Lebech)

Technical University Lyngby: High-pressure X-ray diffraction (L. Gerward)

University of Copenhagen: High pressure X-ray diffraction (J. Staun-Olsen)

FINLAND

VTT Nuclear Engineering Laboratory: TRANSURANUS fuel pin development (S. Kelppe)

FRANCE

Commissariat à l'Énergie Atomique (CEA)
CEA, Cadarache: Transmutation of actinides - irradiation experiments: DEC (J.L. Faugère, R. Ginier, Y. Guerin, C. Prunier, D. Warin); DER (A. Lanquille, J. Rouault); DRN (M. Salvatores); TRANSURANUS fuel pin development (Y. Guerin); PHEBUS PF programme, (B. Adroguer): post irradiation examinations (L. Codron, P. von der Hardt), Inert matrices (M. Beauvy)
CEA, Marcoule: Partitioning of actinides, DIAMEX process (C. Madic)
CEN, Grenoble: Neutron diffraction, magnetic studies, transport properties and Mössbauer studies (P. Burlet, J.P. Sanchez, B. Fåk, D. Braithwaite and F. Bourdarot)
CEN, Saclay: Neutron diffraction (J.M. Mignot, L. Paolasini); Post-irradiation examinations (J.I. Blanc, F. Couvreur)

CERCA, Romans: MTR fuel development (J.P. Durand, B. Lelievre)

CNRS
Lab. de Cristallographie, Grenoble: Crystallography of phase transitions (J.C. Marmeggi) Orsay: Basic studies on spent UO_2 fuel (J.C. Dran)

COGEMA
La Hague: On-site laboratory
Branche Combustible Nucléaire, Vélizy: Development of MOX fuels (Mme M. Trotabas)

Électricité de France (EDF)
Septen, Villeurbanne: Transmutation of actinides (M. Rome, G. Vambenepe), TRANSURANUS fuel pin code development (C. Bernaudat); RIM effect (M. Baron); Chemical and mechanical interactions fuel/cladding (thermal reactor) and determination of mechanical properties of irradiated UO_2 (M. Baron)

ESRF, Grenoble: Synchrotron studies on actinides (C. Vettier, G. Grübel)

FRAGEMA: Post-irradiation examinations (Blanpain, Van Scherp, Gentil)

FRAMATOME, Lyon: TRANSURANUS fuel pin code development (P. Blanpain)

ILL, Grenoble: Polarized neutron diffraction and neutron inelastic scattering (P.J. Brown, C. Zeyen, A. Hiess, N. Bernhoeft)

Institut National de la Santé et de la Recherche Médicale (INSERM), Nantes: (α-immunotherapy by Bi-213 (J. F. Chatal)

OECD Nuclear Energy Agency, AEN-NEA, Paris: Database on fuel performance (E. Sartori)

University of Grenoble: Transport measurements (J.M. Fournier)

GERMANY

Apparatebau Rothemühle, Wenden: Acoustic aerosol scavenging (W. Niggeschmidt, N. Seyfert)

Gesellschaft für Schwerionenforschung (GSI) Darmstadt: High energy ion implantation (C. Trautmann, J. Vetter)

Hahn-Meitner-Institut (HMI), Berlin: Ranges of ions in solids, B-profiles in leached glasses (D. Fink, J. Biersack); High-energy ion implantation (S. Klaumünzer)

Forschungzentrum Jülich GmbH (KFA)
Institut für Festkörperforschung: Electrical resistivity under pressure (J. Wittig)

Forschungszentrum Karlsruhe (FZK)
Institut für Kernphysik (IK-III): On-site laboratory training; K-edge densitometry (H. Ottmar, H. Eberle)
Institut für Neutronenphysik und Reaktortechnik (INR): Neutron collar development; Beryllium blanket modelling: ANFIBE-FUTURE (M. Dalle Donne)
Institut für Nukleare Festkörperphysik (INFP): Radiation damage studies, RBS analyses, channeling, ion implantation (O. Meyer, G. Linker)
Institut für Technische Chemie (ITC): Susceptibility and crystal preparation (B. Kanellakopulos)
Projekt Nukleare Sicherheitsforschung (PSF): Irradiation experiment CAPRA-TRABANT (G. Heusener, G. Mühling)

Max-Planck Research Group 'Theory of Complex and Correlated Systems', Dresden: Theory of the Kerr-effect (P.M. Oppeneer)

Siemens/KWU, Erlangen: Post-irradiation fuel rod examination (R. Manzel)

Technischer Überwachungsverein Bayern e.V., München: TRANSURANUS fuel pin code development (G. Sauer)

Technischer Überwachungsverein Hannover/Sachsen-Anhalt e.V.: TRANSURANUS fuel pin code development (H. Märtens, H. Bour)

Technischer Überwachungsverein Norddeutschland e.V., Hamburg: TRANSURANUS fuel pin code development (H. Schmidt)

Technischer Überwachungsverein Südwest e .V., Mannheim: TRANSURANUS fuel pin code development (I. Brestrich)

Technische Universität München: Mössbauer and (SR studies (M. Kalvius, W. Potzel, L. Asch)

Universität Stuttgart, IKE: Source term studies (H. Hocke);

VGB-Forschungsstiftung, Essen: Flue gas cleaning (J.P. Jacobs, H. Krüger)

HUNGARY

Atomic Energy Research Institute, Budapest: TRANSURANUS fuel pin code development (S. Elo)

Hungarian Atomic Energy Commission, Budapest: TRANSURANUS fuel pin code development (M. Gado)

ISRAEL

Technion, Haifa: Waste glass studies (Y. Eyal)

ITALY

Centro Ceramico Bologna: Leaching studies, Indentation techniques (L. Esposito)

Centro Legnaro/Padova: RBS, Ion implantation, H-analysis on leached waste matrices (G. Della Mea, V. Rigato)

University of Padova: Analysis of glass surfaces (P. Mazzoldi)

University of Pisa, Chemistry Department: Instrumental analytical techniques for traces analysis (R. Fuoco)

University of Trento: Indentation techniques (R. DalMaschio)

University of Ancona: Neutron and bulk magnetization studies (R. Caciuffo);

University of Aquila, Physics Department: Theory of optical properties (P. Monachesi)

JAPAN

Central Research Institute of Electricity Producing Industries (CRIEPI), Tokyo: Preparation and characterization of minor actinide alloys (T. Inoue); Dissolution studies on high burn-up fuel (T. Tsukada); Spent fuel characterization (S. Matsumura), Rim effect studies (M. Kinoshita)

JAERI, Tokai Mura: Radiation damage in oxide fuels (K. Fukuda); DIDPA actinide separation process (Y. Morita)

Tohoku University, Inst. for Materials Research, Sendai, Japan: Reduction of Np metal, solid states physics (Y. Shiokawa)

Tokohu University, Sendai, Japan: Studies of heavy fermium uranium compounds (N. Sato, T. Komatsubara, Y. Endoh)

NORWAY

OECD Halden Reactor Project: TRANSURANUS fuel pin development (W. Wiesenack)

THE NETHERLANDS

Alpha medical, St. Marten: Separation of alpha-emitting nuclides (M. Geerlings)

ECN, Petten: Transmutation of fission products (W. Franken, M. Gruppelaar)

Interfaculty Reactor Institute, Delft: Gas release (A. van Veen)

KEMA, Arnhem: Flue gas cleaning (R. Hunik, R. Tanke)

University of Amsterdam: Low temperature magnetization and resistivity (F. R. de Boer, J. Franse, E. Brück)

POLAND

Institute of Atomic Energy, Otwock/Swierk: TRANSURANUS fuel pin code development (M. Szuta)

Institute for Low Temperature and Structure Research, Warsaw: Bulk properties and neutron scattering (R. Troc, W. Suski)

Nuclear Institute, Warsaw: Channeling techniques, Radiation damage studies (A. Turos)

PORTUGAL

LNETI, Sacavem: Physical chemistry of actinides (A. Piros de Matos, M. Almeida)

University of Aveiro, Department of Physics: Kerr effect theory (T. Gasche)

University of Coimbra: Neutron and X-ray studies (J.A. Paixão)

ROMANIA

University for Nuclear Research, Pitetsi: TRANSURANUS fuel pin code development (G. Horhoianu)

RUSSIA

Academy of Sciences, IVTAN, Moscow: Equation of uranium dioxide (I. Iosiliewski); Studies on high-melting materials (Brykin, Bacharin)

High Energy Density Research Centre, Moscow: Critical Point of UO_2 (Lomonasov)

High Temperature Institute, Moscow: Thermodynamic database (Yungman)

Institute for Chemical Physics, Chernogslovka: Thermodynamics of liquid UO_2 (Gryaznov)

Nuclear Power Plant, Leningrad: PIE, non destructive examinations (V.C. Shevchenko)

Radium Khlopin Institute, St. Petersburg: Field testing of a robotized system for safeguards analysis (N. Shulyak)

Russian Research Centre „Kurchatov Institute" Institute of Nuclear Reactor WWER Division: TRANSURANUS fuel pin code development (E.P. Ryanzantzev)

State Scientific Centre of Russian Federation, A.A. Bochvar Institute of Inorganic Materials: TRANSURANUS fuel pin code development (Yu. K. Bibilashvili)

SLOVAK REPUBLIC

Nuclear Power Plant Research Institute, Trnava: TRANSURANUS fuel pin code development (M. Cvan)

SPAIN

CIEMAT, Madrid: TRANSURANUS fuel pin code development (J. Lopez Jimenez)

ENRESA: Waste management, leaching tests (J.A. Esteban-Hernandez)

Instituto de Acústica, Madrid: Acoustic aerosol scavenging (J.A. Gallego-Juarez)

SWEDEN

ABB ATOM AB Fuel Division, Västeras: TRANSURANUS fuel pin code development (A. Massih)

Infrasonik AB, Årsta: manufacture of infraphones (M. Olsson)

University of Uppsala: Solid state theory of actinides (B. Johansson, O. Eriksson)

SWITZERLAND

ETH, Zürich: Single crystal growth, magnetic, optical and transport properties, preparation of U and Th compounds (O. Vogt, P. Wachter, K. Mattenberger)

Paul-Scherrer-Institut, Villigen TRANSURANUS fuel pin code development (H.K. Kohl); Post-irradiation structural investigations by electron microscopy

UKRAINE

State Scientific and Technical Centre on Nuclear and Radiation Safety, Kyiv: TRANSURANUS fuel pin code development (M. Eremenko)

Shelter Center Chernobyl: Analysis of the Unit IV Sarcophagus (E.M. Pazukhin)

University of Odessa: Liquid state models (E. Yakub)

UNITED KINGDOM

Birkbeck College: neutron and magnetization studies (K. McEwen)

BNFL, Sellafield: On-site laboratory (R. Strong, J. Reed)

BFNL Eng. Department, Risley: Laboratory infrastructure (R. Johnson)

NNC, Risley: Engineering design support (B. Rowney)

NCC, Workington: QA consultancy (W.G. Smith)

University of Liverpool: X-ray and neutron scattering (W.G. Stirling)

University of Warwick: Compton scattering (M.J. Cooper); Equation of state of irradiated fuel (G. Hyland); Radiative properties at high temperatures (G. Hyland)

UNITED STATES OF AMERICA

Argonne National Laboratory: Neutron scattering and X-ray arbsorption spectroscopy (L. Soderholm, S. Kern)

Battelle Pacific Nothwest Laboratories, Richland: Modelling, transfer of the TRANSURANUS burnup model 'tubrnp' (D.D. Lanning)

Brookhaven National Laboratory: High-resolution and magnetic X-ray scattering (D. Gibbs, J. Axe, G. Watson)

Lawrence Livermore National Laboratory: Forensic nuclear analysis (S. Niemeyer); Photoemission and Synchrotron studies (C. Colmenares, J. Tobin)

Los Alamos National Laboratory: Materials preparation and photoemission (B. Cort, A.J. Arko); Radiation damage in ceramics (K. Sickafus)

Memorial Sloan Kettering Cancer Center, New York: (α-immunotherapy by Bi-213 (D.A. Scheinberg)

National Institute of Health, Bethesda: (α-immunotherapy by Bi-213 (Dr. O.A. Gansow)

Oak Ridge National Laboratory: Material preparation, high pressure X-ray and optical studies (R.G. Haire, J.R. Peterson)

University of New Mexico, Albuquerque: High resolution TEM, radiation damage (R. Ewing, L.M. Wang)

University of West-Virginia, Morgantown, W.- Virginia: Actinide theory (B.R. Cooper)

UZBEKISTAN

Physical Technical Institute, Tashkent: Radiative properties of UO_2 at high temperatures (T. Salikhov)

ANNEX III

Human and Financial Resources

Staff situation (12.96)

Total staff: 221
Statutory staff: 186

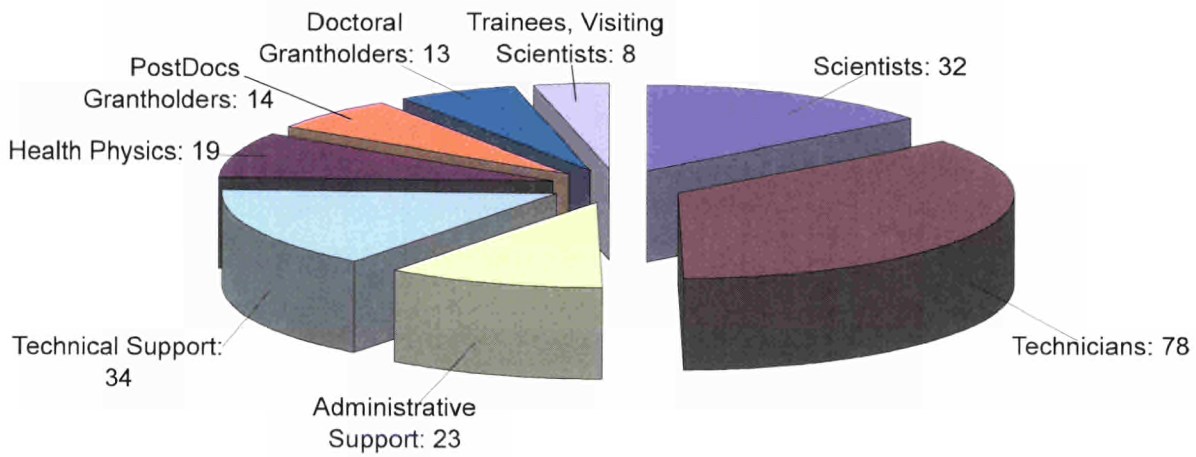

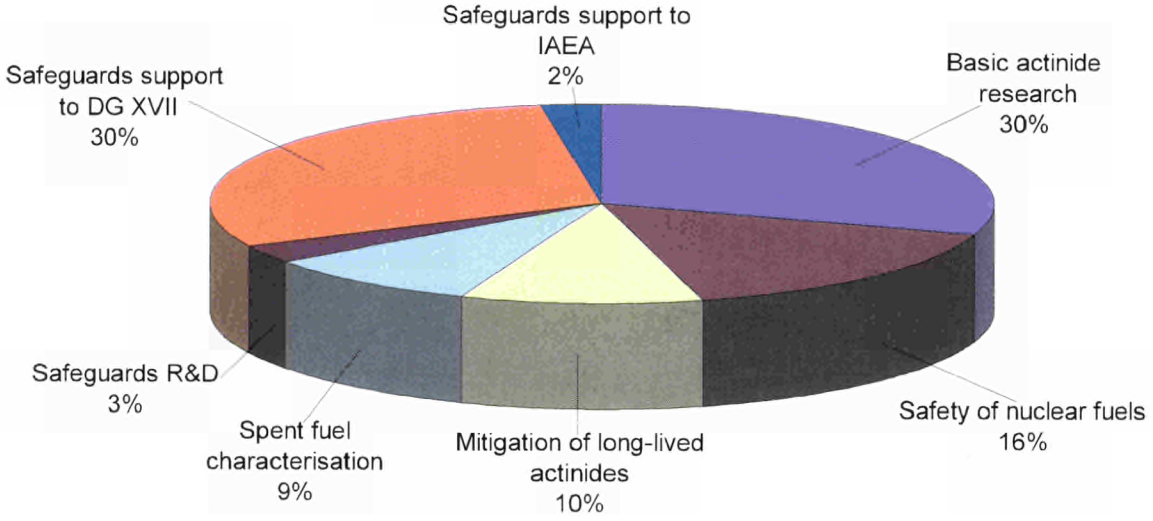

Distribution of staff to scientific / technical activities

Budget distribution

Institutional Activities	30,2	MECU	*(88%)*
Competitive activities	3,9	MECU	*(12%)*
	34,1	MECU	

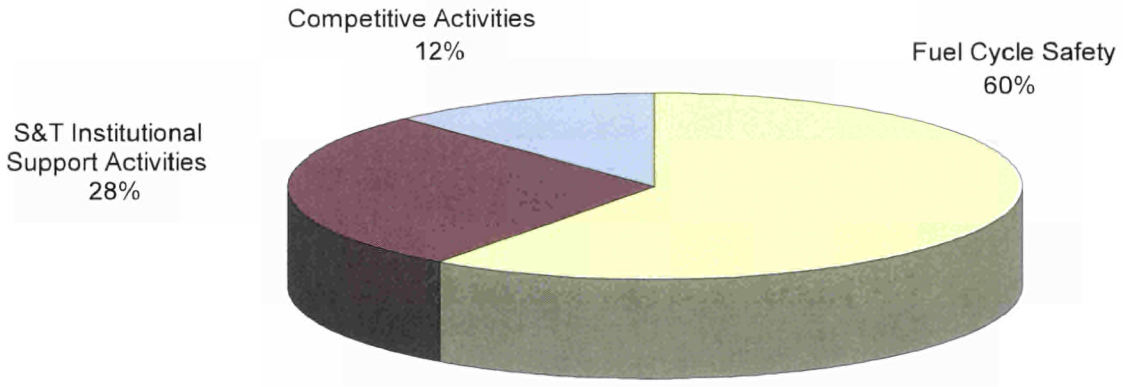

Major activities

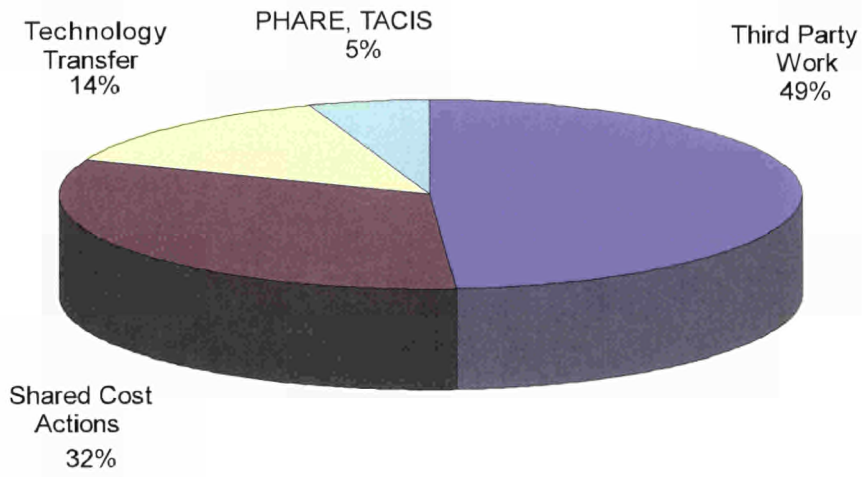

Origin of competitive funds 1996

Annex IV

Organizational Chart

Institute Director	Jacques VAN GEEL
Adviser, acting as Institute Deputy Director	Jean FUGER
Adviser (Programmes)	Roland SCHENKEL
Personnel, Administration and Infrastructure	Gérard SAMSEL
Radiation Protection	Klaas BUIJS (until 30.6.1996) Jean-Luc VASAMILIETTE (acting, since 1.7.1996)
S/T Services:	
- Technical Physics	Michel COQUERELLE
- Applied Physics	Hansjoachim MATZKE
- Nuclear Technology	Karl RICHTER
- Nuclear Chemistry	Lothar KOCH
- Actinide Research	Gerard LANDER

ANNEX V
Glossary of Acronyms and Abbreviations

ABB-CE: Asea Brown Boveri – Combustion Engineering
ACTINEAU: Incinération des ACTINides dans les réacteurs à EAU
AEA: Atomic Energy Authority (United Kingdom)
AECL: Atomic Energy of Canada Ltd.
ADS: Accelerator Driven hybrid reactor Systems
a/o: (at.%) atomic percent
ANTICORP: Technetium transmutation experiment in Phénix
ARTINA: Analysis of Radioisotope Traces for the Identification of Nuclear Activities

BIBLIS: PWR reactor, Biblis/Rhein (Germany)
BNFL: British Nuclear Fuel plc, Springfields (United Kingdom)
B&W: Babcock and Wilcox fuel company
BW: Boiling Water Reactor

C++: Programming Language
CANDU: CANadian Deuterium Uranium reactor
CAPRA: Consommation Accrue de Plutonium dans les (réacteurs) RApides
CCAM: Commission Consultative des Achats et des Marchés, European Commission
CCD: Charged Coupled Device
CEA: Commissariat à l'Énergie Atomique (France)
CEN: Centre d'Etudes Nucléaires, Grenoble (France)
CdZnTe: Cadmium-Zinc-Telluride (detector)
CKED: Compact K-Edge Densitometer
CLASH: Continuous LAser Surface Heating
CLC: Charge Loss Corrector
COGEMA: COmpagnie GEnérale des MAtériaux nucléaires, Vélizy (France)
COMPUCEA: COMbined Product-Uranium Concentration and Enrichment Assay
CRIEPI: Central Research Institute of the Electric Power Industry, Tokyo (Japan)
CSA: Cost Shared Action
CV: Cyclovoltammetry
CW: Continuous Wave

DESY: Deutsches Elektronen-Synchrotron, Hamburg (Germany)
DG I: Directorate-General I 'Internal Economic Relations' of the European Commission
DG XII: Directorate-General 'Science, Research and Development' of the European Commission
DG XIII: Directorate-General XIII 'Telecommunication' Information Market and Exploitation of 'Research' of the European Commission
DG XVII: Directorate-General 'Energy' of the European Commission,
DIAMEX: DIAMide EXtraction process
DTA: Differential Thermal Analysis
DTPA: Diethylene Triamine Penta Acetic acid

ECN: Energie Centrum Nederland, Petten (Netherlands)
ECSAM: European Commission's Safeguards Analytical Measurements
EDAX: Energy-Dispersive Analysis with X-rays
EDAM: Euratom Destructive Analysis Management system
EDF: Électricité de France
EDX: Energy-Dispersive X-ray analysis
EDX: Energy-Dispersive X-ray Diffraction
EFTTRA: Experimental Feasibility for Targets and TRAnsmutation
EFPD: Effective Full Power Days
EMPA: Electron Micro-Probe Analysis (also EPMA)
EOS: Equation Of State
EPMA: Electron Probe Micro-Analysis (also EMPA)

ERDA: Elastic Recoil Detection Analysis
ESARDA: European SAfeguard Research and Development Association
ESD: European Safeguards Directorate, Luxembourg
ESRF: European Synchrotron Research Facility, Grenoble (France)
ETH: Eidgenössische Technische Hochschule, Zürich (Switzerland)
EURATOM: EURopean ATOMic energy community
EXAFS: Extended X-ray Absorption Fine Structure

FBR: Fast Breeder Reactor
FCCI: Fuel Clad Chemical Interaction
FCMI: Fuel Clad Mechanical Interaction
FERONIA: fuel rod modelling and performance project,
FIAP: Fraction of Inventory in the Aeqeous Phase
FP: Fission Products
FZK: ForschungsZentrum Karlsruhe (Germany)
FWHM: Full Width at Half Maximum

GAN: Russian Safeguards and Control Authority
GDMS: Glow Discharge Mass Spectrometry (Spectrometer)
GKN: GemeinschaftsKernkraftwerk Neckarwestheim/Neckar
GSI: Gesellschaft für SchwerIonenforschung, Darmstadt (Germany)
GSP: Gel Supported Precipitation
GWd/tM: Gigawatt-day per (metric) ton metal

HALW: Highly Active Liquid Waste
HAW: Highly Active Waste
HBRP: High Burnup RIM Project
HEU: Highly Enriched Uranium
HFR: High Flux Reactor, Petten (Netherlands)
HLW: High Level Waste
HLLW: High Level Liquid Waste
HMI: Hahn Meitner Institut, Berlin (Germany)
HPGe: High Purity low energy Germanium detector
HPLC: High-Pressure Liquid Chromatography
HPTA: High Precision Trace Analysis
HRGS: High Resolution Gamma Spectrometry
HRTEM: High Resolution Transmission Electron Microscopy

IAEA: International Atomic Energy Agency, Vienna (Austria)
IABAT: Impact of Accelerator BAsed Technologies on nuclear fission safety
IAM: Institute for Advanced Materials, Petten (Netherlands)
IAM: Instituto de Acústica de Madrid (Spain)
IASSC: Iodine Assisted Stress Corrosion Cracking
IBM: International Business Machine, Corporation
IC-ICP-MS-IDA: Ion Chromatography Inductively Coupled-Plasma Mass Spectrometry Isotopic Dilution Analysis
ICP-AES: Inductively Coupled Plasma Atomic Emission Spectroscopy
ICP-MS: Inductively Coupled Plasma Mass Spectrometry
IDA: Isotope Dilution Analysis
ID-ICP-MS: Isotope Dilution ICP-MS
IDMS: Isotope Dilution Mass Spectrometry
ILL: Institut Max von Laue – Paul Langevin, Grenoble (France)
IMF: Institut für Materialforschung, FZK (Germany)
INE: Institut für Nukleare Entsorgungstechnik, FZK (Germany)
INR: Institut für Neutronenphysik und Reaktortechnik, FZK (Germany)
INRAM: INfiltration of RAdioactive Materials
INRNE: Institute for Nuclear Research and Nuclear Energy, Bulgarian Academy of Science
INTAS: INTernational ASsociation for the promotion of Cooperation with Scientists from the Independent States of the former Soviet Union
IRMM: Institute for Reference Materials and Measurements, Geel (Belgium)
IPSN: Institut de Protection et de Sureté Nucléaire, Cadarache (France)
ISO: International Standard Organisation
ISTC: International Science and Technology Center, Moscow (Russia)

ITC: Institut für Technische Chemie, FZK, Karlsruhe (Germany)
ITU: Institute for Transuranium Elements, Karlsruhe (Germany)
ITN: Instituto Tecnológico e Nuclear, Savacem (Portugal)
IVTAN: Institute for High Temperature Physics, Moscow (Russia)

JAERI: Japan Atomic Energy Research Institute (Japan)
JRC: Joint Research Center

KEDG: K-EDGe densitometer
KENO-ORNL: Improved Monte Carlo criticality program with supergrouping, Oak Ridge (USA)
KGB: Kernkraftwerk Gundremmingen Betreibergesellschaft (Germany)
KKGg: KernKraftwerk Gösgen (Germany)
KKI: KernKraftwerk Isar, Eschenbach/Isar (Germany)
KKK: KernKraftwerk Krümmel (Germany)
KKP: KernKraftwerk Philippsburg (Germany)
KNK II: Kompakte Natriumgekühlte Kernreaktoranlage (Germany)
KORIGEN: FZK development of the ORIGEN code
KRI: Khlopin Radium Institute (Russia)
KWO: KernkraftWerk Obrigheim/Neckar (Germany)
KWU: KraftWerk-Union, Germany
KWW: Kernkraftwerk Würgassen/Weser (Germany)

LA: Laser Ablation
LA-ICP-MS: LAser induced Inductively Coupled Plasma Mass Spectrometry
LA-OES: Laser Ablation Optical Emission Spectroscopy
LEU: Low Enriched Uranium
LIF: Laser-Induced Fluorescence
LOCA: LOss-of-Coolant Accident
LSD: Large Size Dried spikes
LSS: Laboratoire Sur Site, La Hague (France)
LWR: Light Water Reactor

MA: Minor Actinides (Np, Am, Cm)
MAGNOX: Magnesium Non Oxidizing (fuel sheath)
MAGNOX reactor: graphite-moderated, gas cooled reactor type in the United Kingdom
MAPI: Mitsubishi Atomic Power Industries (Japan)
MOX: Mixed OXide fuel
MWd/tM: Megawatt day per (metric) ton of (heavy) Metal
MWd/tU: Megawatt day per (metric) ton of Uranium

NCC: Neutron-Coincidence Counter
Nd-YAG: Neodymium-Yttrium Aluminium Garnet laser
NDA: Non-Destructive Assay (Analysis)
NDT: Non-Destructive Testing
NEA: Nuclear Enery Agency, Paris (France)
NEWPART: NEW PARTitioning techniques programme
NNC: National Nuclear Corporation, Ltd. Risley (U.K.)
NSLS: National Synchrotron Light Source, Brookhaven, NY (USA)

OCOM: Optimized CO-Milling
OECD: Organization for Economic Cooperation and Development, Paris (France)
OES: Optical Emission Spectroscopy
ORACLE: Relational database program
ORIGEN: Oak Ridge Isotope GENeration and depletion code
ORNL: Oak Ridge National Laboratory, Oak Ridge, TN (USA)
OS-2: Operating System-2, IBM
OSL: On-Site Laboratory

PCI: Pellet Clad Interaction
PCMI: Pellet Clad Mechanical Interaction
PCRS: Pre-Construction Safety Report
PHARE: Pologne-Hongrie: Aide à la Reconstruction Économique
PHEBUS: French test reactor, Cadarache (France)

PHEBUS-FP: Programme to study fission product release and their distribution in the primary circuit
PHENIX: French prototype fast reactor
PHS: Perturbed Hard-Spheres
PIE: Post-Irradiation Examination
PKED: Product K-Edge Densitometer
PNC: Power reactor and Nuclear fuel development corporation
PSI: Paul Scherrer Institut, Würenlingen, (Switzerland)
PTA: Post-Test Analysis
PWR: Pressurized Water Reactor

QA: Quality Assurance
QC: Qualtity Control

RBMK: graphite moderated Boiling Water Reactor (BWR), (Russia)
RBS: Rutherford Backscattering Spectroscopy
REELS: Reflection Electron Energy Loss Spectra

SAL: Seibersdorf Analytical Laboratory, Vienna (Austria)
SCA: Shared Cost Action
SCALE: Modular code system for performing Standardised Computer Analyses for Licensing Evaluation (ORNL), Oak Ride (USA)
SEM: Scanning Electron Microscopy
SGN: Société Générale pour les Techniques Nouvelles, (France)
SIMFUEL: SIMulated high burnup FUEL (with major non-volatile fission products)
SIMS: Secondary Ion Mass Spectrometry
SOFIT: Joint Soviet-Finish Research Programme of VVER-440 Fuel Performance
SUBATECH: Laboratoire de physique SUBAtomique et de TECHnologies associés, Nantes (France)
SUPERFACT: Minor Actinide Irradiation in Phenix (France)

TACIS: Technical Assistance to the Commonwealth of Independent States
TAMS: Transuranium Analysis Management System
TEM: Transmission Electron Microscopy
THORP: Thermal Oxide Reprocessing Plant, Sellafield (U.K.)
TIG: Tungsten Inert Gas welding
TIMS: Thermal Ionization Mass Spectrometry
TLD: ThermoLuminescence Dosimeter
TOF: Time-Of-Flight
TRABANT: TRAnsmutation and Burning of Actinides in TRIOX
TRANSURANUS: Fuel behaviour code (ITU), Karlsruhe (Germany)
TRIOX: HFR irradiation capsule, Petten (The Netherlands)
TRIM: TRansport of Ions in Matter code
TRU: TRansUranium
TUAR: Annual Report of the Institute for Transuranium Elements (ITU), Karlsruhe (Germany)
TUBRNP: TransUranus BuRNuP model (ITU)

URP-UCD: Unité de Redissolution du Pu – Unité de Conditionnement des Déchets

VAX: Minicomputer (DEC)
VNIINM: All-Russia Research Institute of Inorganic Materials
v/o: (vol %) volume percent
VVER: (also WWER) Pressurized Water Reactor (PWR) built by Russia

WAPD: Westinghouse Atomic Power Division

w/o: (wt %) weight percent
WWER: (also VVER) Pressurized Water Reactor (PWR) built by Russia

XPS: X-ray induced Photoelectron emission Spectroscopy
XRD: X-Ray Diffraction
XRF: X-Ray Fluorescence analysis

Annex VI

List of Contributors to the Various Chapters

1. Basic Actinide Research

G. H. Lander, M.S.S. Brooks, E. Gómez Marín, T. Gouder, S. Heathman, A. Hiess, E. Higgins, V. Ichas, S. Langridge, L. Pereira de Jesus, J. Rebizant, F. Wastin, S. Zwirner – L. Koch, C. Apostolidis, W. Janssens

2. Safety of Nuclear Fuels

M. Coquerelle, J. Cobos-Sabate, J. Spino, A. Stalios, C. Walker – Hj. Matzke, M. Cheindlin, J.P. Hiernaut, K. Laßmann, C. Ronchi, T. Wiss, – K. Richter, A. Fernandez, J. Somers

3. Mitigation of Long Lived Actinides and Fission Products

M. Coquerelle, A. Stalios, L. Koch, C. Apostolidis, J.-P. Glatz – Hj. Matzke, V.V. Rondinella – K. Richter, J.F. Babelot, J. Somers, J.F. Gueugnon

4. Spent Fuel Characterization in View of Long Term Storage

M. Coquerelle, D. Bottomley, D. Papaioannou, J. Spino, B. Sätmark, D. Wegen – Hj. Matzke, V.V. Rondinella, J. Garcia-Serrano – L. Koch, J.-P. Glatz, G. Nicolaou

5. Safeguards Research and Development

L. Koch, K. Abbas, M. Betti, J.-P. Glatz, , G. Nicolaou

6. Scientific and Technical Support to DG XVII

L. Koch, O. Cromboom, P. Daures, K. Mayer, H. Ottmar, H.-G. Schneider, A. Schubert, H. van der Vegt, D. Wojnowski

7. Scientific and Technical Support to DG I

L. Koch, M. Betti, K. Mayer

8. Shared Cost Actions

M. Coquerelle, D. Bottomley, Ch. Papaioannou, D. Wegen – L. Koch, J.-P. Glatz, G. Nicolaou – K. Richter, J.F. Babelot, J.F. Gueugnon, J. Magill – Hj. Matzke: M. Cheindlin, J.P. Hiernaut, C. Ronchi

9. Competitive Support Activities

K. Richter, P. Capéran, J. Somers

10. Third Party Work

M. Coquerelle, D. Bottomley, J. Spino, E. Toscano, A. Stalios – L. Koch, J.-P. Glatz, G. Nicolaou Hj. Matzke, K. Laßmann – K. Richter, J.F. Babelot, P. Capéran, J.F. Gueugnon, J. Somers

11. Other Community Activities

L. Koch, K. Mayer, A. Schubert – Hj. Matzke, M. Cheindlin, J.P. Hiernaut, K. Laßmann, C. Ronchi

13. Quality Management

W. Krischer

Annex VII

Previous Progress Reports of the Institute for Transuranium Elements

TUSR	Period	COM Nr	EUR-Nr
1	Jan - Jun 1966	1580	–
2	Jul - Dec 1966	1522	–
3	Jan.- Jun. 1967	1745	–
4	Jul - Dec 1967	2007	–
5	Jan - Jun 1968	2172	–
6	Jul - Dec 1968	2300	–
7	Jan - Jun 1969	2434	–
8	Jul - Dec 1969	2576	–
9	Jan - Jun 1970	2664	–
10	Jul - Dec 1970	2750	–
11	Jan - Jun 1971	2833	–
12	Jul - Dec 1971	2874	–
13	Jan - Jun 1972	2939	–
14	Jul - Dec 1972	3014	–
15	Jan - Jun 1973	3050	–
16	Jul - Dec 1973	3115	–
17	Jan - Jun 1974	3161	–
18	Jul - Dec 1974	3204	–
19	Jan - Jun 1975	3241	–
20	Jul - Dec 1975	3289	–
21	Jan - Jun 1976	3358	–
22	Jul - Dec 1976	3384	–
23	Jan - Jun 1977	3438	6475 EN
24	Jul - Dec 1977	3484	7209 EN
25	Jan - Jun 1978	3526	7459 EN
26	Jul - Dec 1978	3582	7227 EN
27	Jan - Jun 1979	3657	7483 EN
28	Jul - Dec 1979	3714	7509 EN
29	Jan - Jun 1980	3822	7857 EN
30	Jul - Dec 1980	3846	8230 EN
31	Jan - Jun 1981	3898	8447 EN
32	Jul - Dec 1981	3927	8777 EN
33	Jan - Jun 1982	3990	9581 EN
34	Jul - Dec 1982	4048	10251 EN
35	Jan - Jun 1983	4094	10266 EN
36	Jul - Dec 1983	4117	10454 EN
37	Jan - Jun 1984	4150	10470 EN
38	Jul - Dec 1984	4165	11013 EN
39	Jan - Jun 1985	4201	11835 EN
40	Jul - Dec 1985	4263	11836 EN

TUAR	Period	COM Nr	EUR-Nr
86	Jan - Dec 1986	4302	12233 EN
87	Jan - Dec 1987		12385 EN
88	Jan - Dec 1988		12233 EN
89	Jan - Dec 1989		12849 EN
90	Jan - Dec 1990		13815 EN
91	Jan - Dec 1991		14493 EN
92	Jan - Dec 1992		15154 EN
93	Jan - Dec 1993		15741 EN
94	Jan - Dec 1994		16152 EN
95	Jan - Dec 1995		16368 EN
96	Jan - Dec 1996		17296 EN

Previous Programme Progress Reports were confidential for a period of two years. Between 1977 and 1987 they had been made freely accessible after that period as EUR-Reports (on microfiches) and since 1988 they have been issued as regular EUR-Reports. They can be ordered from the Office for Official Publications of the European Communities, 2 rue Mercier, L-2985 Luxembourg, Tel. 499 28-1, Telex 1322 PUBOF LU. Since 1996 (TUAR-95) the reports are available on the Web page: http://www.jrc.org/

European Commission

EUR 17296 EN - Institute for Transuranium Elements - Annual report 1996
Editors: R. Schenkel, J. Richter, J. Magill, D. Pel
Luxembourg: Office for Official Publications of the European Communities
1997 - 171 pp.; - 21.0 x 29.7 cm
Scientific and Technical Research series
ISBN 92-828-0049-0 Catalogue number: GC-NA-17296-EN-C

The safety of actinides in the nuclear fuel cycle continued to be the major institutional contribution of the Institute to the Nuclear Fission Safety Programme. Major research areas were basic actinide research, safety of nuclear fuels, mitigation of long-lived actinides and spent fuel characterisation.
Basic actinide research is being carried out to elucidate the electronic structure of actinide elements. The preparation of new compounds, and synthesis of single crystals play a key role in this endeavour. Important results have been obtained in the understanding of uranium-based heavy-fermion superconductors. Other themes include pressure studies, the theory of light-solid interactions; and the use of neutron and synchrotron experiments to complement the bulk-property measurements obtained in Karlsruhe. Several batches of ^{225}Actinium - ^{213}Bismuth were delivered to the Memorial Sloan Kettering Cancer Center in New York. The first treatment of patients with ^{213}Bi alpha-immunotherapy took place at the end of 1996.
In the area of safety of nuclear fuel, porosity distribution and mechanical properties of fuel at very high burn-up (up to 60 GWd/t) was measured and evaluated. Structural properties of fuel with simulated burn-ups of up to 200 GWd/t were examined and compared with real high burn-up fuel to improve understanding of the rim effect formation processes. Oxidation and creep measurements on SIMFUEL were carried out and radiation damage studies on UO2 yielded, for the first time, direct visible evidence of tracks of fission fragments in this material.
With regard to mitigation of long-lived actinides and fission products, ITU continued its collaborative work with leading national laboratories, in order to study the further reduction of radiotoxicity of highly active wastes. During 1996, a new fabrication procedure based on the infiltration of radioactive materials (INRAM) into matrices was developed, tested and successfully applied for the fabrication of americium containing incineration targets. Actinides were separated from irradiated fuel (Superfact 1) on a 100 g scale, including a final separation step for lanthanides. Radiation damage and basic physical property studies were performed on different inert matrices.
On the characterization of spent fuel, investigations centered mainly on the oxidation kinetics and corrosion effects of irradiated UO_2 and MOX fuel. Leaching tests on UO_2 and on fuel rod segments with pre-set defects were carried out. The chemical interaction of fuel and cladding has been further investigated. Initial electrochemical measurements show lower corrosion rates for MOX fuel than for uranium fuel.
Within safeguards R & D, the Secondary Ion Mass Spectrometer (SIMS) for the measurement of particles from swipe samples went into operation and the first environmental samples were received and analysed. Major progress was achieved towards the implementation of the on-site laboratory at Sellafield.
The technical specifications for the on-site laboratory at Cap la Hague were discussed with the architect engineering company in charge of the pre-project. ITU also continued to receive and analyse seized nuclear materials. A nuclear material data bank was set up in close collaboration with the Bochvar Institute in Moscow.

Information on European Commission publications in the areas of research and innovation can be obtained from

- CORDIS, the Community R&D Information Service. For more information, contact CORDIS Customer Service, BP 2373, L-1023 Luxembourg (Tel.: +352 401162-240, Fax: +352 401162-248, E-mail: helpdesk@cordis.lu) or visit the CORDIS website at http://www.cordis.lu/
- *Euroabstracts*, the European Commission's periodical on research publications, issued every two months. For a subscription (1 year; ECU 65) write to the address below.

15 GC-NA-17296-EN-C

OFFICE FOR OFFICIAL PUBLICATIONS
OF THE EUROPEAN COMMUNITIES

L-2985 Luxembourg

ISBN 92-828-0049-0

9 789282 800492 >